The role of IFITM1 in promoting breast cancer aggression and aromatase inhibitor resistance

By

Asona J. Lui

Submitted to the graduate degree program in Molecular and Integrative Physiology and the Graduate Faculty of the University of Kansas in partial fulfillment of the requirements for the degree of Doctor of Philosophy.

_____

Co-Chair: Joan Lewis-Wambi, Ph.D.

_____

Co-Chair: Paige Geiger, Ph.D.

_____

Shrikant Anant, Ph.D.

_____

Fariba Behbod, PharmD, Ph.D.

_____

Dan Dixon, Ph.D.

_____

Animesh Dhar, Ph.D.

_____

Timothy Fields, M.D., Ph.D.

Date defended: 3/28/17

The Dissertation Committee for Asona J. Lui

certifies that this is the approved version of the following dissertation:

The role of IFITM1 in promoting breast cancer aggression and aromatase-inhibitor resistance

_____

Co-Chair: Joan Lewis-Wambi, Ph.D.

_____

Co-Chair: Paige Geiger, Ph.D.

Date approved: 5/12/17

ABSTRACT

Breast cancer remains the leading malignancy among women in the United States, affecting an estimated 246,660 women in 2016. Breast cancer can be separated into three groups known as estrogen receptor/ progesterone receptor positive (ER+/PR+), Her2/neu positive (HER2+), and triple negative (ER-/PR-/HER2-) subtypes. The majority of breast cancers rely on estrogen to stimulate their growth and survival. Estrogen is produced from precursor hormones by the aromatase enzyme, whose action can be blocked with aromatase inhibitors (AIs). Unfortunately ~40% of breast cancer patients are resistant to this treatment and their breast tumors either continue to grow or recur despite depletion of circulating estrogen. The precise cause of AI-resistance is not known. Our lab aims to determine the mechanisms that allow breast cancer cells to survive in estrogen-depleted conditions. We have previously reported the generation of an AI-resistant breast cancer cell line, MCF-7:5C, which was isolated under estrogen-free conditions from the estrogen-dependent breast cancer cell line MCF-7. The MCF-7:5C cell line is highly aggressive and overexpresses several interferon stimulated genes including, interferon inducible transmembrane protein 1 (IFITM1).

IFITM1 is a type 1 interferon (IFN) stimulated gene (ISG) that is not expressed in normal breast tissue, and is only induced by the type1 IFNs (IFNα and β) to protect the host from viral infections. IFNα signals through a specific receptor, IFNAR, which uses JAK/STAT signaling to produce the ISGs. ISGs are known to drive the progression of other cancer types, to inhibit apoptosis and promote DNA damage resistance. However, the significance of constitutive overexpression of ISGs in AI-resistant breast cancer is

not known. We hypothesize that IFITM1 overexpression contributes the AI-resistant phenotype and promotes breast cancer cell aggression and survival.

In this thesis, we demonstrate that IFITM1 is overexpressed in breast tumors and is correlated with poor response to endocrine therapy using *in silico* analysis of breast tumor expression databases and a human tissue microarray. Gain and loss of function studies in an IFITM1-overexpressing AI-resistant breast cancer cell line, MCF-7:5C, and an IFITM1-null AI-sensitive breast cancer cell line, MCF-7, reveal that IFITM1 promotes the AI-resistant aggressive phenotype and estrogen-independent growth. Additionally, the orthotopic (mammary fat pad) and mouse mammary intraductal (MIND) models of breast cancer evaluate the role of IFITM1 in tumor growth and invasion respectively. We report that loss of IFITM1 induced cell death in AI-resistant MCF-7:5C cells results in marked increases in p21/Waf1/Cip1 transcription, expression and nuclear localization. Notably, p21 transcriptional upregulation was mediated by STAT1 activation. These findings suggest IFITM1 overexpression contributes directly to breast cancer progression and that it may be a therapeutically relevant target in the treatment of endocrine-resistant breast cancer.

Mechanistic studies reveal that MCF-7:5C cells produce elevated levels of IFNα as compared to MCF-7 cells and that this cytokine binds to the type 1 IFNα receptor, IFNAR, and induces JAK/STAT signaling, ultimately resulting in the overexpression of IFITM1. Independently, we also find that mucin 1 (MUC1) associates with STAT1 and stabilizes its phosphorylated form, thereby contributing directly to IFITM1 expression. MUC1 expression is hormonally controlled and is normally enhanced by estrogen stimulation. We find that MUC1 expression is dysregulated in AI-resistant MCF-7:5C

cells and is instead reduced by estrogen stimulation. MCF-7:5C cells are sensitive to apoptosis following exposure to estrogen, which can be enhanced by loss of IFITM1 expression. Loss of MUC1 expression similarly enhances estrogen-induced apoptosis, suggesting that the communication between MUC1 and STAT1 also influences estrogen signaling in AI-resistant breast cancer. In this thesis, we conduct investigations into the mechanisms and functional significance of IFITM1 expression in AI-resistant breast cancer and conclude that IFITM1overexpression may be a targetable marker of AI-resistant disease.

ACKNOWLEDGEMENTS

I would like to start by thanking my mentor, Dr. Joan Lewis-Wambi, who took a chance on an eager student in the summer of 2013 even though she wasn't planning on bringing a student into her brand new laboratory yet. I had no background in cancer research, but I was directed by the many independent recommendations that I received from both her peers and mine. I was always told that your mentor was more important than your thesis project and I was fortunate to find both an exciting project and a wonderful mentor in Dr. Lewis-Wambi. Our discussions have encouraged me to think critically about my research, but also my training and career goals. Ultimately, she has helped me map out a plan that I am confident will lead to a successful career as a Physician Scientist. I will be forever thankful that I was steered in the direction of the Lewis-Wambi lab.

I would like to show my appreciation for the members of my dissertation committee, Drs. Paige Geiger, Shrikant Anant, Fariba Behbod, Dan Dixon, Animesh Dhar and Timothy Fields, who made up a dream team to support my training. Thank you to them for providing invaluable guidance and intellectual rigor during this educational journey. Their involvement in my training has augmented my development as a scientist and has made it possible to complete these projects.

I want to take this opportunity to express my gratitude to the Department of Molecular and Integrative Physiology from their well-structured graduate program and unwavering support of their students. Being a member of this department has made the process of graduate school a logical and reasonable process. I applaud their commitment to student voices and involvement through the Physiology Society, which brought fun and opportunity to my four year tenure in the department. I was very

fortunate to also be a member of the Cancer Biology Department during this time, which provided the coursework, facilities and faculty necessary to developing a young cancer biologist. Being a member of the KU Cancer Center has allowed me access to the pre-award grant support and intellectual environment necessary to submit my F30 fellowship to the National Cancer Institute, for which I will always be grateful. Thank you to Dr. Shrikant Anant especially, who was willing to serve as my co-sponsor and to share his secrets in the art of grant writing, which I am lucky to take with me into my future career.

I would also like to thank the members of the Wambi Lab; Dr. Hye-Joung Choi, Dr. Joshua Ogony, Erin Hayes, Jordan Marquess and Eric Geanes who made it possible to get through the ninth repeat of a western blot, the pain of MIND injections and 21 days straight of oral gavage with laughter. A special thank you to Dr. Kelli Valdez and the members of the Behbod lab for training me in the amazing MIND model and helping me through large experiments when I found myself the sole member of the Wambi Lab during the Summer of 2016. And a big thank you to Jordan Marquess and Marco Chacon who made it possible to complete critical experiments in a wheelchair during that same period.

I am grateful to the MD/PhD Physician Scientist Training Program at the University of Kansas Medical Center which extended me the opportunity to learn to heal patients and also satisfy my need to ask, “Why?” and, “How?” Dr. Fields, Dr. Rongish and Janice Fletcher are the heart and soul of the MD/PhD program and I will always be thankful for their open doors, open hearts and commitment to bringing together the right students for this long journey. They have provided me with a network of life-long friends

who also happen to be fellow MudPhuds. I am also grateful to Dr. Erhart and Dr. He at Chicago State University for giving me the chance to discover the joy of basic science research, and without whom I never would have applied to KUMC.

I would like to thank the Flow Cytometry Core (and Rich Hastings), the Confocal Imaging Core (and Pat St John), the Electron Microscopy Core (and Barb Fegley), the Biospecimen Repository (and Marsha Danley) for the use of key pieces of equipment and training in elegant scientific techniques. I also want to recognize the dedicated staff and many mice in the Animal Facility at KUMC for making an *in vivo* component to the project a reality.

I acknowledge the financial support that made this research possible, including the KUMC Biomedical Research Training Program (BRTP to AL), the National Cancer Institute (1F30CA203160-01 to AL), the American Medical Association (AMA) Foundation (to AL), start-up funds from the University of Kansas Medical Center (KUMC) (to JLW), and the University of Kansas Cancer Center (CCSG grants P30 CA168524-0 to JLW).

I am most indebted to my family who has given unconditional support throughout my life, and especially my parents who provided the opportunities and education they never had. “The one thing that no one can ever take away from you.”

TABLE OF CONTENTS

Abstract ..... **iii**

Acknowledgements ..... **vi**

Table of Contents ..... **ix**

List of Abbreviations ..... **xii**

List of figures and Tables ..... **xiv**

Figures xiv

Tables xvi

Supplementary Figures xvi

Chapter 1 : Background and Introduction **1**

Breast Cancer Statistics and Risk Factors 1

Estrogen and Estrogen Signaling in Breast Cancer 1

Aromatase inhibitor Resistance in ER+ Breast Cancer 4

The Paradoxical Effects of Estrogen 5

The IFN Family 7

IFN Signaling and IFN Stimulated Genes 8

IFN Stimulated Genes in Solid Tumors 10

Interferon Induced Transmembrane Protein 1 (IFITM1) 13

Summary 17

Chapter 2 : IFITM1 is overexpressed in breast cancer and is correlated with clinical outcome and response to therapy 19

Introduction 19

Results 21

Discussion 29

Materials and Methods 32

Chapter 3 : Functional significance of IFITM1 overexpression in AI-resistant breast cancer 36

Introduction 36

Results 38

Discussion 52

Materials and Methods 54

Supplemental Figures 63

Chapter 4 : Role of IFITM1 in controlling cell cycling and survival 68

Introduction 68

Results 71

Discussion 77

Materials and Methods 78

Chapter 5 : Regulation of IFITM1 by JAK/STAT signaling in AI-resistant breast cancer 82

Introduction....82

Results....86

Discussion....103

Materials and Methods....107

Supplemental Figures....110

Chapter 6 : Conclusion and future directions....111

References....115

Appendix A: Manuscript-Everolimus downregulates estrogen receptor and induces autophagy in aromatase inhibitor-resistant breast cancer cells....138

LIST OF ABBREVIATIONS

4OHT	4- hydroxytamoxifen
AI	Aromatase inhibitor
CAV-1	Calveolin-1
Dox	doxycycline
ERα	Estrogen receptor alpha
ER+	estrogen receptor-positive
ERE	estrogen response element
FUL	Fulvestrant
GAS	gamma associated sequence
HER2	human epidermal growth factor receptor 2
IFI27	Interferon-inducible protein 27
IFIT1	Interferon induced protein with tetratricopeptide repeats 1
IFITM	interferon induced transmembrane protein
IFNα/β	interferon alpha and beta
IFNAR	type 1 interferon receptor
IHC	immunohistochemistry
IRF-7	IFN regulatory factor
IRF-9	IFN regulatory factor 9
ISGs	interferon stimulated genes
ISGF3	IFN-stimulated gene factor 3
ISRE	interferon stimulated response element

JAK1/2	Janus kinase 1 and 2
MIND	mouse mammary intraductal model
mTOR	Mammalian target of rapamycin
OAS 1,2,3	2-5-oligoadenylate synthetase 1,2,3
p21	Cyclin dependent kinas inhibitor 1
p53	tumor protein 53
PARP	poly ADP ribose polymerase
PI	propidium iodide
PI3K	Phosphoinositide 3-kinase
Pim-1	murine leukemia virus
PLSCR1	phospholipid scramblase 1
PR	Progesterone receptor
PTEN	Phosphatase and tensin homolog
Rux	ruxolitinib (Jakafi™)
SOCS1,2	suppressor of cytokine signaling 1
STAT1/2	signal transducer and activator of transcription 1 and 2
U-ISGF3	unphosphorylated IFN-stimulated gene factor 3

LIST OF FIGURES AND TABLES

FIGURES

Figure 1.1 Estrogen production and signaling in postmenopausal women. 2

Figure 1.2 Mechanisms of action of endocrine therapy 3

Figure 1.3 Mechanisms of AI-resistance. 5

Figure 1.4 Types of IFN Signaling. 7

Figure 1.5 Proposed causes and results of endogenous IFN production by breast cancer cells. 13

Figure 1.6 IFITM proteins inhibit virus entry at different stages of cell trafficking. 14

Figure 1.7 IFITM protein topology and domain organization. 15

Figure 2.1 IFITM1 is overexpressed in breast cancer. 22

Figure 2.2 High IFITM1 expression is associated with AI-resistance. 23

Figure 2.3 staining intensities for ER+ breast cancer patients. 27

Figure 2.4 IFITM1 overexpression is correlated with poor clinical outcome. 28

Figure 3.1 ISGs are overexpressed AI-resistant MCF-7:5C cells 40

Figure 3.2 Loss of IFITM1 induced death in AI-resistant MCF-7:5C cells. 41

Figure 3.3 Loss of IFITM1 inhibited MCF-7:5C tumor growth and promoted cell death *in vivo*. 42

Figure 3.4 A comparison of the orthotopic and MIND models of breast cancer. 43

Figure 3.5 Loss of IFITM1 reduced aromatase inhibitor-resistant tumor cell invasion in the MIND model. 45

Figure 3.6 Loss of IFITM1 decreased cell proliferation and increased cell death in the MIND model of breast cancer. 46

Figure 3.7 Overexpression of IFITM1 enhances the aggressive phenotype of MCF-7 breast cancer cells in vitro. 48

Figure 3.8 Overexpression of IFITM1 promoted breast cancer cell proliferation and invasion *in vivo*. 49

Figure 3.9 Loss of IFITM1 reduces blood vessel density and MMP1 expression. 51

Figure 4.1 Nuclear and cytoplasmic functions of $p21^{waf1}$.....69

Figure 4.2 Loss of IFITM1 expression was associated with increased p21 expression, which mediated cell death. 72

Figure 4.3 IFITM1 knockdown increases p21 expression via enhanced STAT1 activity. 74

Figure 4.4 Loss of IFITM1 induces p21 nuclear translocation. 76

Figure 4.5 Loss of p21 drives cell death through regulation of p21 expression and cellular localization. 78

Figure 5.1 Elevated IFNa production drives constitutive overexpression of IFITM1 through IFNAR 87

Figure 5.2 IFNα production is driven by interferon regulatory factor 7 (IRF-7). 89

Figure 5.3 ISG expression in MCF-7 and MCF-7:5C cells in response to IFNα exposure. 91

Figure 5.4 IFITM1 overexpression is driven by JAK/STAT signaling at GAS and ISRE motifs. 93

Figure 5.5 STAT1, STAT2 and MUC1 are recruited to an ISRE in the IFITM1 promoter 94

Figure 5.6 Inhibition of JAK/STAT signaling with Ruxolitinib decrease IFITM1 expression and reduced the growth of aromatase inhibitor-resistant MCF-7:5C tumors.....96

Figure 5.7 MUC1 expression is dysregulated in MCF-7:5C cells.....98

Figure 5.8 MUC1 stabilizes JAK/STAT signaling through interaction with p-STAT1 100

Figure 5.9 Loss of MUC1 induces death of AI-resistant MCF-7:5C cells.....101

Figure 5.10 MUC1 and IFITM1 co-occur in breast cancer 102

Figure 5.11 The role of MUC1 in JAK/STAT mediated IFITM1 overexpression and estrogen-induced apoptosis 104

Figure 6.1 IFITM1 overexpression is driven by JAK/STAT signaling from IFNAR and is stabilized by MUC1. 112

TABLES

Table 1.1 Interferon Stimulated Genes (ISGs) associated with cancer progression and resistance to chemotherapy, radiation and hormonal therapy.[6] 11

Table 2.1 Staining intensity for IFITM1 expression in AI-resistant TMA 24

Table 2.2 Distribution of clinical and histologic parameters in ER+ invasive ductal carcinoma samples 25

Table 2.3 IFITM1 staining intensity in normal and cancerous breast tissues.....25

SUPPLEMENTARY FIGURES

Supplemental Figure 3.1 Doxycycline induced IFITM1 shRNA expression is specific to MCF-7:5C/IFsh cells. 63

Supplemental Figure 3.2 MIND injection of MCF-7:5C/IFsh and MCF-7:5C/C9Con cells. 64

Supplemental Figure 3.3 Expression of ERα is higher in MIND verses orthotopic mouse tumors. 65

Supplemental Figure 3.4 Overexpression of IFITM1 promoted breast cancer cell proliferation and invasion. 66

Supplemental Figure 3.5 IFITM1 expression is associated with angiogenesis. 67

Supplemental Figure 5.1 Inhibition of JAK/STAT signaling with Ruxolitinib (Jakafi) decreased IFITM1 expression and reduced the growth of IFITM1 overexpressing MDA-MB-468 cells. 110

CHAPTER 1 : BACKGROUND AND INTRODUCTION

BREAST CANCER STATISTICS AND RISK FACTORS

Breast cancer remains the most prevalent malignancy among women, accounting for about 30% of all cancer cases diagnosed in the United States, and a total of 246,660 new cases in 2016.[10,11] While the incidence of breast cancer has decreased continuously in recent decades, it is still estimated that 1 in 8 women will develop breast cancer in her lifetime.[12,13] Additionally, several risk factors for the development of a breast malignancy have been identified. It is known that having a personal or family history of breast cancer, as well as certain genetic mutations, such those in the BRCA1/2 DNA repair genes increases breast cancer risk. The remaining well-known risk factors: female gender, age, use of hormone replacement therapy or oral contraceptives, early menarche, late menopause, obesity and alcohol intake all increase the chance of developing breast cancer because they increase a woman's lifetime exposure to estrogen.[14,15]

ESTROGEN AND ESTROGEN SIGNALING IN BREAST CANCER

Estrogen is a steroid hormone that is essential for normal development of the female reproductive organs, as well as the bones and heart.[16] Estrogen promotes the growth and differentiation of target tissues by binding to the estrogen receptor (ER). Traditionally, ER functions as a classic steroid hormone receptor. Ligand activated ER enters the nucleus and dimerizes allowing for transcription factor function. [17] Active ER then binds to estrogen responsive elements (ERE) in the promoters of hundreds of genes, most of which promote cell cycle progression and growth.[16] ER can also be palmitoylated, which localizes it to the cell membrane. There ER interacts with the

adaptor proteins Shc and calveolin-1.[18] These interactions allow ER to signal through rapid phosphorylation cascades, using many cell signaling mediators, including G-protein coupled receptors, Src tyrosine kinases and PI3K.[17,18] The latter interaction also mediates cell growth and survival by facilitating Akt activation, which promotes the expression of cell cycle and pro-survival genes as well. Rapid signaling through membrane bound ER is also known to recruit β-tubulin, which increases promotes cell migration.[18] Due to the many beneficial effects of ER signaling, most breast cancers utilize estrogen to facilitate their growth, survival and invasion (Figure 1.1).

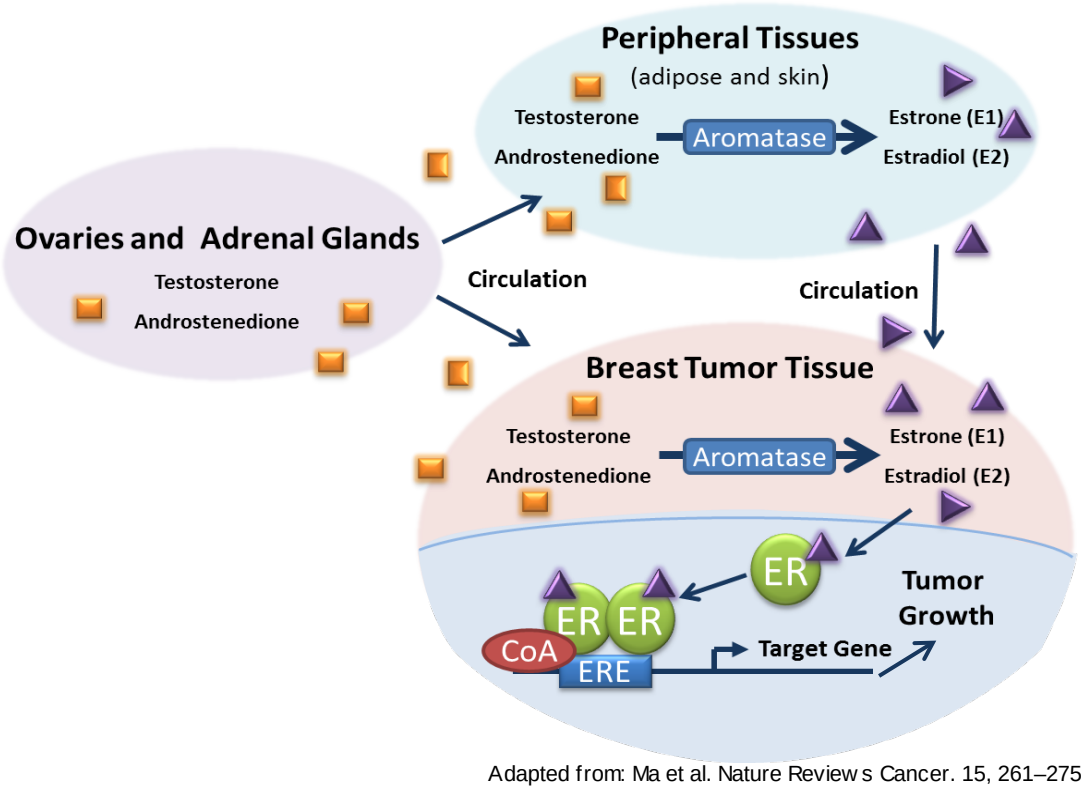

Adapted from: Ma et al. Nature Reviews Cancer. 15, 261–275 (2015).

Figure 1.1 Estrogen production and signaling in postmenopausal women.

In postmenopausal women, the ovaries and adrenal glands produce the hormones testosterone and androstenedione. Estrogen is synthesized in peripheral tissues such as adipose tissue, breasts and skin through the action of aromatase, which converts androstenedione and testosterone to estrone and estradiol. Estrogen receptor-positive (ER^+) breast cancer cells can also express aromatase, leading to intratumoral estrogen production. CoA, co-activator; ERE, estrogen response element.[5]

Roughly 75% of breast cancers are estrogen receptor positive (ER+) and the number of ER+ tumors is expected to continue to rise over the next decade.[10,11,13] Therefore, it is not surprising that women with higher circulating levels of estrogen have a higher risk of developing breast cancer. [16] This is not only because ER signaling promotes cell growth and proliferation, but also because estrogen metabolites are powerful carcinogens. Estrogen metabolites form DNA adducts, cleave purine bases, and generate free radicals, all of which induce DNA damage and promote epithelial transformation.[19-21] Due to the many cancer promoting actions of estrogen, the predominate treatment for ER+ breast tumors is blockade of ER signaling. The main

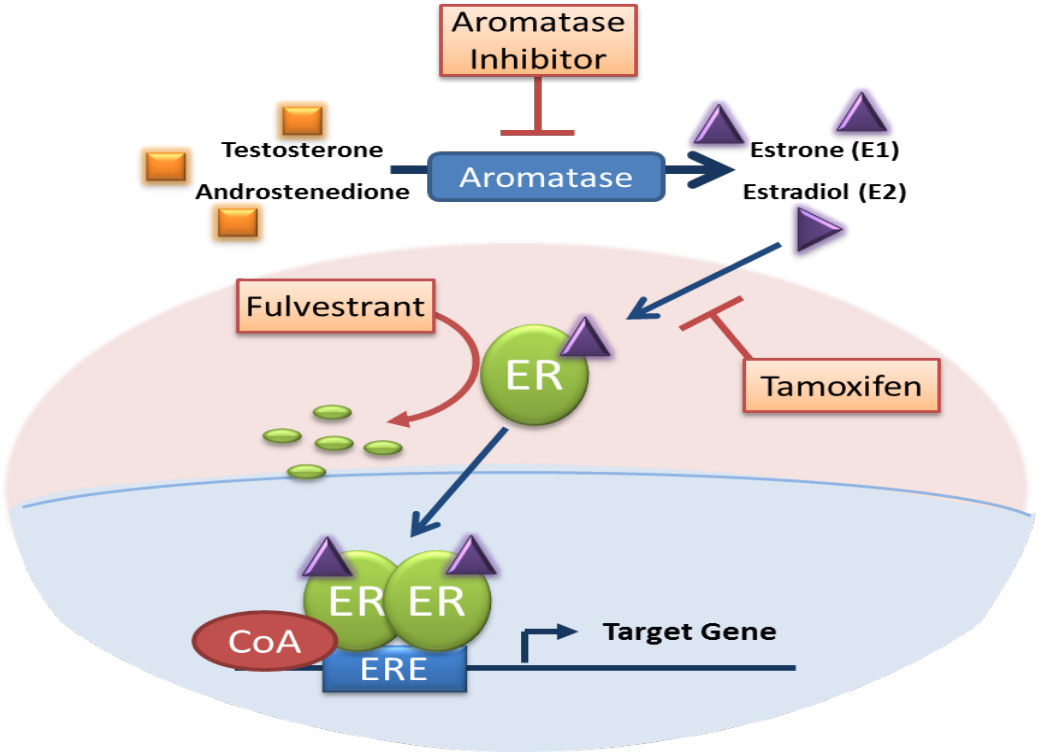

Adapted from: Johnston & Dow sett. *Nature Reviews Cancer* **3**, 821-831 (2003).

Figure 1.2 Mechanisms of action of endocrine therapy

Estradiol binds to the estrogen receptor (ER), leading to dimerization, conformational change and binding to estrogen response elements (EREs) upstream of estrogen-responsive genes including those responsible for proliferation. Tamoxifen competes with estradiol for ER binding whereas aromatase inhibitors reduce the synthesis of estrogens from their androgenic precursors. Fulvestrant in turn binds to and induces degradation of ER. CoA, coactivator. [8]

therapies for ER+ breast cancer target the estrogen receptor, estrogen production or estrogen signaling (i.e. endocrine therapy). This is accomplished by depletion of circulating estrogen with aromatase enzyme inhibition (AI), by blockade of ER signaling with selective estrogen receptor modulators (SERMs) such as tamoxifen, and by degradation of ER itself, with selective estrogen receptor down-regulators (SERDs) such as fulvestrant (Figure 1.2). All of these therapies have had profound anti-tumor benefits in the clinic.[22,23] The introduction of endocrine therapy has resulted in significant reductions in ER+ breast cancer-related mortality.

AROMATASE INHIBITOR RESISTANCE IN ER+ BREAST CANCER

The AIs prevent estrogen production from precursor hormones by targeting the aromatase enzyme. These include non-steroidal anastrozole and letrozole as well as steroidal exemestane (Figure 1.2).[11,24] All three compounds deplete circulating estrogen, effectively starving the breast cancer cells and stimulating cell cycle arrest and cell death, which results in tumor shrinkage and prevention of metastasis.[25,26] Due to the unsurpassed effect on tumor progression, AI therapy is now the standard of care for women with ER+ breast cancer. Unfortunately, approximately 30% of women receiving AI treatment eventually develop resistance and the tumors continue to grow and metastasize despite the absence of estrogen.[25-28] These AI-resistant tumors are typically more aggressive and are less responsive to other types of endocrine therapy, leaving radiation and chemotherapy as the main treatments available to these patients.[28] The mechanism by which AI resistance develops in breast cancer and the molecular factors driving its aggressive phenotype are still not completely known.[5] While it is not known what drives AI-resistance, alterations in ER, growth factor,

PI3K/Akt/mTOR, apoptosis and autophagy signaling have been identified as potential mechanisms in both preclinical and clinical studies (Figure 1.3).[27,29-31]

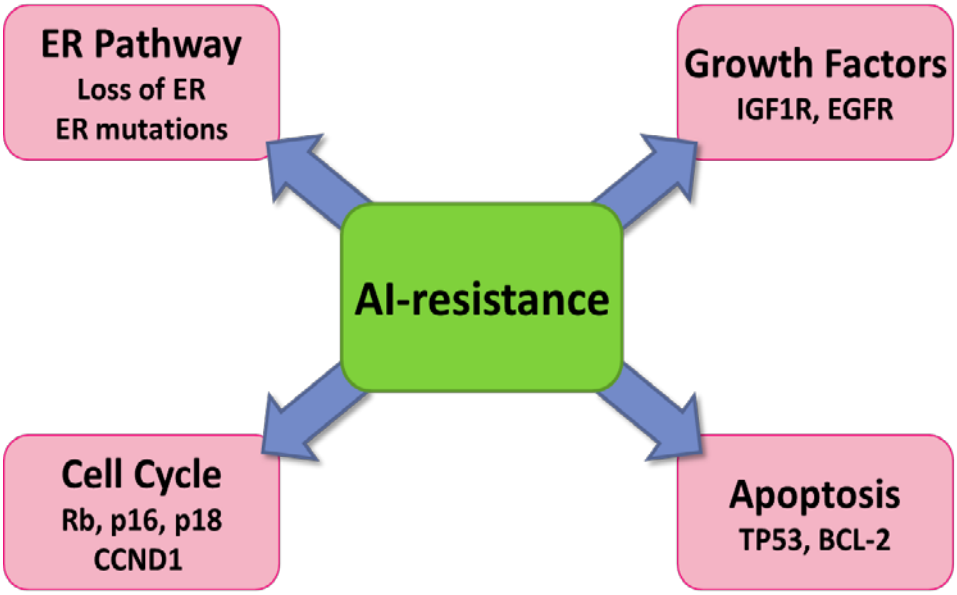

Ma et al. Nature Reviews Cancer. 15, 261–275 (2015).

Figure 1.3 Mechanisms of AI-resistance.
Several cell-autonomous and non-cell-autonomous mechanisms in estrogen receptor-positive (ER^+) breast cancer and the tumor microenvironment could lead to aromatase inhibitor (AI) resistance. These include alterations in estrogen receptor (ER), such as mutations in/or loss of ER expression. Enhanced growth factor signaling can compensate for the loss of estrogen stimulation and changes in apoptosis or cell cycle proteins can promote cell survival and proliferation. IGF1R, insulin-like growth factor; EGFR, epidermal growth factor receptor; TP53, tumor protein 53; BCL-2, B cell lymphoma 2; Rb, retinoblastoma protein; CCND1, cyclin D1 [5]

THE PARADOXICAL EFFECTS OF ESTROGEN

Remarkably, in addition to the growth stimulating effects of estrogen, estrogen and estrogenic compounds can also have a pro-apoptotic role in breast cancer cells, known as the "estrogen paradox."[32] It should be noted that synthetic estrogens and estradiol were used for the treatment of advanced breast cancer starting in the 1940s until the advent of tamoxifen therapy in the 1970s.[33,34] In fact, synthetic estrogens and tamoxifen exhibited similar tumor regression rates to tamoxifen in clinical trials and were only replaced as standard of care for breast cancer treatment because of a better side-

effect profile.[35,36] As the number of patients developing resistance to endocrine therapy grew, the use of estrogens was investigated again in patients that had failed several rounds of hormone therapy.[23,37-39] In these studies, a significant group of patients experienced marked decreases in tumor size, burden and mortality when treated with estrogens as compared to standard endocrine therapy. This concept, known as the "estrogen gap hypothesis" addresses the fact that high dose estrogen therapy is significantly effective in breast tumors that have been deprived of estrogen for at least 5 years and also explains why older post-menopausal women have a lower incidence of breast cancer when placed on estradiol replacement therapy late in life.[40,41]

Development of the long-term estrogen deprived (LTED) cell lines from ER+ MCF-7 and T47-D cells has allowed for investigation into the mechanism of estrogen-induced tumor regression.[42-44] Studies by our laboratory and others have revealed that estrogen induces stress response, intrinsic caspase-mediated and Fas death receptor mediated apoptosis in LTED cells.[45-48] Estrogen-induced apoptosis is an ER-mediated phenomenon that likely results after adaptive hypersensitivity to estrogen in LTED cells. This hypersensitivity is thought to be due to upregulated growth-factor signaling in the estrogen-deprived state.[49] In response to estrogen treatment, LTED cells receive growth and death signals simultaneously. The growth signals are thought to be mediated by insulin-like growth factor (IGF) signaling, while the pro-apoptotic signals seem to begin with Akt degradation in the endoplasmic reticulum.[50] Competing signals on the PI3K pathway likely maintains homeostasis in normal tissues but becomes out of balance in the LTED state.[47] While investigation into the exact mechanism of estrogen-induced apoptosis continues, our laboratory has begun compiling a genetic profile that defines

tumors that are sensitive to estrogen therapy. One pathway that is overactive in LTED is the interferon (IFN) signaling pathway.[46]

THE IFN FAMILY

The IFN family consists of several cytokines that are known to have both pro- and anti-tumor functions.[2] These proteins are produced by all nucleated cells in the body, including the cells of the immune system and epithelial cells at the site of inflammation or pathogen specific immune response.[2,51] They all have antiviral activity, inhibit cell growth and control cell fate.[51,52] The IFNs are transcribed by interferon

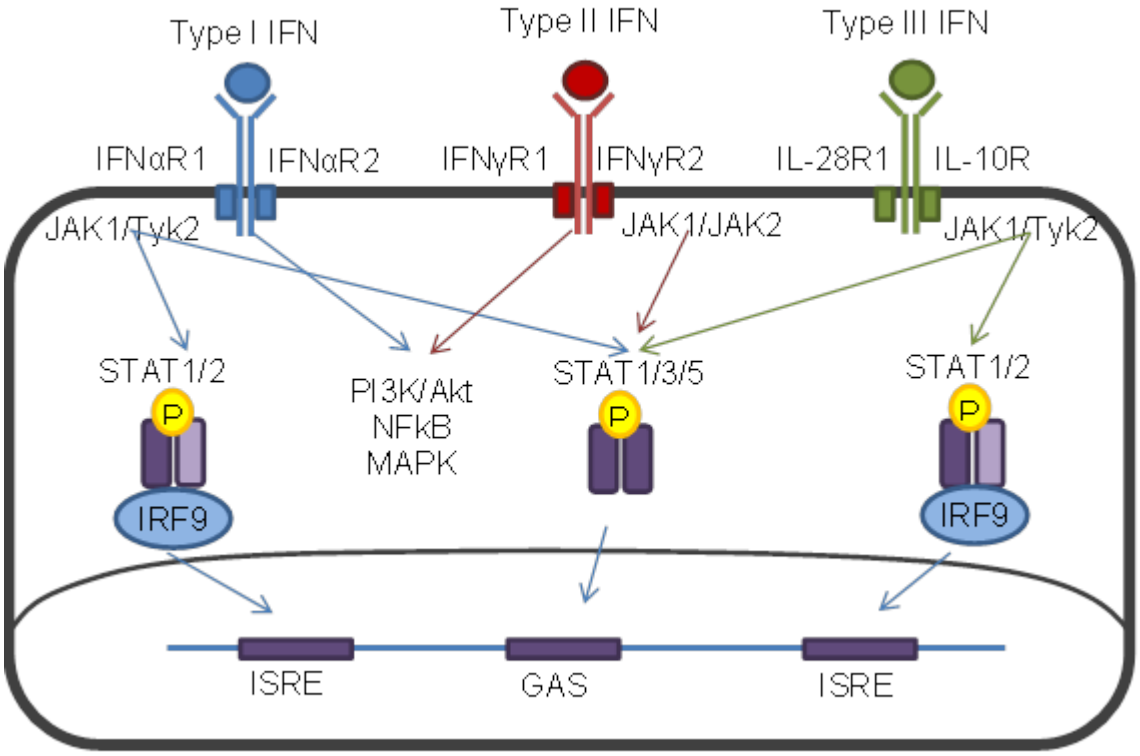

Figure 1.4 Types of IFN Signaling.
The IFNs bind to specific receptors which are heterodimers. The JAK family of kinases phosphorylates STAT proteins, which form a variety of transcription factor complexes. The STATs can homodimerize, heterodimerize and interact with other proteins which gives diversity to this signaling pathway. The activated complexes then enter the nucleus where they recognize specific promoter elements and transcribe the effector genes. The Type I and II IFNS can also activate other phosphorylation signaling cascades. [2,3]

response factors (IRFs) and actively secreted into the extracellular space where they signal in an autocrine and paracrine fashion, serving as a warning to adjacent epithelial and immune cells.[51-53] The type I IFN family includes IFNα, IFNβ and IFNω. These cell-to-cell messengers have been best characterized by their function in the immune system where they aid in defending host tissues from viral infection.[2,53,54] The type I IFNs can be produced by any nucleated cell in the body when the presence of viral DNA or RNA is detected.

The type II IFN family consists of only IFNγ, which facilitates the inflammatory response of the adaptive immune system. IFNγ is predominantly produced by T-cells when they are stimulated by specific antigens.[2] This cytokine then activates other members of the adaptive immune system and modulates the immunogenicity of epithelial cells. The type III IFN family, which includes IFNλ1 and IFNλ2/3 (aka IL-29 and IL-28A/B), also exhibits potent antiviral activity, but their impact on epithelial cells is still being characterized.[3,55,56] Both IFNα and IFNγ have been used successfully as therapy for both blood and solid cancers because of their potent inhibition of cell proliferation, stimulation of MHCI expression and induction of pro-apoptotic genes.[2,57]

IFN SIGNALING AND IFN STIMULATED GENES

The IFNs all bind to specific integral cell membrane receptors that facilitate intracellular signaling through a variety of pathways, including phosphorylation cascades and Janus kinase (JAK)/signal transducer and activator of transcription (STAT) signaling (Figure 1.4). The type I IFNs all bind to the type I IFN receptor (IFNAR) on the cell surface. IFNα and β utilize the JAK/STAT system, while IFN ω relies

on the phosphorylation cascade of the MAPK pathway.[2] IFNγ binds a specific receptor, IFNγR, which uses JAK/STAT signaling in addition to the NFκB pathway and the PI3K/Akt and MAPK phosphorylation cascades for signaling.[2] The Type III IFN receptor is a heterodimer comprised of one chain that it shares with the IL-10 receptor (IL-10R2) and also the IFN specific IL-28R1 chain. The type III IFNs rely predominantly on the JAK/STAT signaling pathway to mediate their antiviral functions.[3] The IFNs and their receptors all have JAK/STAT signaling in common but different STAT proteins are preferred by different members of the IFN family.

The signal transducer and activator of transcription (STAT) superfamily of proteins are latent transcription factors that are activated by the Janus kinase (JAK) family of phosphorylation proteins. Currently six STAT proteins have been identified and all enter the nucleus upon phosphorylation where they bind to specific elements in the promoters of their target genes. The STAT proteins can form homo- and heterodimers and also interact with other proteins to form a variety of transcription factor complexes, including the interferon response factor family (IRFs).[6] This variety provides differing specificity for certain promoter elements. For example, the type I and type III IFNs both stimulate the formation of the IFN-stimulated gene factor 3 (ISGF3) complex, which is comprised of STAT1, STAT2 and IRF9.[3,56] This results in the production of a similar array of interferon stimulated genes in both immune cells and epithelial cells. ISGF3 binds to interferon stimulated response elements (ISREs) in the promoters of ISGs.[58] IFNγ, however, stimulates the formation of STAT1 homodimers which recognize gamma associated sequences (GASs). Traditionally, the STATs must be phosphorylated in order to enter the nucleus and facilitate transcription but recent studies have found that

activity of the unphosphorylated STATs are capable of transcribing the ISGs.[6] This phenomenon is thought to contribute to radiation, chemotherapeutic and hormonal resistance in cancer.[54,59]

IFN stimulated genes (ISGs) mediate the effects of IFN signaling. There are thousands of ISGs and their specific roles in the antiviral response and modulation of cell fate are still being elucidated. Thus far the ISGs are known to prevent the fusion of viruses with the cell membrane, inhibit the translation of viral DNA, recognize viral RNA, bind and inhibit viral proteins, modulate the expression of cell cycle proteins and control the availability and activation of pro-apoptotic mitochondrial proteins.[60-63] Expression of these ISGs is critical for preventing and controlling infection by a wide variety of DNA and RNA viruses and also determining cell fate.[56,62,64-66] STAT1 and STAT2 themselves are considered ISGs and are overexpressed in breast cancer.[67-69] Interestingly, STAT1 knock out mice develop spontaneous ER positive mammary tumors, which highlights the critical role for STAT signaling in mammary development and the dual role that IFN/JAK/STAT signaling can play in cancer.[70,71] Through the actions of the ISGs, IFN signaling can promote the controlled death of an infected cell and at the same time the survival of adjacent cells in an epithelial cell layer. It is the duality of IFN signaling that allows the same system to mediate IFN anti-cancer therapy and simultaneously augment tumor progression.[6,54,59,72,73]

IFN STIMULATED GENES IN SOLID TUMORS

Due to their modulation of cell fate, the ISGs have the potential to impact the development and progression of tumors. Acute high doses of IFNs tend to be cytotoxic, and so are used as anti-tumor therapy [72,74], but chronic exposure to low amounts of IFN

stimulates the production of a unique subset of ISGs, which includes the Interferon Related DNA Damage Resistance Signature (IRDS), and these ISGs have been linked to cancer progression as well as chemotherapy, radiation and hormonal resistance (Table 1.1).[6,59,75,76] Additionally, expression of several ISGs (i.e. PLSCR1, IFITM1 and IFITM3) by various epithelial cancers promotes aggressive growth, invasion and tumor progression in both in vitro and in vivo models of colon, ovarian and breast cancer and in some clinical studies.[59,73,75,77-79] The mechanism(s) by which ISGs facilitate tumor progression has not been elucidated.

Adapted from: Chen et al. PNAS. 2009 Jun 9;106(23):9373-8

Table 1: ISGs Associated with Cancer Progression and Drug Resistance				
BST2	ISG15	IFI27	IFI35	IFI44
IFI44L	IFIT1	IFIT3	OAS1	OAS2
OAS3	OASL	STAT1	STAT2	MX1
PLSCR1	IFITM1	IFITM3	IRF7	IRF9

Table 1.1 Interferon Stimulated Genes (ISGs) associated with cancer progression and resistance to chemotherapy, radiation and hormonal therapy.[6]

While the exact role that ISGs play in breast cancer is not yet known, there is strong evidence that aberrations of IFN signaling do have an impact on breast tumorigenesis and progression. Enhanced JAK/STAT signaling is pro-survival, pro-proliferative and has been shown to confer resistance to chemotherapy and radiation in breast cancer specifically.[54,75,80] The suppressors of cytokine signaling (SOCS) family specifically inhibits the phosphorylation capabilities of the JAK family, thus shutting down canonical JAK/STAT signaling. Silencing and down-regulation of SOCS proteins has been seen in both breast and ovarian cancer, and re-expression of SOCS1 can reduce cell growth.[81,82] Conversely, higher expression of several SOCS family members confers a better prognosis for patients with breast cancer.[81,83,84] Additionally,

interferon response factor 1 (IRF1), which also modulates ISG expression, exhibits some control over breast cancer cell death and is required for the apoptotic actions of anti-estrogen therapy.[85-87] In addition to DNA-damage resistance, STAT1 and type 1 IFN signaling specifically have been linked to endocrine-resistance in breast cancer by several groups [59,68,73,88] and may actually define a separate molecular subtype of breast cancer termed "luminal-like." [89] The luminal-like subset has been characterized by high ISG expression, including IFITM1, IFIT1, ISG15, IFI27 and MX1, and downregulation of ERBB2 and lipid signaling. This results in poorer prognosis than luminal breast tumors but better prognosis than the basal-like subtype.[89]

The source of IFNs in the breast tumor microenvironment is still under investigation, but studies suggest that MAMs, dendritic cells, T-cells and the breast tumor cells themselves all are potential sources.[59,72,73,90] IFN production by the mammary epithelial cells could be induced through stress, viral infection, persistent DNA damage, loss of p53 function or acquired genetic alterations (Figure 1.5).[72,91] In breast cancer, the presence of stromal cells also seems to be crucial to ISG expression by the neoplastic epithelial cells. Stromal cell-induced ISG expression is dependent on STAT1 expression in the breast cancer cells and has been shown to induce radiation resistance in a mouse model.[92] Modification of IFN signaling influences the drug sensitivity and prognosis of breast cancer but the specific role of individual ISGs remains to be elucidated.

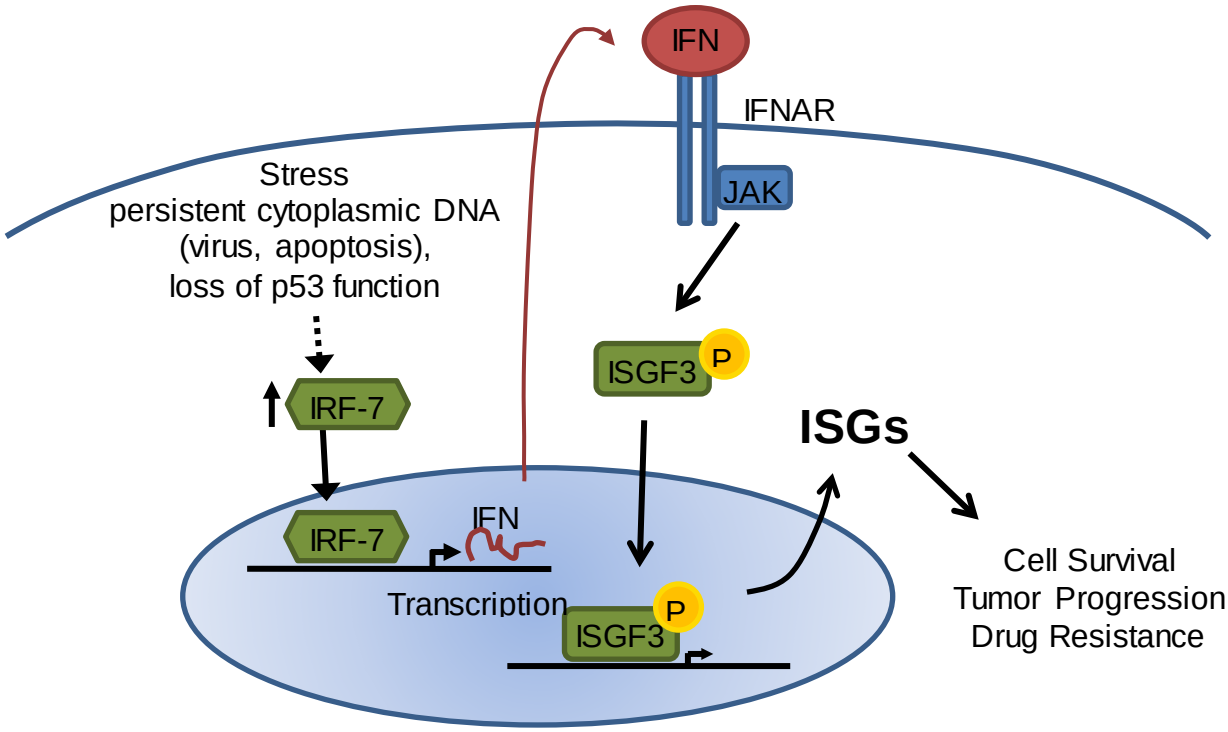

Figure 1.5 Proposed causes and results of endogenous IFN production by breast cancer

Stress response, persistent exposure to cytoplasmic DNA (DNA damaging chemicals, viruses) and loss of p53 function can all lead to endogenous type 1 IFN production through IRF7 induction. Chronic exposure to type 1 IFN leads to persistent JAK/STAT signaling and expression of ISGs that promote cell survival, resistance to therapy and tumor progression.

INTERFERON INDUCED TRANSMEMBRANE PROTEIN 1 (IFITM1)

Interferon-induced transmembrane protein 1 (IFITM1) is a member of the IFN-inducible transmembrane protein family whose expression is strongly induced by type 1 IFNs. [93] It was initially identified as a leukocyte antigen that is part of a membrane complex involved in the transduction of anti-proliferative and homotypic cell adhesion signals in lymphocytes.[94] The IFITM proteins family includes IFITM1, 2 , 3, 4, 5 and 10 which likely arose from an early gene duplication event in vertebrates. IFITM1, 2, 3 and 5 are present in humans and are clustered in a 26kb region at the end of the short arm of chromosome 11, while IFITM10 is located closer to centromere and has an unknown function and tissue distribution.[9,62] Interestingly, IFITM5 is expressed only in bone and is

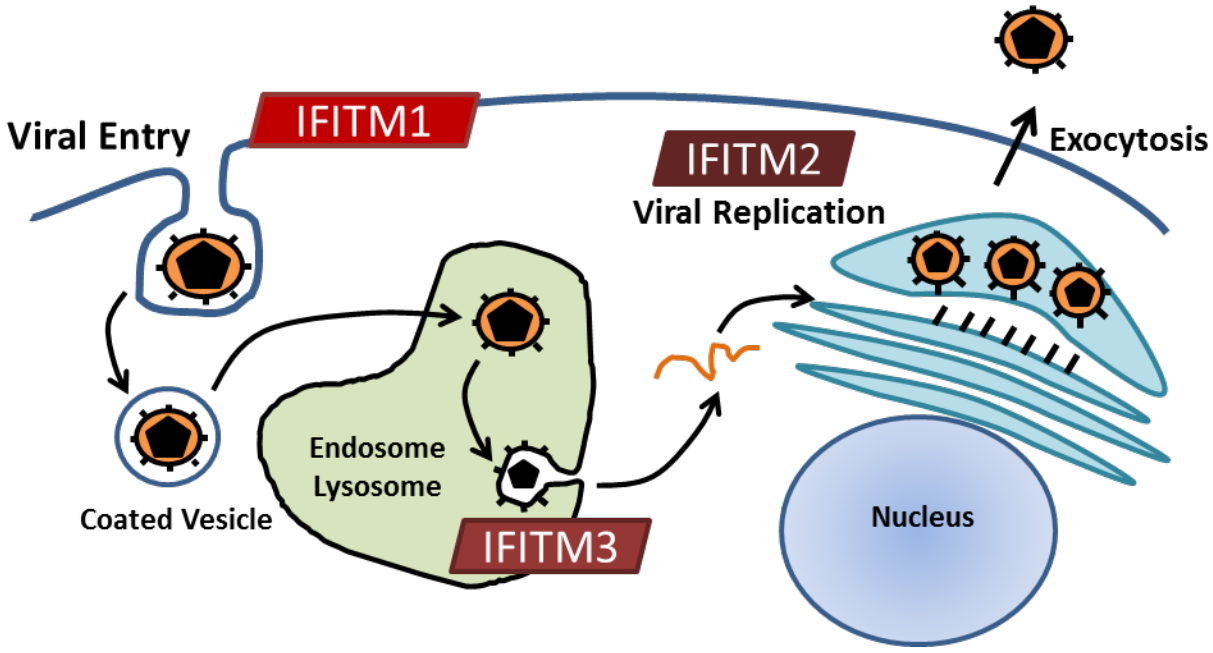

Adapted From: Smith et al. Current Opinion in Virology 2014, 4:71–77

Figure 1.6 IFITM proteins inhibit virus entry at different stages of cell trafficking.

Viruses enter cells by fusing with or penetrating a limiting cellular membrane. For most enveloped viruses fusion occurs either at the cell surface or, following uptake by endocytosis, from within endosomes. Trafficking through the endocytic system, from early to late endosomes, exposes virions to increasingly acidic environments. IFITM proteins (green) can inhibit entry, infection and replication by a number of viruses that fuse/penetrate at the cell surface or from within endosomes. IFITM1 is expressed primarily at the cell surface, while IFITM2 and 3 are primarily intracellular. IFITM3 has been localized to endosomal compartments, but the distribution of IFITM2 still needs to be clearly established.

not an ISG, instead playing an important role in bone mineralization. The remaining IFITM proteins, IFITM1, 2 and 3, are potent inhibitors of viral entry and replication, with predominant expression on cell membranes in the endocytic pathway (Figure 1.6). IFITM proteins have very similar amino acid sequence with two transmembrane domains linked by a highly conserved intracellular loop (CIL).[4,65] Several topologies have been proposed for IFITM protein conformation in cell membranes. The most

current theory is that only one transmembrane domain spans the membrane, leaving the N-terminal and CIL on the inner leaflet and the C-domain on the outer leaflet (Figure 1.7).[9,62] This arrangement is consistent with highly conserved and palmitoylated cysteine residues that are present where the CIL and transmembrane proteins meet.[1,9]

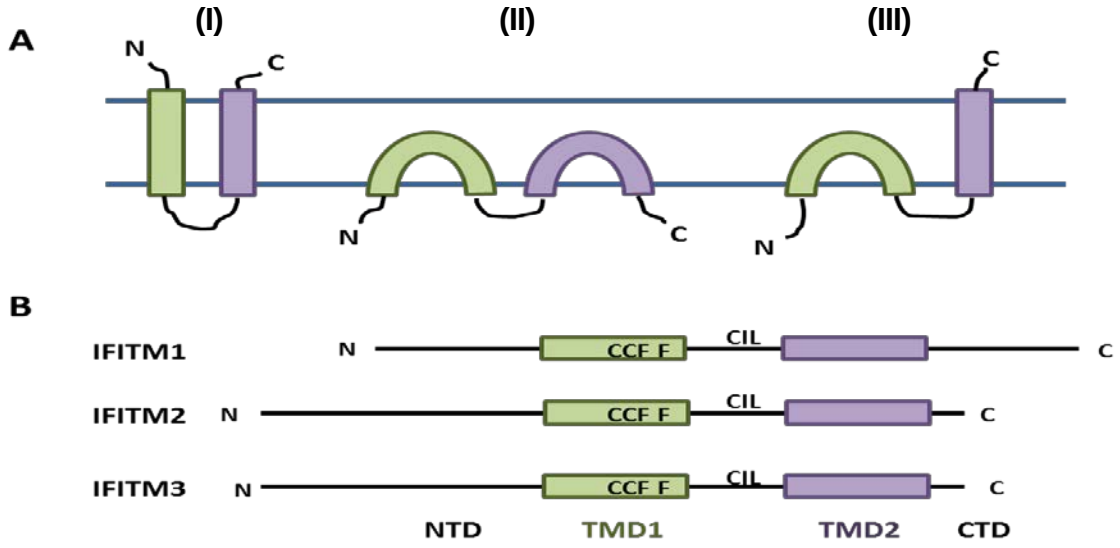

Smith et al. Current Opinion in Virology 2014, 4:71–77

Figure 1.7 IFITM protein topology and domain organization.

Panel **(a)** Topological models for IFITM proteins. (I) Represents an initial model for the proteins as transmembrane molecules with both the N-terminal and C-terminal domains (NTD and CTD) extracellular and the conserved intracellular loop (CIL) facing the cytoplasm.[1] Subsequently, an alternative model (II) was proposed with the NTD, CTD and CIL all positioned intracellularly, and neither transmembrane domain (TMD1 and TMD2, green and purple respectively) spanning the bilayer.[4] The most recent model (III) combines models I and II, positioning the NTD and CIL in the cytoplasm and the CTD extracellularly. Currently, the topology represented by III is only established for murine IFITM3.[9] **(b)** Linear representation of human IFITM1, 2 and 3 showing key amino acids. In all cases, modifications and functional activities have only been established with IFITM3, but conserved residues in IFITM1 and 2 are shown.

In addition to inhibiting viral entry and replication, ISGs are also known to modulate the decision between cell survival and death.[54,66,72,76] In fact, one study has found that the expression of ISGs increases in mouse models of endocrine resistant breast cancer.[88] IFITM1 specifically is thought to promote the survival of epithelial cells and to allow breast, prostate, lung and brain cancer cells to survive chemotherapy and

radiation.[54,69,76] While the exact structure and functional domains of IFITM1 remain under study (Figure 1.7), recently identified binding partners include caveolin-1 (CAV-1) and CD81/TAPA-1. CAV-1 is a cell surface protein that is necessary to form invaginations in the cell membrane which impacts intracellular vesicle transport, cell cycle control and apoptosis. [95-97] CD81 is a member of the tetraspan family and is known to control proliferation, adhesion, and migration through association with many cell signaling molecules and transmembrane receptors.[98-100] Both CAV-1 and CD81 have been linked to cancer progression and metastasis.[100-102]

Most recently there has been evidence to suggest that IFITM1 might also play a role in tumorigenesis. IFITM1 has been shown to be overexpressed in several types of cancers, including colorectal, gastrointestinal, head and neck, and breast, and its overexpression positively correlates with tumor progression and increased invasiveness.[103-107] Our laboratory has previously shown that the IFN signaling pathway was activated in AI-resistant breast cancer cells as compared to AI-sensitive cell lines.[46,108] Microarray analysis revealed that several ISGs, including IFITM1, were constitutively overexpressed in AI-resistant breast cancer cells.[46] We hypothesize that IFITM1 overexpression contributed to the AI-resistant phenotype and promoted breast cancer cell aggression and survival.

SUMMARY

Due to the high incidence and poor-prognosis of AI-resistant breast cancer, there is a critical need to better understand the mechanism by which this phenomenon occurs so that alternative treatment options can be developed. Our overall research goal is to determine how breast cancer cells gain the ability to survive without estrogen. Notably, ISG expression is related to estrogenic signaling and the success of anti-estrogenic treatments. This thesis will demonstrate how alterations in the expression of one ISG, IFITM1, affect the phenotype of ER+ breast cancer cells. In this study, we validate the importance of IFITM1 overexpression using an in silico approach to mine several large datasets and then an in house retrospective study using tissue microarrays. We use IFITM1-null AI-sensitive MCF-7 and constitutively IFITM1-overexpressing AI-resistant MCF-7:5C cells to investigate the mechanism of IFITM1 overexpression in ER+ breast cancer cells. Gain and loss of function studies in MCF-7 and MCF-7:5C cells demonstrate the functional importance of IFITM1 expression.

The information gained in this study has the potential to be exploited therapeutically due to both the discovery of novel drug targets and the addition of key ISGs to our developing profile of AI-resistant breast tumors. We hope that this profile can be used in the future to recognize which patients are good candidates for AI before initiating the treatment and to identify patients that have developed resistance long before a clinical recurrence of the tumor. We hypothesize that IFITM1 overexpression contributed to the AI-resistant phenotype and promoted breast cancer cell aggression and survival. We address this hypothesis in the following chapters:

Chapter 2: IFITM1 is overexpressed in breast cancer and is correlated with clinical outcome and response to therapy. In this chapter we analyze deposited tumor expression data to determine whether IFITM1 is expressed in breast cancer. We then use the Kaplan-Meier plotter and tissue microarrays to investigate the clinical significance of IFITM1 overexpression.[109]

Chapter 3: Functional significance of IFITM1 overexpression in AI-resistant breast cancer. Here, we use gain and loss of function studies to investigate the functional impact of IFITM1 on the ER+ breast cancer cell phenotype including response to estrogen deprivation. In this chapter we assess the importance of IFITM1 expression in vitro and in two in vivo models of breast cancer.

Chapter 4: Role of IFITM1 in controlling cell cycling and survival**.** We utilize inducible shRNA to knock down IFITM1 expression and determine the effect of IFITM1 loss on survival with particular attention given to the cyclin dependent kinase inhibitor p21.

Chapter 5: Regulation of IFITM1 by JAK/STAT signaling in AI-resistant breast cancer. In this chapter we examine the mechanisms of IFITM1 overexpression including JAK/STAT signaling and ER mediated mucin 1 expression. We then analyze the motifs in the IFITM1 promoter that STAT protein complexes use to drive IFITM1 transcription. Finally, we investigate the feasibility of targeting IFITM1 with the JAK1/2 inhibitor ruxolitinib *in vivo*.

Chapter 6: Conclusion. Summary of results, a discussion on how this research contributes to the field and suggestions for future directions of this work.

CHAPTER 2 : IFITM1 IS OVEREXPRESSED IN BREAST CANCER AND IS CORRELATED WITH CLINICAL OUTCOME AND RESPONSE TO THERAPY

This chapter is adapted from:

Choi HJ & Lui A, Ogony J**,** Jan R, Sims P, Lewis-Wambi J. *Targeting interferon response genes sensitizes aromatase inhibitor resistant breast cancer cells to estrogen-induced cell death.* Breast Cancer Res, 2015. 17(1): p. 6. PMCID:4336497.

Lui A, Ogony J, Geanes E, Behbod F, Valdez K, Marquess J, Jewell W, Tawfik O, Lewis-Wambi J. *IFITM1 suppression blocks proliferation and invasion of aromatase inhibitor-resistant breast cancer in vivo by JAK/STAT-mediated induction of p21*. Cancer Lett. 2017 Apr 12;399:29-43.

INTRODUCTION

Approximately 30% of estrogen receptor expressing (ER+) breast tumors are resistant to anti-hormonal treatment. [26] In addition, as many as 40% of women successfully treated with aromatase inhibitors (AIs) eventually develop resistance to this therapy over time. [30] The ensuing cancer cells are capable of long term estrogen-independent survival and proliferation. Many potential methods for maintaining estrogen-independent growth are available but the true mechanism(s) of aromatase inhibitor-resistance remains unclear. Previous studies have focused on alterations in estrogen receptor (ER) signaling, as well as non-estrogenic processes including those that regulate cell survival, the cell-cycle, and receptor tyrosine kinase activity. [29,30,110] Our lab has reported the development of an AI-resistant breast cancer model that exhibits constitutive overexpression of type-1 interferon (IFN) stimulated genes (ISGs).

The type-1 IFN cytokine family includes IFNα and β. They mediate danger signaling in the immune system by binding the type 1 IFN receptor (IFNAR) and stimulating JAK/STAT signaling through a phosphorylation cascade that promotes the expression of hundreds of ISGs. The ISGs protect from viral infection by preventing viral

entry and replication as well as promoting the survival of adjacent uninfected cells. [58] Despite the positive role of JAK/STAT signaling and the ISGs in the immune system, they have also been implicated in the pathogenesis of some cancers. While it has not been studied in breast cancer, the ISGs interferon transmembrane protein 1 (IFITM1) has been linked to the progression of several aggressive cancer types, including cancers of the cervix, esophagus, colon, ovary and brain.[77,95,101,105,106,111-113]

IFITM1 is a 17-kDa transmembrane protein coded on the short arm of chromosome 11.[62] It belongs specifically belongs to a group of ISGs that are produced in response to lower levels of type 1IFNs, and are thought to promote cancer progression and DNA damage resistance.[54,76,95,101,105,114,115] We began our study by determining whether IFITM1 was indeed expressed in breast cancer and whether it held any promise as a determinant of clinical outcome.

RESULTS

IFITM1 is overexpressed in breast cancer

To determine whether IFITM1 was expressed in breast cancer we used the Oncomine database to compare IFITM1 expression in invasive ductal carcinoma (IDC) and normal breast tissue in four deposited datasets (Figure 2.1). Analysis of 201 IDC and 24 normal breast samples revealed that IFITM1 is significantly overexpressed in IDC as compared to normal breast tissue. In the four analyzed datasets, IFITM1 had a median gene rank of 77 putting it in the top 1-5% of all genes altered in IDC. This result indicates that IFITM1 is indeed a gene significantly upregulated in breast cancer.

IFITM1 is overexpressed in AI-resistant breast cancer

We investigated the clinical significance of IFITM1 expression in AI-resistant (recurrence) breast cancer by performing IHC staining on normal breast tissue, primary breast tumors (N = 40) and AI-resistant recurrence breast tumors (N = 40). We found that IFITM1 proteins was overexpressed in 90% of the AI-resistant (recurrence) tumors (36 of 40 samples) compared with only 20% of the primary tumors (8 out of 40 samples); however, in normal breast tissue IFITM1 was undetectable (Figure 2.2). As shown in Table 2.1, stained slides were scored in terms of intensity and distribution. Normal breast tissue showed no staining for IFITM1 (SI score = 0); primary tumors showed medium staining for IFITM1 and PLSCR1 which correlated with low expression (SI score of ≤3); and AI-resistant (recurrence) tumors showed very strong staining for IFITM1 which correlated with high expression of both proteins (SI score of ≥6). Taken together, these results demonstrate that interferon regulated genes are constitutively

overexpressed in AI resistant breast cancer and they suggest that interferon signaling might be dysregulated in the resistant cells.

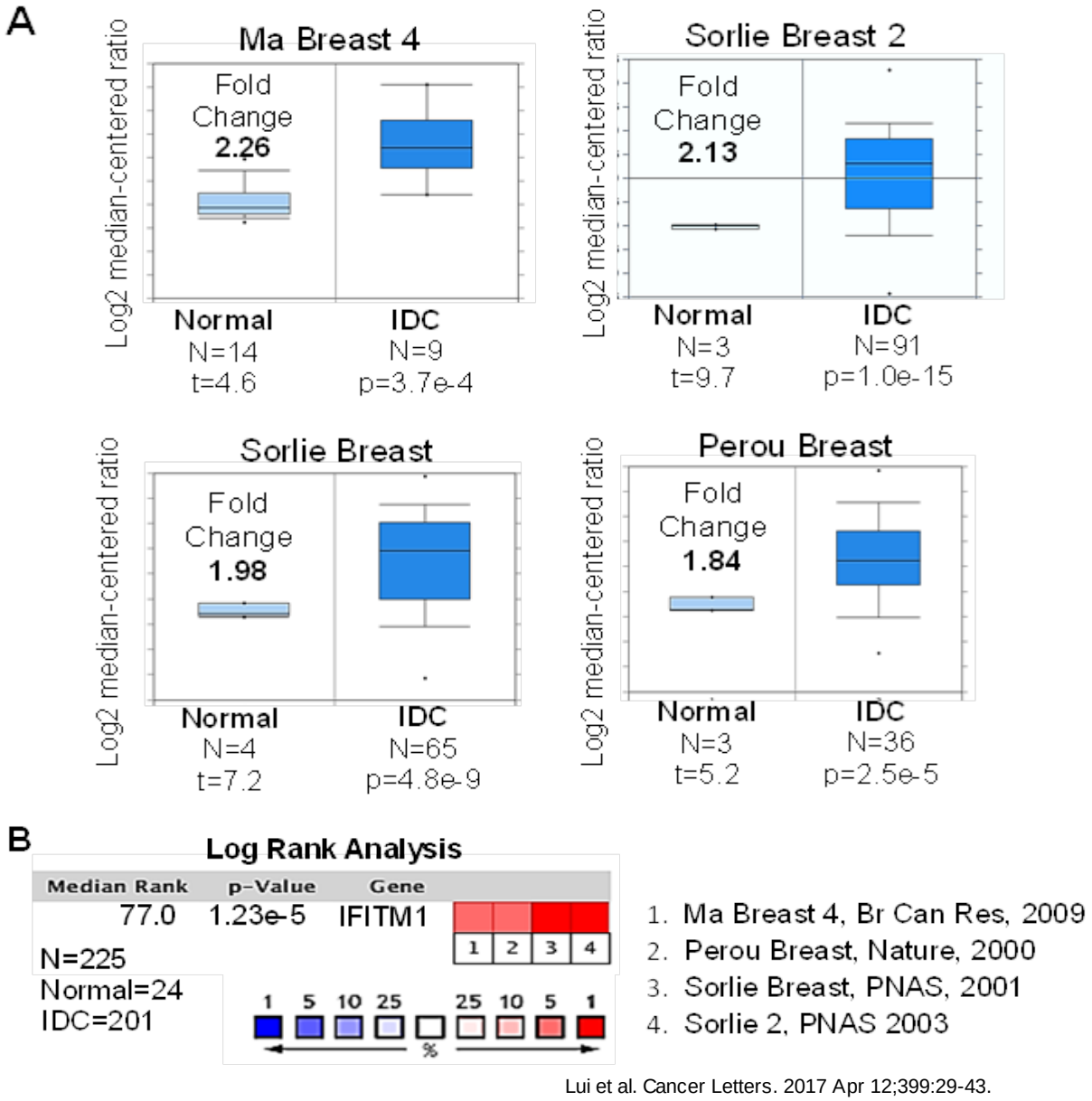

Lui et al. Cancer Letters. 2017 Apr 12;399:29-43.

Figure 2.1 IFITM1 is overexpressed in breast cancer.

(**A**) Relative expression of IFITM1 in normal and invasive ductal carcinoma (IDC) from four Oncomine breast cancer datasets is shown on a log2 scale allowing for comparison of fold change in expression. (**B**) Pooled analysis of relative IFITM1 expression in all four Oncomine datasets using a log rank analysis places IFITM1 in the top 3% of genes most upregulated in breast cancer as compared to normal breast tissue.

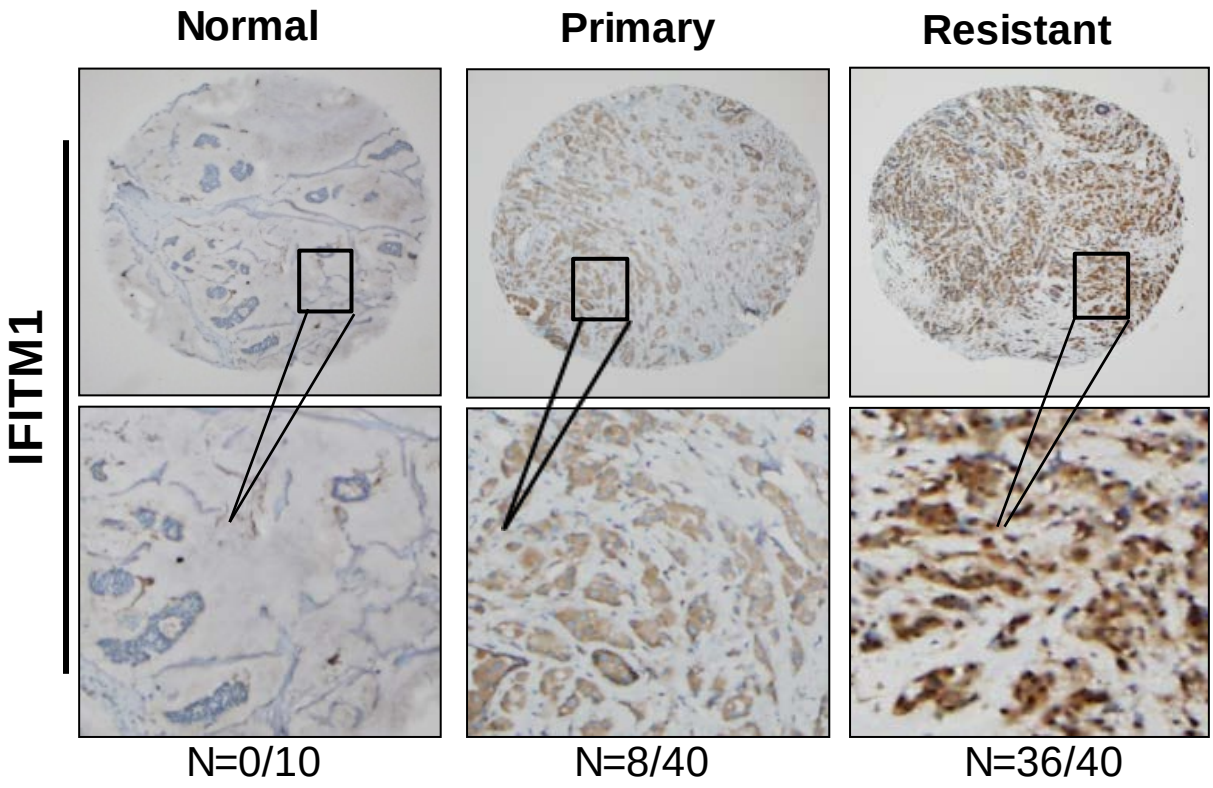

Choi & Lui et al. Breast Cancer Research. 2015 Jan 15;17:6

Figure 2.2 High IFITM1 expression is associated with AI-resistance.

Immunohistochemistry (IHC) staining for IFITM1 was performed on tissue microarrays generated from normal breast tissue (left panel), primary breast tumor tissue (middle panel) and recurrence breast tumor tissue (right panel). For immunohistochemical analysis, the scores were determined by combining the proportion of positively stained tumor cells and the intensity of staining, giving rise to a Staining Index (SI) value for each sample. The proportion of positively stained tumor cells was graded as follows: 0 (<5% positively stained tumor cells), 1 (5% to 25% positive tumor cells), 2 (25% to 50% positive tumor cells), 3 (50% to 75% positive tumor cells) and 4 (>75% positive tumor cells). Representative photomicrographs were taken using a phase-contrast microscope (original magnification, ×200).

Table 2.1 Staining intensity for IFITM1 expression in AI-resistant TMA

	Staining Intensity	IFITM1
Normal tissues	No stain	10/10
	Weak	0/10
	Strong	0/10
Primary tumors	No stain	32/40
	Weak	8/40
	Strong	0/40
Recurrence tumors	No stain	0/40
	Weak	4/40
	Strong	36/40

Choi & Lui et al. Breast Cancer Research. 2015 Jan 15;17:6

Table 2.2 Distribution of clinical and histologic parameters in ER+ invasive ductal carcinoma samples

		Frequency	Percent
Age	30-39	10	11%
	40-49	19	20%
	50-59	23	24%
	60-69	19	20%
	70-79	13	14%
	80+	10	11%
Race	European American	86	91%
	African American	5	5%
	Asian/Pacific Islander	3	3%
Stage	1	20	21%
	2	22	23%
	3	10	11%
	4	5	5%
Her2/Neu	0+	38	40.43%
	1+	15	15.96%
	2+	4	4.26%
	Total	**94**	

Lui et al. Cancer Letters. 2017 Apr 12;399:29-43

Table 2.3 IFITM1 staining intensity in normal and cancerous breast tissues

Tissue Type	Intensity	Frequency	Percent
Normal Breast	**0**	6	100%
	1+	0	0%
	2+	0	0%
	3+	0	0%
	Total	**6**	
Breast Tumors	**0**	7	7%
	1+	24	26%
	2+	48	51%
	3+	22	23%
	Total	**94**	

Lui et al. Cancer Letters. 2017 Apr 12;399:29-43

High IFITM1 expression is correlated with poor clinical outcome

Since 20% of our primary breast tumors expressed IFITM1, we next investigated whether high IFITM1 expression at the time of diagnosis was correlated with clinical outcome in ER+ breast cancer. We examined the overall survival for patients with grade 1 ER+ breast cancer using the Kaplan-Meier Plotter breast cancer survival database and found that high IFITM1 expression correlated with poor overall survival (Figure 2.4A).[109] We next conducted in-house analysis of IFITM1 expression in 94 ER+ breast cancer patient samples using immunohistochemistry. The patients included in this study represented typical patient demographics with an average age of 58.3years. The patients were 91% European American, had mostly stage 1 and 2 disease and were predominately Her2/neu negative (Table 2.2). The 94 samples represented the full range of IFITM1 expression (0-3) (Figure 2.3) and all of the normal breast tissue samples were negative for IFITM1 expression (Table 2.3). High IFITM1 intensity score was correlated with decreased survival but also increased clinical stage and risk of recurrence during endocrine therapy (Figure 2.4). These two separate analyses suggest that high IFITM1 expression in ER+ breast cancer is significantly associated with poor clinical outcome and poor response to endocrine therapy.

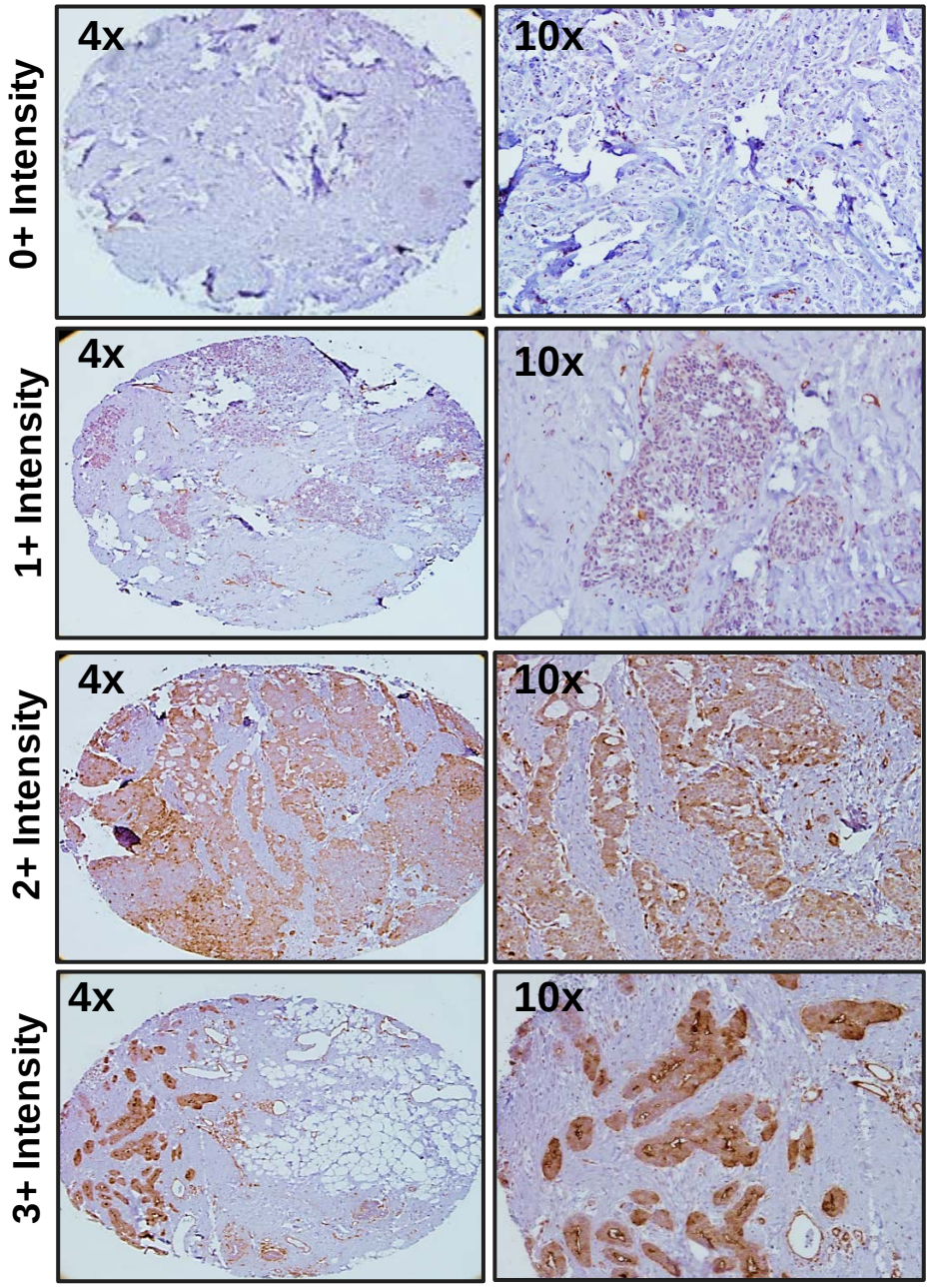

Lui et al. Cancer Letters. 2017 Apr 12;399:29-43

Figure 2.3 staining intensities for ER+ breast cancer

Immunohistochemical staining for IFITM1 expression was conducted in 94 ER+ breast cancer patient samples and 6 normal breast tissue samples. Staining intensity was graded on a scale of 0-3 with representative images of each staining intensity shown.

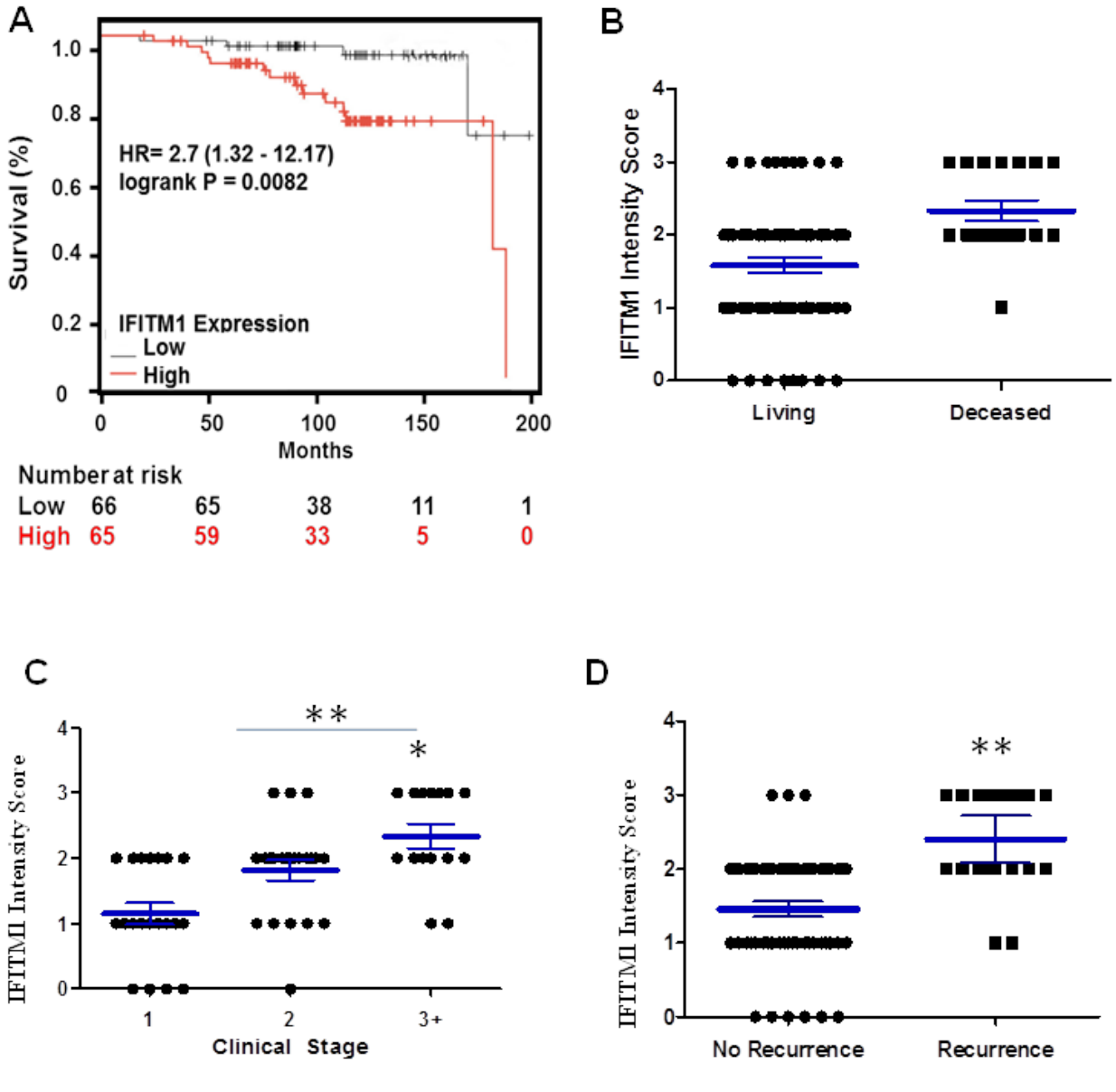

Lui et al. Cancer Letters. 2017 Apr 12;399:29-43

Figure 2.4 IFITM1 overexpression is correlated with poor clinical outcome.

(A) The hazard ratio (HR) and 95 % confidence interval for high IFITM1 expression in ER+ Luminal A breast cancer patients was analyzed using The Kaplan-Meier Plotter database. P-value was determined by log-rank test. Immunohistochemical staining for IFITM1 expression was conducted in 94 ER+ breast cancer patient samples and 6 normal breast tissue samples. Staining intensity was graded on a scale of 0-3. IFITM1 staining intensity was correlated with patient survival (**B**) clinical stage (**C**) and recurrence (**D**). *p < 0.05, ** p< 0.01

DISCUSSION

We had previously reported high IFITM1 expression in AI-resistant breast cancer cell lines. Here, we found that this observation was clinically relevant using *in silico* analysis of deposited patient gene expression data. Notably, we found that there is no IFITM1 expression in normal breast tissue. It is thought that IFITM1 can drive the progression of several types of cancer but it had not been previously investigated in the breast. The IFN signaling pathway may be one of the strategies used by cancer to overcome normal restrictions on proliferation and survival. The fact that IFITM1 is actually expressed in breast cancer allowed us to next assess whether IFITM1 expression had any clinical significance. Stratification of the oncomine datasets by Luminal A and Luminal B breast cancer would provide an interesting comparison of IFITM1 expression in different subsets of ER+ breast cancer and would strengthen this study.

In our tissue microarrays revealed that AI-resistant tumors express significantly higher levels of IFITM1 than even the original tumor prior to AI therapy. This data suggests that estrogen starvation may drive IFITM1 expression. Cross-talk between the type1 IFN-signaling pathway and ER has been speculated due to the critical role of IRF1 in modulating the effects of anti-estrogen therapy. [85,86] Thus far a positive regulatory feedback loop between the IFNs and ERα has been discovered, which opens the possibility that the IFNs can promote breast cancer progression by enhancing estrogen signaling. [116] Conversely, 17b-estradiol has been shown to induce IFNα production by macrophages, closing the feedback loop between the mammary gland macrophages in the tumor microenvironment.[117] It is probable that the interaction

between ER and IFN signaling has implications for breast cancer development and prognosis. Recently, the expression of several cytokine receptors, including IFNAR2 has been associated with breast cancer risk in patients [118] and the expression of a type I IFN gene signature by mammary epithelial cells has been shown to vary by hormonal status in two strains of mice, with the strongest ISG expression occurring during diestrous when estrogen levels are the highest.[119] Additionally, the estrogen-responsive gene mucin1 (MUC1) is frequently upregulated in breast cancer due its ability to prevent apoptosis and is also a known stabilizer of STAT1 phosphorylation in breast cancer cells. [67,120,121] Further study into the collaboration between estrogen and IFN signaling is likely to yield new targets for prevention and therapy.

Since we found that IFITM1 overexpression could be found in some primary tumors, we also investigated whether IFITM1 expression could predict clinical outcome or response to endocrine therapy. In a retrospective clinical trial of ER+ breast tumors we found that high IFITM1 expression was associated with not only overall survival but also clinical stage and risk of recurrence during endocrine therapy. These results support the idea that IFITM1 expression could be used to screen ER+ breast cancer patients for responsiveness to endocrine therapy and may define a resistant subset. In this study ER, PR and Her2 scoring was conducted by the Department of Pathology and Laboratory Medicine at the time of patient diagnosis. We did not independently confirm ER expression in our tumors, which would strengthen our study. Additionally, assessment of the percentage of proliferation with Ki67 staining would allow us to determine whether IFITM1 expression correlates with other markers of aggressive breast cancer currently used in the clinic. In future, including other ISGs that are also

overexpressed in AI-resistant breast cancer to generate a panel of genes that can define this resistant subset would likely be more clinically useful and could better predict response to treatment than IFITM1 expression alone.

MATERIALS AND METHODS

AI-resistant TMA

Paraffin-embedded de-identified human breast cancer tissue samples were collected from the Tumor Bank facility at The Research Institute of Fox Chase Cancer Center (Philadelphia, PA, USA) and the University of Kansas Medical Center (KUMC) and the protocols were reviewed and approved by the Institutional Review Board at Fox Chase Cancer Center and KUMC. The archived tumor samples were collected from patients (N = 40) who were initially treated with Arimidex and either responded or responded but then developed recurrence disease with an average time to disease progression (TTP) of 93 months. Patients provided written informed consent for the use of their tumor samples. Tissue microarray (TMA) slides were constructed from 40 matching primary and AI-resistant tumors using duplicate cores of 0.6 mm per tumor sample. Normal mammary tissue samples (N = 10) were also included on the TMA. For immunohistochemistry assays, tissue microarray slides were incubated at room temperature for 20 minutes with antibodies against IFITM1 (Santa Cruz Biotechnology) and PLSCR1 (Chemicon Inc.) applied at 1:100 dilution in antibody diluent (Dako, Carpenteria, CA, USA). A secondary anti-mouse antibody polymer conjugated with HRP (Dako) was applied for 30 minutes and 3,3-diaminobenzidine(DAB) was used to produce visible, localized staining viewable with light microscopy. Sections without primary antibody served as negative controls. A semi-automated quantitative image analysis system, ACIS II (ChromaVision Medical Systems, Inc., San Juan Capistrano, CA, USA), was used to quantitate the staining of the TMA slides. For immunohistochemical analysis, the scores were determined by combining the proportion of positively stained tumor cells and the intensity of staining, giving rise to a

Staining Index (SI) value for each sample. The proportion of positively stained tumor cells was graded as follows: 0 (<5% positively stained tumor cells), 1 (5% to 25% positive tumor cells), 2 (25% to 50% positive tumor cells), 3 (50% to 75% positive tumor cells) and 4 (>75% positive tumor cells). The intensity of staining was recorded on a scale of 0 (no staining), 1 (weak staining, light brown), 2 (moderate staining, yellowish brown) and 3 (strong staining, brown). The SI value was calculated as follows: SI = staining intensity × proportion of positively stained tumor cells. Scores were evaluated comparatively for the expression of IFITM1 and PLSCR1 in breast tumors by SIs (scored as 0, 1, 2, 3, 4, 6 or 9). An optimal cutoff value was identified, and the SI score of ≥6 was used to define tumors with high expression and SI ≤3 as tumors with low expression of IFITM1 and PLSCR1.

Survival analysis

Survival data were obtained from the Kaplan-Meier Plotter 2014 breast cancer survival database (http://kmplot.com/analysis/index.php?p=service&cancer=breast).[109] The 131 patients with grade 1 ER+ disease as determined by gene expression data were included in the analysis. Patients were stratified by IFITM1 expression (probe set 214022_s_at) relative to median. The P-value was calculated using a log-rank test.

ER+ Tissue Microarray and IHC data analysis

This retrospective study was approved by the Institutional Review Committee at the University of Kansas Medical Center (KUMC). A total of 94 primary ER+ invasive ductal carcinomas diagnosed and removed surgically between 2001 and 2010, and for whom follow-up information was available, were examined. Samples were taken from 6 normal breast tissue samples from routine reduction mammoplasties were also examined.

These tissues were formalin-fixed and paraffin-embedded (FFPE). Clinicopathological data including age, race, clinical stage and Her2 staining are shown in Table 1. At diagnosis, tissue blocks containing the most representative and well-preserved tumor areas were selected for IHC. IHC analysis was performed on tissue fixed with 10% neutral buffered formalin. IHC analyses for ER was performed at the time of diagnosis on all specimens in the Department of Pathology and Laboratory Medicine at KUMC. Samples with greater than 1% of the tumors staining for ER were considered positive and qualified the sample to be included in the tissue microarray. After review of the hematoxylin and eosin slides and marking of tumor areas, 2-mm tissue cores of representative tumor areas were extracted and inserted in recipient blocks. IHC analysis for IFITM1 (Santa Cruz) was performed on tissue microarrays obtained from the same samples (see IHC Staining protocol below). Two cores from each tumor were analyzed in an attempt to account for the impact of tumor heterogeneity on IFITM1 expression. IFITM1 staining intensity was quantified manually on a scale of 0-3 where 0 means no staining, 1+ is faint staining, 2+ is moderate staining and 3+ is strong staining. Cores were scored by three independent individuals prior to accessing patient medical records. Final distribution of IFITM1 expression is shown in Table 2. Histopathologic parameters were extracted from patient pathology records and clinical parameters were obtained from electronic medical records.

IHC staining was performed after tissue deparaffinization by clearance in xylene and hydration through graded ethanol series. Antigen retrieval was conducted at 99˚C in Dako Target retrieval solution (S1700) for 20 min per manufacturer's instructions (Agilent Technologies, Copenhagen, Denmark). For human samples, blocking was

performed using 5% normal horse serum and antibody dilution was performed in 0.01% Triton-X. For mouse xenografts, blocking and antibody dilution were performed using the Mouse on Mouse (MOM™) Kit following manufacturer's instructions (Vector Labs, Burlingame, CA). Sections were stained using primary human antibodies targeted against lFITM1, ERα, phospo-STAT1 (ser701), CD31, MMP1 (Santa Cruz) and Ki67 (Dako) and HRP-conjugated biotinylated secondary antibodies (Vector Labs). Immunoperoxidase signal was produced using 3,3'-Diaminobenzidine (DAB) and amplified using the Vectastain® Elite ABC Kit (Vector Laboratories). Tissue sections were counter stained using hematoxylin and mounted in xylene. Slides were imaged on a Nikon Eclipse 80i Upright Microscope in the Imaging Core of KUMC.

CHAPTER 3 : FUNCTIONAL SIGNIFICANCE OF IFITM1 OVEREXPRESSION IN AI-RESISTANT BREAST CANCER

This chapter is adapted from:

Choi HJ & **Lui A**, Ogony J**,** Jan R, Sims P, Lewis-Wambi J. *Targeting interferon response genes sensitizes aromatase inhibitor resistant breast cancer cells to estrogen-induced cell death.* Breast Cancer Res, 2015. **17**(1): p. 6. PMCID:4336497.

Lui A, Ogony J, Geanes E, Behbod F, Valdez K, Marquess J, Jewell W, Tawfik O, Lewis-Wambi J. *IFITM1 suppression blocks proliferation and invasion of aromatase inhibitor-resistant breast cancer in vivo by JAK/STAT-mediated induction of p21*. Cancer Lett. 2017 Apr 12;399:29-43.

INTRODUCTION

To investigate the role of altered ISG expression in AI-resistance, we will use our previously described model of endocrine-resistant breast cancer.[42] Briefly, MCF-7 cells, which require estrogen for proliferation and survival, were starved long-term through the depletion of estrogen from their serum and utilization of phenol-free media. After many rounds of selection for an estrogen-independent phenotype, the clone MCF-7: 5C was established.[122] The MCF-7:5C cell line maintains fully functional wild type ER and grows robustly without estrogen; however MCF-7:5C cells proliferate more quickly and are more invasive than MCF-7 cells *in vitro* and *in vivo*.[108] A unique feature of the MCF-7:5C cells is their constitutive overexpression of a panel of genes associated with inflammation and inflammatory signaling. Here we use the AI-resistant MCF-7:5C and AI-sensitive MCF-7 cell line to investigate the role of IFITM1 in AI-resistance.

In vivo mouse models are the most common tool used for investigating the clinical relevance of breast cancer studies. Traditionally, the orthotopic model is used to evaluate tumor growth. The breast cancer cells are injected directly into the mammary fat pad and allowed to grow over time, allowing for assessment of proliferation, cell

death, and/or metastasis. Breast cancer, however, originates inside the mammary duct where the cells must invade out of the duct prior to establishing a solid tumor. The mouse mammary intraductal (MIND) model has been developed to study breast cancer cell invasion *in vivo*.[123,124] In this model, breast cancer cells are injected into the mammary duct through the nipple, where they populate the duct and can invade into the surrounding mammary gland. The MIND model provides a tumor microenvironment that permits the *in vivo* study of previously difficult to grow ER+ breast cancer cell lines and faithfully mirrors the behavior of primary breast cancer cells in patients with regard to aggression and response to therapy.[125] The orthotopic model tests the proliferation and survival of tumor cells *in vivo*, modeling an established tumor of several million cells. In comparison, the MIND model more faithfully replicates the early stages of breast cancer development, where a small number of abnormal cells begin to proliferate inside of the duct and eventually gain the ability to bypass the basement membrane and invade into the mammary gland. The MIND model allows for analysis of proliferation and survival but also the investigation of breast cancer invasion and the early stages of the metastatic cascade. In this chapter we establish clones of the MCF-7 and MCF-7:5C cell line with altered IFITM1 expression and use both the orthotpic and MIND models to investigate the impact of IFITM1 expression on breast cancer proliferation and invasion *in vivo*.

RESULTS

IFITM1 is constitutively overexpressed in AI-resistant human breast cancer cells

Microarray studies previously revealed that the interferon signaling pathway was altered in AI-resistant breast cancer cells compared with AI-sensitive cells.[46] To validate our microarray data we measured the basal expression of two well-known interferon stimulated proteins, IFITM1 and PLSCR1, in AI-resistant MCF-7:5C breast cancer cells and AI-sensitive MCF-7 cells. Our data showed that IFITM1 was constitutively overexpressed at the protein (Figure 3.1A) and mRNA level (Figure 3.1B) in AI-resistant MCF-7:5C cells but were almost undetectable at the protein and mRNA level in AI-sensitive MCF-7 cells. Notably, we also found that several other ISGs including PLSCR1, IFI27, IFIT1, OAS1, MX1, STAT1 and STAT2 were constitutively overexpressed in AI-resistant MCF-7:5C cells compared with MCF-7 cells (Figure 3.1C).

Loss of IFITM1 induces the death of aromatase inhibitor-resistant breast cancer cells.

To assess the functional significance of IFITM1 overexpression in AI-resistant MCF-7:5C breast cancer cells, we used three siRNAs (siIFITM1A, siIFITM1B, siIFITM1C) to silence its expression (Figure 3.2A). We found that all three siRNAs completely reduced IFITM1 expression in MCF-7:5C cells and that loss of IFITM1 resulted in cell death which was quantified using AnnexinV/PI staining and TUNEL staining (Figure 3.2B and Figure 3.2C). To further investigate the effects of IFITM1 loss on proliferation and death in AI-resistant cells, we developed the MCF-7:5C/shIF cell line which expresses IFITM1 shRNA under the control of a tetracycline/doxycycline-inducible promoter. Our lentivirus-inducible system showed that upon doxycycline (Dox) exposure, IFITM1 expression was reduced in MCF-7:5C/shIF cells in a concentration-

dependent manner, with maximum reduction at 1 µg/mL Dox (Figure 3.2D). Consistent with our siRNA *in vitro* data, loss of IFITM1 using Dox-inducible shRNA initiated cell death over time, with maximal response after 96 hours, as demonstrated by PARP cleavage (Figure 3.2D) and annexin-PI staining (Figure 3.2E). Notably, Dox treatment had no effect on the survival of un-transduced MCF-7:5C cells or MCF-7:5C cells expressing a scrambled control vector (MCF-7:5C/shCon) (Figure 3.2F). These data demonstrate that IFITM1 overexpression enhances the growth of AI-resistant MCF-7:5C cells and that silencing IFITM1 expression using siRNAs/shRNAs inhibits proliferation and induces death in these cells.

Loss of IFITM1 inhibits AI-resistant breast tumor growth and promotes cell death in vivo.

Generation of the MCF-7:5C/shCon and MCF-7:5C/shIF cells allowed us to assess the effect of IFITM1 loss on the growth of MCF-7:5C cells *in vivo*. MCF-7:5C/shCon and MCF-7:5C/shIF cells were implanted into the 4th mammary fat pad of ovariectomized NOD scid gamma (NSG) mice. After 10 days, mice were randomized to Dox (+ Dox) or vehicle (- Dox) treatment for 22 days. We found that Dox exposure significantly reduced MCF-7:5C/shIF tumor growth compared to the –Dox group (vehicle control) (Figure 3.3A and Figure 3.3B) and that the reduction in tumor growth positively correlated with a loss of IFITM1 expression and a decrease in the proliferation marker Ki67 (Figure 3.3C). TUNEL staining of MCF-7:5C/shIF tumors confirmed that the reduction in tumor growth in the Dox-treated group was due to cell death/apoptosis (Figure 3.3C) Notably, Dox exposure had no effect on the growth of MCF-7:5C/shCon cell tumors (Supplemental Figure 3.1A) or on the expression of IFITM1, Ki67 or TUNEL

(Supplemental Figure 3.1B). This data confirm that IFITM1 overexpression is important for the growth and survival of AI-resistant MCF-7:5C tumors *in vivo*.

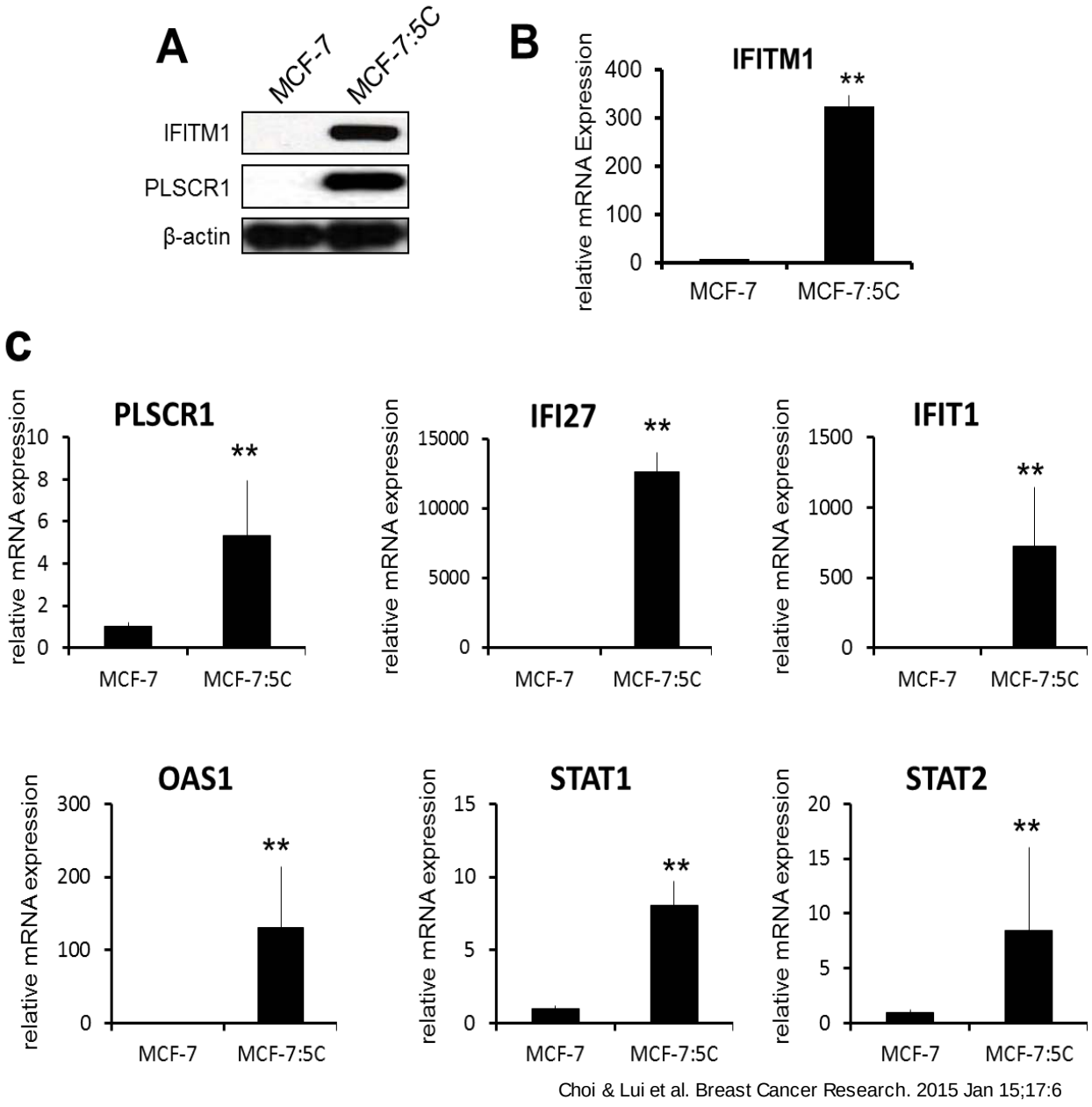

Figure 3.1 ISGs are overexpressed AI-resistant MCF-7:5C cells

(**A**) Whole cell lysate from MCF-7 and MCF-7:5C cells was immunoblotted for IFITM1, PLSCR1 protein expression. Total RNA was extracted from MCF-7 and MCF-7:5C cells and mRNA expression for (**B**) IFITM1 and PLSCR1, IFIT27, IFIT1, OAS1, STAT2 and STAT2 (**C**) was determined by real-time PCR. Fold change is reported relative to MCF-7 expression.

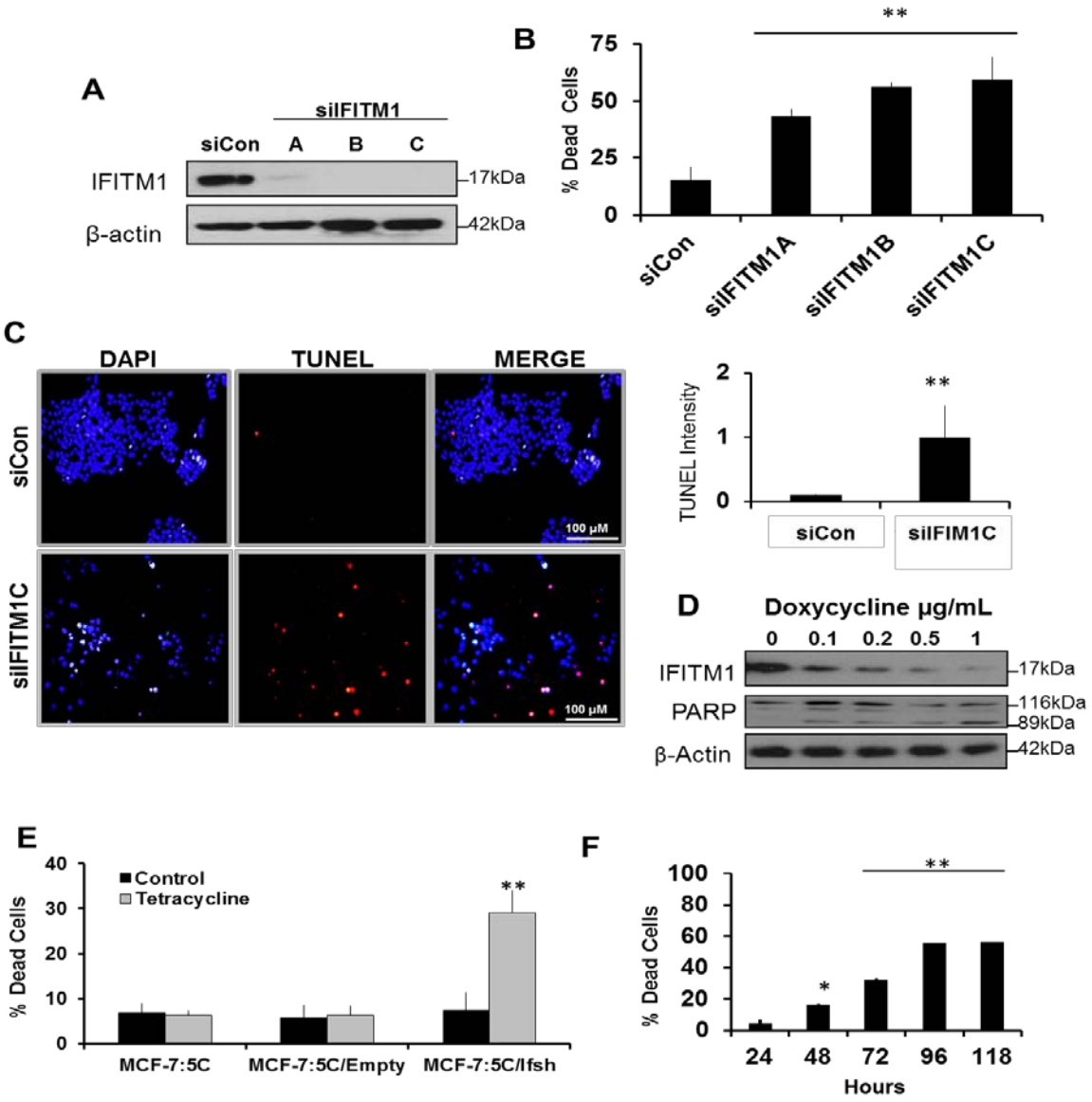

Lui et al. Cancer Letters. 2017 Apr 12;399:29-43

Figure 3.2 Loss of IFITM1 induced death in AI-resistant MCF-7:5C cells.

(**a**) Cell lysates from MCF-7:5C cells transfected with scrambles control siRNA (siCon) or three different IFITM1 siRNA sequences (siIFITM1 A, B, C) were immunoblotted for IFITM1 expression. (**b**) Dual annexin/PI staining was used to quantify cell death in each transfection group. Data represent means ± SD from two experiments conducted in duplicate. (**c**) MCF-7:5C cells were transiently transfected with siCon or siIFITM1C. The intensity of TUNEL (red) staining was used to assess the effect of IFITM1 knockdown on cell survival and was quantified using five separate images with Image J Software (*right panel*). (**d**) MCF-7:5C/shIF cells were treated with the indicated concentrations of doxycycline to induce IFITM1 shRNA expression. IFITM1 and PARP protein expression levels were determined by immunoblotting. (e) MCF-7:5C/shIF cells were treated with 10μg/mL doxycycline over a 118 hour period. Annexin V/ Propidium Iodide staining quantified the percent of dead cells over the accompanying untreated (control) sample. (**f**)MCF-7:5C, MCF-7:5CshCon and MCF-7:5C/shIF cells were treated with 1ug/mL Dox and the percent dead cells determined by Annexin V/PI staining. Data represents two independent experiments conducted in duplicate. * $p<0.05$ ** $p< 0.01$

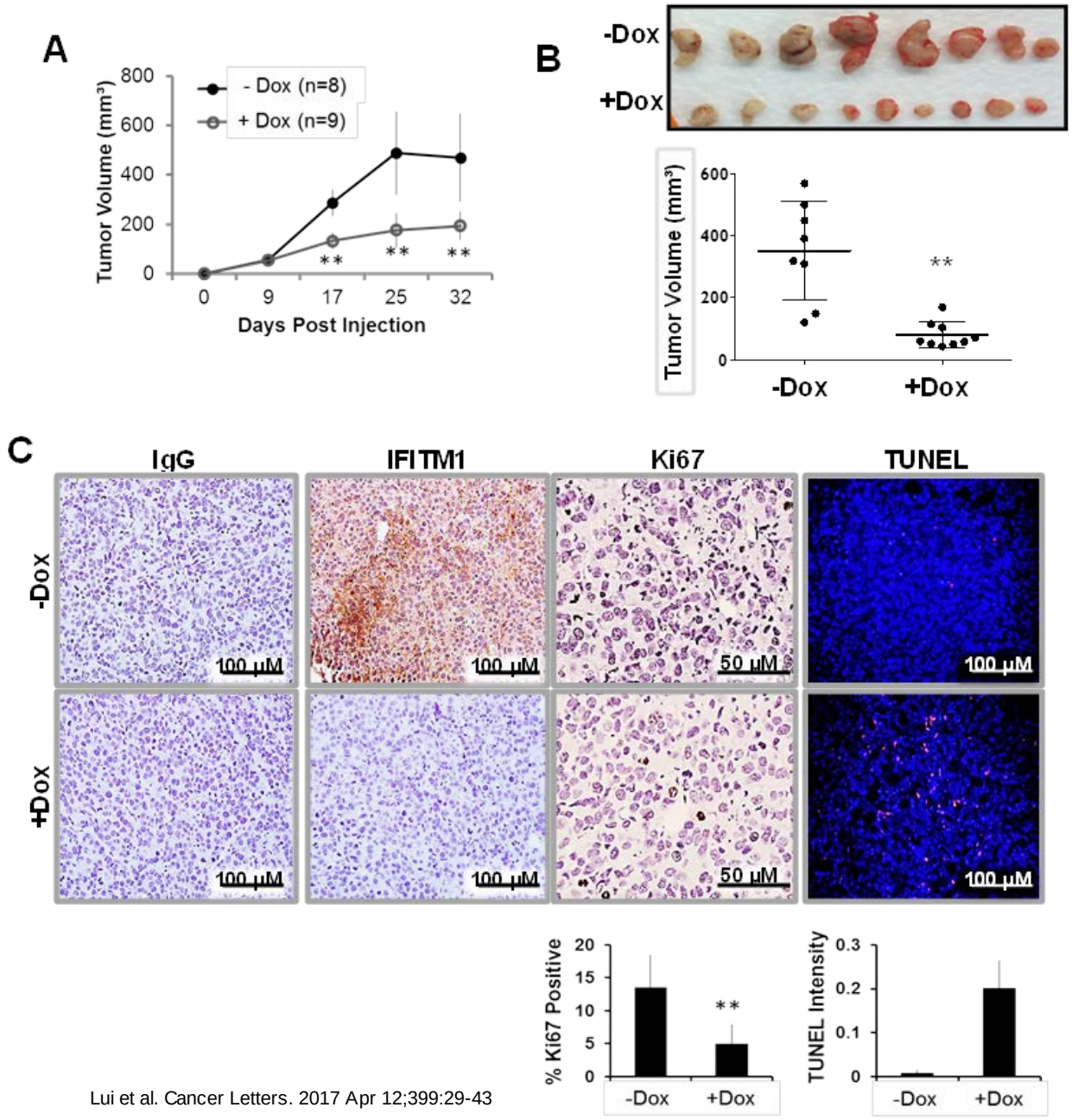

Lui et al. Cancer Letters. 2017 Apr 12;399:29-43

Figure 3.3 Loss of IFITM1 inhibited MCF-7:5C tumor growth and promoted cell death *in vivo*.

(a) 3 million MCF-7:5C/shIF cells were injected into the 4th mammary fat pad of ovariectomized female NSG mice. 9 days after orthotopic injection, mice were randomized to treatment groups and half were provided doxycycline (Dox)-treated drinking water. Tumors were measured by digital calipers and tumor volume (mm3) displayed over time. (b) At the end of the experiment tumors were excised and are shown. Tumor volumes were determined by digital caliper measurement. (c) IFITM1 and Ki67 expression was determined by immunohistochemical staining. The percent of Ki67 positive cells was determined by counting four separate 40X fields. Cell death was analyzed by TUNEL staining and quantified by Image J software. ** $p < 0.01$

Loss of IFITM1 blocks aromatase inhibitor-resistant tumor cell invasion out of the mammary duct.

Since our previous studies indicated that loss of IFITM1 inhibited cell invasion *in vitro*, we used the mammary intraductal (MIND) model of breast cancer to investigate the effect of reduced IFITM1 expression on AI-resistant tumor cell invasion *in vivo* (Figure 3.4) [59,73]. After three weeks of Dox exposure, we confirmed that the MIND model was able to accurately assess tumor cell invasion out of the mammary duct using immunofluorescent staining (Figure 3.5A). Immunofluorescent staining verified that Dox exposure resulted in IFITM1 loss in the MIND model (Figure 3.5A). Smooth muscle actin (SMA) was used to stain the myoepithelial layer of the mammary duct and human keratin 19 (K19) was used to label the breast cancer cells (Figure 3.5A). Hematoxylin and eosin (H&E) staining further revealed the architecture of the mammary glands, demonstrating that invasive IFITM1-expressing cells breach the mammary duct and

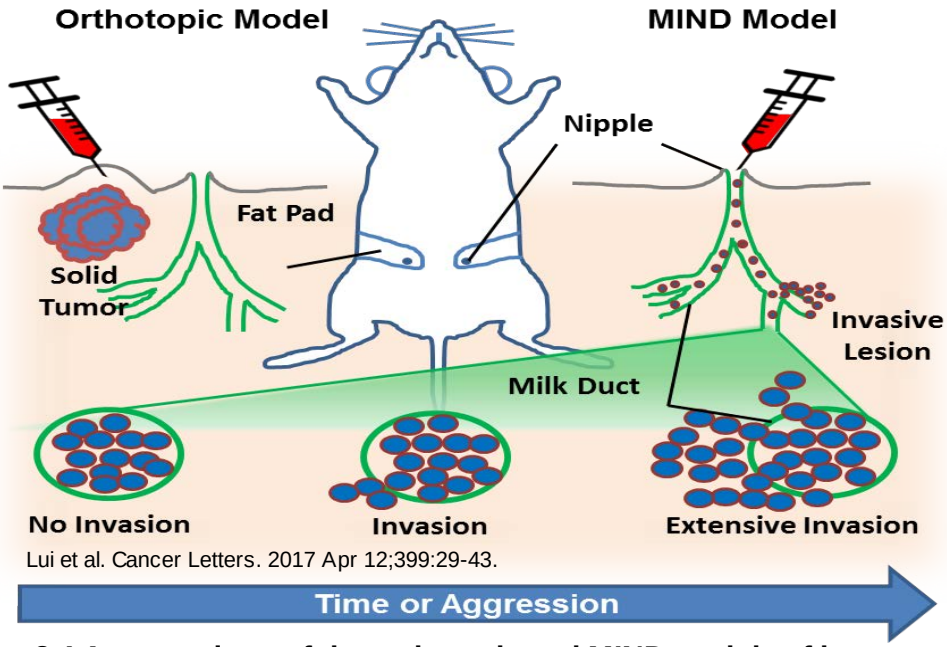

Figure 3.4 A comparison of the orthotopic and MIND models of breast cancer.
A diagram of the two breast cancer models where cells are injected into the mammary fat pad (Orthotopic Model) or through the nipple (MIND Model).

invade into the mammary gland stroma (Figure 3.5B). Immunohistochemical staining for SMA was used to visualize the extent of tumor burden in the mammary gland parenchyma (Figure 3.5B) and to quantify the extent of invasion (Lesions/Duct) (Figure 3.5C). The MIND model revealed that MCF-7:5C/shIF cells were highly invasive, however, loss of IFITM1 (+Dox) completely blocked the ability of these cells to invade out of the mammary duct as demonstrated by the lack of K19-stained cells outside of the duct (Figure 3.5A and Figure 3.5C). Using Ki67 and TUNEL staining, we found that loss of IFITM1 expression also reduced cell proliferation and increased cell death in the MIND model of breast cancer (Figure 3.6). This experiment demonstrates that the MIND model can be used to assess the impact of individual gene expression on ERα+ tumor cell invasion *in vivo* and that it faithfully replicates effects on cell survival and proliferation seen *in vitro* or the orthotopic model of breast cancer.

Immunohistochemistry staining verified that Dox exposure resulted in IFITM1 loss in the MIND model. Hematoxylin and eosin (H&E) staining further revealed the architecture of the mammary glands, demonstrating that invasive IFITM1-expressing cells breach the mammary duct and invade into the mammary gland stroma. When IFITM1 expression is lost, breast cancer cells remain confined within the duct and the majority of the stoma is comprised of adipose tissue (Figure 3.6B). Using Ki67 and TUNEL staining, we found that loss of IFITM1 expression reduced cell proliferation and increases cell death in the MIND model of breast cancer (Figure 3.6B). Dox exposure had no effect on the invasion, proliferation or survival of MCF-7:5C/shCon cells in either *in vivo* model (Supplemental Figure 3.2). Interestingly, we also found that the MIND model maintains higher estrogen receptor α (ERα) expression than the orthotopic model

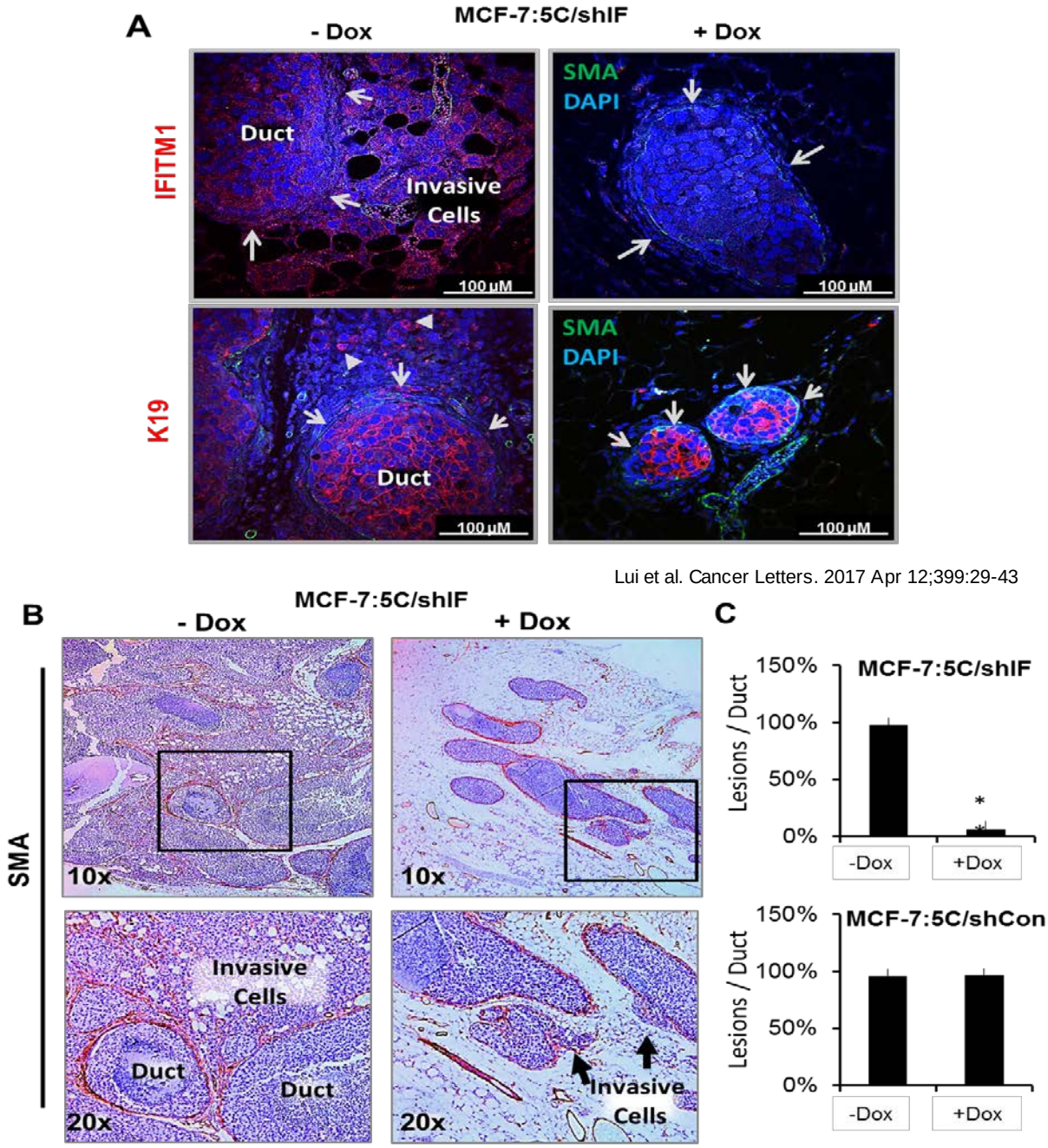

Lui et al. Cancer Letters. 2017 Apr 12;399:29-43

Figure 3.5 Loss of IFITM1 reduced aromatase inhibitor-resistant tumor cell invasion in the MIND model.

5,000 MCF-7:5C/shIF cells were injected into the duct of the 4th mammary gland of female ovariectomized NSG mice use the MIND injection protocol. After 10 days, mice were randomized to treatment groups and half were provided doxycycline (Dox)-treated drinking water. After 3 weeks, mammary glands were removed. (a) Mammary glands were fixed and processed onto glass slides. Immunofluorescent staining of the breast cancer cells for IFITM1, human keratin 19 (HuK19-red) and the mammary duct for smooth muscle actin (SMA-green) was conducted. Arrows indicate the mammary duct wall. (b) The milk duct was identified by immunohistochemistry. SMA was used to delineate invasive areas at 10X (upper panel) and 20X (lower panel). (c) Number of invasive lesions were quantified per duct in a 10X field. Numbers represent averages of 5 fields in 3 different mammary glands for each treatment group. ** p< 0.01

for both MCF-7 and MCF-7:5C cells (Supplemental Figure 3.3). This experiment demonstrates that the MIND model can be used to assess the impact of individual gene expression on ERα+ tumor cell invasion *in vivo* and that it faithfully replicates effects on cell survival and proliferation seen *in vitro* or the orthotopic model of breast cancer.

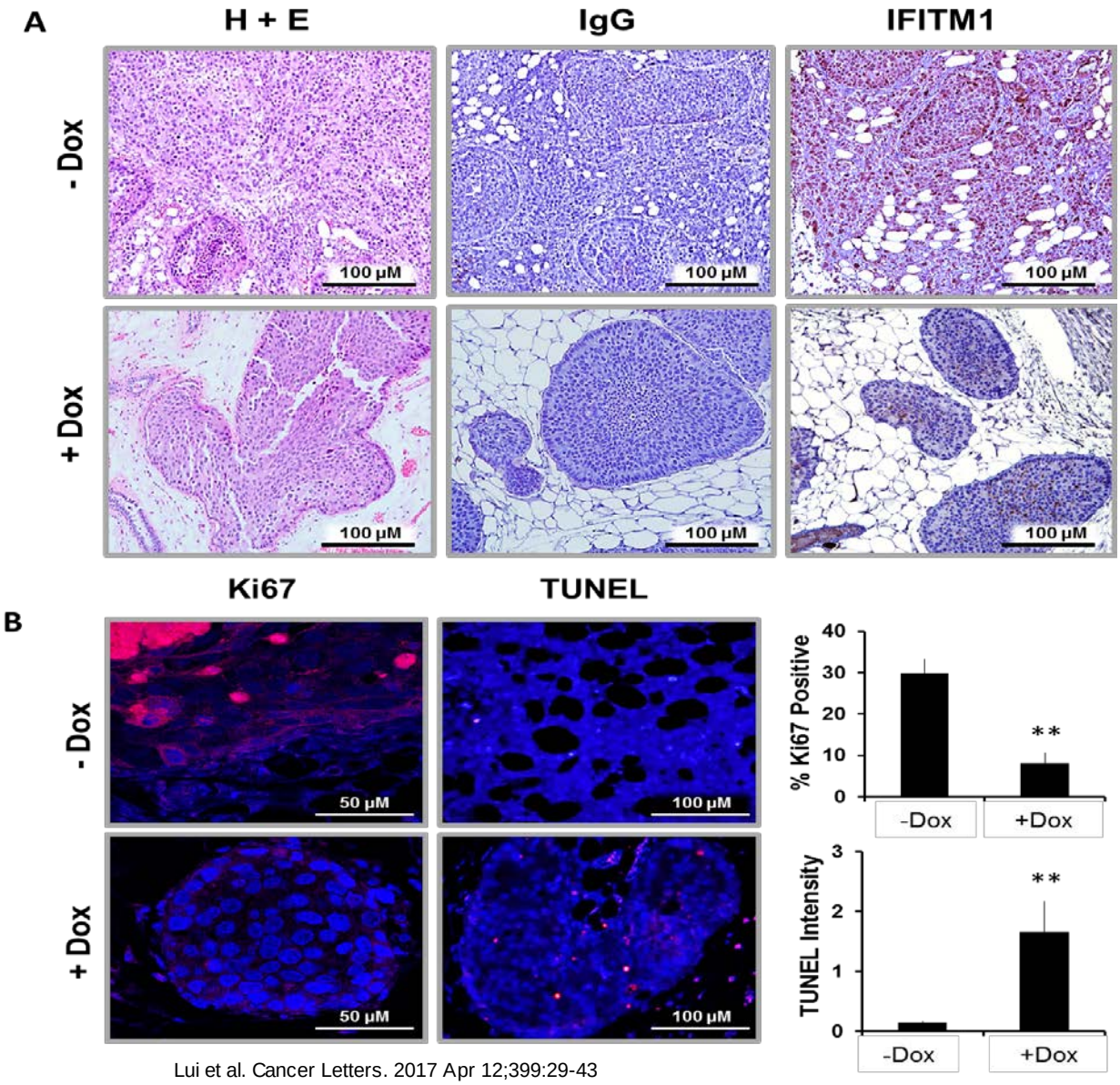

Lui et al. Cancer Letters. 2017 Apr 12;399:29-43

Figure 3.6 Loss of IFITM1 decreased cell proliferation and increased cell death in the MIND model of breast cancer.

(**a**) H&E, IgG (negative staining control) and IFITM1 staining in MIND injected mammary glands from untreated and doxycycline (Dox) treated mice. (**b**) Immunofluorescent staining for Ki67 on these glands is shown (*left panel*) and quantified (*right panel*). The percent of Ki67 positive cells was determined by counting five separate 40X fields. Cell death was analyzed by TUNEL staining and quantified by Image J software. ** p< 0.01

Overexpression of IFITM1 promotes breast cancer cell aggression in vitro and in vivo.

To validate the importance of IFITM1 in the ER+ breast cancer cell phenotype, we overexpressed IFITM1 in parental MCF-7 cells using CRISPR/Cas9 guided transcription. Two clones, MCF-7/IF-1 and MCF-7/IF-2 were generated which expressed moderate and high levels of IFITM1 respectively (Figure 3.7A), as compared to control scrambled guiding-RNA expressing MCF-7/C9Con cells which lack IFITM1. IFITM1 overexpression enhanced MCF-7 cell proliferation in a 96 hour cell viability assay (Figure 3.7B). Additionally, IFITM1 overexpression enhanced the aggressive phenotype and tumorigenic potential of MCF-7 cells as demonstrated by soft agar anchorage-independent growth (Figure 3.7D) and wound healing cell migration assays (Figure 3.7E). To determine whether IFITM1 overexpression contributes directly to AI-resistance, we cultured the MCF-7/IF clones (MCF-7/IF1 and MCF-7/IF2) in estrogen-deprived conditions to mimic AI treatment, and we found that overexpression of IFITM1 in MCF-7 cells increased their proliferation, tumorigenicity, and estrogen-independent growth (Figure 3.7C) compared to MCF-7 and MCF-7/C9Con cells (Supplemental Figure 3.4).

To assess the role of IFITM1 overexpression *in vivo,* we transplanted the MCF-7/C9Con, MCF-7/IF-1 and MCF-7/IF-2 cells into intact (not ovariectomized) female NSG mice using both the orthotopic and MIND models of breast cancer. Overexpression of IFITM1 resulted in the enhanced growth of MCF-7/IF-2 solid tumors (Figure 3.8A and Figure 3.8B). Immunohistochemistry revealed that the MCF-7/IF-2 tumors continued to express IFITM1 *in vivo* and had increased ki67 positivity (Figure 3.8C). Additionally,

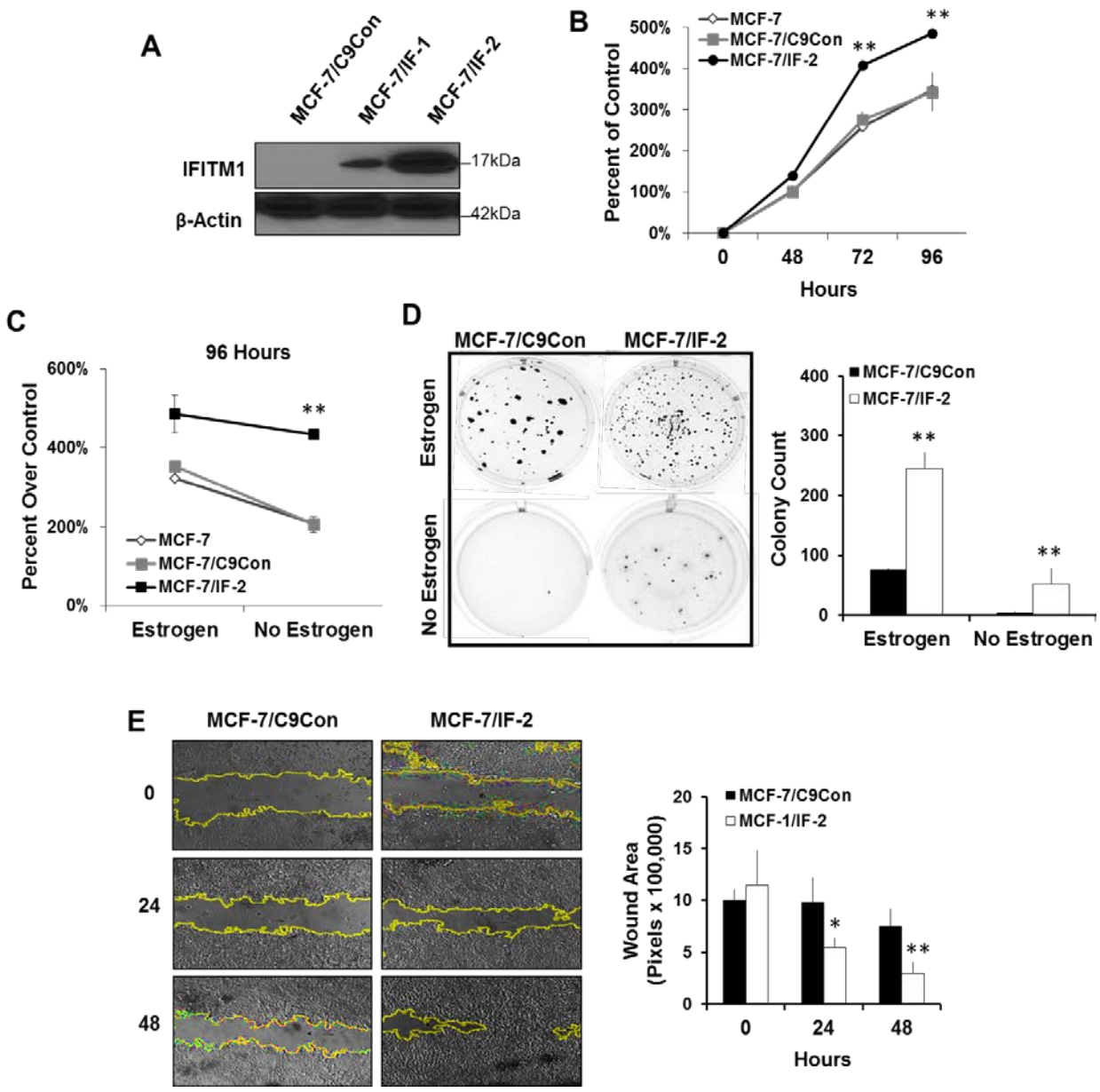

Lui et al. Cancer Letters. 2017 Apr 12;399:29-43

Figure 3.7 Overexpression of IFITM1 enhances the aggressive phenotype of MCF-7 breast cancer cells in vitro.

(**a**) IFITM1 expression in MCF-7 cells expressing scrambled control (MCF-7/C9Con) or an IFITM1 guided Cas9 overexpression vector (MCF-7/IF-1 and MCF-7/IF-2) was determined by immunoblotting and compared to expression in MCF-7:5C cells. (**b**) The proliferation of parental MCF-7, MCF-7/C9Con and MCF-7/IF-2 cells in estrogen containing media was measured over 96 hours by Cell Viability assay. (**c**) A direct comparison of proliferation in estrogen and estrogen free media is shown at 96 hours. (**d**) MCF-7/C9Con and MCF-7/IF-2 were subjected to soft agar anchorage independent growth assay. Plates were imaged after 21 days and the number of colonies was quantified using Image J (lower panel). Values represent two independent experiments conducted in duplicate. (**e**) Scratch assay was conducted on 70 % confluent plates of MCF-7/C9Con and MCF-7/IF-2 cells. Plates were imaged at 0, 24 and 48 hours and the size of the wound was quantified by image J (right panel). Values represent two independent experiments conducted in triplicate. *p < 0.05, ** p< 0.01

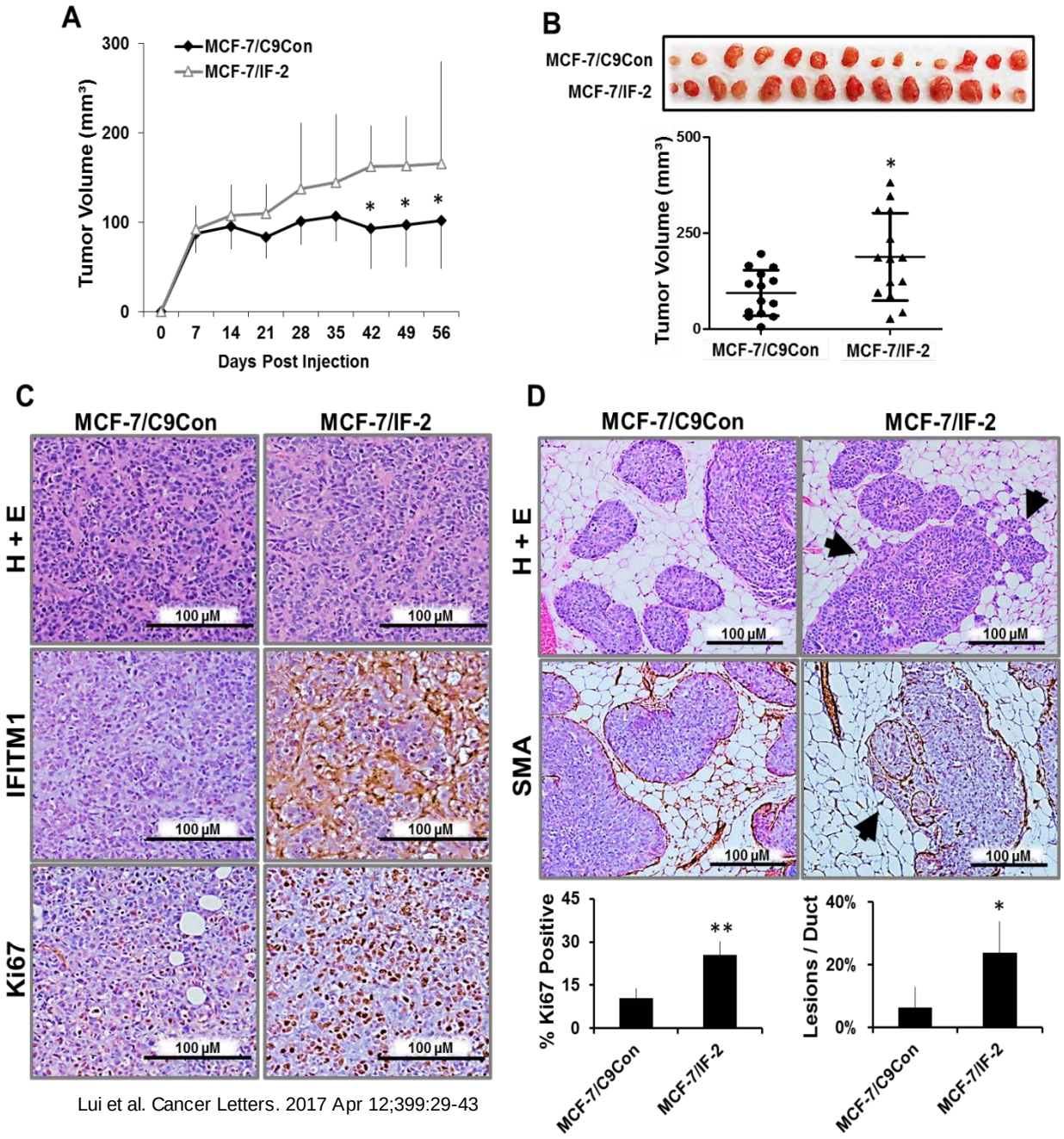

Lui et al. Cancer Letters. 2017 Apr 12;399:29-43

Figure 3.8 Overexpression of IFITM1 promoted breast cancer cell proliferation and invasion *in vivo*.

(**a**) Intact female NSG mice were orthotopically injected with MCF-7/C9Con and MCF-7/IF-2 cells and tumors measured by digital calipers weekly. Tumor volume (mm^3) was calculated and charted over time. (b) The tumors were excised and imaged at day 56 and final tumor volume (mm^3) determined. (c) IFITM1 and Ki67 expression was determined by immunohistochemical staining. The percent of Ki67 positive cells was determined by counting four separate 40X fields (*lower panel*). (d) Intact female NSG mice were injected with MCF-7/C9Con and MCF-7/IF-2 cells using the MIND model. Smooth muscle actin (SMA) staining by immunohistochemistry elucidated the milk duct. Arrow heads indicate invasive lesions which were quantified per duct in a 10X field. Numbers represent averages of 5 fields in 3 different mammary glands for each group (*lower panel*). *p < 0.05, ** p< 0.01

MCF-7/IF-2 cells were significantly more invasive than MCF-7/C9Con cells. We found that IFITM1 overexpression increased angiogenesis in MCF-7 xenografts (Supplemental Figure 3.4). Similar results were seen in moderately IFITM1-overexpressing MCF-7/IF-1 cells (Supplemental Figure 3.4), further demonstrating that IFITM1 expression alone can promote the proliferation, migration and invasion of MCF-7 cells *in vitro* and *in vivo*.

High IFIM1 expression is associated with increased blood vessel density and MMP1 expression.

Notably, we found that loss of IFITM1 significantly reduced angiogenesis in both the MIND and orthotopic models of breast cancer, as demonstrated by CD31 staining (Figure 3.9A and Figure 3.9B). This was seen in the doxycycline-treated MCF-7:5C/shIF groups in both the orthotopic and MIND models of breast cancer. Immunohistochemistry for CD31 expression demonstrated a significant decrease in blood vessel density in both models. Increased blood vessel density was also seen in MCF-7 tumors overexpressing IFITM1 as compared to control (Supplemental Figure 3.5).

Since IFITM1 expression positively correlated with invasion we also measured matrix metalloproteinase 1 (MMP1) expression in our MIND xenografts. We found that MMP1 was upregulated in AI-resistant MCF-7:5C/shIF cells at the leading edge of invasion, while the non-invasive cells inside of the duct remain MMP1 negative (Figure 3.9C, left panel). Notably, loss of IFITM1 (+Dox) reduced the number and extent of invasive lesions and was associated with lower MMP1 expression (Figure 3.9C, right panel). The upregulation of MMP1 likely facilitates colonization of the mammary gland parenchyma.

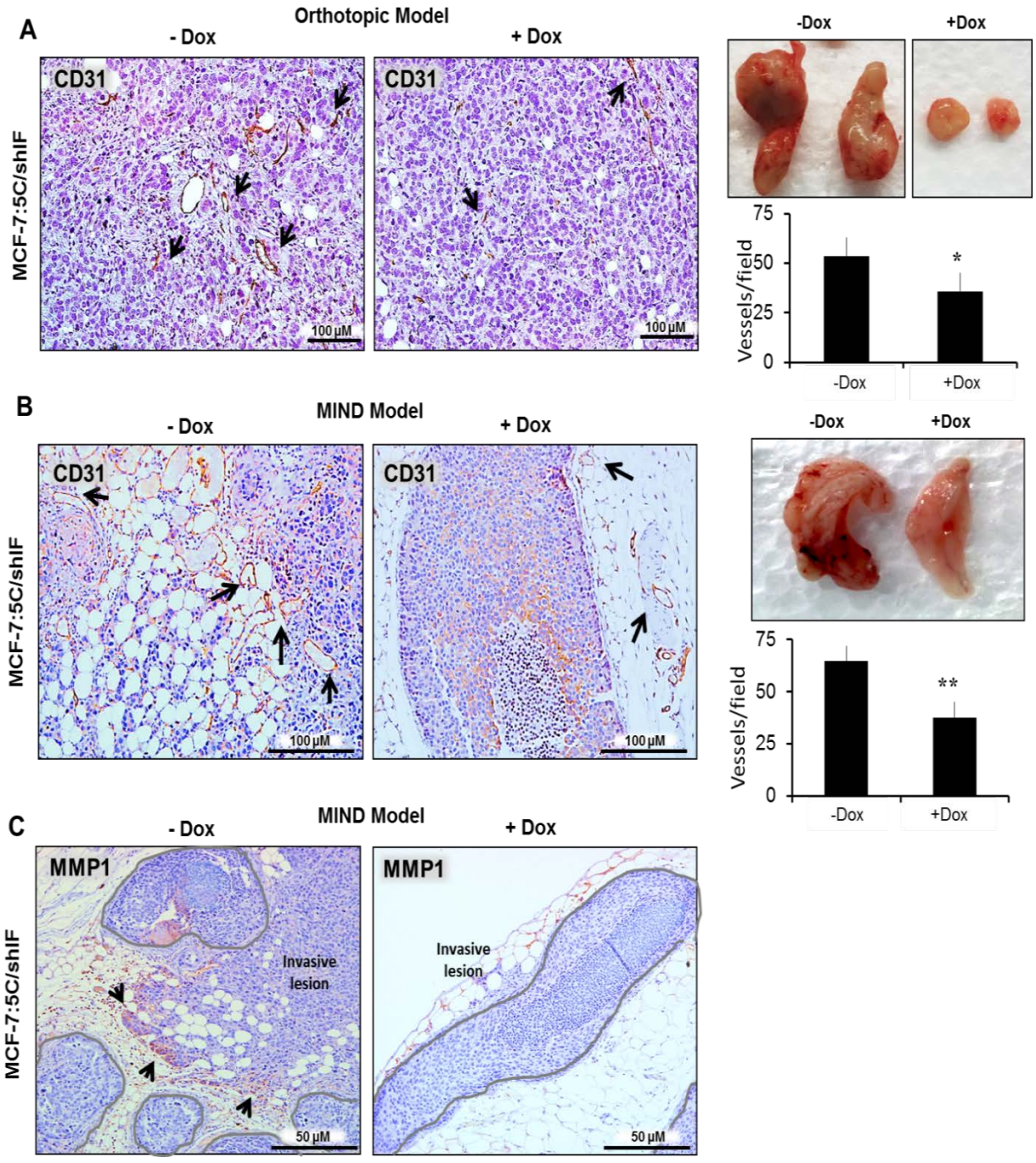

Lui et al. Cancer Letters. 2017 Apr 12;399:29-43

Figure 3.9 Loss of IFITM1 reduces blood vessel density and MMP1 expression.

MCF-7:5C/shIF xenografts from the orthotopic (**a**) and MIND model experiments were stained for CD31 expression using immunohistochemistry. Blood vessel density was determined by counting the number of CD31 positive blood vessels in at least 4 random 10X fields in each group from three separate samples. Graphs represent the average number of vessels per field. (**c**) Immunohistochemistry staining for matrix metalloproteinase 1 (MMP1) is shown. Mammary ducts are outlined in gray and MMP1 positive invasive cells indicated with arrows. ** $p < 0.01$

DISCUSSION

Previous work in our lab demonstrated that AI-sensitive cell lines and patient tumors do not express IFITM1, while AI-resistant cells and tumors express IFITM1 at a high level.[59] It is not known what drives AI-resistance, however, alterations in ER, growth factor, PI3K/Akt/mTOR, apoptosis and autophagy signaling have been identified as potential mechanisms in both preclinical and clinical studies.[27,29-31] Notably, when we overexpressed IFITM1 in MCF-7 cells (MCF-7/IF-1 and MCF-7/IF-2) we found that IFITM1 overexpression enhanced MCF-7 cell proliferation and tumorigenicity. It is significant that IFITM1 overexpression also improved breast cancer cell survival and aggression under estrogen-deprived conditions. IFITM1 expression is driven by type 1 IFN mediated JAK/STAT signaling.[2,66,72] Notably, enhanced STAT protein expression and activation have been linked to breast cancer development, progression and therapeutic resistance.[54,67,69,126] IFITM1 overexpression is likely one of the ways that JAK/STAT signaling drives breast cancer development, aggression and therapeutic resistance.

Using the orthotopic model we found that overexpressing IFITM1 increased tumor proliferation in the mammary fat pad and that loss of IFITM1 in AI-resistant cells reduced cell proliferation and induced death *in vivo*. The effect of IFITM1 expression on tumor proliferation and survival was likely due in part to the effect that IFITM1 had an effect on CD31+ blood vessel density *in vivo*. IFITM1 in endothelial cells is known to promote angiogenesis but the mechanism by which cancer cell IFITM1 expression drives angiogenesis warrants further study in our system.[127] The MIND model was developed to study the progression of ductal carcinoma *in situ* (DCIS) to invasive breast cancer.[123,124] While the orthotopic model is the most common method of studying breast

cancer in animals we used and validated the use of the MIND model as *in vivo* invasion assay. We discovered that IFITM1 expression can increase MCF-7 cell invasion while loss of IFITM1 can inhibit invasion out of the mammary duct. Recently, it has been shown that the MIND model can be used to study ER+ breast cancer invasion and metastasis and that the model maintains the phenotype of ER+ breast cancer cells more faithfully than the orthotopic model.[125] Specifically, the MIND model maintains higher ERα expression than the orthotopic model, which has implications for *in vivo* investigations of ER+ breast cancer.[128] We found that results from the MIND model also reflected the differences in MCF-7 and MCF-7:5C cells aggression. AI-resistant MCF-7:5C MIND xenografts were significantly more invasive than AI-sensitive MCF-7 xenografts. Notably, invasive lesions showed an induction in matrix metalloproteinase 1 (MMP1) at the leading edge of invasion. IFITM1 is thought to promote invasion and inflammation through control of the expression of several matrix metalloproteinases (MMPs).[129-131] The mechanism of IFITM1 control over MMP expression and activity remains unknown and warrants further study in our IFITM1-overexpression breast cancer cell lines.

MATERIALS AND METHODS

Cell lines and culture conditions

The MCF-7 cell line [42,132] was obtained from Dr. V. Craig Jordan (University of Texas MD Anderson Cancer Center, Houston) and maintained in RPMI-1640 medium supplemented with 10% fetal bovine serum, 2 mM glutamine, Antibiotic/Antimitotic mix, MEM Non-Essential Amino Acids (Invitrogen, Waltham, MA), and bovine insulin at 6 ng/mL (Sigma Aldrich, St. Louis, MO). The long-term estrogen deprived human breast cancer cell lines; MCF-7:5C and MCF-7:2A [122,132] were cloned from parental MCF-7 cells following long term (> 12 months) culture in estrogen-free medium composed of phenol red-free RPMI-1640, 10% fetal bovine serum treated three times with dextran-coated charcoal (SFS), 2 mM glutamine, bovine insulin at 6 ng/mL, Antibiotic/Antimitotic mix, and MEM Non-Essential Amino Acids (Invitrogen). The MCF10A cell line was purchased from the American Type Tissue Culture Collection. They are maintained in Dulbecco's Modified Eagle Medium: Nutrient Mixture F-12 (DMEM/F12) in a 1:1 mixture and supplemented with 5% horse serum, Antibiotic/Antimitotic mix (100 IU/mL penicillin, 100 µg/mL streptomycin, 25 µg/mL of Fungizone® from Invitrogen, Grand Island, NY), 20ng/ml EGF (Millipore), 0.5mg/ml hydrocortisone, 100ng/ml cholera toxin (Sigma Aldrich). All cell lines were cultured at 37°C under 5% CO_2.

Western blotting

Cells were seeded in 6-well plates, collected using a cell scraper and suspended in RIPA buffer (Thermo Scientific, Pittsburgh, PA) supplemented with protease inhibitor cocktail and phosphatase inhibitor (Sigma Aldrich). Cells were homogenized over ice by sonication. After purification of the sample by centrifugation, protein concentration was

determined by protein assay (Bio-Rad, Hercules, CA). The proteins were separated by 4-12% SDS–polyacrylamide gel electrophoresis (SDS–PAGE) and electrically transferred to a polyvinylidene difluoride membrane (Santa Cruz Biotechnology). After blocking the membrane using 5% non-fat milk, target proteins were detected using anti-IFITM1, anti-PARP, anti-ERα, anti-phospho-STAT1 (ser701), anti-STAT1, anti-p21, anti-p53 or anti-laminin B (Santa Cruz Biotechnology) antibodies. Membranes were stripped and re-probed for β-actin (Cell Signaling). The appropriate horseradish peroxidase (HRP)-conjugated secondary antibody was applied and the positive bands were detected using Amersham ECL Plus Western blotting detection reagents (GE Health care, Piscataway, NJ) and exposed to autoradiography film (Midwest Scientific).

RNA isolation and RT-PCR analysis

Total RNA was isolated from cultured cells using the RNeasy® Mini Kit(Qiagen, Venlo, Netherlands) according to the manufacturer′s procedure. First strand cDNA synthesis was performed from 2.5 µg total RNA using Super- Script Reverse Transcriptase (Invitrogen). cDNA was amplified in a 15-µl PCR mixture containing 1 mm dNTPs, 1× PCR buffer, 2.5 mm MgCl2, and 1 U DNA Taq polymerase (Promega, Madison, WI) with 25 pmol of primers specific for human PLSCR1 (sense: 5′-CATTCACCGGGCTCTCTAC-3′; antisense: 5′-GGCAGCTGGGCA ATCTTGCA-3′), IFITM1 (sense: 5′-GGATTTCGGCTTGTCCCGAG-3′; antisense: 5′- CCATG TGGAAGGGAGGGCTC-3′), IRF9 (sense: 5’-TTCTGTCCCTGGTGTAGAGCCT-3’, antisense: 5’- TTTCAGGACACGATTATCACGG-3’), IRF7 sense: 5’-GAGCCCTTACCTCCC CTGTTAT-3’, antisense: 5’-CCACTGCAGCCCCTCATAG-3’, IFI27 (sense: 5’- GCCTCTGG CTCTGCCGTAGTT-3’, antisense: 5’-

ATGGAGGACGAGGCGATTCC-3'), IFIT1 (sense 5'-TCTCAGAGGAGCCTGGCTAA-3', antisense 5'-CCAGACTATCCTTGACCTGATGA-3'), MX1 (sense: 5'-CTTTCCAGTCCAGCTCGGCA-3', antisense: 5'-AGCTGCTGGCCGTACGT CTG-3'), OAS1 sense: 5'-TGAGGTCCAGGCTCCACGCT-3', antisense: 5'-GCAGGTC GGTGCACTCCTCG-3'), STAT1 (sense: 5'-GGCACCAGAACGAATGAGGG-3', antisense: 5'-CCATCGTGCACATGGTGGAG-3', STAT2 (sense: 5'-GCAGCACAATTTGCGGAA-3', antisense: 5'-ACAGGTGTTTCGAGAACTGGC-3'). The condition in the logarithmic phase of PCR amplification was as follows: 5 min initial denaturation at 94°C, 1 min denaturation at 94°C, 35 sec annealing at 67°C, and 1.5 min extension at 72°C for 30 cycles. The number of amplification cycles during which PCR product formation was limited by template concentration was determined in pilot experiments. PUM1 was used as the internal control (sense: 5′-TCACCGAGGCCCCTCTGAACCCTA-3′; antisense: 5′-GGCAGTAATCTCCTTCTGCATCC T-3′). The reproducibility of the quantitative measurements was evaluated by three independent cDNA syntheses and PCR amplification from each preparation of RNA. Densitometric analysis was performed using Scion Image software (Scion Corp, Frederick, MD), and the relative mRNA expression level was determined as the ratio of the signal intensity of the target to that of PUM1.

TUNEL Staining

TUNEL staining was conducted using the Invitrogen Click-iT™ Plus TUNEL assay kit on either methanol fixed cell lines grown on chamber slides or deparaffinized tissue (See below) following manufacturer's instructions (Thermo Fisher Scientific). The average

TUNEL intensity was quantified using the red color channel on Image J software from a minimum of three images.

Plasmid DNA construction

shRNA cloning was performed utilizing Gateway® Technology (Invitrogen Life Technologies). Double stranded IFITM1 shRNA was generated as previously described.[133] The vectors used for cloning were a kind gift from Eric Campeau. Briefly, double stranded IFITM1 shRNA (5'-GATCGCTGTGACAGTCTACCATATTTCAAGAGAATATGGTAGACTGTCACAG-3') and scrambled shRNA sequences (5'-CATCGCCTAAGGTTAAGTCGCCCTCGCTCG AGCGAGGGCGACTTAACCTTAGG-3',) were inserted into the pENTR/pTER+ vector (430-1) (Addgene #17453), placing their expression under the control of the inducible H1/TO promoter which contains a Tet-operator (TetO). The pENTR/pTER+ shRNA constructs were then incubated with LR clonase II enzyme mix (Invitrogen) and pLentiX2-Hygro-DEST (w17-1) (Addgene #17295) vector to generate pLentiX2 DEST/shIFITM1 and pLentiX2 DEST/shCon constructs.

Virus preparation and transduction

Lentivirus preparation was performed as previously described.[133] Briefly, pLentiX2 DEST constructs were co-transfected with pVSVG packaging vectors into HEK293T cells using Lipofectamine 2000 (Invitrogen). Medium was changed after 24 hours and viral supernatant was harvested 48 hours later. Virus-containing medium was then filtered using a 0.45μM syringe filter (Millipore). MCF-7:5C cells were then seeded in 6-well plates and allowed to reach 70% confluence overnight. 400 μL of viral supernatant of the filtered supernatant and 1mL

Lentivirus expressing pLenti CMV rtTA3 BLAST (TetR) vector (w756-1) was another kind gift from Eric Campeau purchased from Addgene.[133] First, transduction of MCF-7:5C cells with the construct was accomplished using 100 μL virus-containing medium in 2 mL normal medium and 3 μg/mL polybrene which generated MCF-7:5C/TetR cells which express the TetR gene under a CMV promoter. TetR expression occupies TetO sites, keeping target-genes silenced until tetracycline or doxycycline exposure. MCF-7:5C/TetR cells were then transduced with the pLentiX2 DEST constructs which produced the MCF-7:5C/TetR/shCon (MCF-7:5C/shCon) and MCF-7:5C/TetR/shIFITM1 (MCF-7:5C/shIF) cell lines.

CRISPR /Cas9 Lentiviral Activation of IFITM1

IFITM1 Lentiviral Activation Particles (Santa Cruz sc-416878-LAC) is a synergistic activation mediator (SAM) transcription activation system designed to specifically and efficiently upregulate gene expression via lentiviral transduction of cells. IFITM1 Lentiviral Activation Particles (h) contain the following SAM Activation elements: a deactivated Cas9 (dCas9) nuclease (D10A and N863A) fused to the transactivation domain VP64, an MS2-p65-HSF1 fusion protein and a target-specific 20 nt. guide RNA. Upon transduction, the SAM complex binds to a site-specific region approximately 200-250 nt. upstream of the transcriptional start site and provides robust recruitment of transcription factors for highly efficient gene activation. Viral transduction and cloning was conducted per manufacturer's protocol.

Cell Viability

Cells were assayed for viability in 24-well plates in triplicate in either estrogen or estrogen-free medium (see Cell Culture Conditions). At each time point, a measure of the viable cells was taken using the Cell-Titer Blue Assay Kit (Promega, Madison, WI) per the manufacturer's instructions. Assay plates were kept at 37˚C in 5% CO_2 for 3 hours and read at 560-590 nM on a BioTek Synergy 4 microplate reader using the Gen 5 data analysis software (BioTek Instruments, Winooski, VT).

Soft Agar Anchorage-independent Growth Assay

6-well plates were coated with 1 mL of 0.8% agarose in the appropriate culture media. Cells were then suspended in 0.48% agarose and immediately overlaid on the pre-coated plates. Once the agarose was solid, 1mL of culture medium with or without estrogen (see Cell Culture Conditions) and every 4 days for 20 days. Cultures were then stained with 50 µl of MTT solution (5 mg/mL) was added to each well at a final concentration of 500 µg/mL, and the plates were further incubated for 2 h at 37^{o}C. Plates were imaged at 1X in a Bio-Rad ChemiDoc™ XRS+ System with Image Lab™ Software (Bio-Rad). Colonies were counted and measured using Image J software (NIH).

Wound healing assay

Cell lines were seeded in 6-well culture plates so that they would reach 70% confluence overnight. The next day, a single wound was made on the plates for each cell line by scratching the attached cells using a 200 µl sterile pipette tip. The plates were washed with complete medium to remove cellular debris from the scraped surface. The images of the cells were taken at 10X immediately, and after 24 and 48 hours using phase-

contrast microscope. The area of the wound was quantified using the MRI Wound Healing Tool in Image J Software (NIH).

Animals

Recipients were 8- to 10-week-old virgin female NOD-SCID IL2Rgamma^{null} (NSG) mice which were purchased from Jackson Laboratories or bred (a gift from Thomas Yankee, PhD at The University of Kansas Medical Center). Animal experiments were conducted following protocols approved by the University of Kansas School of Medicine Animal Care and Use.

Orthotopic Cell Line Transplantation

Cells were suspended in 50:50 PBS/Matrigel (Corning) were bilaterally into 4th mammary fat pads of NSG mice, as described previously. [48] 3 x 10^6 cells were delivered per injection in a volume of 100µL. The length (L) and width (W) of tumors was measured weekly with digital calipers, and the tumor volume was calculated by the formula $L^2/(2W)$. When tumors reached a mean volume of 0.20 cm^3, groups of 5-15 mice were randomly assigned to treatment groups. For doxycycline treatment, mice were provided with 50 µg/mL doxycycline in dark water bottles to induce IFITM1 shRNA expression. Water was replaced weekly to maintain efficacy. Where indicated, mice were given 50 µg/kg body weight of Ruxolitinib suspended in methylcellulose by oral gavage every other day. When using MCF-7 cells, capsules made of medical grade silastic tubing (Dow-Corning) containing 1:4 estradiol/cholesterol (Sigma Aldrich) were implanted subcutaneously in the mice where indicated. These capsules produce a mean serum estradiol level of ~80 pg/mL, which is similar to postmenopausal serum levels of estradiol. For the control group, the mice did not receive any treatment.

Mammary intraductal transplantation (MIND) method

MIND injections were conducted as previously described using 8-10 weeks old ovariectomized NSG mice. [123,134] Briefly, cells were resuspended as single cells in PBS and counted. A 30-gauge Hamilton syringe, 50-µl capacity, with a blunt-ended 1/2-inch needle was used to deliver the cells. The mice were anesthetized by ketamine/xylene injection, and a Y-incision was made on the abdomen, allowing exposure of the inguinal mammary fat pads. The nipple of the inguinal gland is snipped so that the needle can be directly inserted through the nipple. Two microliters of cell-culture medium (with 0.1% trypan blue) containing cells at a concentration of 2,500 to 5,000 cells/µl were injected. Successfully injection was confirmed by visual detection of trypan blue in the ductal tree branches. The skin flaps were then repositioned normally and held together with wound clips. When required, mice were provided with 50 µg/mL doxycycline in dark water bottles to induce IFITM1 shRNA expression. Water was replaced weekly to maintain efficacy.

Tissue Harvesting and Preparation

Mammary glands and solid tumors were removed and fixed in 4% paraformaldehyde for 72 hours and then 70% ethanol. Fixed glands were then processed, embedded and sectioned by the Biospecimen Repository at the University of Kansas Medical Center. For immunohistochemical staining procedure see above.

Immunofluorescent (IF) staining of tissue

IF was performed as previously described [124] after tissue deparaffinization by clearance in xylene and hydration through graded ethanol series. Antigen retrieval was conducted at 99˚C in Dako Target retrieval solution (S1700) for 20 min per manufacturer's instructions (Agilent Technologies, Copenhagen, Denmark). Washes were performed in IF buffer (130 mM NaCl, 7 mM Na_2HPO_4, 3.5 mM NaH_2PO_4, 7.7 mM NaN_3, 0.1% bovine albumin, 0.2% Triton X-100, 0.5% Tween-20). Due to use of mouse antibodies on mouse tissue, blocking and antibody dilution were performed using the Mouse on Mouse (MOM™) Kit following manufacturer's instructions (Vector Labs, Burlingame, CA). Sections were stained using human antibodies targeted against Keratin 19 (Neomarkers #MS-198-P1), anti- actin smooth muscle (Spring Biosciences #E2464), anti-ki67 (Dako #M7240), or anti-IFITM1 (Santa Cruz Technology). Secondary antibodies were FITC or Texas Red conjugated (Santa Cruz). Sections were mounted using ProLong® Gold Antifade Reagent with DAPI (Cell Signaling) and visualized on a Leica TCS SPE confocal microscope in the Confocal Imaging Core at The University of Kansas Medical Center. Images were collected and analyzed using the Leica LAS AF Lite software (Leica Biosystems, Nussloch, Germany). For quantification, mean fluorescent intensity was determined using Image J software on single color channel images.

SUPPLEMENTAL FIGURES

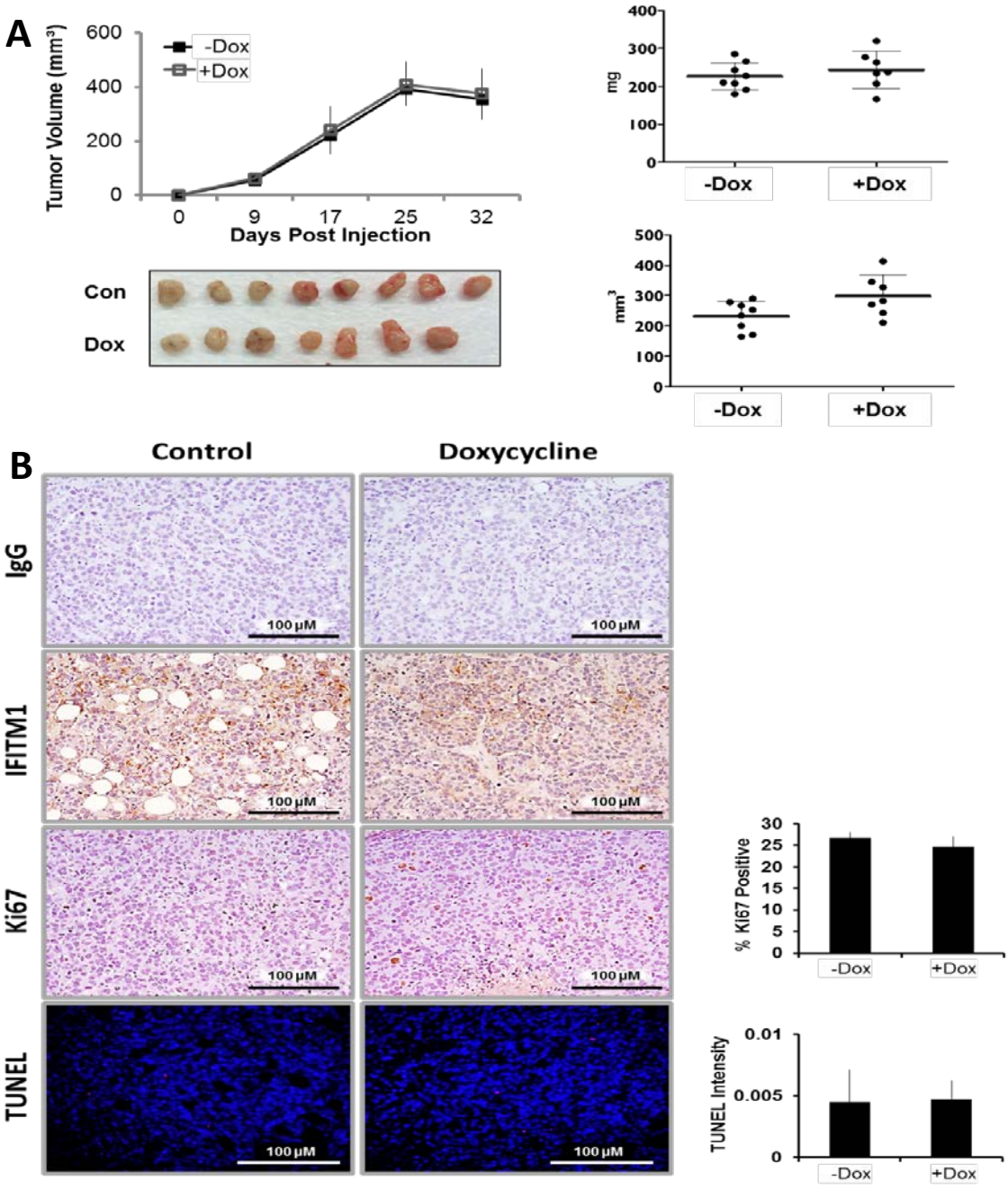

Lui et al. Cancer Letters. 2017 Apr 12;399:29-43

Supplemental Figure 3.1 Doxycycline induced IFITM1 shRNA expression is specific to MCF-7:5C/IFsh cells.

(**a**) 3 million MCF-7:5C/Con cells were injected in an accompanying experiment. Tumors were measured by digital calipers and tumor volume (mm^3) displayed over time (*left panel*). Excised tumor weight (mg) and volume (mm^3) was measured (*right panel*). (**b**) Excised tumors were fixed, embedded in paraffin and sectioned onto glass slides. IFITM1 and Ki67 expression was determined by immunohistochemical staining. The percent of Ki67 positive cells was determined by counting four separate 40X fields. Cell death was analyzed by TUNEL staining and quantified by Image J software analysis of six separate 20X images. Representative images are shown. ** $p<0.01$

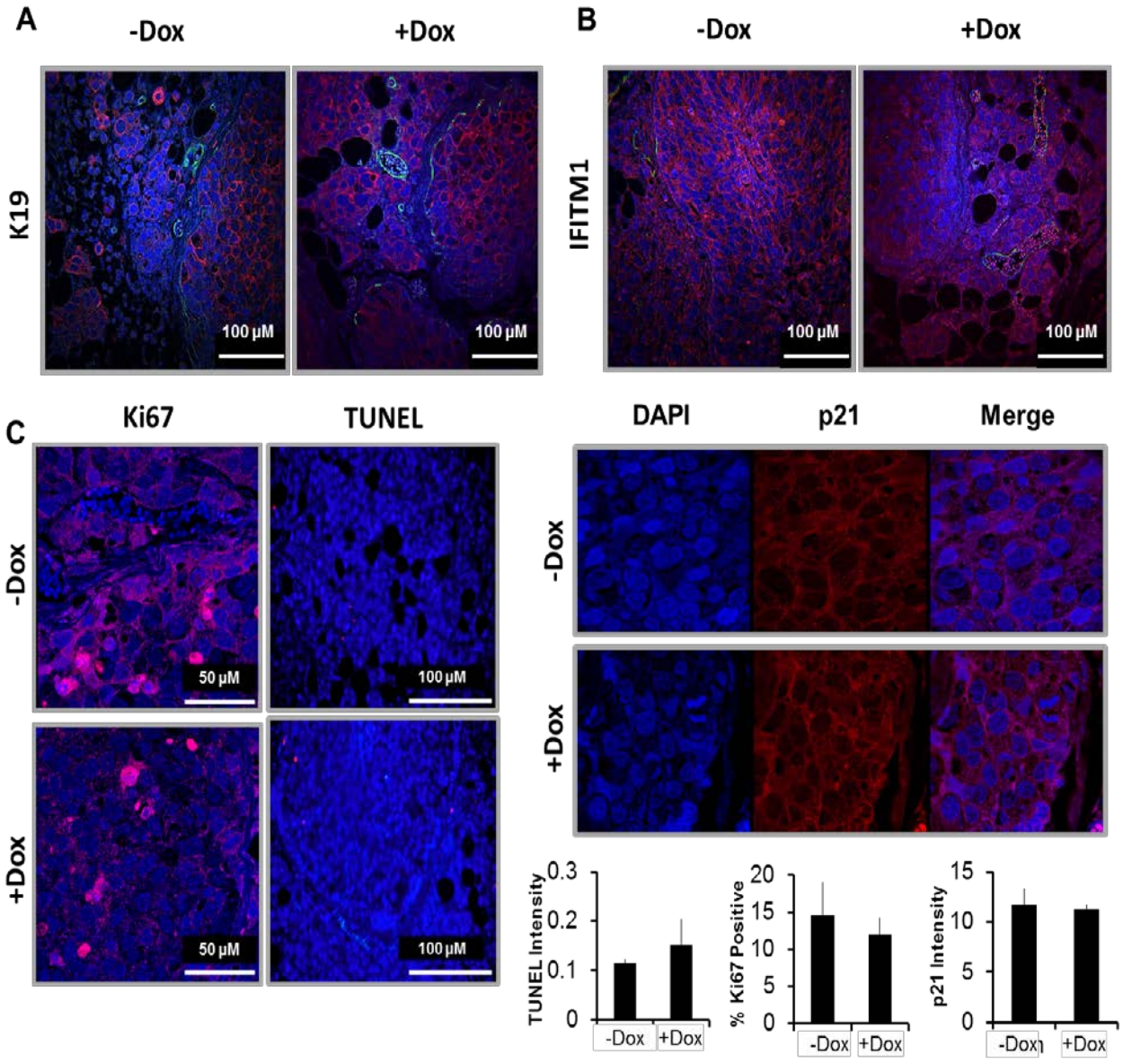

Lui et al. Cancer Letters. 2017 Apr 12;399:29-43

Supplemental Figure 3.2 MIND injection of MCF-7:5C/IFsh and MCF-7:5C/C9Con cells.

5,000 (a-d) MCF-7:5C/C9Con cells were injected into the duct of the 4^{tn} mammary gland of female ovarectomized NSG mice by the MIND injection protocol. After 10 days, mice were randomized to treatment groups and half were provided doxycycline (Dox)-treated drinking water. After 3 weeks, mammary glands were removed and processed. Immunofluorescent staining of the breast cancer cells for (b) human keratin 19 (HuK19-red), or (c) IFITM1 and the mammary duct for smooth muscle actin (SMA-green) was conducted. As well as (d) Ki67, TUNEL (*quantified on the right*) and (e) p21 staining (*quantified in lower panel*)

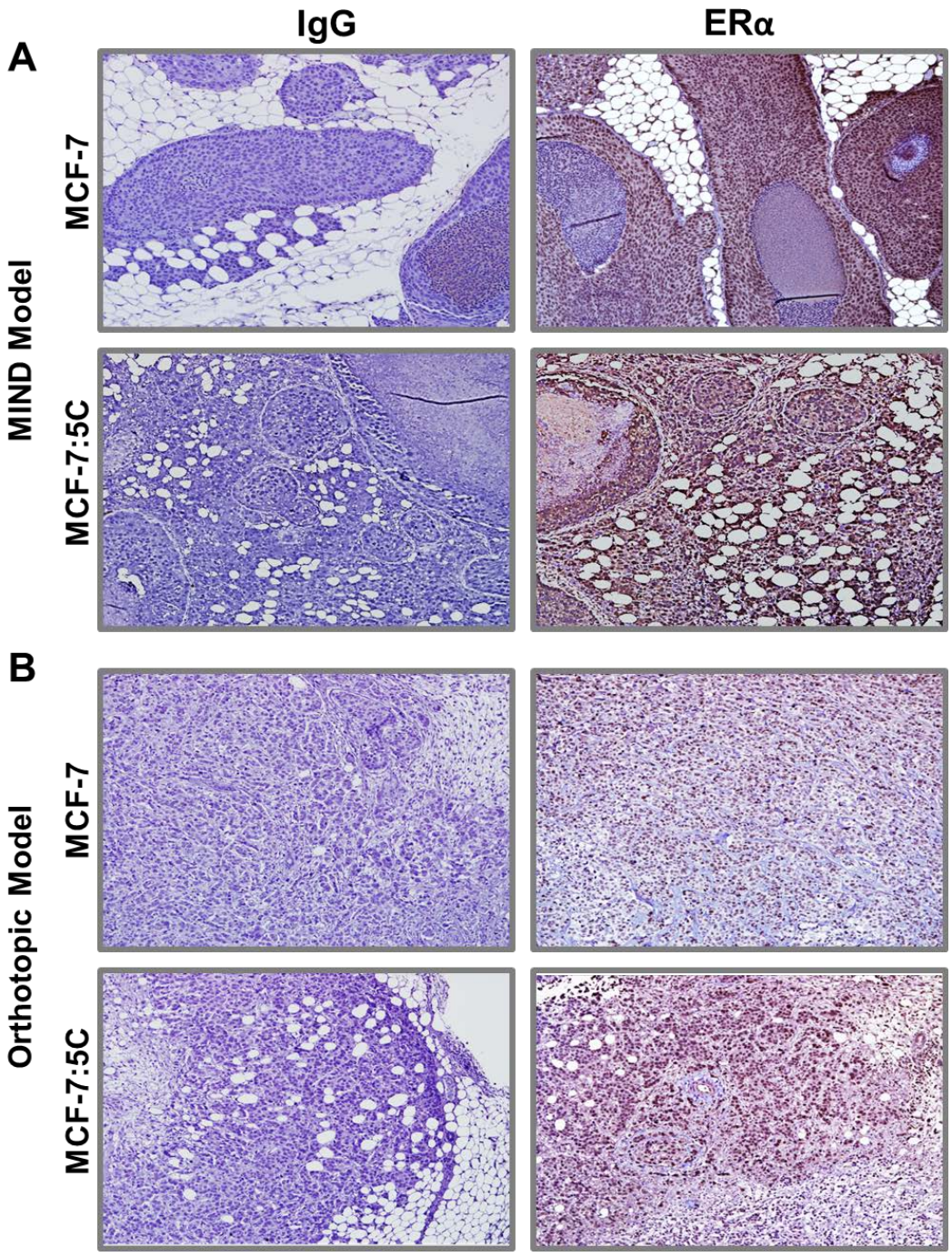

Lui et al. Cancer Letters. 2017 Apr 12;399:29-43

Supplemental Figure 3.3 Expression of ERα is higher in MIND verses orthotopic mouse tumors.

(a) 5,000 MCF-7 or MCF-7:5C cells were injected into the duct of the 4^{tn} mammary gland of female NSG mice use the MIND injection protocol. After 4 weeks, mammary glands were removed. Mammary glands were fixed and processed onto glass slides. ERα expression was determined by immunohistochemistry. (b) 3 million MCF-7 or MCF-7:5C cells were injected into the 4th mammary fat pad of female NSG mice. After 43 days, tumors were excised, fixed, embedded in paraffin and sectioned onto glass slides. ERα expression was determined by immunohistochemistry.

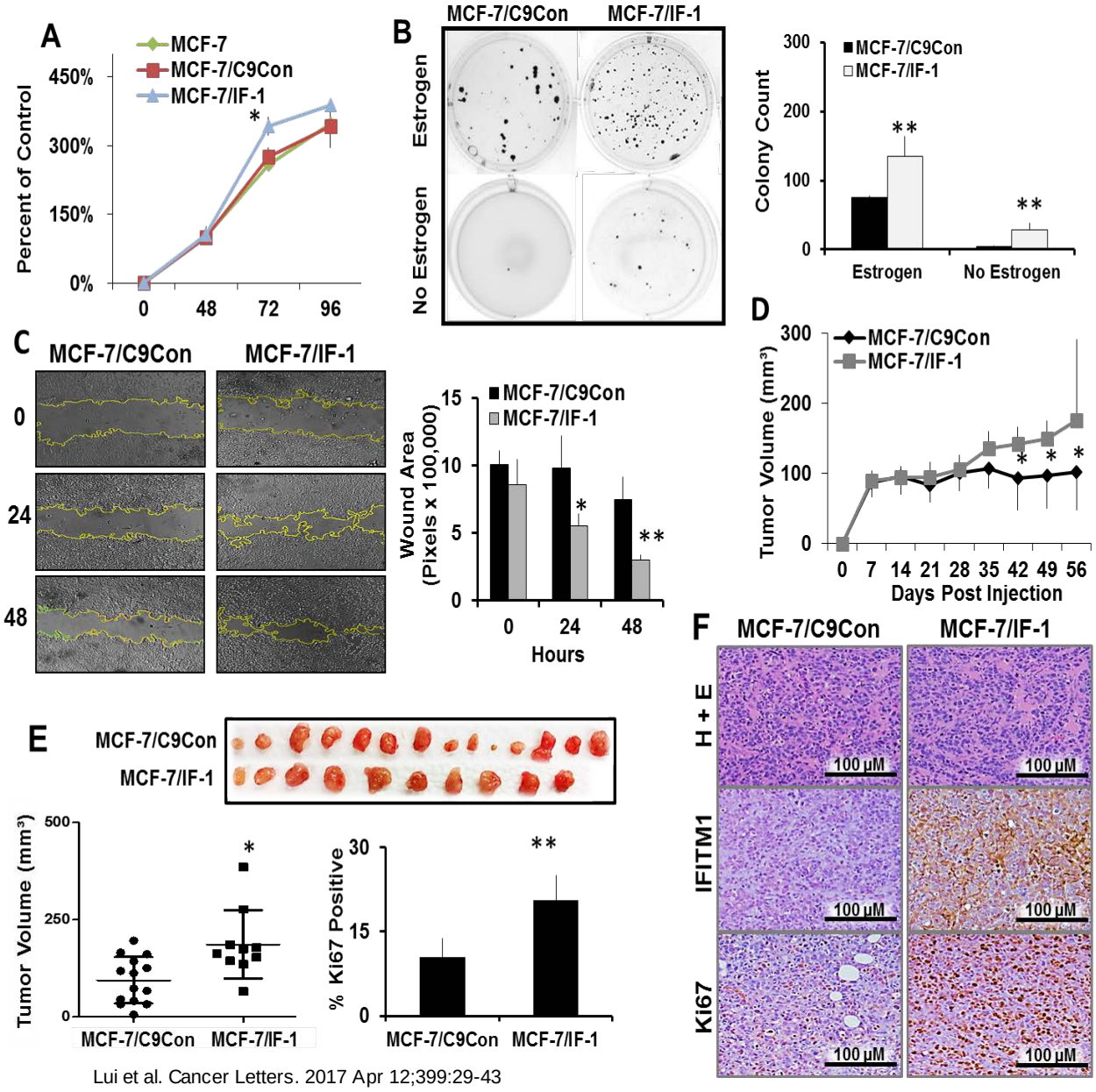

Lui et al. Cancer Letters. 2017 Apr 12;399:29-43

Supplemental Figure 3.4 Overexpression of IFITM1 promoted breast cancer cell proliferation and invasion.

(a) The proliferation of parental MCF-7, MCF-7/C9Con and MCF-7/IF-1 was measured over 96 hours by Cell Viability assay. (b) MCF-7/C9Con and MCF-7/IF-1 cells were subjected to soft agar anchorage independent growth assay. After 21 days the number of colonies was quantified using Image J (*right panel*). Values represent two independent experiments conducted in duplicate. (c) Scratch assay was conducted on 70 % confluent plates of MCF-7/C9Con and MCF-7/IF-1 cells. Plates were imaged at 0, 24 and 48 hours and the size of the wound was quantified by image J (*right panel*). Values represent two independent experiments conducted in triplicate. (d) Intact female NSG mice were orthotopically injected with MCF-7/C9Con and MCF-7/IF-1 cells. Tumor volume (mm^3) was calculated and charted over time. (e) Tumors were imaged and final tumor volume (mm^3) determined. (f) IFITM1 and Ki67 expression was determined by immunohistochemical staining. The percent of Ki67 positive cells was determined by counting four separate 40X fields (*left panel*).

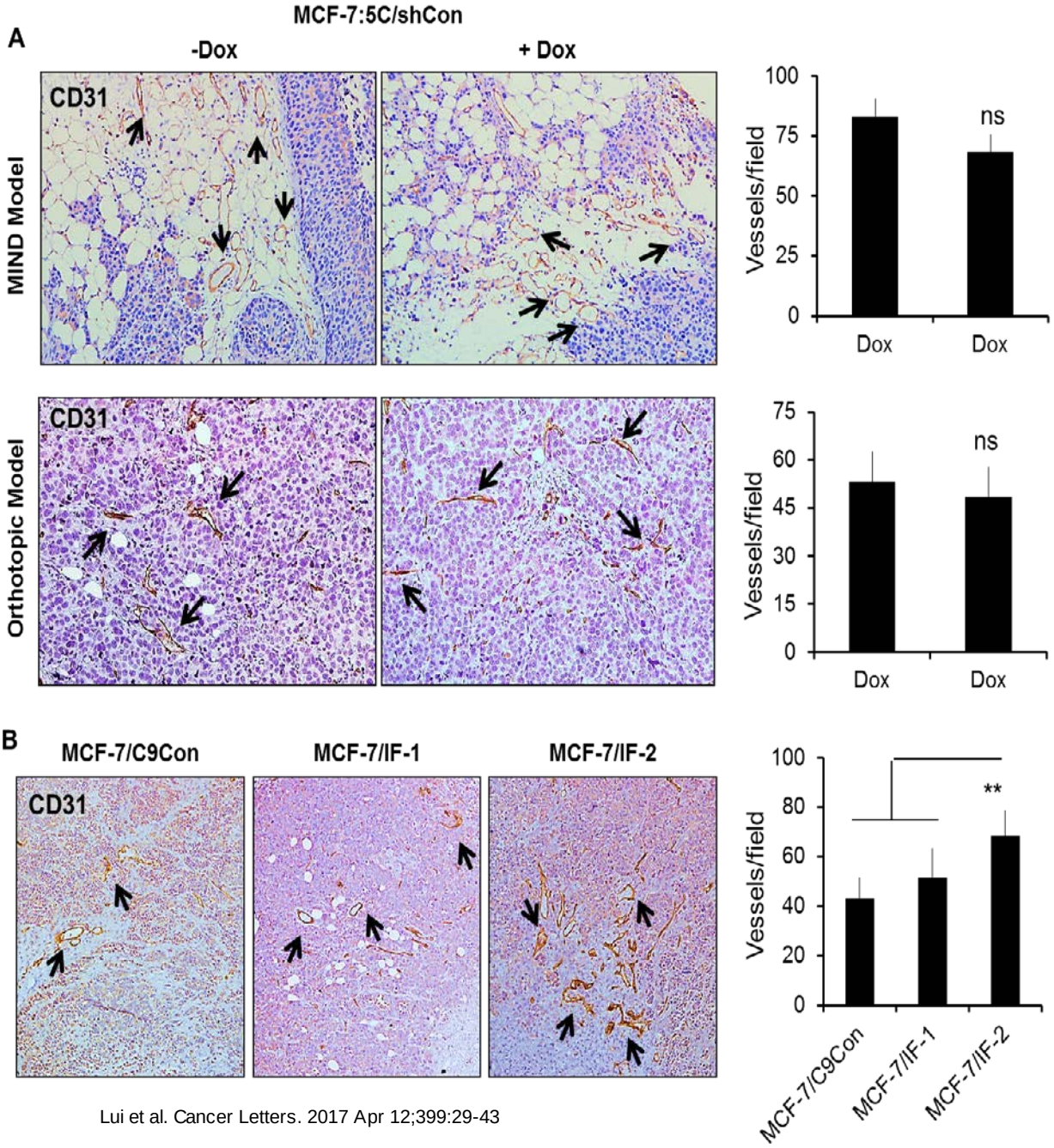

Lui et al. Cancer Letters. 2017 Apr 12;399:29-43

Supplemental Figure 3.5 IFITM1 expression is associated with angiogenesis.

(a) MCF-7:5C/shCon cells were injected into the 4^{tn} mammary gland of ovarectomized female NSG mice using either the MIN or orthotopic model. (b) 3 million MCF-7/C9Con, MCF-7/IF-1, MCF-7/IF-2 cells were injected into the 4th mammary fat pad of female NSG mice. Immunohistochemical staining for CD31 visualized the blood vessels in each tumor. The number CD31 positive blood vessels was quantified using at least 4 random 10x fields in each group.

CHAPTER 4 : ROLE OF IFITM1 IN CONTROLLING CELL CYCLING AND SURVIVAL

This chapter is adapted from:

Lui A, Ogony J, Geanes E, Behbod F, Valdez K, Marquess J, Jewell W, Tawfik O, Lewis-Wambi J. *IFITM1 suppression blocks proliferation and invasion of aromatase inhibitor-resistant breast cancer in vivo by JAK/STAT-mediated induction of p21*. Cancer Lett. 2017 Apr 12;399:29-43.

INTRODUCTION

IFITM1 is a transmembrane interferon stimulated gene (ISG) that is normally induced in response to IFN exposure to aid in resistance to viral infections. In addition to inhibiting viral entry and replication, ISGs are also known to modulate the decision between cell survival and death.[54,66,72,76] In fact, one study has found that the expression of ISGs increases in mouse models of endocrine resistance.[88] IFITM1 specifically is thought to promote the survival of epithelial cells and to allow cancer cells to survive chemotherapy and radiation.[54,76] These therapies function mainly by inducing DNA damage which initiates cell cycle arrest and cell death.

p21

The cell cycle is tightly controlled by a variety of proteins and signaling cascades. Cell cycle progression is driven by cyclin dependent kinases (CDKs) which phosphorylate target proteins such as the retinoblastoma susceptibility protein (Rb). CDKs are activated by interaction with cyclin proteins (Cyclin A, B , D and E) and are regulated by the CDK inhibitors of the INK and Cip/Kip families.[135,136] The CDK inhibitor p21 ($p21^{waf1/cip1}$) is the most prominent member of the Cip/Kip family and is known to arrest the cell cycle at the G1/S and G2/M checkpoints through inhibition of CDK and cyclin protein complex activity. The most well-known activator of p21 is p53, which is a

transcription factor that drives p21 expression in response to DNA damage (ie chemotherapy and radiation).[137,138] p21 is a potent driver of cell cycle arrest and so is often silenced in cancer due to its role as a tumor suppressor. Conversely, p21 is also frequently overexpressed in the cytoplasm of cancer cells and is associated with poor prognosis because cytoplasmic p21 can inhibit apoptosis through prevention of caspase activation, repression of E2F-1 activity and inhibitory interactions with pro-apoptotic proteins in the cytoplasm like apoptosis signal regulating kinase 1 (ASK1) (Figure

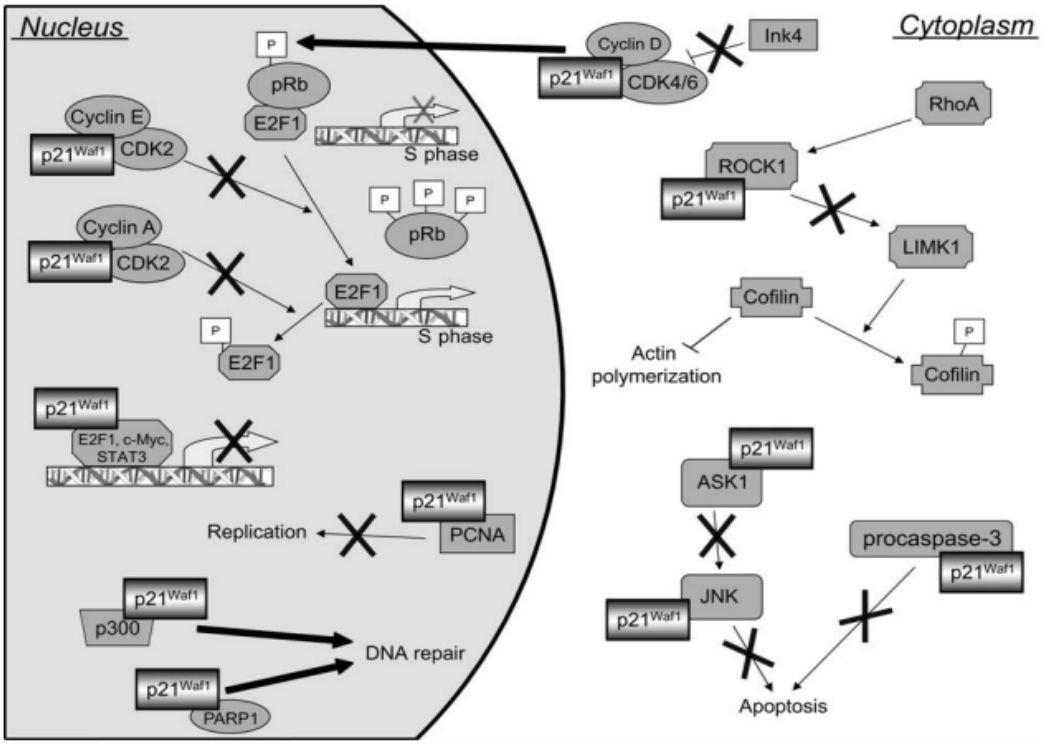

Figure 4.1 Nuclear and cytoplasmic functions of p21^{waf1}

Depending on intracellular localization, p21Waf1 is implicated in regulation of the cell cycle, DNA repair, apoptosis, and reorganization of the actin cytoskeleton. For example, in the nucleus the Cterminus of p21Waf1 interacts with a DNApolymerase δ subunit, PCNA, and thereby inhibits DNA replication. p21Waf1 can directly interact with PARP1 enzyme, a marker of both single and doublestranded DNA breaks that plays an important role in DNA repair via interacting with many repair proteins. Beside the traditional role of cytoplasmic p21Waf1 in regulating cyclin CDK2 complex inactivation, the cytoplasmic p21Waf1 can also bind to and regulate the Rhoassociated kinase 1 (ROCK1) cascade. This cascade is required for actin stress fiber and focal contact formation, which allows for cancer cell migration. Additionally cytoplasmic p21Waf1 can inhibit apoptosis by blocking procaspase-3 cleavage and apoptosis signal-regulating kinase 1 (ASK1). [7]

4.1).[139,140] When p21 is in the cytoplasm it is no longer a negative regulator of the cell cycle. Instead, cytoplasmic p21 can be stabilized by phosphorylation in response to pro-survival signals like PI3K/Akt and Ras signaling and there is growing evidence that cytoplasmic p21 is oncogenic, protecting many cancers from DNA damage-induced apoptosis. [7] Interestingly, cytoplasmic p21 is also thought to control reorganization of the actin cytoskeleton through interaction with Rho-associated kinase 1 (ROCK1) which also gives p21 a role in cell migration.[7,138] The cellular localization of p21 is important in determining the role that it plays in cancer.

RESULTS

Loss of IFITM1 induces p21 expression in AI-resistant cells.

We previously demonstrated in chapter 3 that IFITM1 knockdown induced cell death of AI-resistant MCF-7:5C cells. It is known that IFN signaling and ISGs modulate cell cycle progression and cell survival, so we assessed the mechanism by which IFITM1 loss induces cell death in AI-resistant MCF-7:5C cells. Our mechanistic studies focused on p21 and p53 which are important regulators of cell cycle progression and cell death. We found that siRNA knockdown of IFITM1 in the MCF-7:5C cells induced p21, while having no effect on p53 (Figure 4.2A) and this effect was true for all three siRNA constructs as well as the inducible IFITM1 shRNA system (Figure 4.2B). The induction of p21 was associated with cell cycle arrest (Figure 4.2C). Notably, doxycycline-induced loss of IFITM1 significantly reduced the percentage of MCF-7:5C/shIF cells that were in G0/G1 phase (Figure 4.2C); however, doxycycline exposure did not affect the cycling of wild type MCF-7:5C or MCF-7:5C/shCon cells. Concurrent knockdown of IFITM1 and p21 demonstrated that p21 was necessary for the induction of cell death using either the siRNA (Figure 4.2D) or shRNA approaches (*data not shown*). We should note that IFITM1 knockdown not only increased p21 expression but also increased STAT1 phosphorylation which was blocked by concurrent p21 knockdown (Figure 4.2E). Concurrent knockdown of IFITM1 and p53 had no effect on cell death or STAT1 activation (*data not shown*).

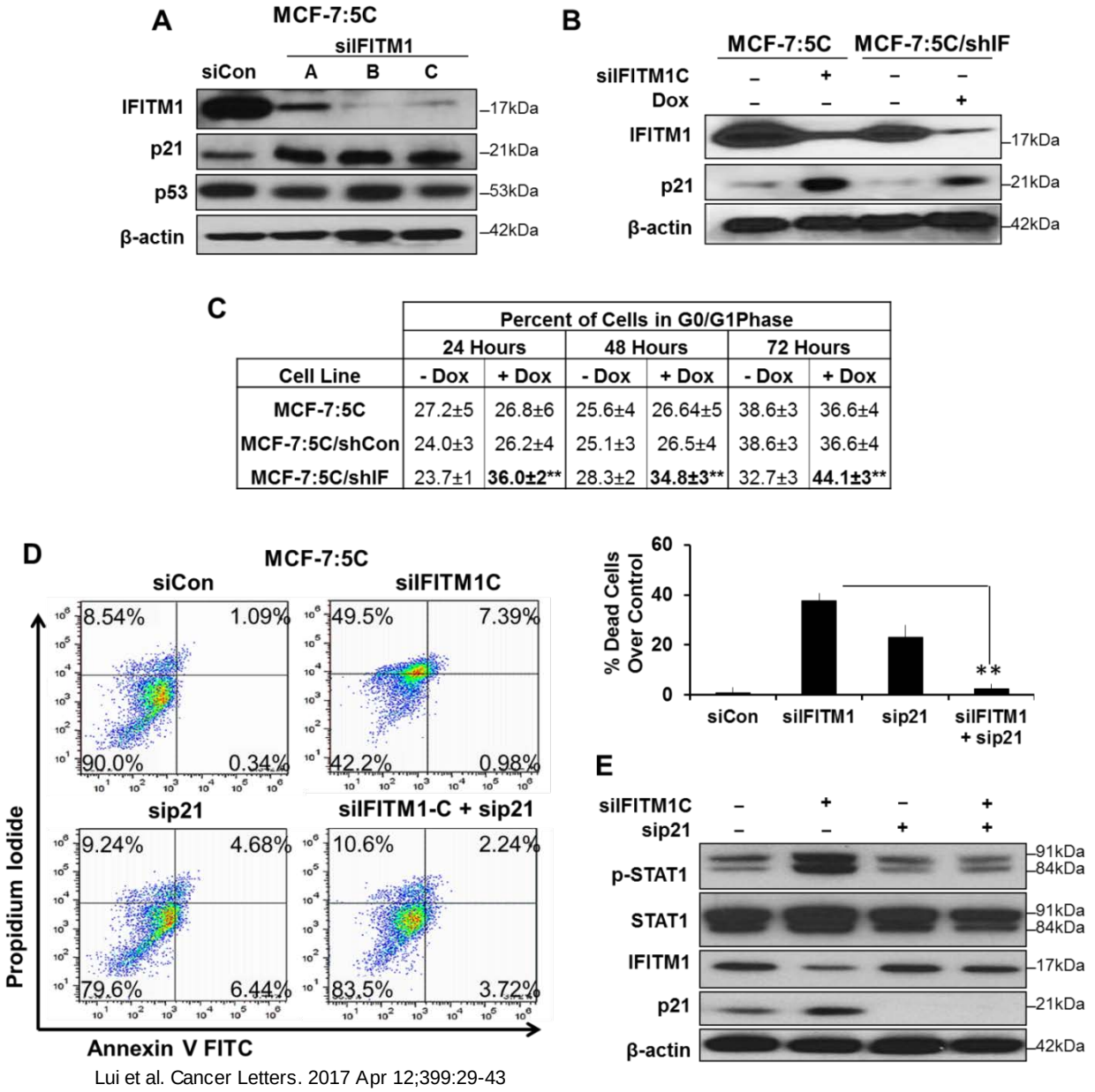

Lui et al. Cancer Letters. 2017 Apr 12;399:29-43

Figure 4.2 Loss of IFITM1 expression was associated with increased p21 expression, which mediated cell death.

(a) Cell lysates from MCF-7:5C cells transfected with scrambles control siRNA (siCon) or three different IFITM1 siRNA sequences (siIFITM1 A, B, C) were immunoblotted for IFITM1, p53 and p21 expression. (b) MCF-7:5C cells were transiently transfected with siCon or siIFITM1C while MCF-7:5C/shIF cells were treated with vehicle or 1μM doxycycline (Dox). Cells were harvested after 48 and 72 hours respectively and then lysates were immunoblotted for IFITM1 and p21 expression. (c) MCF-7:5C, MCF-7:5C/shCon and MCF-7:5C/shIF cells were treated with vehicle or control over 72 hours. Samples were harvested and fixed at 24, 48 and 72 hours for cell cycle analysis. The percent of cells in G0/G1 phase is displayed and represents means from two experiments conducted in duplicate ± standard deviation. MCF-7:5C cells were transfected with siCon, siIFITM1C, p21 siRNA (siP21) or siIFITM1-C with sip21. (d) Dual Annexin V/Propidium Iodide staining was used to quantify cell death in each transfection group as compared to siCon. Data represent means ± SD from two experiments conducted in duplicate (*right panel*). (e) Whole cell lysates were immunoblotted for p-STAT1, STAT1, IFITM1 and p21 expression. ** $p<0.01$

IFITM1 knockdown increased p21 expression through enhanced STAT1 activity.

The p21 promoter is known to have binding motifs for a variety of transcription factors including p53, SP1, AP2 and STAT1.[135,137] Since IFITM1 knockdown induced STAT1 phosphorylation we investigated whether loss of IFITM1 had an effect on p21 transcription. Using a p21 promoter luciferase reporter, we found that STAT1 but not STAT2 activated p21 transcription in MCF-7:5C cells and that loss of IFITM1 expression significantly increased p21 promoter activity (Figure 4.3A). To test whether the enhanced transcriptional activity at the p21 promoter was mediated by STAT1 we used a STAT1 motif luciferase reporter. We found enhanced basal STAT1 transcriptional activity in the MCF-7:5C cells which was completely abrogated by inhibiting STAT1 phosphorylation with the JAK1/2 inhibitor ruxolitinib (Rux). Significantly, IFITM1 knockdown doubled STAT1 transcriptional activity in AI-resistant MCF-7:5C cells (Figure 4.3B).

To demonstrate that the increase in p21 transcription was indeed mediated by STAT1 activation, we knocked down IFITM1 in the presence and absence of Rux. Inhibition of STAT1 phosphorylation (activation) prevented the increase in p21 expression normally seen when IFITM1 is lost (Figure 4.3C). The direct effect on p21 transcription was demonstrated using the p21 promoter luciferase reporter using both IFITM1 siRNA (Figure 4.3D) and inducible shRNA (*data not shown*). The importance of JAK/STAT signaling during IFITM1 knockdown-induced cell death was further elucidated by cell viability and annexin V/PI staining. Rux treatment significantly blunted the negative effects of IFITM1 loss on cell survival (Figure 4.3F).

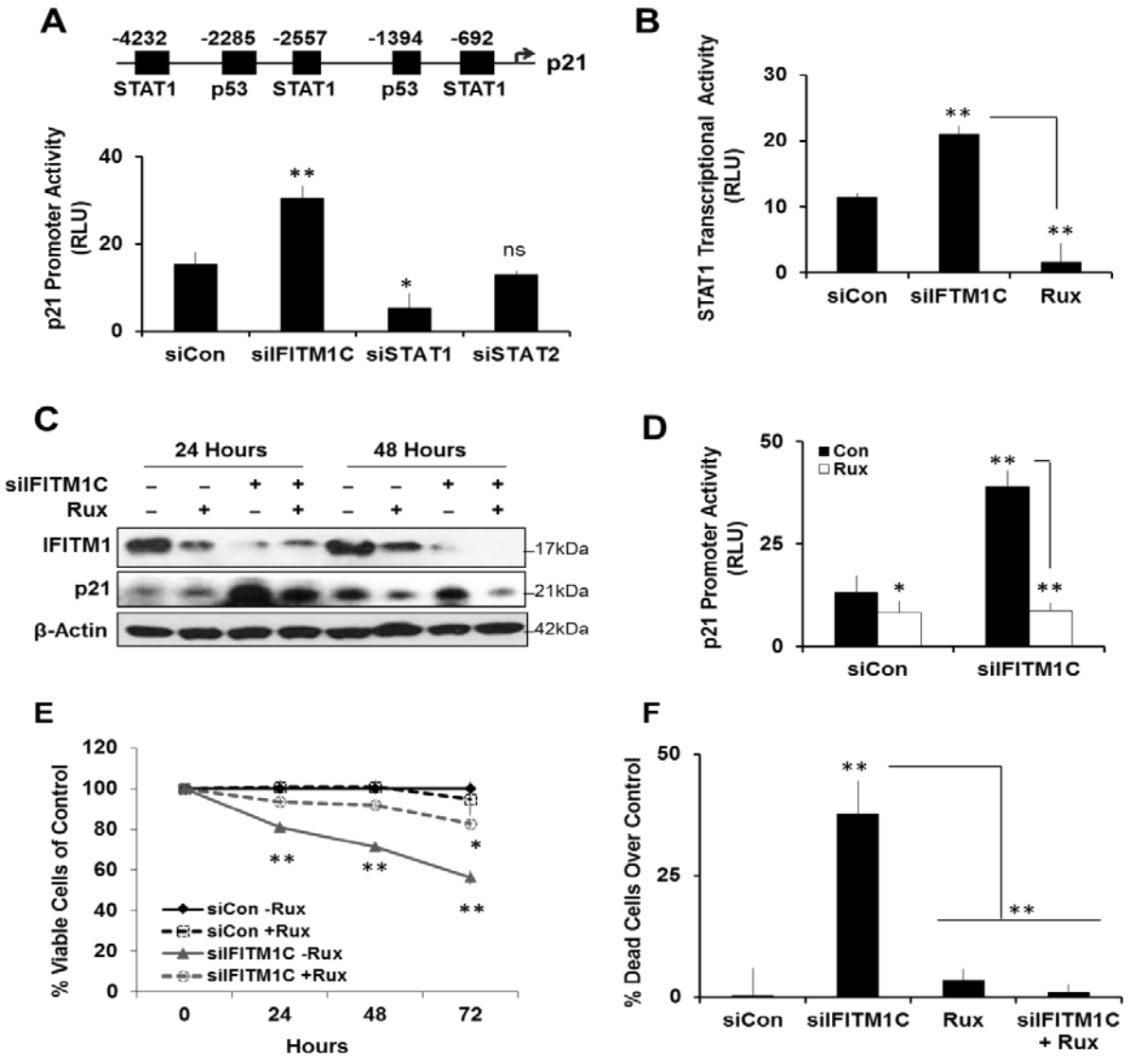

Lui et al. Cancer Letters. 2017 Apr 12;399:29-43

Figure 4.3 IFITM1 knockdown increases p21 expression via enhanced STAT1 activity.

(a) Activity at the p21 promoter was determined by luciferase assay. MCF-7:5C cells were transfected with p21 luciferase reporter and renilla reporter constructs with scrambled control (siCon) or IFITM1C siRNA (siIFITM1). (b) STAT1 transcriptional activity was determined by gamma associated sequence (GAS) luciferase assay cocktail. MCF-7:5C cells were transfected with GAS luciferase cocktail and with siCon or siIFITM1 or treated with 10μM ruxolitinib (Rux). (c) MCF-7:5C cells transfected with either siCon or siIFITM1 were also treated with 10μM Rux or vehicle. Whole cell lysates after 24 and 48 hours of treatment were immunoblotted for phospho-STAT1 (p-STAT1), STAT1, IFITM1 and p21 expression. (d) p21 luciferase assay determined relative activity at the p21promoter when MCF-7:5C cells were transfected with siCon or three IFITM1 siRNA sequences (siIFITM1A, B, C). After overnight transfection, cells were then treated with 10μM Rux or vehicle (Con) and assayed after 24 hours of Rux treatment. (e) The percent of viable cells after siCon or siIFITM1-C (siIFITM1) transfection with and without 10μM Rux was determined by cell titer blue cell viability assay after 24, 48 and 72 hours of treatment. Values are means ± SD of two independent experiments conducted in triplicate. (f) MCF-7:5C cells were transfected with siCon or siIFITM1C, treated with 10μM Rux or transfected with siIFITM1C and treated10μM Rux in combination. Dual annexin/PI staining was used to quantify cell death in each transfection group as compared to untreated siCon. *p < 0.05, ** p< 0.01

Loss of IFITM1 is associated with nuclear translocation of p21.

The cellular localization of p21 also plays a role in cell survival. To investigate whether localization of p21 is altered in MCF-7:5C cells we fractionated the cytoplasmic and nuclear fractions of AI-sensitive parental MCF-7 cells and AI-resistant MCF-7:5C cells and found significantly diminished p21 expression in the nuclear fraction of MCF-7:5C cells. Low nuclear to cytoplasmic ratio of p21 is associated with cancer aggression and resistance to therapy (Figure 4.4A). We then used our MCF-7:5C/shIF cells to determine the effect of IFITM1 loss on p21 localization. Both cell lysate fractionation and immunofluorescent staining revealed that loss of IFITM1 is associated with increased nuclear translocation of p21 (Figure 4.4B and Figure 4.4C). Interestingly, treatment with Rux prevented not only enhanced p21 expression, but also prevented induced nuclear translocation (Figure 4.4B and Figure 4.4C). Our data suggest that IFITM1 expression is inversely related to p21 nuclear localization and that p21 nuclear translocation may be a key step in IFITM1 knockdown-induced cell death.

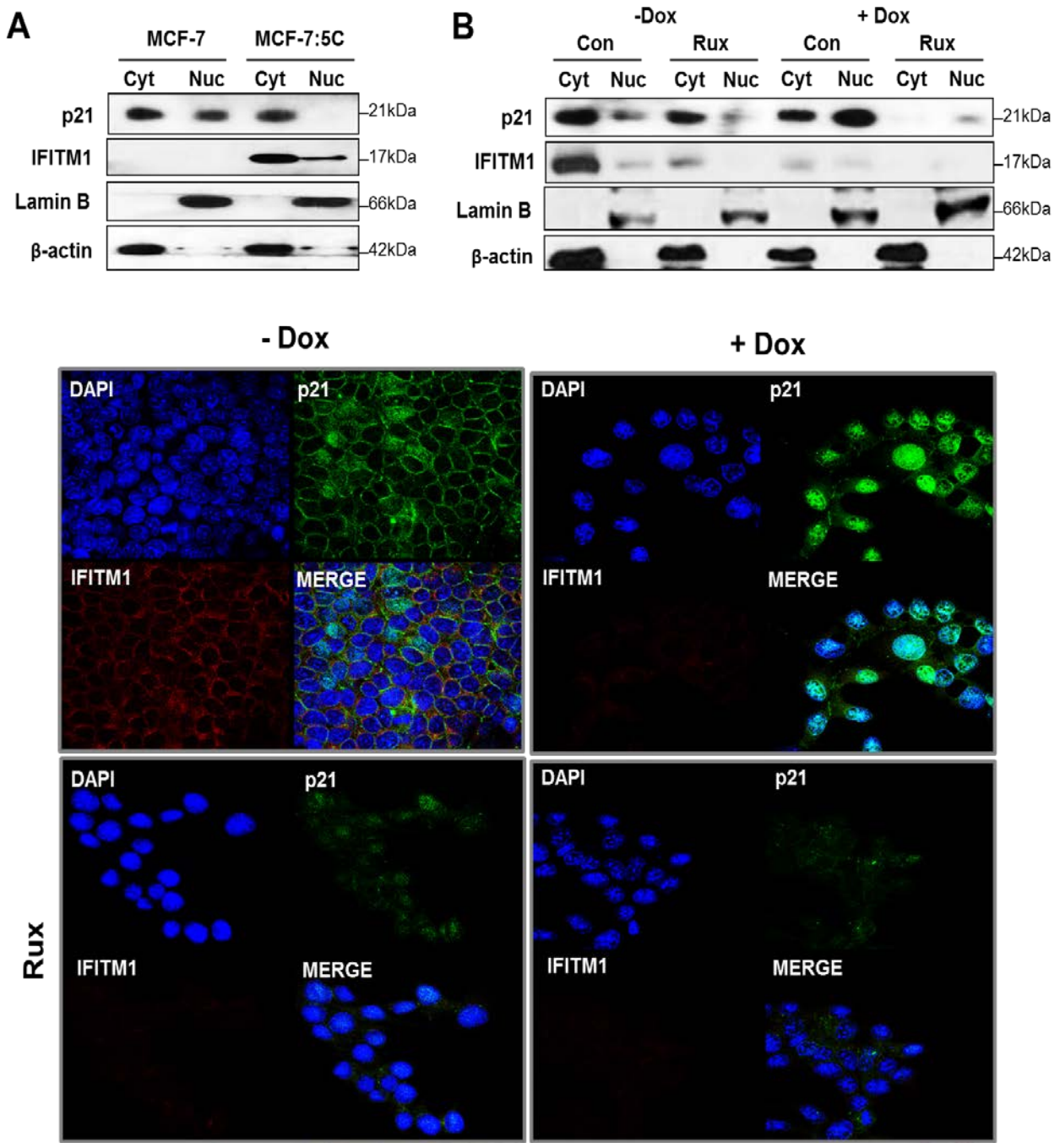

Lui et al. Cancer Letters. 2017 Apr 12;399:29-43

Figure 4.4 Loss of IFITM1 induces p21 nuclear translocation.

(a) Fresh whole cell lysates from 80% confluent MCF-7, and MCF-7:5C were separated into nuclear (laminin B) and cytoplasmic (β-actin) fractions. Protein expression of p21 and IFITM1 was determined by immunoblotting. (b) MCF-7:5C/shIF cells with and without doxycycline (± Dox) exposure were also treated with 10μM ruxolitinib (Rux). After 48 hours Rux treatment, cells were harvested and fresh whole cell lysates were fractionated and immunoblotted for p21, phospho-STAT1 (p-STAT1), STAT1 and IFITM1 protein expression. (c) MCF-7:5C/shIF cells with and without doxycycline (± Dox) exposure were also treated with 10μM ruxolitinib (Rux). After 48 hours Rux treatment, p21 and IFITM1expression and localization as determined by immunofluorescent staining.

DISCUSSION

We generated an inducible model of IFITM1 loss in MCF-7:5C cells and found that IFITM1 expression was critical to the survival of AI-resistant cells. In particular, we discovered that IFITM1 overexpression was required to maintain the survival and aggressive phenotype of AI-resistant MCF-7:5C cells whereas loss of IFITM1 induced cell cycle arrest and apoptosis. Mechanistic studies revealed that loss of IFITM1 markedly induced p21 expression which was dependent on STAT1 activation but not p53. While p53 is a well-known transcriptional regulator of p21, several other transcription factors also activate p21 expression in a p53-independent manner.[139] Indeed, DNA-binding elements for several transcription factors are present in the proximal p21 promoter, including three STAT1 binding sites.[139] These responsive elements are utilized to regulate p21 expression in response to various stimuli and stress signals. We have previously reported that total STAT1 and p(Y701)-STAT1 are significantly elevated in AI-resistant MCF-7:5C cells and that constitutive activation of the JAK/STAT pathway plays a critical role in driving IFITM1 overexpression in these cells.[59] In the present study, increased p21 expression was associated with cell cycle arrest and cell death, which is consistent with similar studies in other cancer models (Figure 4.5).[139] High expression of cytoplasmic p21 is known to promote cell survival and cell cycling while higher nuclear p21 stimulates cell death.[135,141,142] Cancers with high p21 cytoplasmic/nuclear ratio are thought to be more aggressive, hence our finding that AI-resistant MCF-7:5C cells have very high expression of IFITM1 but very low nuclear p21 expression is consistent with their highly aggressive phenotype both *in vitro* and *in vivo*.[140,143,144] Notably, loss of IFITM1 drove p21 nuclear translocation which can be induced by p21 threonin-145 phosphorylation by Akt1 and murine leukemia virus

(Pim-1).[135,136] Pim-1 is known to promote tumor aggression and high Pim-1 expression is associated with poor prognosis in various cancers.[145-147] Specifically Pim-1 is thought to promote inflammation induced tumorigenesis, and promote cancer cell survival of chemotherapy and radiation treatment.[148-151] In breast cancer, high Pim-1 expression is associated with PI3K/Akt mediated drug resistance.[152] The PI3K/Akt pathway has long been associated with endocrine resistance in ER+ breast cancer.[153-157] In fact, we have investigated the efficacy of FDA approved mTOR inhibitor everolimus/Afinitor™ in targeting AI-resistant breast cancer (Appendix A). Interestingly, Pim-1 expression itself is mediated by JAK/STAT signaling and stress signals including cytokine exposure and viral infection in a similar manner to IFITM1.[158,159] Significantly, in this study, overexpression of IFITM1 promoted MCF-7 cell survival in estrogen-deprived conditions. Whether IFITM1 modulates Akt1 and Pim-1 activity and p21 phosphorylation requires further study.

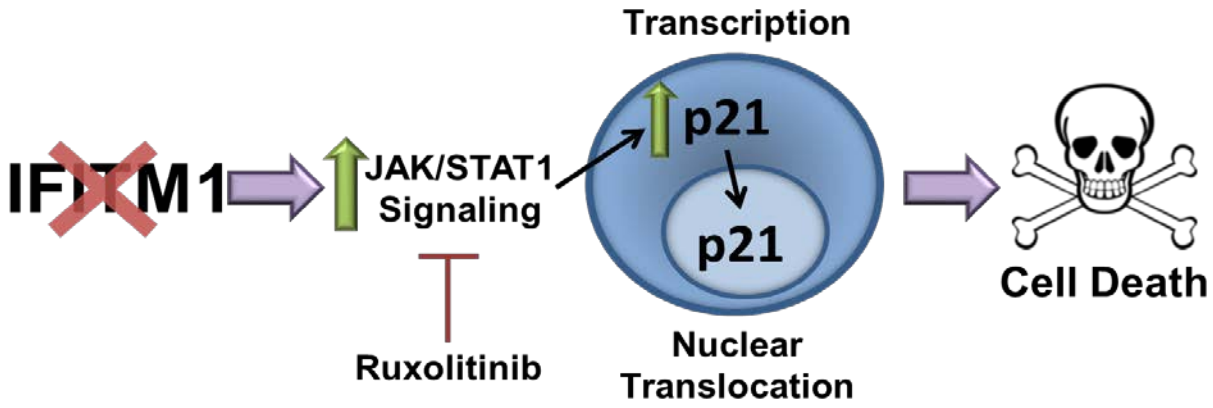

Figure 4.5 Loss of p21 drives cell death through regulation of p21 expression and cellular localization.

Loss of IFITM1 expression drives JAK/STAT mediated increases in p21 transcription and nuclear translocation. This change in p21 expression and localization drives cell death and can be blocked with the JAK1/2 inhibtior, ruxolitinib.

MATERIALS AND METHODS

RNA Isolation and Real Time PCR

Cells were harvested by cell scraping in RLT lysis buffer and total RNA was isolated using the Qiagen RNeasy kit (Venlo, Limburg). First strand cDNA synthesis was performed from 3 µg total RNA using MulV Reverse Transcriptase (Applied Biosystems, Carlsbad, CA) on a Bio Rad MyCycler™. RT-PCR was conducted using the ViiA™ 7 Real-Time PCR system (Applied Biosystems) and SYBR Green Reagent (Life Technologies, Carlsbad, CA) with 25 pmol primers specific for human PLSCR1 (sense: 5′-CATTCACCGGGCTCTCTAC-3′; antisense: 5′-GGCAGCTGGGCA ATCTTGCA-3′), IFITM1 (sense: 5′-GGATTTCGGCTTGTCCCGAG-3′; antisense: 5′-CCATGTGGAAGGGAGGGCTC-3′). Relative mRNA expression level was determined as the ratio of the signal intensity to that of PUM1 using the formula: $2^{-\Delta CT}$. When cells were treated, fold change in ERα expression was normalized to PUM1 and then compared to the untreated value for that cell line using the formula: $2^{-\Delta\Delta CT}$.

Small interfering RNA (siRNA) transfections

Cells were transiently transfected with siRNA for IFITM1 (cat# sc-44549A/B/C), p21, MUC1 or a scrambled negative control (cat# sc-37007) (Santa Cruz Biotechnology, Santa Cruz, CA). All of the siRNAs were pools of three target specific 20 to 25 nt siRNAs. Cells were seeded the night before transfection and allowed to reach 60% confluence by the time of transfection. Twenty nmol of each siRNA was introduced using Lipofectamine 2000 in OptiMEM Reduced-Serum Medium (Invitrogen, San Diego, CA, USA) according to the manufacturer's instructions. After overnight incubation, the

transfection mixture was replaced with normal culture medium containing 1 µg/mL doxycycline, only where indicated.

Annexin V Apoptosis Assay

The annexin V–FITC-labeled Apoptosis Detection Kit I (BD Pharmingen, San Diego, CA) was used to detect and quantify apoptotic cells by flow cytometry according to the manufacturer's instructions. In brief, cells were seeded in 6-well plates and cultured for up to 118 hours in their regular media or with 1 µg/mL doxycycline, where indicated. Media was changed at 72 hours for longer experiments. Cells were then harvested by trypsinization and resuspended in 1 × binding buffer (HEPES buffer, 10 mM, pH 7.4, 150 mM NaCl, 5 mM KCl, 1 mM MgCl2, and 1.8 mM CaCl2). Samples were stained simultaneously with FITC-labeled annexin V (25 ng/mL) and propidium iodide (PI) (50 ng/mL). Cells were analyzed using the BD FACSAria™ II Flow Cytometer (BD, Franklin Lakes, NJ) in the Flow Cytometry Core Facility at the University of Kansas Medical Center, and the data was analyzed with FlowJo software (Ashland, OR).

Cell Cycle Analysis

Cells were incubated in the appropriate cell culture media with and without doxycycline treatment. Cells were harvested at the indicated time points by trypsinization and then fixed with 0.9% NaCl and ice cold ethanol. Once all samples were collected, DNA was stained with 50 µg/mL Propidium Iodide and 100 µg/mL RNase A in PBS (Invitrogen). Samples were analyzed using a BD FACSAria™ II Flow Cytometer in the flow cytometry core at The University of Kansas Medical Center (BD, Franklin Lakes, NJ). The data were analyzed with FlowJo software (Ashland, OR).

Luciferase Assays

For IFITM1 and p21 promoter assays, 0.8 µg of plasmid DNA and the pRL CMV Renilla vector were used as previously described.[73] For analysis of IFITM1 promoter activity, the pGL3 plasmid with the first 750 nucleotides of the IFITM1 promoter inserted (pGL3-IFITM1 [−750/-1]), was used.[73] The pGL3-Basic-IRES was a kind gift from Joshua Mendell (Addgene #64784).[160] For analysis of p21 promoter activity, the pGL2-p21 promoter-Luc plasmid was used, which as a kind gift from Martin Walsh (Addgene #33021).[161] After 24 hours, transfection reagent was replaced with normal cell culture media containing ruxolitnib where indicated. Luciferase and Renilla activities were measured 24 h later using the Dual-Luciferase® reporter assay kit (Promega) according to the manufacturer's instructions on a BioTek Synergy 4 microplate reader using the Gen 5 data analysis software (BioTek Instruments).

CHAPTER 5 : REGULATION OF IFITM1 BY JAK/STAT SIGNALING IN AI-RESISTANT BREAST CANCER

This chapter is adapted from:

Choi HJ & **Lui A**, Ogony J**,** Jan R, Sims P, Lewis-Wambi J. *Targeting interferon response genes sensitizes aromatase inhibitor resistant breast cancer cells to estrogen-induced cell death.* Breast Cancer Res, 2015. **17**(1): p. 6. PMCID:4336497.

Lui A, Ogony J, Geanes E, Behbod F, Valdez K, Marquess J, Jewell W, Tawfik O, Lewis-Wambi J. *IFITM1 suppression blocks proliferation and invasion of aromatase inhibitor-resistant breast cancer in vivo by JAK/STAT-mediated induction of p21*. Cancer Lett. 2017 Apr 12;399:29-43.

INTRODUCTION

JAK/STAT signaling and ISGs

Interferons (IFNs) are a class of glycoproteins known as cytokines that are produced by immune cells of most vertebrates and are secreted in response to viral infections, tumors, and other pathogenic microbial agents.[72,162,163] IFNs diffuse to the surrounding cells and bind to high affinity cell surface type I (IFNα/β) and type II (IFNγ) receptors (IFNAR1/2), leading to phosphorylation and activation of JAK1, JAK2 and Tyk2. Activated JAKs phosphorylate and activate STAT1 and STAT2, resulting in the formation of STAT1/STAT1 homodimers and STAT1/STAT2 heterodimers. The dimers are transported to the nucleus by importins and bind to gamma associate sequences (GAS/STAT1) and IFN-stimulated response elements (ISREs) in ISG promoters to drive transcription.[162,164,165]

Traditionally the STATs are phosphorylated and associate with interferon regulatory factor 9 (IRF-9) to form the phosphorylated interferon-stimulated gene factor 3 (p-ISGF3) which enters the nucleus to initiate transcription at ISREs. Recently, however, studies have found that activity of the unphosphorylated STATs, which form

the unphosphorylated ISGF3 (U-ISGF3), are capable of stabilizing the ISGs in chemotherapeutic and radiation resistant cancers. [6,54] The interferon signaling pathway plays an important role in the proper functioning of the immune system and there is strong evidence that its dysregulation, resulting in constitutive overexpression of ISGs contributes to tumorigenesis and drug resistance. [69,75,114]

IFITM1 expression is classically driven by type 1 IFN mediated JAK/STAT signaling.[2,66,72] Notably, enhanced STAT protein expression and activation have been linked to breast cancer development, progression and therapeutic resistance.[54,67,69,126] In contrast, the suppressors of cytokine signaling (SOCS) family of proteins specifically inhibits STAT phosphorylation. Silencing and down-regulation of SOCS proteins has been associated with breast cancer while high SOCS expression confers a better prognosis for patients.[81-84] IFITM1 overexpression is likely one of the ways that JAK/STAT signaling drives breast cancer development, aggression and therapeutic resistance.

JAK/STAT signaling itself is pro-survival and has been shown to confer resistance to chemotherapy and radiation in breast cancer.[54,75] Increased signaling through this pathway also offers one potential method of maintaining estrogen-independent growth in AI-resistant cancer cells.[80] In this chapter we utilize the JAK1/2 inhibitor ruxolitinib (Afinitor™) to assess the role of JAK/STAT signaling in IFITM1 expression. Ruxolitinib is also FDA approved for the treatment of myelofibrosis. Here we also investigate whether oral ruxolitinib treatment can be used to target IFITM1 *in vivo* using orthotopic tumor xenografts. We demonstrate that ruxolitinib therapy holds promise for IFITM1-overexpressing ER+ and ER- breast cancers.

Mucin 1 (MUC1) in breast cancer

The human mucin family consists of 21 that function to protect epithelial linings in the body. Mucin 1 (MUC1) is an O-glycosylated transmembrane heterodimer localized on the apical borders of epithelial cells.[166-168] These glycoproteins can be either secreted or embedded in the plasma membrane where they contribute to the formation of mucous barriers, transmitting growth signals and promoting survival under stress.[121] The N-terminus supports the mucous layer, functions in cell adhesion and also aids in the trapping of microbes.[169-171] The C-terminus of this protein is responsible for the intracellular signaling with links to diverse signaling molecules in the cytoplasm, nucleus and mitochondria that control cell proliferation and survival.[166,172]

Due to the normal functions of MUC1 it is overexpressed in many epithelial cancers including breast, ovarian, lung, pancreatic, prostate, gastric, bladder and rectal carcinoma.[173-178] The high levels of MUC1 allow movement of this protein from the apical surfaces to the entire cytoplasm, providing enhanced interaction with other known cancer modulators such as GSK3β, Wnt/β-catenin, NFκB, HER2 and p53.[121,179-182] This diffuse expression of MUC1 contributes to invasion and metastasis by augmenting the epithelial to mesenchymal transition and encouraging attachment of carcinoma cells to distant sites by first interrupting adherens and tight junctions and then binding intracellular adhesion molecule 1 (ICAM-1) and e-selectin. [169,183] MUC1 is also known to act on the mitochondria and directly inhibit apoptosis by preventing the actions of Bcl-2-associated X protein (Bax), preventing cleavage of caspase-8, release of cytochrome c and protecting from reactive oxygen species (ROS) induced mitochondrial changes.[172,184,185] This allows MUC1 to confer resistance to death even in the presence

of hypoxia and chemotherapeutic drugs, making MUC1 overexpressing cancers a clinical challenge.[186,187] MUC1 is overexpressed in approximately 90% of breast cancers and, due to its effect on invasion, metastasis and chemosensitivity, is associated with poor patient outcomes.[121,188-192]

The effect of MUC1 expression on prognosis is also largely due to the intimate relationship between MUC1 and hormonal signaling. MUC1 is known to bind directly to estrogen receptor alpha (ERα) in MCF-7 cells and enhance the activities of estrogen by preventing ubiquitination of ERα.[193,194] MUC1 expression itself is also influenced by estrogen due to half an estrogen response element (ERE) in the promoter, making both MUC1's levels and interactions hormonally controlled.[120,195] Clinically, MUC1 expression correlates with ERα levels in breast tumors and also is associated with resistance to anti-hormonal therapy.[193,196] [189,197] In this chapter we investigate a connection between estrogen signaling, apoptosis and IFITM1 expression.

MUC1 is also known to promote JAK/ STAT signaling by stabilizing phosphorylation of STAT1.[67] STAT1 must be phosphorylated in order to enter the nucleus and function as a transcription factor.[67,75] Here we investigate whether MUC1 supports JAK/STAT signaling and IFITM1 expression in estrogen-independent MCF-7:5C cells. It should be noted that MCF-7:5C cells undergo estrogen-induced apoptosis due to dysregulation of estrogen signaling. In fact, low-dose estrogen therapy is currently under clinical study as a potential treatment option for patients with AI-resistant breast cancer.[22]

RESULTS

IFNα drives overexpression of IFITM1 in AI-resistant MCF-7:5C cells by stimulating JAK/STAT signaling through IFNAR

Binding of interferon alpha (IFNα) to the IFN alpha Type 1 receptor (IFNAR) complex initiates a signaling cascade comprising phosphorylation and dimerization of STAT1/2 molecules followed by their translocation to the nucleus, where they regulate the expression of ISGs. To investigate whether constitutive overexpression of IFITM1 in resistant MCF-7:5C cells is driven by the canonical IFNα signaling pathway, we first measured intracellular IFNα level in the supernatant and lysate of AI-resistant MCF-7:5C and parental MCF-7 cells using ELISA. IFNα protein level was significantly higher in the supernatant and lysate of resistant MCF-7:5C cells compared to parental MCF-7 cells (Figure 5.1A). IFNα mRNA expression was also significantly elevated in resistant MCF-7:5C cells compared to MCF-7 cells (Figure 5.1B). Canonically, STAT1 and STAT2 form a heterodimer when IFNAR is stimulated by type 1 IFNs. We confirmed that STAT1 and STAT2 both drove IFITM1 expression (Figure 5.1C). Next, we used a neutralizing antibody against the type 1 interferon receptor, IFNAR1/2, to see whether blocking the receptor reduces IFITM1 expression in the resistant cells. As shown in Figure 5.1D, α-IFNAR-Ab markedly reduced the basal expression of IFITM1 and PLSCR1 in resistant MCF-7:5C cells in addition to basal STAT1/2 phosphorylation. IFNAR neutralization also completely blocked exogenous IFNα induction of IFITM1 in parental MCF-7 cells.

We further tested whether suppression of the IFNα level is capable of reducing IFITM1 expression in the resistant cells. Induction of IFNα production is primarily controlled at the transcription level by the transcription factor IRF-7, hence, we

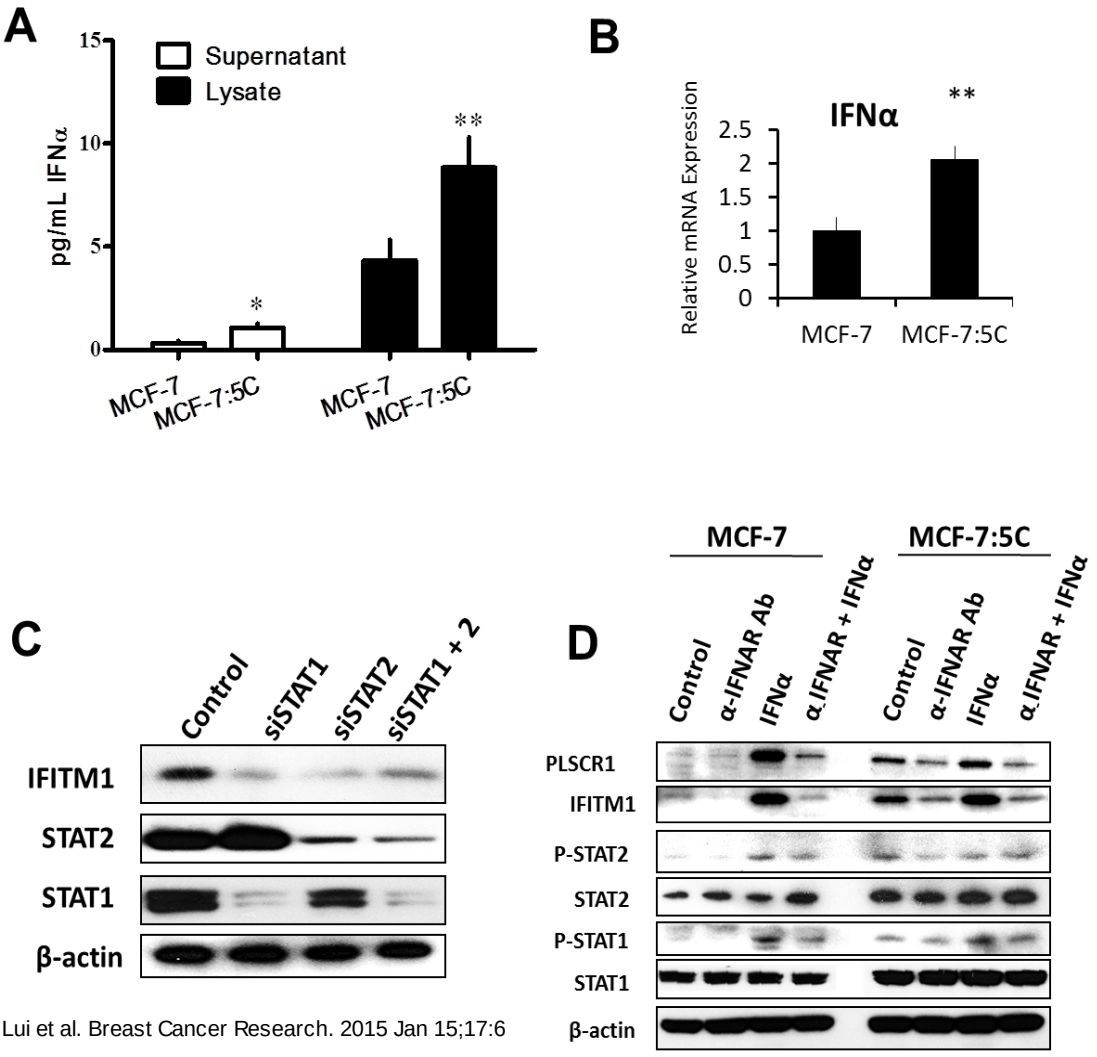

Choi & Lui et al. Breast Cancer Research. 2015 Jan 15;17:6

Figure 5.1 Elevated IFNa production drives constitutive overexpression of IFITM1 through IFNAR

(A) IFNα levels in MCF-7 and MCF-7:5C cells was measured in the supernatants and cell lysates by ELISA as described in Methods. All the illustrated data were performed in duplicate and are expressed as mean values of three independent experiments ± SD. (B) Measurement of IFNα mRNA was determined by real-time PCR. Fold change was calculated by means of the ΔΔCT method using PUM1 as an internal control. Values are displayed as relative to MCF-7 cells and are means of triplicate measurements ± SD in three independent experiments. (D) MCF-7 and MCF-7:5C cells were treated with type 1 interferon receptor, IFNAR1neutralizing antibody and/or 100 IU IFNα. After 24 hoursm whole cell lysates ere immunoblotted for PLSCR1, IFITM1, p-STAT1/2 and STAT1/2. (C) siRNA knockdown of STAT1 and/or STAT2 was conducted in MCF-7:5C cells. STAT1, STAT2 and IFITM1 expression was determined by immunoblotting.

performed siRNA knockdown of IRF-7 to suppress intracellular IFNα level in the resistant cells. We should note that IRF-7 mRNA and IRF-7 protein (Figure 5.2A) were constitutively overexpressed in resistant MCF-7:5C cells compared to parental MCF-7 cells. IRF-7 siRNA markedly reduced and IFNα mRNA level and protein expression in resistant MCF-7:5C cells (Figure 5.2B) in addition to IFITM1 expression (Figure 5.2C). We also found that siRNA knockdown of IFNα reduced its protein level in the supernatant by 100% and in the lysate by 50% (Figure 5.2D). SiRNA knockdown of both IFNα and IRF-7 completely reduced IFITM1 protein expression in the resistant cells (Figure 5.2C). Taken together, these data indicate that IFNα is significantly elevated in the supernatant and lysate of AI-resistant MCF-7:5C breast cancer cells and that activation of the canonical IFNα/IFNAR signaling pathway plays a critical role in driving the constitutive overexpression of IFITM1 and other ISGs in the resistant cells.

Dysregulation of type 1 IFNα signaling in AI-resistant

Since IFITM1 and PLSCR1 were constitutively overexpressed in the resistant cells, we wanted to assess the functional integrity of the interferon signaling pathway in the resistant cells compared to parental MCF-7 cells. Cells were treated with 1,000 IU/ml of IFNα for 0 to 24 hours and protein levels of IFITM1 and PLSCR1 were determined by Western blot analysis. We found that in parental MCF-7 cells, IFNα treatment significantly increased PLSCR1, IFITM1, protein expression in a time-dependent manner with maximum induction at 24 hours of exposure (Figure 5.3A). In contrast, we found that IFITM1 and PLSCR1 were constitutively overexpressed in

resistant MCF-7:5C cells and that treatment with exogenous IFNα did not significantly increase the level of IFITM1 or PLSCR1 at any of the time points (<2-fold increase in

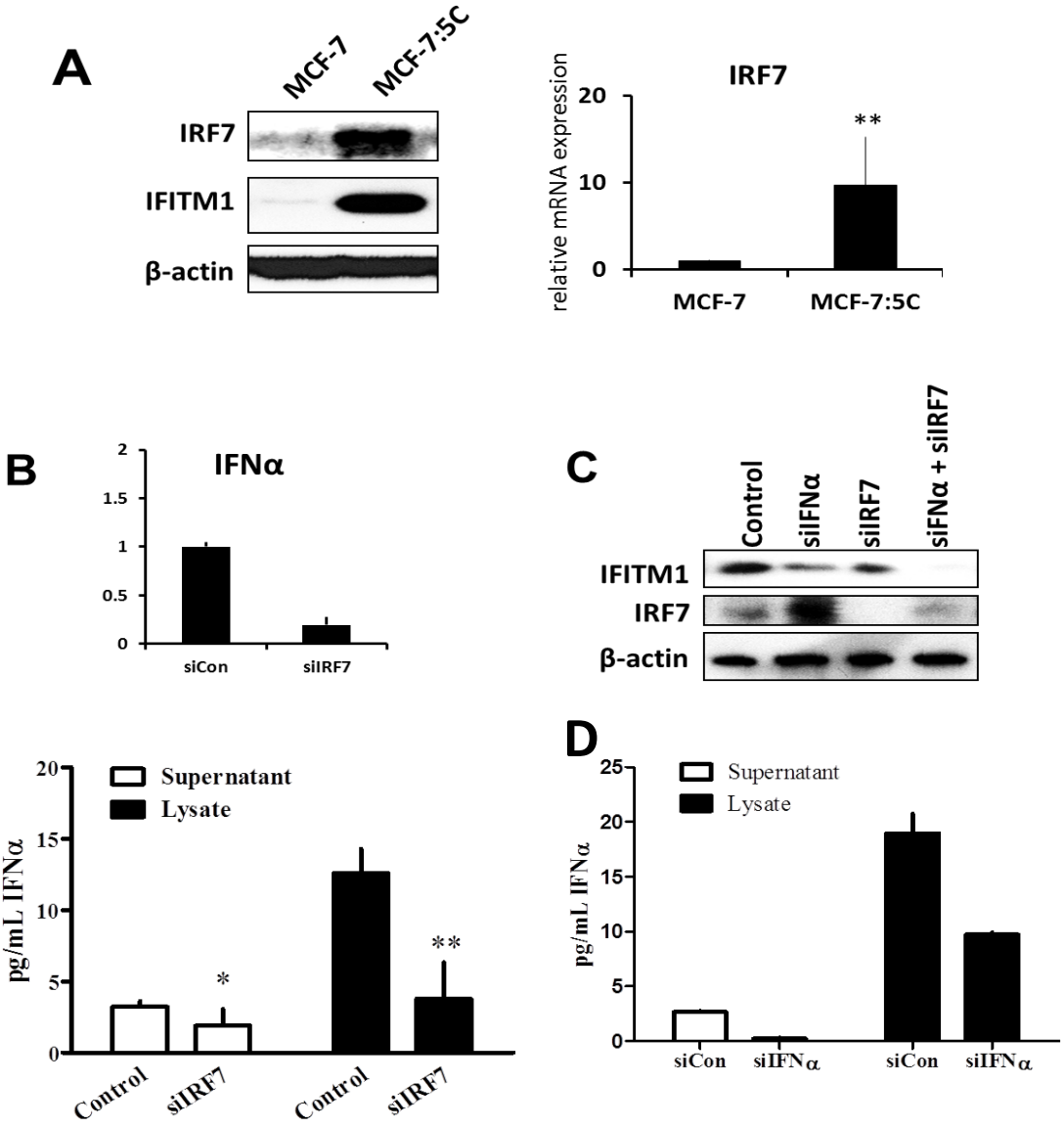

Choi & Lui et al. Breast Cancer Research. 2015 Jan 15;17:6

Figure 5.2 IFNα production is driven by interferon regulatory factor 7 (IRF-7).
(A) Whole cell lysates from MCF-7 and MCF-7:5C cells were immunoblotted for IRF-7 and IFITM1 expression. B) Measurement of IRF-7 mRNA was determined by real-time PCR. Fold change was calculated by means of the ΔΔCT method using PUM1 as an internal control. Values are displayed as relative to MCF-7 cells and are means of triplicate measurements ± SD in three independent experiments. (b) The effect of IRF-7 knockdown on IFNα expression is determined by RT-PCR and ELISA. (c) The effect of IFNα or IRF-7 knockdown on IFITM1 expression is sown by immunoblotting. (d) Confirmation of IFNα siRNA knockdown is determined by ELISA. *p <0.05 or **p <0.01.

PLSCR1 and IFITM1 at 24 hours) (Figure 5.3B). A similar trend was observed at the mRNA level for IFITM1 andPLSCR1 in resistant MCF-7:5C cells compared to parental MCF-7 cells (Figure 5.3C and Figure 5.3D). In MCF-7 cells, exogenous IFNα induced IFITM1 mRNA by approximately 374-fold, PLSCR1 mRNA by approximately 9-fold and STAT1 mRNA by approximately 11-fold at 48 hours, whereas, in resistant MCF-7:5C cells, treatment with IFNα induced IFITM1 mRNA by approximately 3-fold, PLSCR1 mRNA by approximately 2-fold, and STAT1 mRNA by approximately 2-fold. Similar results were seen when assessing IFIT1, IFI27, MX1 and OAS1 expression in MCF-7 and MCF-7:5C cells after 48 hours IFNα exposure (Figure 5.3E). These findings suggest that IFITM1 and other ISGs are constitutively overexpressed in the resistant cells due to dysregulation of interferon signaling, whereas, in parental MCF-7 cells, the interferon signaling pathway functionally intact and the induction of IFITM1 and other ISGs is tightly controlled.

STAT proteins use ISRE and GAS motifs to drive IFITM1 expression

Next, we investigated the ISRE and GAS transcriptional activity in the AI-resistant MCF-7:5C cells. Luciferase reporters with tandem GAS/STAT1 or ISRE motifs indicated that there was basal activity of both types (Figure 5.4A and Figure 5.4C). Knockdown of STAT1 and STAT2 abrogated both GAS and ISRE activity. Interestingly, knockdown of both STATs equally inhibited transcription at ISRE sites while STAT1 knockdown was more efficient at inhibiting GAS activity. These results suggest that both STAT1 and STAT2 may drive transcription at GAS and ISRE sites in MCF-7:5C cells. Inhibition of STAT phosphorylation with the JAK1/2 inhibitor ruxolitinib (Rux)

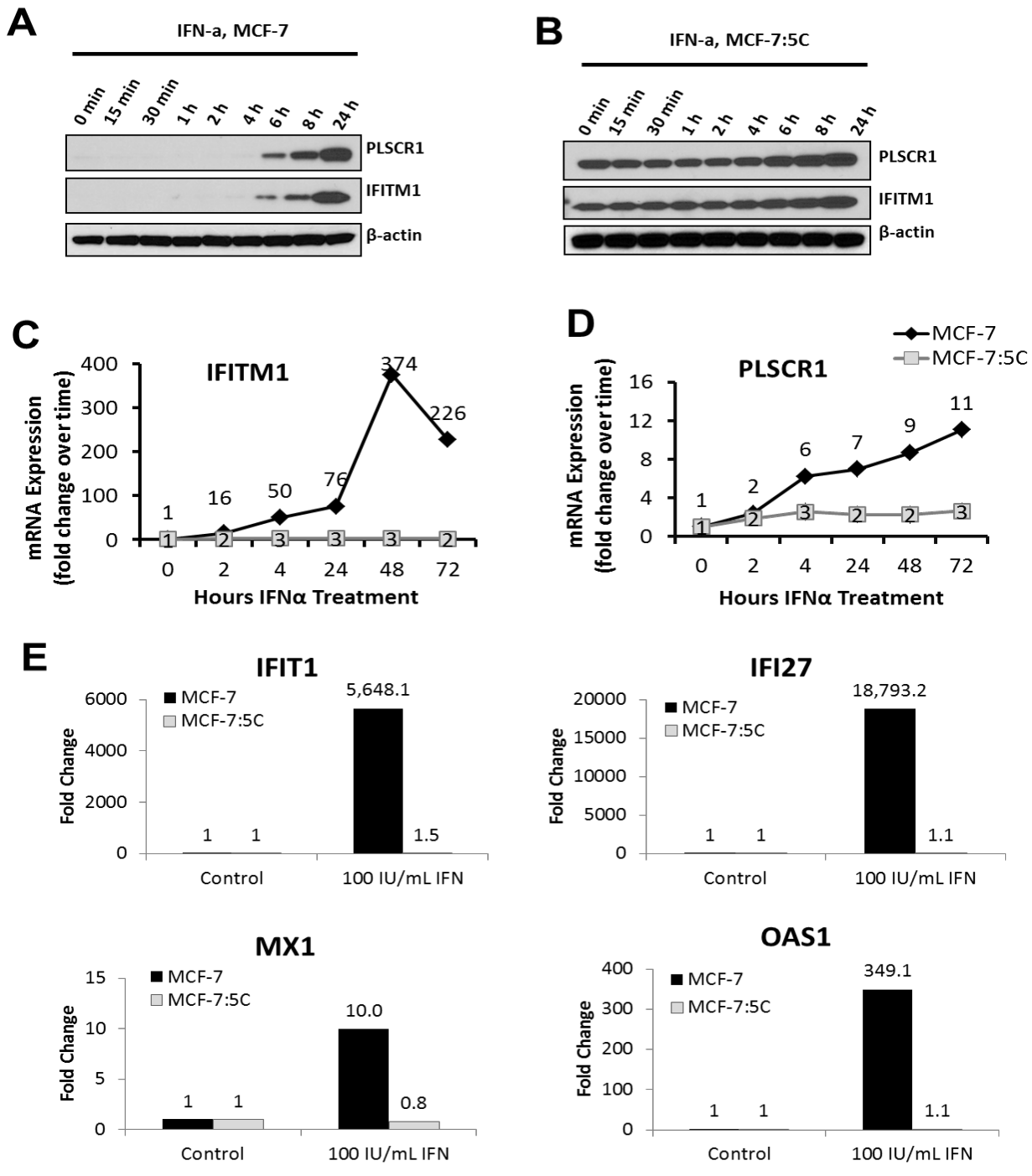

Choi & Lui et al. Breast Cancer Research. 2015 Jan 15;17:6

Figure 5.3 ISG expression in MCF-7 and MCF-7:5C cells in response to IFNα exposure.

MCF-7 and MCF-7:5C cells were treated with 100 I/U IFNα for 0-72 hours. (A and B) Whole cell lysates were harvested at the indicated time points and immunoblotted for PLSCR1 and IFITM1 expression. (C and D) Measurement of IFITM1 and PLSCR1 mRNA over time was determined by real-time PCR. Fold change was calculated by means of the ΔΔCT method. Values are displayed as relative to day 0 and are means of triplicate measurements ± SD in three independent experiments.

dramatically reduced GAS and ISRE activity in MCF-7:5C cells underscoring the importance of STAT activation in JAK/STAT signaling (Figure 5.4B and Figure 5.4D). Notably, IFITM1 promoter luciferase assay indicated that JAK/STAT signaling drove IFITM1 expression in MCF-7:5C cells. Knockdown of STAT1 and STAT2 both significantly inhibited IFITM1 transcription and IFNAR neutralization and Rux treatment had similar effects (Figure 5.4E).

To determine which specific promoter elements drive IFITM1 transcription we conducted an analysis of the IFITM1 promoter sequence using MatInspector (Genomatix). MatInspector identified several promising ISRE and STAT1 motifs, with one potential STAT1/GAS sequence at -3157 and an ISRE sequence at the -1 upstream from the transcription start site also being supported binding locations from other deposited data (Figure 5.5A). The IFITM1 promoter is classically about 750 kb and so we used chromatin immunoprecipitation (ChIP) assays to assess STAT1 and STAT2 binding at the suggested ISRE motif. ChIP assays determined that both STAT1 and STAT2 bind to the IFITM1 promoter at the -1 position and that this binding is specific to activated STATs (Figure 5.5B). There was significantly higher STAT1 and STAT2 recruitment to this site in MCF-7:5C than in MCF-7 cells (Figure 5.5B) and inhibition of STAT phosphorylation with Rux dramatically reduced STAT protein recruitment (Figure 5.5C). Taken together, these data highlight the abnormal JAK/STAT activation in MCF-7:5C cells and confirm that classic STAT signaling drives IFITM1 expression.

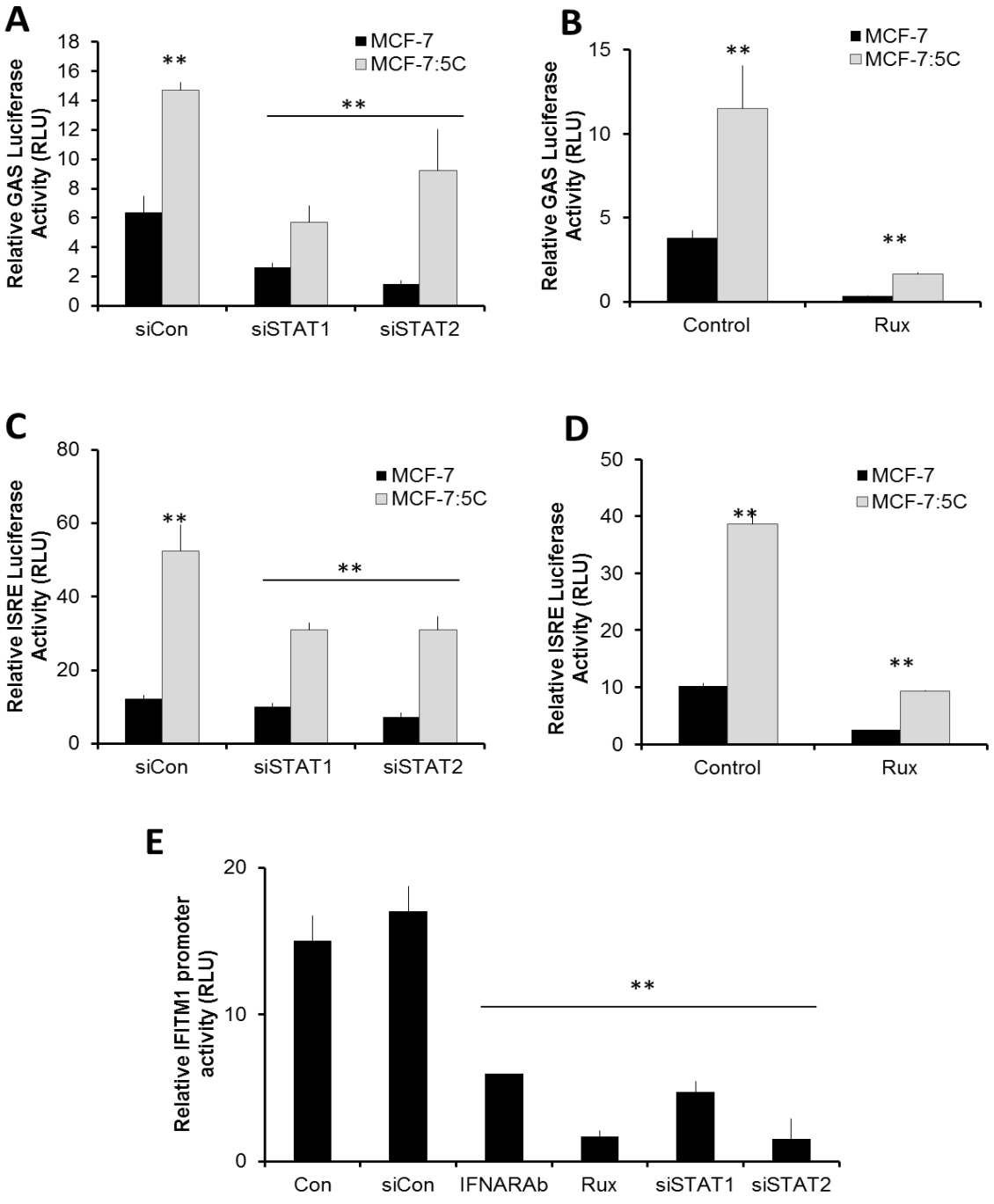

Figure 5.4 IFITM1 overexpression is driven by JAK/STAT signaling at GAS and ISRE motifs.

Relative transcriptional activity at gamma associated sequence (GAS) sites is determined by luciferase assay (A) before and after STAT1/2 siRNA transfection or (B) Rux treatment in MCF-7 and MCF-7:5C cells. Relative transcriptional activity at interferon stimulated response elements (ISRE) is determined by luciferase assay (C) before and after STAT1/2 siRNA transfection or (D) Rux treatment in MCF-7 and MCF-7:5C cells. (E) Relative transcriptional activity at the IFITM1 promoter before and after IFNAR neutralization, Rux treatment or STAT1/2 siRNA transfection is determined by IFITM1 promoter luciferase reporter.

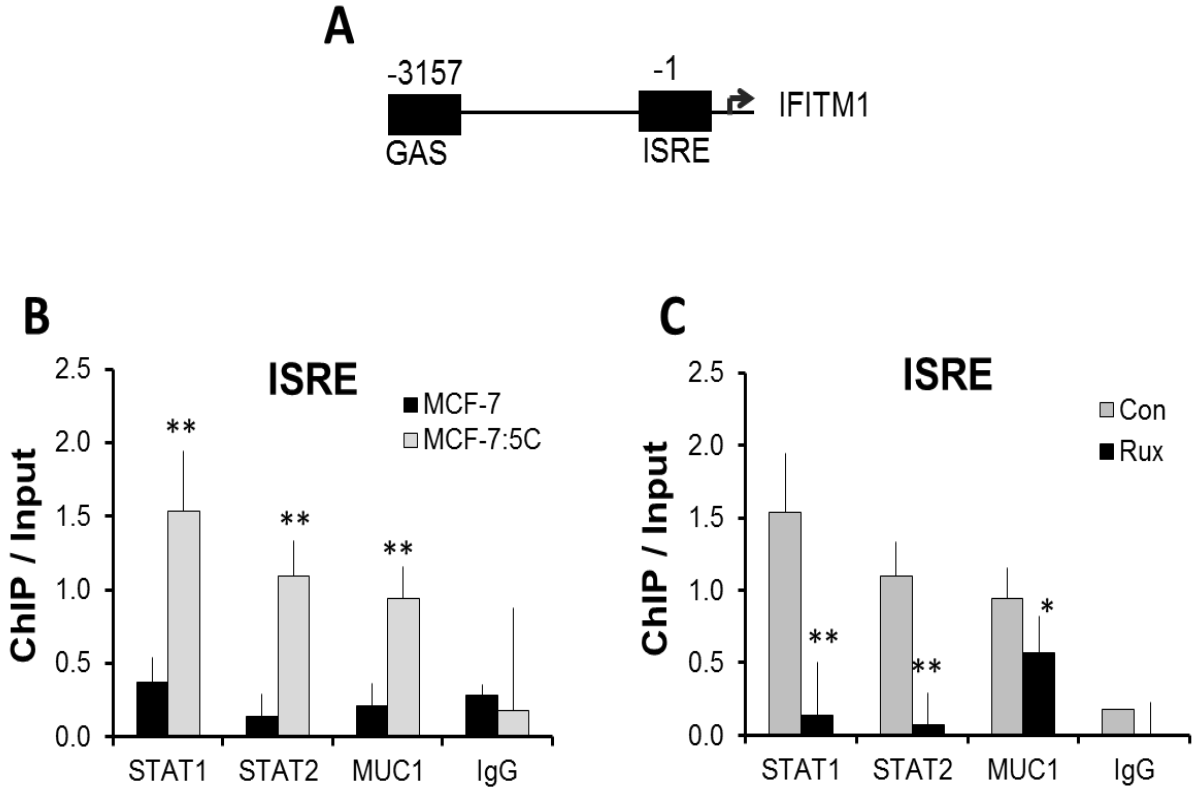

Figure 5.5 STAT1, STAT2 and MUC1 are recruited to an ISRE in the IFITM1 promoter

(**a**) ISRE and GAS binding site were identified in the IFITM1 promoter in silico using MatInspector (Genomatix). (**b**) Fixed MCF-7 and MCF-7:5C cell lysates were subjected to chromatin immunoprecipitation (ChIP) with antibodies against STAT1, STAT2, MUC1 or species specific IgG control. (**c**) Fixed whole cell lysates from MCF-7:5C cells treated with 10μM Ruxolitinib/Jakafi (Rux) for 24 hours. qPCR was performed on the isolates DNA using primers designed to amplify the ISRE regulatory regions. Recruitment of the indicates proteins to the ISRE site was compared to input DNA and displayed as mean ± SD of technical triplicates in two independent experiments.

IFITM1 can be targeted through JAK/STAT inhibition with Ruxolitinib (Jakafi™) in vivo

We previously reported that the FDA approved JAK inhibitor, Ruxolitinib (Jakafi™) dramatically reduced STAT1 phosphorylation and IFITM1 expression in the MCF-7:5C cells (Figure 5.4A). To determine whether Rux may have potential clinical relevance for IFITM1-expressing breast cancer, we used the orthotopic model to determine whether IFITM1 can be targeted *in vivo* by Rux. IFITM1-null MCF-7 and IFITM1-expressing MCF-7:5C cells were transplanted into the 4th mammary fat pad of female NSG mice and after 25 days mice were randomized to receive either vehicle (Control) or 50 mg/kg ruxolitinib by oral gavage. Rux treatment reduced STAT1 phosphorylation in MCF-7:5C tumors (Figure 5.6B) and caused a reduction in MCF-7:5C tumor growth while having little effect on MCF-7 tumor size (Figure 5.6C and Figure 5.6D). Immunohistochemistry confirmed that IFITM1 and phosphorylated STAT1 (p-STAT1) were lost in the MCF-7:5C tumors (Figure 5.6E). Notably, Rux treatment of IFITM1 expressing MDA-MB-468 tumors also resulted in smaller tumor size and loss of IFITM1 expression (Supplemental Figure 6). These data suggest that IFITM1 expression may define a subset of breast tumors that are sensitive to therapies that target JAK/STAT signaling.

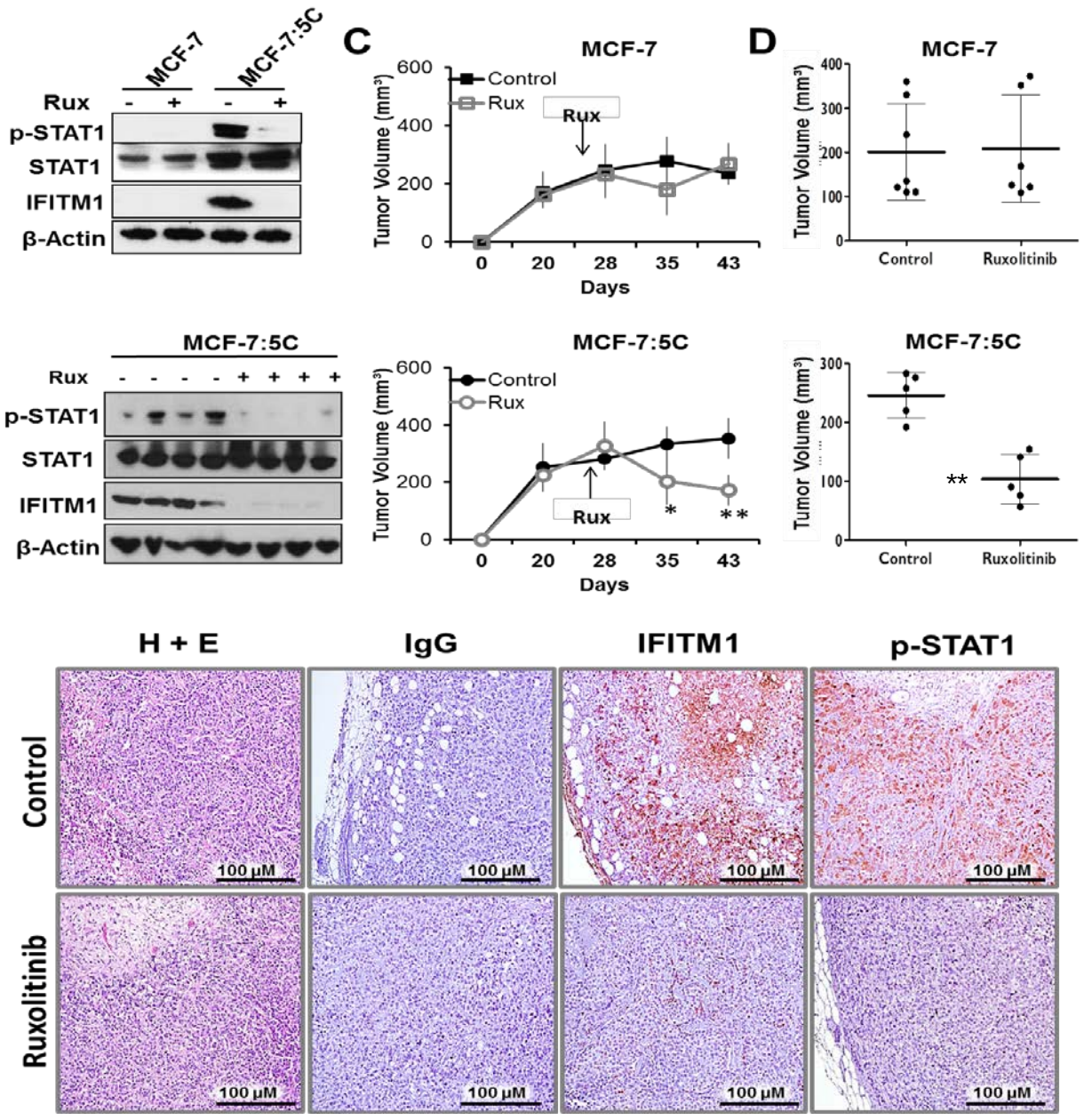

Lui et al. Cancer Letters. 2017 Apr 12;399:29-43

Figure 5.6 Inhibition of JAK/STAT signaling with Ruxolitinib decrease IFITM1 expression and reduced the growth of aromatase inhibitor-resistant MCF-7:5C tumors

(a) Whole cell lysates from MCF-7 and MCF-7:5C cells treated with 10μM Ruxolitinib/Jakafi™ (Rux) for 24 hours were immunoblotted for phospho-STAT1 (p-STAT1), STAT1 and IFITM1 protein expression. (b) 3 million MCF-7 or MCF-7:5C cells were injected into the 4th mammary fat pad of female NSG mice. After 22 days of tumor growth, mice were randomized to treatment groups and half were given 50 mg/kg Rux by oral gavage every other day. Tumor expression of phospho-STAT1 (p-STAT1), STAT1 and IFITM1 after 21 days of treatment was determined by immunoblot. (c) Tumors were measured by digital calipers and tumor volume (mm^3) displayed over time. (d) At the end of the experiment tumors were excised and tumor volumes were determined by digital caliper measurement. (e) Tumors were fixed, embedded in paraffin and sectioned onto glass slides. Hematoxylin and Eosin (H+E) staining revealed tumor architecture and IFITM1 and phospho-STAT1 (p-STAT1) expression was determined by immunohistochemistry.

MUC1 expression is dysregulated in AI-resistant MCF-7:5C cells

Since MUC1 is one of the most overexpressed proteins in breast cancer and is known to interact with JAK/STAT signaling, we next investigated whether MUC1 was actually expressed in MCF-7:5C cells. We found that MUC1 is more highly expressed in AI-resistant MCF-7:5C cells than in expressed in parental MCF-7 cells (Figure 5.7A). Notably, another estrogen-independent clone, MCF-7:2A, that does not express IFITM1 or have constitutive JAK/STAT signaling also expressed MUC1 at low levels (Figure 5.7A). MUC1 is an estrogen-responsive gene that is normally transcribed in response to estrogen exposure so we next investigated the hormonal regulation of MUC1 expression in MCF-7:5C cells. Treatment with 1nM estradiol (E2) significantly reduced MUC1 expression at the protein and mRNA level which is directly in contrast to the effect of E2 on MCF-7 cells (Figure 5.7). Treatment with the pure anti-estrogen fulvestrant (FUL or ICI) had the opposite effect and instead increased MUC1 mRNA and protein expression in MCF-7:5C cells (Figure 5.7). These data indicate that MUC1 expression is hormonally controlled in a manner in direct contrast to canonical regulation and is unique to IFITM1 overexpressing AI-resistant breast cancer cells.

MUC1 stabilizes JAK/STAT signaling which is necessary for IFITM1 expression

It should be noted that JAK/STAT signaling is also known to contribute to MUC1 expression. We found that both STAT1 knockdown and Rux treatment reduce IFITM1 and MUC1 expression indicating that in the MCF-7:5C cells, constitutive JAK/STAT activation helps to maintain MUC1 expression in the absence of estrogen (Figure 5.8A). Next, we investigated whether MUC1 plays a role in IFITM1 expression. Co-immunoprecipitation studies revealed that MUC1 and p-STAT1 interact (Figure 5.8B).

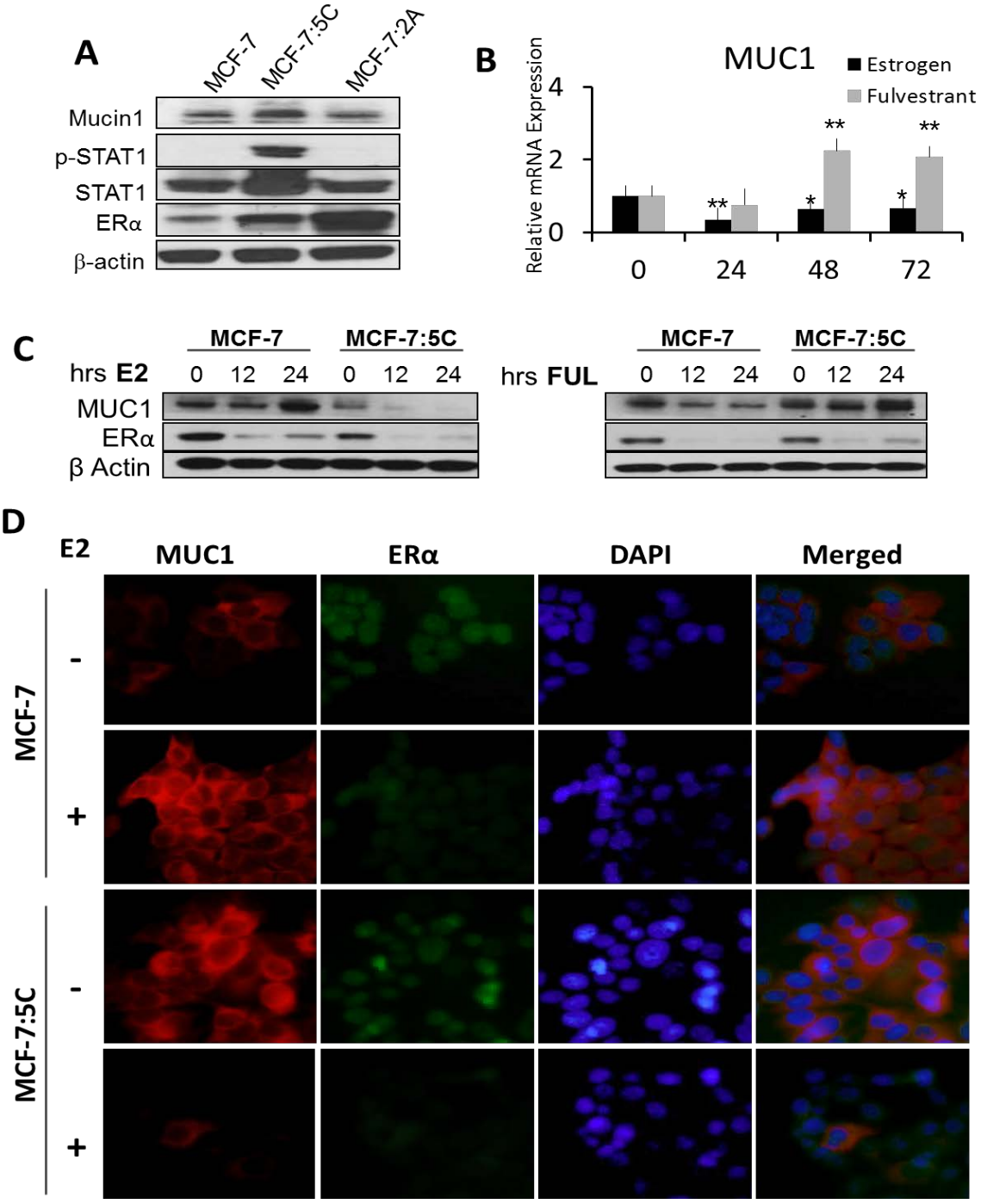

Figure 5.7 MUC1 expression is dysregulated in MCF-7:5C cells

(a) Whole cell lysates for MCF-7, MF-7:5C and MCF-7:2A cells were immunoblotted for MUC1, p-STAT1, STAT1 and ERα expression. (b) MCF-7:5C cells were treated with 1nM estradiol (E2) or 1uM fulvestrant (FUL). MUC1 mRNA expression was determined by RT-PCR at 0, 24, 48 and 72 hours. Fold change was calculated by the ΔΔCT method. Values are displayed as relative to day 0 and are means of triplicate measurements ± SD in two independent experiments. (c) Whole cell lysates were collected at 0, 12 and 24 hours and immunoblotted for MUC1 and ERα protein expression. (d) MCF-7 and MCF-7:5C cells were treated with 1nM estradiol and fixed after 24 hours. Immunofluorescent staining was used to asses MUC1 and ERα expression and localization. *p<0.05 ** p<0.01

Notably, when STAT1 is not phosphorylated (Rux treated) MUC1 binding is significantly reduced, suggesting that STAT1 must be phosphorylated prior to MUC1 interaction (Figure 5.8B). Loss of MUC1 activity either with siRNA knockdown or treatment with the MUC1 inhibitor GO-201 reduced STAT1 phosphorylation and IFITM1 expression (Figure 5.8C and Figure 5.8D). This result indicates that MUC1 stabilizes the phosphorylation status of STAT1 protein and that this phosphorylation is required for IFITM1 transcription. Significantly, MUC1 knockdown reduced IFITM1 mRNA expression and transcription (Figure 5.8E and Figure 5.8F).

MUC1 knockdown enhances estrogen-induced death through additive inhibition of IFITM1 expression

Since we have previously reported that loss of IFITM1 induces cell death of AI-resistant MCF-7:5C cells, we next investigated the effect of MUC1 knockdown on cell survival. Annexin V/ PI staining revealed that MUC1 knockdown also induces cell death, likely due to the inhibition of IFITM1 expression that results (Figure 5.9A). Here, we reported that estradiol treatment reduces MUC1 expression, which is critical to the maintenance of JAK/STAT signaling and IFITM1 expression in AI-resistant MCF-7:5C cells. Notably, MUC1 knockdown enhanced estrogen-induced death, suggesting a role for targeting MUC1 in conjunction with estrogen therapy (Figure 5.9B). We then determined whether estradiol directly affected IFITM1 expression and found that indeed, estradiol exposure reduced IFITM1 expression over time (Figure 5.9C). This finding is consistent with previous reports that estrogen induces apoptosis in MCF-7:5C and other LTED cell lines and tumors. We conclude that IFITM1 loss may be one of the mechanisms of estrogen-induced apoptosis which explains why both MUC1 knockdown

and estrogen treatment induce cell death. Finally, we conducted in silico analysis of deposited tumor expression data at cbioportal.org and we found that MUC1 and IFITM1 overexpression co-occurs in 4 separate breast cancer datasets (Figure 5.10).

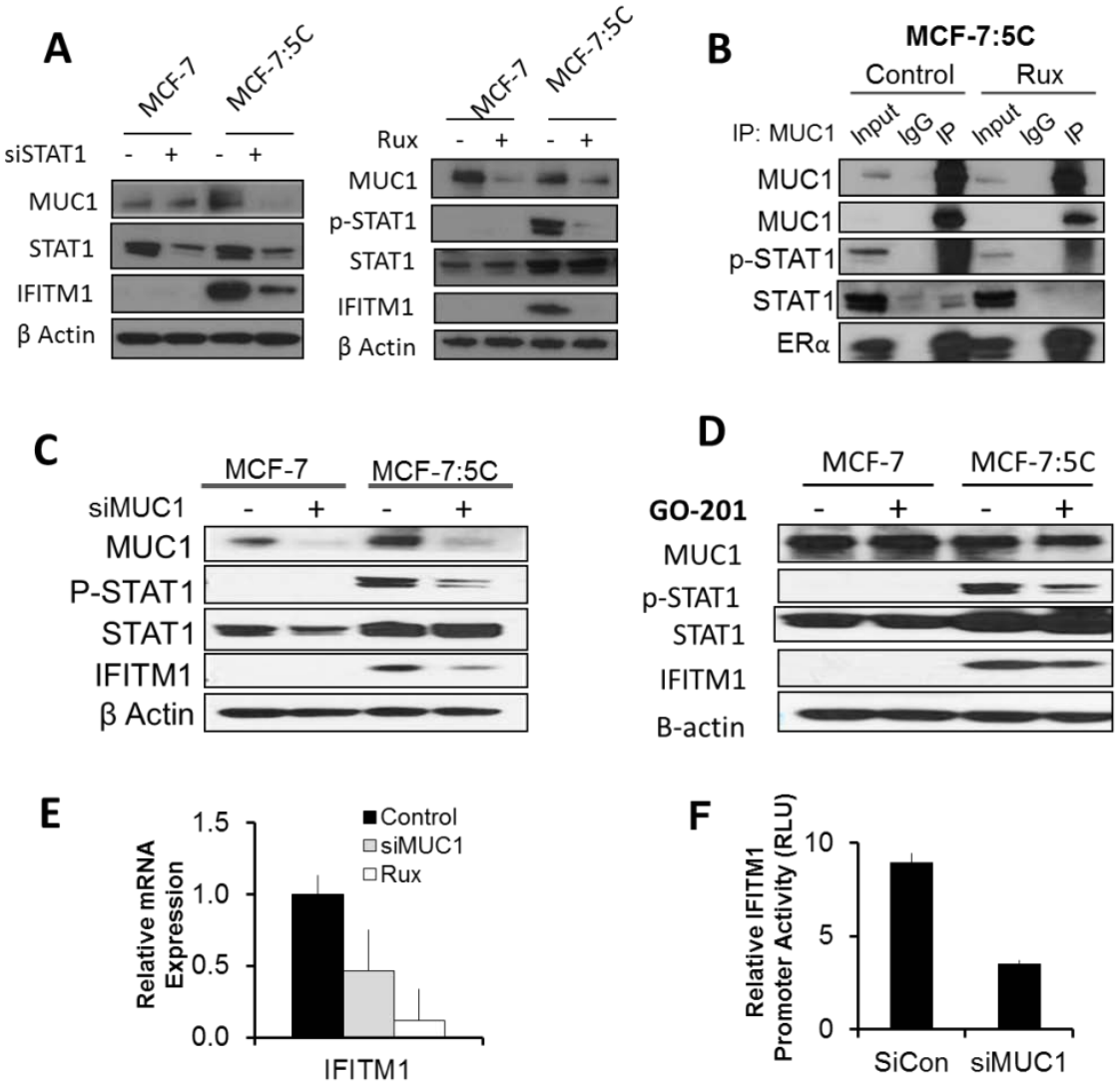

Figure 5.8 MUC1 stabilizes JAK/STAT signaling through interaction with p-STAT1

(a) MCF-7 and MCF-7:5C cells were either transfected with STAT1 siRNA or treated with 10μM Ruxolitinib/Jakafi (Rux). Whole cell lysates were immunoblotted for MUC1, p-STAT1, STAT1 and IFITM1 expression. (**b**) Whole cell lysates from MCF-7:5C cells treated with vehicle (Con) 10μM Ruxolitinib/Jakafi (Rux) for 24 hours were immunoprecipitated with anti-MUC1 antibody or rabbit IgG and samples immunoblotted for MUC1, ERα, p-STAT1 and STAT1 protein interaction. MCF-7 and MCF-7:5C cells were transiently transfected with MUC1 siRNA (c) or treated with MUC1 inhibitor (GO-201) (d). After 24 hours, MUC1, p-STAT1, STAT1 and IFITM1 expression were determined by immunoblotting. (e) MCF-7:5C cells were transiently transfected with control or MUC1 siRNA or treated with Rux. After 24 hours, mRNA expression of IFITM1 was determined by RT-PCR. (f) IFITM1 promoter activity was measured by luciferase assay in MCF-7:5C cells transiently transfected with control or MUC1 siRNA. Relative light units (RLU). *p<0.05 ** p<0.01

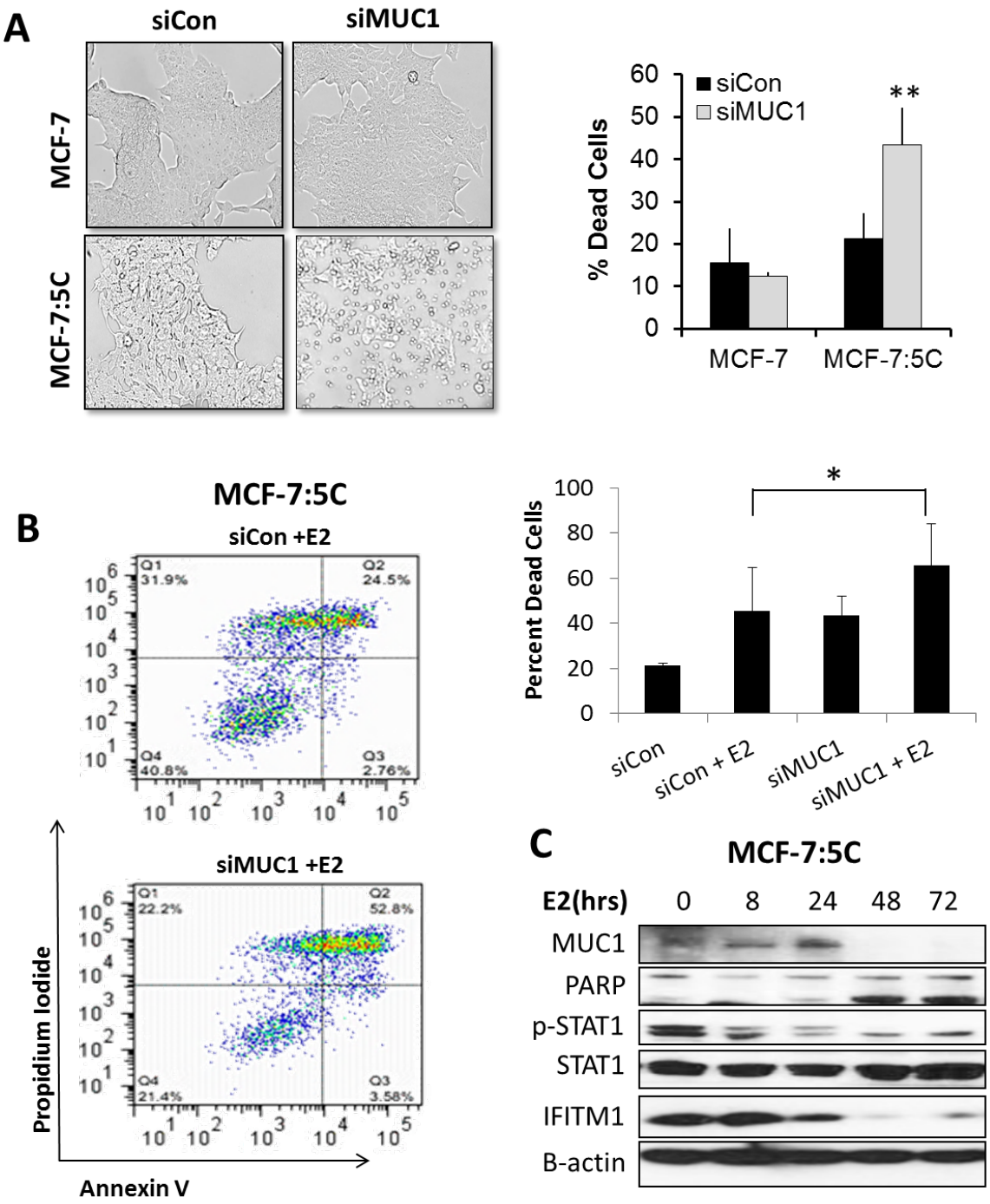

Figure 5.9 Loss of MUC1 induces death of AI-resistant MCF-7:5C cells

(a) MCF-7 andMCF-7:5C cells were imaged at 20X 72 hours after transient transfection with control (siCon) or MUC1 (siMUC1) siRNA and the percent of dead cells was determined by AnnexinV/PI Staining (right panel). (b) After transient siCon or siMUC1 transfection, MCF-7:5C cells were treated with 1nM estradiol (E2) for 72 hours and the percent dead cells measured by Annexin V/PI staining (quantified in right panel). (c) Whole cell lysates from MCF-7:5C cells were treated with 1 nM E2 for 0-72 hours and immunoblotted for MUC1, PARP, p-STAT1, STAT1, and IFITM1 expression. *p<0.05 ** p<0.01

A

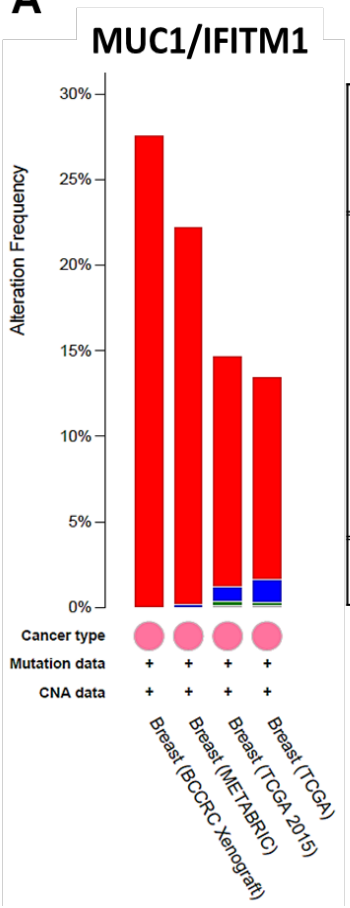

B

	Sample Size (n)	p-value (Fisher Exact Test) MUC1/IFITM1	Log odds ratio MUC1/IFITM1	Result
BCCRC Xenograft	116	0.014	3	Association towards co-occurrence (Significant)
METABRIC	2509	0.051	0.392	Association towards co-occurrence
TCGA 2015	817	0.115	0.935	Association towards co-occurrence
TCGA	825	0.002	1.484	Association towards co-occurrence (Significant)
Total (n)/AVG	**4151**	**0.0455**	**1.453**	
Std Dev		0.0566	1.124	

Log odds ratio > 0 : Association towards co-occurrence
Log odds ratio <= 0 : Association towards mutual exclusivity
p-Value < 0.05 : Significant association

Figure 5.10 MUC1 and IFITM1 co-occur in breast cancer

(a) In silico analysis of tumor gene expression using the cbioportal.org database for deposited breast tumor expression for both MUC1 and IFITM1 expression resulted in four datasets with singificant overexpression of both proteins. (b) Fisher Exact test on each of the four datasets was conducted to determine likelihood of co-occurrence of MUC1 and IFITM1 in breast cancer.

DISCUSSION

Inflammation is often thought of as a double edged sword in the human body. While it is known that uncontrolled inflammation in general causes disease, we also know that some inflammatory response is necessary for the clearing of infections and the healing of wounds. In cancer, inflammation has also exhibited this contradiction. The role of inflammation in increasing the risk for gastrointestinal cancers is well accepted. Alternatively, the presence of inflammatory cells in other solid tumors has been established as a positive prognostic sign because it indicates the successful anti-tumor activity of the immune system. One possible reason for this contradiction is the lack of distinction between an inflammatory immune response and an IFN-related gene signature within a tissue.[53] While inflammation and IFN signaling is necessary for the cells of the immune system to launch a successful defense against pathogens and tumors, it also seems to aide epithelial cells in altering their restraints on growth and proliferation, ultimately resulting in cancer.[198,199] The majority of studies into the relationship of IFNs to the cancer process focus on the actions of IFNγ on the immune system and tumors themselves but the actions of type I IFNs are less well-known. Short-term AI-therapy has been shown to induce an inflammatory gene signature in breast cancer patients but mechanisms remain unclear. [200] Within a cancer cell, the type I IFN pathway is one of the systems that can be utilized to promote survival. In several types of solid cancers, a number of ISGs have been implicated in DNA damage resistance, making the tumor insensitive to chemotherapy and radiation (Table 1.1).

Here, we found that IFITM1 overexpression is mediated by constitutive production of IFNα which drives JAK/STAT signaling through IFNAR. We reported that

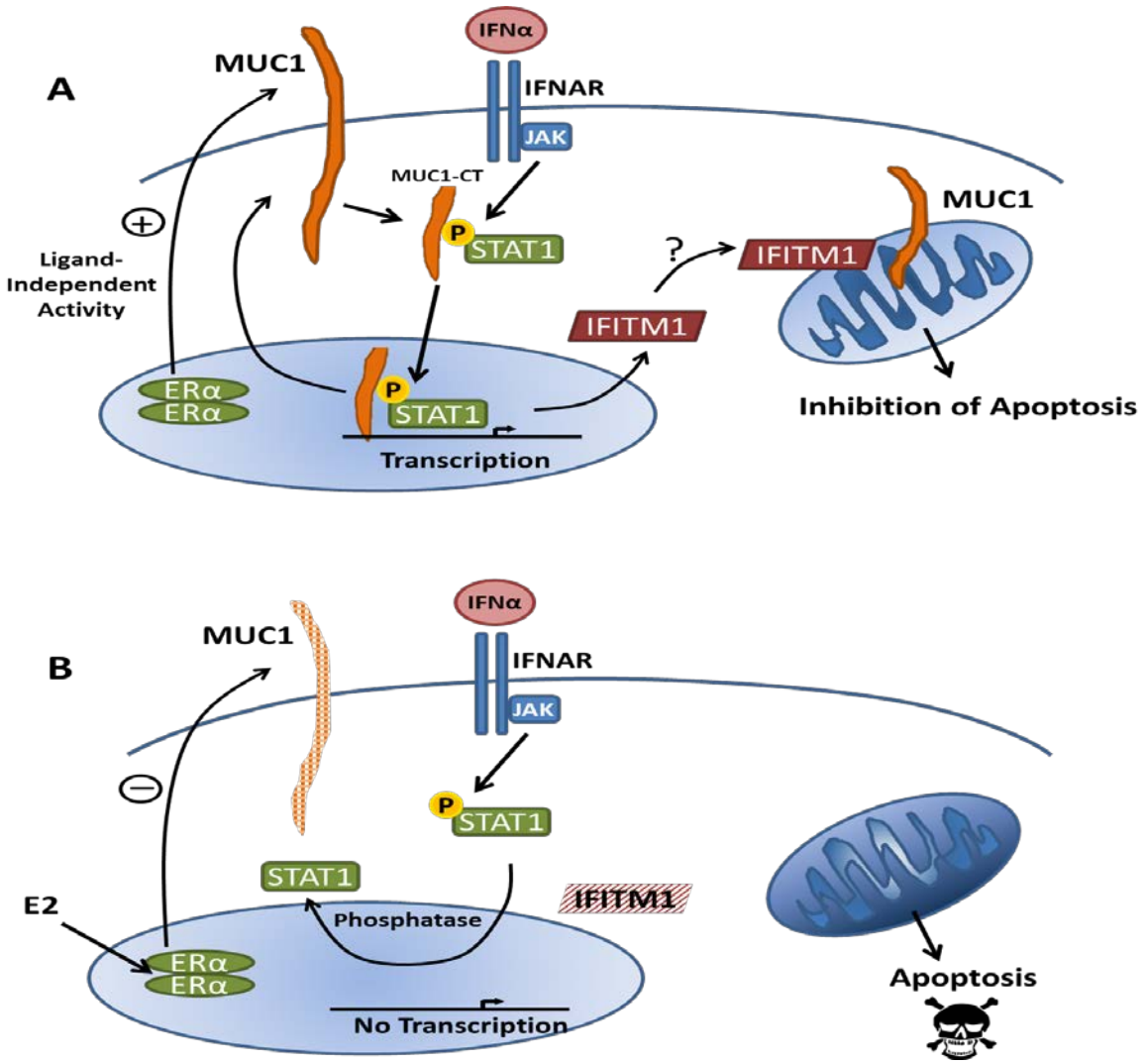

Figure 5.11 The role of MUC1 in JAK/STAT mediated IFITM1 overexpression and estrogen-induced apoptosis

(a)In MCF-7:5C cells IFITM1 expression is stimulated by JAK/STAT signaling from IFNAR. Mucin 1 (MUC1), an estrogen receptor (ERα) controlled gene is constitutively expressed by ligandindependent activity of ERα. MUC1 is expressed on cellular and mitochondrial membranes wherer it inhibits apoptosis. IFITM1 and other ISGs may also be present on the mitochondrial membrane to prevent apoptosis. MUC1 is cleaved at the membrane and the C-terminus of MUC1 (MUC1-CT) binds to and stabilizes STAT phosphorylation. Upon estrogen exposure, MUC1 is lost and JAK/STAT signaling is no longer maintained leading to a loss of IFITM1 expression and apoptosis.

STAT1 and STAT2 are continually phosphorylated which allows for continual transcription at ISRE and GAS motifs in AI-resistant cells, especially an ISRE sequence directly adjacent to the IFITM1 transcription start site. The fact that knockdown of IFNα dramatically reduced IFITM1 expression in the resistant cells and its loss significantly

induced cell death highlights the potential dependency of the resistant cells on elevated IFNα to maintain their resistant phenotype and to drive the constitutive overexpression of IFITM1 and the other ISGs in the cells. We should note that elevated IFN production has previously been reported in many pathological conditions, such as chronic inflammation and cancer, as well as in virus infections.[201] In cancers, IFN production is thought to be increased by infiltrating immune cells or by the cancer cells themselves.[72,202] Notably, we also discovered that MUC1 promotes IFITM1 expression by stabilizing the phosphorylated status of STAT1 in MCF-7:5C cells. MUC1 expression itself is dysregulated in the MCF-7:5C cell line, with estrogen treatment reducing not only MUC1 expression but also IFITM1 during estrogen-induced death. These data underscore the key role that MUC1 plays in driving JAK/STAT mediated IFITM1 overexpression (Figure 5.11). It is possible that combination of IFITM1 and MUC1 inhibition may hold promise as the basis of a novel therapy for AI-resistant breast cancer.

Ruxolitinib (Jakafi®) is a JAK1/2 inhibitor that prevents STAT phosphorylation and is currently approved by the FDA for treatment of myelofibrosis. We have found previously that IFITM1 expression in breast cancer is driven by IFNα production and constitutive JAK/STAT activity.[59,73] Ruxolitinib treatment prevents IFITM1 expression and is currently being investigated in clinical trials as an alternative therapy in treatment-refractory breast cancer (NCT01562873, NCT02041429, NCT01594216). Our study suggests that high IFITM1 expression may define a subset of breast cancer that is most sensitive to ruxolitinib therapy. In fact, we have found that oral ruxolitinib treatment can cause shrinkage of MCF-7:5C xenografts. We and others propose that harnessing

ruxolitinib therapy for use in treatment of solid tumors should be explored.[203] It should be noted that ruxolitinib treatment is associated with several side effects including anemia, neutropenia, thrombocytopenia, dizziness and gastrointestinal distress. Additionally, ruxolitinib suppresses the immune system and there is concern for increased susceptibility to infection. This study suggests that MUC1 overexpression may also help define the subset of ISG-dependent breast cancers and that MUC1 inhibition could be developed for treatment of ISG-overexpressing breast cancer. Developing alternative methods for inhibiting IFITM1 will require further study into the drivers of IFITM1 overexpression and a better understanding of structure and function of this protein.

MATERIALS AND METHODS

ELISA

Measurement of human interferon-α (IFNα) was conducted by ELISA (PBL Interferon Source, Piscataway, NJ). One million MCF-7 or MCF-7:5C cells were seeded in 6-well plates and allowed to acclimatize overnight. Cells and supernatants were harvested after 24 hours and kept at -80°C until analysis. Protein was extracted by sonication in RIPA buffer supplemented with protease and phosphatase inhibitors. Supernatants and lysates were purified by centrifugation and analyzed for the presence of IFNα according to the manufacturer's instructions.

IFNAR neutralization

In order to achieve neutralization of IFNAR, cells were pretreated with 5μg/mL anti-IFNAR2/MMHAR2 from Millipore, Temecula, CA (cat# MAB1155) for 4 hours and then overnight with 20 U/mL human recombinant IFNα (Sigma) or 1nM E2 (Sigma) where indicated. Cells were harvested by cell scraping for western blot and by trypsinization for cell viability analysis with trypan blue.

Luciferase Assays

For Gamma Associated Sequence (GAS/STAT1) assays and Interferon Stimulated Response Element (ISRE) assays, the Cignal™ Reporter Assay (#CCS-009L and #CCS-008L) were used for analysis of STAT1/STAT1 homodimer and STAT1/STAT2 heterodimer transcriptional activity, respectively and was utilized according to manufacturer's instructions. Briefly, the reverse transcription protocol was used where cells were suspended in Opti-MEM and seeded in 96-well plates on top of already aliquoted transfection cocktail. This cocktail contained Lipofectamine 2000™ and the

GAS Reporter, which is a mixture of an inducible reporter plasmid containing tandem GAS-responsive elements upstream of a firefly luciferase construct and a constitutively expressing Renilla luciferase construct. After overnight incubation, the mixture was replaced with normal media containing Ruxolitinib where indicated. Luciferase and Renilla activities were measured 24 h later using the Dual-Luciferase® reporter assay kit (Promega) according to the manufacturer's instructions on a BioTek Synergy 4 microplate reader using the Gen 5 data analysis software (BioTek Instruments).

Co-immunoprecipitation

For co-immunoprecipitation (CoIP) experiments, cell lysates were collected in RIPA buffer supplemented with protease and phosphatase inhibitors and sonicated on ice. Cell lysates containing equivalent protein concentrations (5 µg) were pre-cleared with 50:50 Protein A/G coated magnetic beads (Roche Diagnostics) then incubated overnight at 4°C with 2 µg appropriate antibody or control IgG. 50:50 Protein A/G coated magnetic beads were then added for the final 1 h of incubation time. Immune complexes were washed three times with PBS and, resuspended in Laemmli sample buffer containing dithiothreitol and β-mercaptoethanol (Invitrogen) boiled for 5 min and subjected to western blotting analysis.

Chromatin Immunoprecipitation (ChIP) Assay

ChIP was performed using the ChIP-IT Express Kit (Active Motif) according to the manufacturer's instructions using sonication as the method for chromatin shearing. Lysates were immunoprecipitated (IP) overnight (18 h) with the following antibodies STAT1, STAT2, MUC1 (Santa Cruz) or an equal amount of mouse or rabbit IgG. Resulting DNA was analyzed using qPCR as described previously [204], and data are

represented as a percentage of input DNA. *In silico* analysis using MatInspector (Genomatix) identified potential STAT1-binding sites and ISREs.

Oral Treatment of Mice with Ruxolitinib

See Orthotopic Cell Line Transplantation above.

SUPPLEMENTAL FIGURES

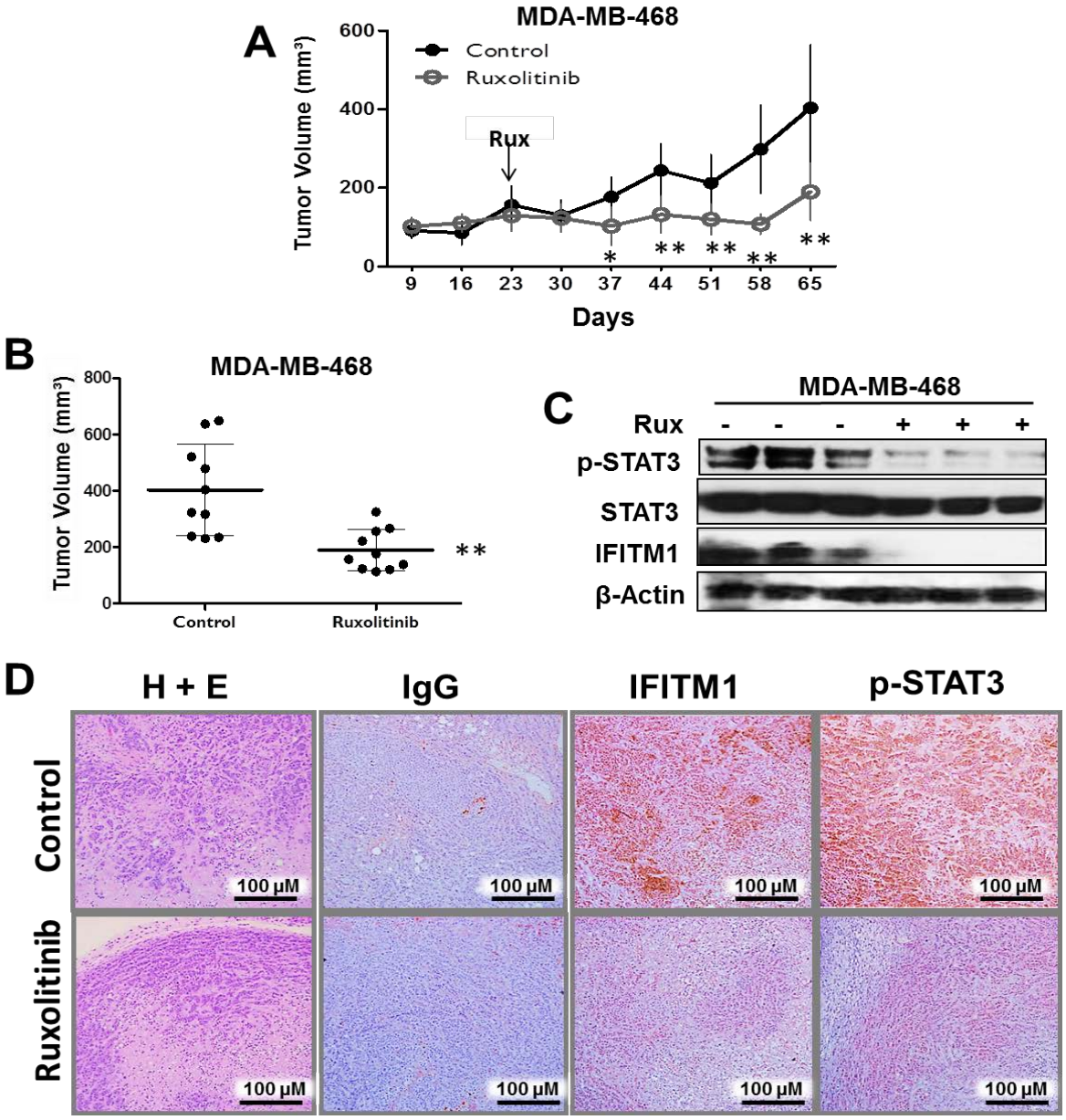

Lui et al. Cancer Letters Cancer Letters. 2017 Apr 10;600:80-43

Supplemental Figure 5.1 Inhibition of JAK/STAT signaling with Ruxolitinib (Jakafi) decreased IFITM1 expression and reduced the growth of IFITM1 overexpressing MDA-MB-468 cells.

3 million MDA-MB-468 cells were injected into the 4^{tn} mammary fat pad of female NSG mice. After 23 days of tumor growth, mice were randomized to treatment groups and half were given 50 mg/kg Rux by oral gavage three times per week. (**a**) Tumors were measured weekly by digital calipers and tumor volume (mm^3) displayed over time. (**b**) At the end of the experiment tumors were excised and final tumor volumes were determined by digital caliper measurement. (**c**) Immunoblotting on lysates from three tumors in separate mice determined expression of phospho-STAT3 (p-STAT3), STAT3 and IFITM1 after 42 days of treatment. (**d**) Tumors were fixed, embedded in paraffin and sectioned onto glass slides. Hematoxylin and Eosin (H+E) staining revealed tumor architecture and IFITM1 and phospho-STAT3 (p-STAT3) expression was determined by immunohistochemistry.

CHAPTER 6 : CONCLUSION AND FUTURE DIRECTIONS

This thesis demonstrated that overexpression of the ISG IFITM1 is driven through constitutive hyperactivation of JAK/STAT signaling which promotes AI-resistant breast cancer cell aggression and survival (Figure 6.1). The MIND model served as a tool for assessing invasion *in vivo* in addition to reflecting the effect of IFITM1 on proliferation and survival seen in the orthotopic model. Loss of IFITM1 caused cell death through an induction of p21 transcription and nuclear translocation (Figure 4.5 and Figure 6.1). Future studies are needed to determine the role that IFITM1 plays in p21 cellular localization. Our data suggests that IFITM1 may be a targetable marker of aggressive breast cancer and that development of an IFITM1 specific inhibitor may hold promise for treatment refractory breast cancer. Until that therapy is developed, this work suggests that some combination of estrogen therapy with MUC1 or JAK/STAT inhibition can be harnessed as an alternative therapy for AI-resistant breast cancer. MUC1 and JAK inhibitors are currently under study in clinical trials for stage IV breast cancer.

Type I interferons (IFNs $\alpha$and β) are known to drive the expression of ISGs that encode proteins that possess anti-viral, anti-proliferative, pro-apoptotic and pro-inflammatory functions; however, many experimental data have shown that high expression of IFN-induced genes, including STAT1 itself, promotes tumor growth, metastasis and resistance to chemotherapy and radiation.[67-69,126,205] Normally, IFNs induce rapid activation of STATs through phosphorylation on the C-terminal tyrosine residues (Y701 for STAT1 and Y690 for STAT2) which drives the expression of ISGs.[206] Several important negative feedback mechanisms collaborate to terminate the expression of these genes several hours after IFN stimulation; for example, expression

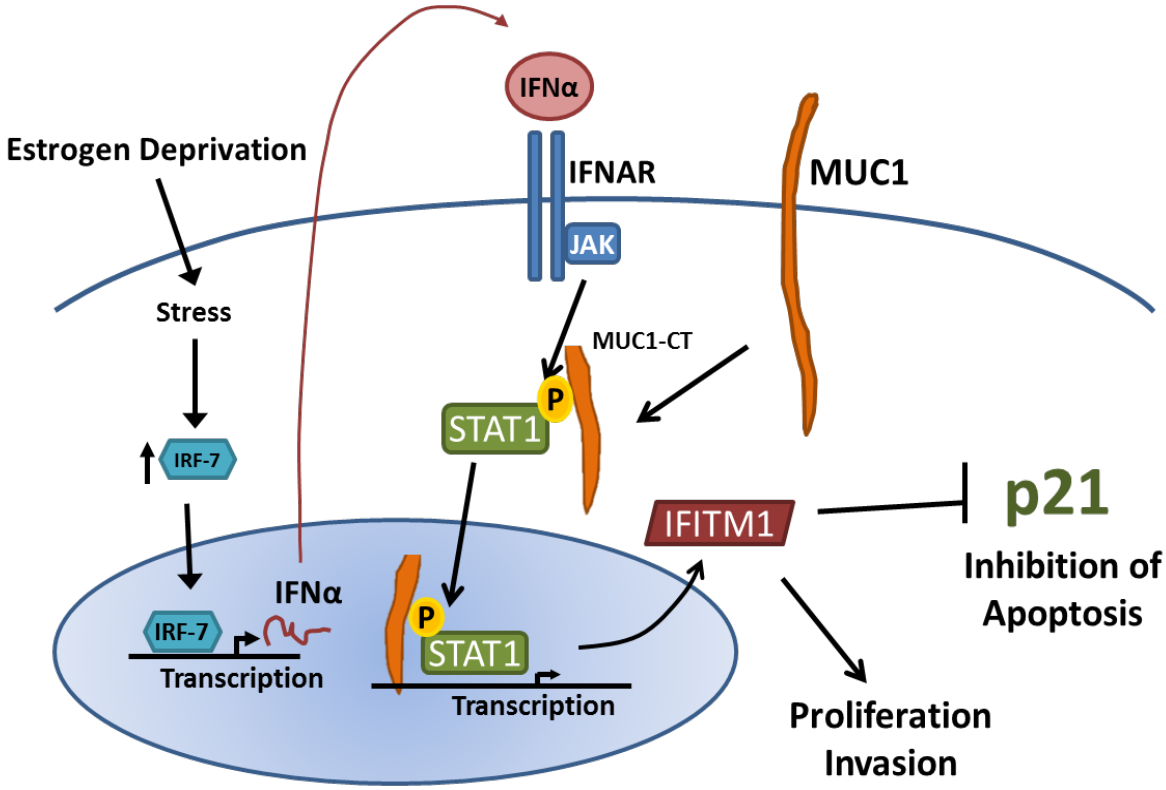

Figure 6.1 IFITM1 overexpression is driven by JAK/STAT signaling from IFNAR and is stabilized by MUC1.

of the potent negative regulator SOCS1 is rapidly induced by IFNs.[207] Sustained expression of ISGs and their encoded proteins was previously thought to be deleterious to cell survival; however, recent studies suggest that sustained expression of a subset of ISGs and their encoded proteins might provide a survival advantage to cells.[6,54] We should note that ER+ breast cancer cells are dependent on estrogen for survival and growth and when they are deprived of estrogen they tend to die. Long term, however, some breast cancer cells develop strategies to allow them to survive and grow in an estrogen-depleted environment.[46,48,108] In our working model shown in Figure 6.1 IFITM1 overexpression is driven by JAK/STAT signaling from IFNAR and is stabilized by MUC1., we propose that in AI-resistant MCF-7:5C breast cancer cells long term

estrogen deprivation induces the transcription factor and stress response gene IRF-7 to stimulate the production of IFNα which is then secreted from the cells and binds to the IFNAR1/2 to induce JAK/STAT signaling and the expression of ISGs (including IFITM1, PLSCR1, IFIT1, IFI21, OAS1, MX1, STAT1, STAT2, IRF-7, IRF-9). MUC1 stabilizes the constitutive JAK/STAT signaling in MCF-7:5C cells and allows for persistent STAT-mediated transcription in the nucleus. We have found that IFITM1 promotes cell survival, AI-resistance and tumor proliferation and invasion. Thus, we propose that constitutive overexpression of the ISGs provides a survival advantage to the resistant cells that allows them to adapt and grow in an estrogen-depleted environment.

There have been many studies into the mechanism(s) of AI-resistance which have revealed the role of several other cellular pathways that control cell proliferation, survival and growth. The proposed project differs from previous studies because of the unique model of AI-resistance that is being utilized and the distinctive cellular pathway that is altered in this model. Other popular models of AI-resistance rely upon artificial expression of the human aromatase enzyme, maintenance in cellular media that contains estrogen precursors and then long-term treatment with an aromatase inhibitor.[208] Our model of AI-resistance more directly mimics what a breast cancer experiences during AI therapy. As breast epithelium does not normally express the aromatase enzyme, a breast cancer cell does not develop resistance by direct action of the drug but by depleting the circulating estrogen. A breast cancer cell experiences a sudden drastic decrease in the estrogen available for growth and proliferation. The simplicity of long-term estrogen deprivation makes our model more relevant. The other major difference in our system is the intrinsic up-regulation of type 1 IFN signaling in

direct response to estrogen deprivation. ISGs play a role in the progression of colorectal, pancreatic and ovarian cancer but the expression of ISGs has not been seen in previous models of breast cancer much less in AI-resistant breast cancer. Our system provides a novel tool for investigating the novel role that this pathway plays in AI-resistance. Identification of another AI-resistant cell line that constitutively overexpresses IFITM1 remains a goal of the laboratory.

Breast cancer can be separated into estrogen receptor/ progesterone receptor positive (ER+/PR+), Her2/neu positive (HER2+), and triple negative (ER-/PR-/HER2-) subtypes. We have, screened a panel of nine cell lines that represent all major subtypes of breast cancer and found IFITM1 overexpression in triple negative MDA-MB-468 and MDA-MB-157, and triple negative inflammatory SUM149 cells. Inflammatory breast cancer is a highly lethal subtype of breast carcinoma that may express any of the three aforementioned receptors. Notably, knockdown of IFITM1 in SUM149 cells using CRISPR/Cas9 dramatically reduces aggression *in vitro* and *in vivo* in a similar manner to AI-resistant MCF-7:5C cells. While there is marked inhibition of tumor proliferation and invasion, IFITM1 knockdown does not induce cell death in this model. We recently have also gained access to a triple negative breast cancer tissue microarray and found elevated IFITM1 expression as compared to normal breast tissue. Interestingly, this overexpression is most pronounced in TNBC tumors from African American (AA) patients. It should be noted the MDA-MB-468, MDA-MB-157 and SUM149 cell lines were all isolated from AA patients. Further studies by our laboratory into the role of IFITM1 and other ISGs in driving multiple aggressive subtypes of breast cancer are ongoing.

REFERENCES

1. JS Yount, Moltedo B, Yang YY, et al. *Palmitoylome profiling reveals S-palmitoylation-dependent antiviral activity of IFITM3*. Nature chemical biology 2010;6:610-4.

2. S Pestka, Krause CD, Walter MR. *Interferons, interferon-like cytokines, and their receptors*. Immunological reviews 2004;202:8-32.

3. A Lasfar, Cohen-Solal KA. *Emergence of IFN-lambda as a Potential Antitumor Agent*2011.

4. JS Yount, Karssemeijer RA, Hang HC. *S-palmitoylation and ubiquitination differentially regulate interferon-induced transmembrane protein 3 (IFITM3)-mediated resistance to influenza virus*. The Journal of biological chemistry 2012;287:19631-41.

5. CX Ma, Reinert T, Chmielewska I, Ellis MJ. *Mechanisms of aromatase inhibitor resistance*. Nature reviews Cancer 2015;15:261-75.

6. H Cheon, Stark GR. *Unphosphorylated STAT1 prolongs the expression of interferon-induced immune regulatory genes*. Proceedings of the National Academy of Sciences of the United States of America 2009;106:9373-8.

7. VS Romanov, Pospelov VA, Pospelova TV. *Cyclin-dependent kinase inhibitor p21(Waf1): contemporary view on its role in senescence and oncogenesis*. Biochemistry Biokhimiia 2012;77:575-84.

8. SR Johnston, Dowsett M. *Aromatase inhibitors for breast cancer: lessons from the laboratory*. Nature reviews Cancer 2003;3:821-31.

9. CC Bailey, Kondur HR, Huang IC, Farzan M. *Interferon-induced transmembrane protein 3 is a type II transmembrane protein*. The Journal of biological chemistry 2013;288:32184-93.

10. CE DeSantis, Lin CC, Mariotto AB, et al. *Cancer treatment and survivorship statistics, 2014*. CA: a cancer journal for clinicians 2014.

11. KD Miller, Siegel RL, Lin CC, et al. *Cancer treatment and survivorship statistics, 2016*. CA: a cancer journal for clinicians 2016;66:271-89.

12. R Siegel, Naishadham D, Jemal A. *Cancer statistics, 2013*. CA: a cancer journal for clinicians 2013;63:11-30.

13. WF Anderson, Katki HA, Rosenberg PS. *Incidence of breast cancer in the United States: current and future trends*. Journal of the National Cancer Institute 2011;103:1397-402.

14. L Bernstein. *Epidemiology of endocrine-related risk factors for breast cancer*. Journal of mammary gland biology and neoplasia 2002;7:3-15.

15. HK Seitz, Maurer B. *The relationship between alcohol metabolism, estrogen levels, and breast cancer risk*. Alcohol research & health : the journal of the National Institute on Alcohol Abuse and Alcoholism 2007;30:42-3.

16. HV Thomas, Reeves GK, Key TJ. *Endogenous estrogen and postmenopausal breast cancer: a quantitative review.* Cancer causes & control : CCC 1997;8:922-8.

17. L Bjornstrom, Sjoberg M. *Mechanisms of estrogen receptor signaling: convergence of genomic and nongenomic actions on target genes*. Molecular endocrinology (Baltimore, Md) 2005;19:833-42.

18. M Le Romancer, Treilleux I, Bouchekioua-Bouzaghou K, Sentis S, Corbo L. *Methylation, a key step for nongenomic estrogen signaling in breast tumors*. Steroids 2010;75:560-4.

19. RJ Santen, Yue W, Wang JP. *Estrogen metabolites and breast cancer*. Steroids 2014.

20. JD Yager, Davidson NE. *Estrogen carcinogenesis in breast cancer*. The New England journal of medicine 2006;354:270-82.

21. JL Bolton, Thatcher GR. *Potential mechanisms of estrogen quinone carcinogenesis*. Chemical research in toxicology 2008;21:93-101.

22. JS Lewis, Jordan VC. *Selective estrogen receptor modulators (SERMs): mechanisms of anticarcinogenesis and drug resistance*. Mutation research 2005;591:247-63.

23. PE Lonning. *The potency and clinical efficacy of aromatase inhibitors across the breast cancer continuum*. Annals of oncology : official journal of the European Society for Medical Oncology / ESMO 2011;22:503-14.

24. WR Miller. *Aromatase inhibitors: mechanism of action and role in the treatment of breast cancer*. Seminars in oncology 2003;30:3-11.

25. RW Brueggemeier. *Aromatase, aromatase inhibitors, and breast cancer*. American journal of therapeutics 2001;8:333-44.

26. S Chumsri, Howes T, Bao T, Sabnis G, Brodie A. *Aromatase, aromatase inhibitors, and breast cancer*. The Journal of steroid biochemistry and molecular biology 2011;125:13-22.

27. WR Miller, Larionov AA. *Understanding the mechanisms of aromatase inhibitor resistance*. Breast cancer research : BCR 2012;14:201.

28. Z Suba. *The pitfall of the transient, inconsistent anticancer capacity of antiestrogens and the mechanism of apparent antiestrogen resistance*. Drug design, development and therapy 2015;9:4341-53.

29. R Clarke, Liu MC, Bouker KB, et al. *Antiestrogen resistance in breast cancer and the role of estrogen receptor signaling*. Oncogene 2003;22:7316-39.

30. S Ali, Coombes RC. *Endocrine-responsive breast cancer and strategies for combating resistance*. Nature reviews Cancer 2002;2:101-12.

31. CK Osborne, Schiff R. *Mechanisms of endocrine resistance in breast cancer*. Annual review of medicine 2011;62:233-47.

32. VC Jordan. *The new biology of estrogen-induced apoptosis applied to treat and prevent breast cancer*. Endocrine-related cancer 2015;22:R1-31.

33. A Haddow, Watkinson JM, Paterson E, Koller PC. *Influence Of Synthetic Oestrogens Upon Advanced Malignant Disease*. The British Medical Journal 1944;2:393-8.

34. GG Binnie. *Regression of Tumours following Treatment by Stilbœstrol and X-ray Therapy, with Notes on a Case of Breast Tumour which regressed with Stilbœstrol alone*. The British Journal of Radiology 1944;17:42-5.

35. JN Ingle , Ahmann DL, Green SJ, et al. *Randomized Clinical Trial of Diethylstilbestrol versus Tamoxifen in Postmenopausal Women with Advanced Breast Cancer*. New England Journal of Medicine 1981;304:16-21.

36. L Beex, Pieters G, Smals A, Koenders A, Benraad T, Kloppenborg P. *Tamoxifen versus ethinyl estradiol in the treatment of postmenopausal women with advanced breast cancer*. Cancer treatment reports 1981;65:179-85.

37. H Iwase, Yamamoto Y, Yamamoto-Ibusuki M, et al. *Ethinylestradiol is beneficial for postmenopausal patients with heavily pre-treated metastatic breast cancer after prior aromatase inhibitor treatment: a prospective study*. British journal of cancer 2013;109:1537-42.

38. P Chalasani, Stopeck A, Clarke K, Livingston R. *A pilot study of estradiol followed by exemestane for reversing endocrine resistance in postmenopausal women with hormone receptor-positive metastatic breast cancer*. The oncologist 2014;19:1127-8.

39. MJ Ellis, Gao F, Dehdashti F, et al. *Lower-dose vs high-dose oral estradiol therapy of hormone receptor-positive, aromatase inhibitor-resistant advanced breast cancer: a phase 2 randomized study*. Jama 2009;302:774-80.

40. HJT Coelingh Bennink, Verhoeven C, Dutman AE, Thijssen J. *The use of high-dose estrogens for the treatment of breast cancer*. Maturitas 2017;95:11-23.

41. GL Anderson, Chlebowski RT, Aragaki AK, et al. *Conjugated equine oestrogen and breast cancer incidence and mortality in postmenopausal women with hysterectomy: extended follow-up of the Women's Health Initiative randomised placebo-controlled trial*. The Lancet Oncology 2012;13:476-86.

42. SY Jiang, Wolf DM, Yingling JM, Chang C, Jordan VC. *An estrogen receptor positive MCF-7 clone that is resistant to antiestrogens and estradiol*. Molecular and cellular endocrinology 1992;90:77-86.

43. RXD Song, Mor G, Naftolin F, et al. *Effect of Long-Term Estrogen Deprivation on Apoptotic Responses of Breast Cancer Cells to 17β-Estradiol*. JNCI: Journal of the National Cancer Institute 2001;93:1714-23.

44. Y Zhang, Zhao H, Asztalos S, Chisamore M, Sitabkhan Y, Tonetti DA. *Estradiol-Induced Regression in T47D:A18/PKCα Tumors Requires the Estrogen Receptor and Interaction with the Extracellular Matrix*. Molecular Cancer Research 2009;7:498-510.

45. J Szelei, Soto AM, Geck P, et al. *Identification of human estrogen-inducible transcripts that potentially mediate the apoptotic response in breast cancer*. The Journal of steroid biochemistry and molecular biology 2000;72:89-102.

46. EA Ariazi, Cunliffe HE, Lewis-Wambi JS, et al. *Estrogen induces apoptosis in estrogen deprivation-resistant breast cancer through stress responses as identified by global gene expression across time*. Proceedings of the National Academy of Sciences of the United States of America 2011;108:18879-86.

47. P Fan, Cunliffe HE, Maximov PY, et al. *Integration of Downstream Signals of Insulin-like Growth Factor-1 Receptor by Endoplasmic Reticulum Stress for Estrogen-Induced Growth or Apoptosis in Breast Cancer Cells*. Molecular cancer research : MCR 2015;13:1367-76.

48. JS Lewis, Meeke K, Osipo C, et al. *Intrinsic mechanism of estradiol-induced apoptosis in breast cancer cells resistant to estrogen deprivation*. Journal of the National Cancer Institute 2005;97:1746-59.

49. R Santen, Jeng MH, Wang JP, et al. *Adaptive hypersensitivity to estradiol: potential mechanism for secondary hormonal responses in breast cancer patients*. The Journal of steroid biochemistry and molecular biology 2001;79:115-25.

50. P Fan, Griffith OL, Agboke FA, et al. *c-Src Modulates Estrogen-Induced Stress and Apoptosis in Estrogen-Deprived Breast Cancer Cells*. Cancer research 2013;73:4510-20.

51. J Bekisz, Schmeisser H, Hernandez J, Goldman ND, Zoon KC. *Human interferons alpha, beta and omega*. Growth factors (Chur, Switzerland) 2004;22:243-51.

52. I Garcia-Tunon, Ricote M, Ruiz AA, Fraile B, Paniagua R, Royuela M. *Influence of IFN-gamma and its receptors in human breast cancer*. BMC cancer 2007;7:158.

53. D Choubey, Moudgil KD. *Interferons in autoimmune and inflammatory diseases: regulation and roles*. Journal of interferon & cytokine research : the official journal of the International Society for Interferon and Cytokine Research 2011;31:857-65.

54. H Cheon, Holvey-Bates EG, Schoggins JW, et al. *IFNbeta-dependent increases in STAT1, STAT2, and IRF9 mediate resistance to viruses and DNA damage*. The EMBO journal 2013;32:2751-63.

55. RP Donnelly, Kotenko SV. *Interferon-lambda: a new addition to an old family*. Journal of interferon & cytokine research : the official journal of the International Society for Interferon and Cytokine Research 2010;30:555-64.

56. N Ank, West H, Bartholdy C, Eriksson K, Thomsen AR, Paludan SR. *Lambda interferon (IFN-lambda), a type III IFN, is induced by viruses and IFNs and displays potent antiviral activity against select virus infections in vivo*. Journal of virology 2006;80:4501-9.

57. M Ferrantini, Capone I, Belardelli F. *Interferon-alpha and cancer: mechanisms of action and new perspectives of clinical use*. Biochimie 2007;89:884-93.

58. LE Reid, Brasnett AH, Gilbert CS, et al. *A single DNA response element can confer inducibility by both alpha- and gamma-interferons*. Proceedings of the National Academy of Sciences of the United States of America 1989;86:840-4.

59. HJ Choi, Lui A, Ogony J, Jan R, Sims PJ, Lewis-Wambi J. *Targeting interferon response genes sensitizes aromatase inhibitor resistant breast cancer cells to estrogen-induced cell death*. Breast cancer research : BCR 2015;17:6.

60. MS Diamond, Farzan M. *The broad-spectrum antiviral functions of IFIT and IFITM proteins*. Nat Rev Immunol 2013;13:46-57.

61. AH Talukder, Bao M, Kim TW, et al. *Phospholipid scramblase 1 regulates Toll-like receptor 9-mediated type I interferon production in plasmacytoid dendritic cells*. Cell research 2012;22:1129-39.

62. S Smith, Weston S, Kellam P, Marsh M. *IFITM proteins-cellular inhibitors of viral entry*. Current opinion in virology 2014;4:71-7.

63. GI Vladimer, Gorna MW, Superti-Furga G. *IFITs: Emerging Roles as Key Anti-Viral Proteins*. Frontiers in immunology 2014;5:94.

64. KK Conzelmann. *Transcriptional activation of alpha/beta interferon genes: interference by nonsegmented negative-strand RNA viruses*. Journal of virology 2005;79:5241-8.

65. JC Hach, McMichael T, Chesarino NM, Yount JS. *Palmitoylation on conserved and nonconserved cysteines of murine IFITM1 regulates its stability and anti-influenza A virus activity*. Journal of virology 2013;87:9923-7.

66. JW Schoggins, Rice CM. *Interferon-stimulated genes and their antiviral effector functions*. Current opinion in virology 2011;1:519-25.

67. N Khodarev, Ahmad R, Rajabi H, et al. *Cooperativity of the MUC1 oncoprotein and STAT1 pathway in poor prognosis human breast cancer*. Oncogene 2010;29:920-9.

68. R Huang, Faratian D, Sims AH, et al. *Increased STAT1 signaling in endocrine-resistant breast cancer*. PloS one 2014;9:e94226.

69. NN Khodarev, Beckett M, Labay E, Darga T, Roizman B, Weichselbaum RR. *STAT1 is overexpressed in tumors selected for radioresistance and confers protection from radiation in transduced sensitive cells*. Proceedings of the National Academy of Sciences of the United States of America 2004;101:1714-9.

70. SR Chan, Vermi W, Luo J, et al. *STAT1-deficient mice spontaneously develop estrogen receptor alpha-positive luminal mammary carcinomas*. Breast cancer research : BCR 2012;14:R16.

71. AE Koromilas, Sexl V. *The tumor suppressor function of STAT1 in breast cancer*. Jak-stat 2013;2:e23353.

72. H Cheon, Borden EC, Stark GR. *Interferons and their stimulated genes in the tumor microenvironment*. Seminars in oncology 2014;41:156-73.

73. J Ogony, Choi HJ, Lui A, Cristofanilli M, Lewis-Wambi J. *Interferon-induced transmembrane protein 1 (IFITM1) overexpression enhances the aggressive phenotype of SUM149 inflammatory breast cancer cells in a signal transducer and activator of transcription 2 (STAT2)-dependent manner*. Breast cancer research : BCR 2016;18:25.

74. Q Yu, Katlinskaya YV, Carbone CJ, et al. *DNA-damage-induced type I interferon promotes senescence and inhibits stem cell function*. Cell reports 2015;11:785-97.

75. NN Khodarev, Roizman B, Weichselbaum RR. *Molecular pathways: interferon/stat1 pathway: role in the tumor resistance to genotoxic stress and aggressive growth*. Clinical cancer research : an official journal of the American Association for Cancer Research 2012;18:3015-21.

76. RR Weichselbaum, Ishwaran H, Yoon T, et al. *An interferon-related gene signature for DNA damage resistance is a predictive marker for chemotherapy and radiation for breast cancer*. Proceedings of the National Academy of Sciences of the United States of America 2008;105:18490-5.

77. YB Kuo, Chan CC, Chang CA, et al. *Identification of phospholipid scramblase 1 as a biomarker and determination of its prognostic value for colorectal cancer*. Molecular medicine (Cambridge, Mass) 2011;17:41-7.

78. NH Kim, Sung HY, Choi EN, et al. *Aberrant DNA methylation in the IFITM1 promoter enhances the metastatic phenotype in an intraperitoneal xenograft model of human ovarian cancer*. Oncology reports 2014;31:2139-46.

79. D Li, Peng Z, Tang H, et al. *KLF4-mediated negative regulation of IFITM3 expression plays a critical role in colon cancer pathogenesis*. Clinical cancer research : an official journal of the American Association for Cancer Research 2011;17:3558-68.

80. X Rao, Di Leva G, Li M, et al. *MicroRNA-221/222 confers breast cancer fulvestrant resistance by regulating multiple signaling pathways*. Oncogene 2011;30:1082-97.

81. KD Sutherland, Lindeman GJ, Choong DY, et al. *Differential hypermethylation of SOCS genes in ovarian and breast carcinomas*. Oncogene 2004;23:7726-33.

82. W Sasi, Sharma AK, Mokbel K. *The role of suppressors of cytokine signalling in human neoplasms*. Molecular biology international 2014;2014:630797.

83. MC Haffner, Petridou B, Peyrat JP, et al. *Favorable prognostic value of SOCS2 and IGF-I in breast cancer*. BMC cancer 2007;7:136.

84. W Sasi, Jiang WG, Sharma A, Mokbel K. *Higher expression levels of SOCS 1,3,4,7 are associated with earlier tumour stage and better clinical outcome in human breast cancer*. BMC cancer 2010;10:178.

85. KB Bouker, Skaar TC, Fernandez DR, et al. *interferon regulatory factor-1 mediates the proapoptotic but not cell cycle arrest effects of the steroidal antiestrogen ICI 182,780 (faslodex, fulvestrant)*. Cancer research 2004;64:4030-9.

86. ML Bowie, Dietze EC, Delrow J, et al. *Interferon-regulatory factor-1 is critical for tamoxifen-mediated apoptosis in human mammary epithelial cells*. Oncogene 2004;23:8743-55.

87. JL Schwartz, Shajahan AN, Clarke R. *The Role of Interferon Regulatory Factor-1 (IRF1) in Overcoming Antiestrogen Resistance in the Treatment of Breast Cancer*. International journal of breast cancer 2011;2011:912102.

88. SA Dabydeen, Kang K, Diaz-Cruz ES, et al. *Comparison of tamoxifen and letrozole response in mammary preneoplasia of ER and aromatase overexpressing mice defines an immune-associated gene signature linked to tamoxifen resistance*. Carcinogenesis 2015;36:122-32.

89. A Dvorkin-Gheva, Hassell JA. *Identification of a novel luminal molecular subtype of breast cancer*. PloS one 2014;9:e103514.

90. X Sun, Ingman WV. *Cytokine networks that mediate epithelial cell-macrophage crosstalk in the mammary gland: implications for development and cancer*. Journal of mammary gland biology and neoplasia 2014;19:191-201.

91. TA Wallace, Martin DN, Ambs S. *Interactions among genes, tumor biology and the environment in cancer health disparities: examining the evidence on a national and global scale*. Carcinogenesis 2011;32:1107-21.

92. MC Boelens, Wu TJ, Nabet BY, et al. *Exosome transfer from stromal to breast cancer cells regulates therapy resistance pathways*. Cell 2014;159:499-513.

93. G Yang, Xu Y, Chen X, Hu G. *IFITM1 plays an essential role in the antiproliferative action of interferon-gamma*. Oncogene 2007;26:594-603.

94. MC Johnson, Sangrador-Vegas A, Smith TJ, Cairns MT. *Cloning and characterization of two genes encoding rainbow trout homologues of the IFITM protein family*. Veterinary immunology and immunopathology 2006;110:357-62.

95. F Yu, Xie D, Ng SS, et al. *IFITM1 promotes the metastasis of human colorectal cancer via CAV-1*. Cancer letters 2015;368:135-43.

96. RG Parton, Simons K. *The multiple faces of caveolae*. Nature reviews Molecular cell biology 2007;8:185-94.

97. P Liu, Rudick M, Anderson RG. *Multiple functions of caveolin-1*. The Journal of biological chemistry 2002;277:41295-8.

98. C Wilkins, Woodward J, Lau DT, et al. *IFITM1 is a tight junction protein that inhibits hepatitis C virus entry*. Hepatology (Baltimore, Md) 2013;57:461-9.

99. SK Narayana, Helbig KJ, McCartney EM, et al. *The Interferon-induced Transmembrane Proteins, IFITM1, IFITM2, and IFITM3 Inhibit Hepatitis C Virus Entry*. The Journal of biological chemistry 2015;290:25946-59.

100. lK Hong, Byun HJ, Lee J, et al. *The tetraspanin CD81 protein increases melanoma cell motility by up-regulating metalloproteinase MT1-MMP expression through the pro-oncogenic Akt-dependent Sp1 activation signaling pathways*. The Journal of biological chemistry 2014;289:15691-704.

101. I Novita Sari, Yang YG, Hanh Phi LT, et al. *Interferon-induced transmembrane protein 1 (IFITM1) is required for the progression of colorectal cancer*. Oncotarget 2016.

102. CC Ho, Huang PH, Huang HY, Chen YH, Yang PC, Hsu SM. *Up-regulated caveolin-1 accentuates the metastasis capability of lung adenocarcinoma by inducing filopodia formation*. The American journal of pathology 2002;161:1647-56.

103. H Hatano, Kudo Y, Ogawa I, et al. *IFN-induced transmembrane protein 1 promotes invasion at early stage of head and neck cancer progression*. Clinical cancer

research : an official journal of the American Association for Cancer Research 2008;14:6097-105.

104. F Yu, Ng SS, Chow BK, et al. *Knockdown of interferon-induced transmembrane protein 1 (IFITM1) inhibits proliferation, migration, and invasion of glioma cells*. Journal of neuro-oncology 2011;103:187-95.

105. J Lee, Goh SH, Song N, et al. *Overexpression of IFITM1 has clinicopathologic effects on gastric cancer and is regulated by an epigenetic mechanism*. The American journal of pathology 2012;181:43-52.

106. Z Pan, Chen S, Pan X, et al. *Differential gene expression identified in Uigur women cervical squamous cell carcinoma by suppression subtractive hybridization*. Neoplasma 2010;57:123-8.

107. AQ Gomes, Correia DV, Grosso AR, et al. *Identification of a panel of ten cell surface protein antigens associated with immunotargeting of leukemias and lymphomas by peripheral blood gammadelta T cells*. Haematologica 2010;95:1397-404.

108. JS Lewis-Wambi, Cunliffe HE, Kim HR, Willis AL, Jordan VC. *Overexpression of CEACAM6 promotes migration and invasion of oestrogen-deprived breast cancer cells*. European journal of cancer (Oxford, England : 1990) 2008;44:1770-9.

109. B Gyorffy, Lanczky A, Eklund AC, et al. *An online survival analysis tool to rapidly assess the effect of 22,277 genes on breast cancer prognosis using microarray data of 1,809 patients*. Breast cancer research and treatment 2010;123:725-31.

110. EA Musgrove, Sutherland RL. *Biological determinants of endocrine resistance in breast cancer*. Nat Rev Cancer 2009;9:631-43.

111. I Chattopadhyay, Phukan R, Singh A, et al. *Molecular profiling to identify molecular mechanism in esophageal cancer with familial clustering*. Oncology reports 2009;21:1135-46.

112. B Gyorffy, Dietel M, Fekete T, Lage H. *A snapshot of microarray-generated gene expression signatures associated with ovarian carcinoma*. International journal of gynecological cancer : official journal of the International Gynecological Cancer Society 2008;18:1215-33.

113. NT Seyfried, Huysentruyt LC, Atwood JA, 3rd, Xia Q, Seyfried TN, Orlando R. *Up-regulation of NG2 proteoglycan and interferon-induced transmembrane proteins 1 and 3 in mouse astrocytoma: a membrane proteomics approach*. Cancer letters 2008;263:243-52.

114. NN Khodarev, Roach P, Pitroda SP, et al. *STAT1 pathway mediates amplification of metastatic potential and resistance to therapy*. PLoS One 2009;4:e5821.

115. D Borg, Hedner C, Gaber A, et al. *Expression of IFITM1 as a prognostic biomarker in resected gastric and esophageal adenocarcinoma*. Biomarker research 2016;4:10.

116. R Panchanathan, Shen H, Zhang X, Ho SM, Choubey D. *Mutually positive regulatory feedback loop between interferons and estrogen receptor-alpha in mice: implications for sex bias in autoimmunity*. PloS one 2010;5:e10868.

117. C Tasker, Ding J, Schmolke M, Rivera-Medina A, Garcia-Sastre A, Chang TL. *17beta-estradiol protects primary macrophages against HIV infection through induction of interferon-alpha*. Viral immunology 2014;27:140-50.

118. L Quan, Gong Z, Yao S, et al. *Cytokine and cytokine receptor genes of the adaptive immune response are differentially associated with breast cancer risk in American women of African and European ancestry*. International journal of cancer Journal international du cancer 2014;134:1408-21.

119. AM Snijders, Langley S, Mao JH, et al. *An interferon signature identified by RNA-sequencing of mammary tissues varies across the estrous cycle and is predictive of metastasis-free survival*. Oncotarget 2014;5:4011-25.

120. JZ Zaretsky, Barnea I, Aylon Y, Gorivodsky M, Wreschner DH, Keydar I. *MUC1 gene overexpressed in breast cancer: structure and transcriptional activity of the MUC1 promoter and role of estrogen receptor alpha (ERalpha) in regulation of the MUC1 gene expression*. Molecular cancer 2006;5:57.

121. DW Kufe. *Mucins in cancer: function, prognosis and therapy*. Nature reviews Cancer 2009;9:874-85.

122. JS Lewis-Wambi, Kim HR, Wambi C, et al. *Buthionine sulfoximine sensitizes antihormone-resistant human breast cancer cells to estrogen-induced apoptosis*. Breast cancer research : BCR 2008;10:R104.

123. F Behbod, Kittrell FS, LaMarca H, et al. *An intraductal human-in-mouse transplantation model mimics the subtypes of ductal carcinoma in situ*. Breast cancer research : BCR 2009;11:R66.

124. KE Valdez, Fan F, Smith W, Allred DC, Medina D, Behbod F. *Human primary ductal carcinoma in situ (DCIS) subtype-specific pathology is preserved in a mouse intraductal (MIND) xenograft model*. The Journal of pathology 2011;225:565-73.

125. G Sflomos, Dormoy V, Metsalu T, et al. *A Preclinical Model for ERalpha-Positive Breast Cancer Points to the Epithelial Microenvironment as Determinant of Luminal Phenotype and Hormone Response*. Cancer cell 2016;29:407-22.

126. SP Pitroda, Wakim BT, Sood RF, et al. *STAT1-dependent expression of energy metabolic pathways links tumour growth and radioresistance to the Warburg effect*. BMC medicine 2009;7:68.

127. SA Popson, Ziegler ME, Chen X, et al. *Interferon-induced transmembrane protein 1 regulates endothelial lumen formation during angiogenesis*. Arteriosclerosis, thrombosis, and vascular biology 2014;34:1011-9.

128. S Haricharan, Lei J, Ellis M. *Mammary Ductal Environment Is Necessary for Faithful Maintenance of Estrogen Signaling in ER(+) Breast Cancer*. Cancer cell 2016;29:249-50.

129. JY Kim, Kim H, Suk K, Lee WH. *Activation of CD147 with cyclophilin a induces the expression of IFITM1 through ERK and PI3K in THP-1 cells*. Mediators of inflammation 2010;2010:821940.

130. JD He, Luo HL, Li J, Feng WT, Chen LB. *Influences of the interferon induced transmembrane protein 1 on the proliferation, invasion, and metastasis of the colorectal cancer SW480 cell lines*. Chinese medical journal 2012;125:517-22.

131. EM Deraz, Kudo Y, Yoshida M, et al. *MMP-10/stromelysin-2 promotes invasion of head and neck cancer*. PloS one 2011;6:e25438.

132. JJ Pink, Jiang SY, Fritsch M, Jordan VC. *An estrogen-independent MCF-7 breast cancer cell line which contains a novel 80-kilodalton estrogen receptor-related protein*. Cancer research 1995;55:2583-90.

133. E Campeau, Ruhl VE, Rodier F, et al. *A versatile viral system for expression and depletion of proteins in mammalian cells*. PloS one 2009;4:e6529.

134. F Kittrell, Valdez K, Elsarraj H, Hong Y, Medina D, Behbod F. *Mouse Mammary Intraductal (MIND) Method for Transplantation of Patient Derived Primary DCIS Cells and Cell Lines*. Bio-protocol 2016;6.

135. T Abbas, Dutta A. *p21 in cancer: intricate networks and multiple activities*. Nat Rev Cancer 2009;9:400-14.

136. Z Wang, Bhattacharya N, Mixter PF, Wei W, Sedivy J, Magnuson NS. *Phosphorylation of the cell cycle inhibitor p21Cip1/WAF1 by Pim-1 kinase*. Biochimica et biophysica acta 2002;1593:45-55.

137. AL Gartel, Tyner AL. *Transcriptional regulation of the p21((WAF1/CIP1)) gene*. Experimental cell research 1999;246:280-9.

138. A Karimian, Ahmadi Y, Yousefi B. *Multiple functions of p21 in cell cycle, apoptosis and transcriptional regulation after DNA damage*. DNA repair 2016;42:63-71.

139. YS Jung, Qian Y, Chen X. *Examination of the expanding pathways for the regulation of p21 expression and activity*. Cellular signalling 2010;22:1003-12.

140. X Xia, Ji T, Liu R, et al. *Cytoplasmic p21 is responsible for paclitaxel resistance in ovarian cancer A2780 cells*. European journal of gynaecological oncology 2015;36:662-6.

141. ES Child, Mann DJ. *The intricacies of p21 phosphorylation: protein/protein interactions, subcellular localization and stability*. Cell cycle (Georgetown, Tex) 2006;5:1313-9.

142. J Cmielova, Rezacova M. *p21Cip1/Waf1 protein and its function based on a subcellular localization [corrected]*. Journal of cellular biochemistry 2011;112:3502-6.

143. C de Renty, DePamphilis ML, Ullah Z. *Cytoplasmic localization of p21 protects trophoblast giant cells from DNA damage induced apoptosis*. PloS one 2014;9:e97434.

144. P Leisibach, Schneiter D, Soltermann A, Yamada Y, Weder W, Jungraithmayr W. *Prognostic value of immunohistochemical markers in malignant thymic epithelial tumors*. Journal of thoracic disease 2016;8:2580-91.

145. U Weirauch, Beckmann N, Thomas M, et al. *Functional role and therapeutic potential of the pim-1 kinase in colon carcinoma*. Neoplasia (New York, NY) 2013;15:783-94.

146. J Xu, Xiong G, Cao Z, et al. *PIM-1 contributes to the malignancy of pancreatic cancer and displays diagnostic and prognostic value*. Journal of experimental & clinical cancer research : CR 2016;35:133.

147. S Herzog, Fink MA, Weitmann K, et al. *Pim1 kinase is upregulated in glioblastoma multiforme and mediates tumor cell survival*. Neuro-oncology 2015;17:223-42.

148. M Zemskova, Sahakian E, Bashkirova S, Lilly M. *The PIM1 kinase is a critical component of a survival pathway activated by docetaxel and promotes survival of*

docetaxel-treated prostate cancer cells. The Journal of biological chemistry 2008;283:20635-44.

149. M Narlik-Grassow, Blanco-Aparicio C, Cecilia Y, et al. *Conditional transgenic expression of PIM1 kinase in prostate induces inflammation-dependent neoplasia*. PloS one 2013;8:e60277.

150. TJ Pircher, Zhao S, Geiger JN, Joneja B, Wojchowski DM. *Pim-1 kinase protects hematopoietic FDC cells from genotoxin-induced death*. Oncogene 2000;19:3684-92.

151. M Lilly, Sandholm J, Cooper JJ, Koskinen PJ, Kraft A. *The PIM-1 serine kinase prolongs survival and inhibits apoptosis-related mitochondrial dysfunction in part through a bcl-2-dependent pathway*. Oncogene 1999;18:4022-31.

152. X Le, Antony R, Razavi P, et al. *Systematic Functional Characterization of Resistance to PI3K Inhibition in Breast Cancer*. Cancer discovery 2016;6:1134-47.

153. X Chen, Zhao M, Hao M, et al. *Dual Inhibition of PI3K and mTOR Mitigates Compensatory AKT Activation and Improves Tamoxifen Response in Breast Cancer*. Molecular cancer research : MCR 2013;11:1269-78.

154. Y Liu, Zhang X, Liu J, Hou G, Zhang S, Zhang J. *Everolimus in combination with letrozole inhibit human breast cancer MCF-7/Aro stem cells via PI3K/mTOR pathway: an experimental study*. Tumour biology : the journal of the International Society for Oncodevelopmental Biology and Medicine 2014;35:1275-86.

155. I Barone, Cui Y, Herynk MH, et al. *Expression of the K303R estrogen receptor-alpha breast cancer mutation induces resistance to an aromatase inhibitor via addiction to the PI3K/Akt kinase pathway*. Cancer research 2009;69:4724-32.

156. D Zardavas, Fumagalli D, Loi S. *Phosphatidylinositol 3-kinase/AKT/mammalian target of rapamycin pathway inhibition: a breakthrough in the management of luminal (ER+/HER2-) breast cancers?* Current opinion in oncology 2012;24:623-34.

157. J Cidado, Park BH. *Targeting the PI3K/Akt/mTOR pathway for breast cancer therapy*. Journal of mammary gland biology and neoplasia 2012;17:205-16.

158. M Lilly, Le T, Holland P, Hendrickson SL. *Sustained expression of the pim-1 kinase is specifically induced in myeloid cells by cytokines whose receptors are structurally related*. Oncogene 1992;7:727-32.

159. M Bellon, Lu L, Nicot C. *Constitutive activation of Pim1 kinase is a therapeutic target for adult T-cell leukemia*. Blood 2016;127:2439-50.

160. TC Chang, Wentzel EA, Kent OA, et al. *Transactivation of miR-34a by p53 broadly influences gene expression and promotes apoptosis*. Molecular cell 2007;26:745-52.

161. H Nishio, Walsh MJ. *CCAAT displacement protein/cut homolog recruits G9a histone lysine methyltransferase to repress transcription*. Proceedings of the National Academy of Sciences of the United States of America 2004;101:11257-62.

162. GR Stark. *How cells respond to interferons revisited: from early history to current complexity*. Cytokine & growth factor reviews 2007;18:419-23.

163. GR Stark, Kerr IM, Williams BR, Silverman RH, Schreiber RD. *How cells respond to interferons*. Annual review of biochemistry 1998;67:227-64.

164. AR Lewin, Reid LE, McMahon M, Stark GR, Kerr IM. *Molecular analysis of a human interferon-inducible gene family*. European journal of biochemistry 1991;199:417-23.

165. EC Borden, Sen GC, Uze G, et al. *Interferons at age 50: past, current and future impact on biomedicine*. Nature reviews Drug discovery 2007;6:975-90.

166. D Kufe, Inghirami G, Abe M, Hayes D, Justi-Wheeler H, Schlom J. *Differential reactivity of a novel monoclonal antibody (DF3) with human malignant versus benign breast tumors*. Hybridoma 1984;3:223-32.

167. GR Merlo, Siddiqui J, Cropp CS, et al. *Frequent alteration of the DF3 tumor-associated antigen gene in primary human breast carcinomas*. Cancer research 1989;49:6966-71.

168. J Hilkens, Buijs F, Hilgers J, et al. *Monoclonal antibodies against human milk-fat globule membranes detecting differentiation antigens of the mammary gland and its tumors*. International journal of cancer Journal international du cancer 1984;34:197-206.

169. Y Geng, Yeh K, Takatani T, King MR. *Three to Tango: MUC1 as a Ligand for Both E-Selectin and ICAM-1 in the Breast Cancer Metastatic Cascade*. Frontiers in oncology 2012;2:76.

170. Y Geng, Marshall JR, King MR. *Glycomechanics of the metastatic cascade: tumor cell-endothelial cell interactions in the circulation*. Annals of biomedical engineering 2012;40:790-805.

171. HH Habte, Kotwal GJ, Lotz ZE, et al. *Antiviral activity of purified human breast milk mucin*. Neonatology 2007;92:96-104.

172. R Ahmad, Alam M, Rajabi H, Kufe D. *The MUC1-C oncoprotein binds to the BH3 domain of the pro-apoptotic BAX protein and blocks BAX function*. The Journal of biological chemistry 2012;287:20866-75.

173. F Guddo, Giatromanolaki A, Koukourakis MI, et al. *MUC1 (episialin) expression in non-small cell lung cancer is independent of EGFR and c-erbB-2 expression and correlates with poor survival in node positive patients*. Journal of clinical pathology 1998;51:667-71.

174. A Girling, Bartkova J, Burchell J, Gendler S, Gillett C, Taylor-Papadimitriou J. *A core protein epitope of the polymorphic epithelial mucin detected by the monoclonal antibody SM-3 is selectively exposed in a range of primary carcinomas*. International journal of cancer Journal international du cancer 1989;43:1072-6.

175. MD Burdick, Harris A, Reid CJ, Iwamura T, Hollingsworth MA. *Oligosaccharides expressed on MUC1 produced by pancreatic and colon tumor cell lines*. The Journal of biological chemistry 1997;272:24198-202.

176. MP Torres, Chakraborty S, Souchek J, Batra SK. *Mucin-based targeted pancreatic cancer therapy*. Current pharmaceutical design 2012;18:2472-81.

177. Y Ajioka, Allison LJ, Jass JR. *Significance of MUC1 and MUC2 mucin expression in colorectal cancer*. Journal of clinical pathology 1996;49:560-4.

178. M Retz, Lehmann J, Roder C, et al. *Differential mucin MUC7 gene expression in invasive bladder carcinoma in contrast to uniform MUC1 and MUC2 gene expression in both normal urothelium and bladder carcinoma*. Cancer research 1998;58:5662-6.

179. L Huang, Ren J, Chen D, Li Y, Kharbanda S, Kufe D. *MUC1 cytoplasmic domain coactivates Wnt target gene transcription and confers transformation*. Cancer biology & therapy 2003;2:702-6.

180. X Wei, Xu H, Kufe D. *Human mucin 1 oncoprotein represses transcription of the p53 tumor suppressor gene*. Cancer research 2007;67:1853-8.

181. Y Li, Ren J, Yu W, et al. *The epidermal growth factor receptor regulates interaction of the human DF3/MUC1 carcinoma antigen with c-Src and beta-catenin*. The Journal of biological chemistry 2001;276:35239-42.

182. R Ahmad, Raina D, Joshi MD, et al. *MUC1-C oncoprotein functions as a direct activator of the nuclear factor-kappaB p65 transcription factor*. Cancer research 2009;69:7013-21.

183. TM Horm, Schroeder JA. *MUC1 and metastatic cancer: expression, function and therapeutic targeting*. Cell adhesion & migration 2013;7:187-98.

184. N Agata, Ahmad R, Kawano T, Raina D, Kharbanda S, Kufe D. *MUC1 oncoprotein blocks death receptor-mediated apoptosis by inhibiting recruitment of caspase-8*. Cancer research 2008;68:6136-44.

185. L Yin, Kosugi M, Kufe D. *Inhibition of the MUC1-C oncoprotein induces multiple myeloma cell death by down-regulating TIGAR expression and depleting NADPH*. Blood 2012;119:810-6.

186. Q Chen, Li D, Ren J, Li C, Xiao ZX. *MUC1 activates JNK1 and inhibits apoptosis under genotoxic stress*. Biochemical and biophysical research communications 2013;440:179-83.

187. JP Cheng, Yan Y, Wang XY, et al. *MUC1-positive circulating tumor cells and MUC1 protein predict chemotherapeutic efficacy in the treatment of metastatic breast cancer*. Chinese journal of cancer 2011;30:54-61.

188. NN Khodarev, Pitroda SP, Beckett MA, et al. *MUC1-induced transcriptional programs associated with tumorigenesis predict outcome in breast and lung cancer*. Cancer research 2009;69:2833-7.

189. SP Pitroda, Khodarev NN, Beckett MA, Kufe DW, Weichselbaum RR. *MUC1-induced alterations in a lipid metabolic gene network predict response of human breast cancers to tamoxifen treatment*. Proceedings of the National Academy of Sciences of the United States of America 2009;106:5837-41.

190. GD MacLean, Reddish MA, Longenecker BM. *Prognostic significance of preimmunotherapy serum CA27.29 (MUC-1) mucin level after active specific immunotherapy of metastatic adenocarcinoma patients*. Journal of immunotherapy (Hagerstown, Md : 1997) 1997;20:70-8.

191. TJ Duncan, Watson NF, Al-Attar AH, Scholefield JH, Durrant LG. *The role of MUC1 and MUC3 in the biology and prognosis of colorectal cancer*. World journal of surgical oncology 2007;5:31.

192. M Hareuveni, Tsarfaty I, Zaretsky J, et al. *A transcribed gene, containing a variable number of tandem repeats, codes for a human epithelial tumor antigen. cDNA cloning, expression of the transfected gene and over-expression in breast cancer tissue*. European journal of biochemistry / FEBS 1990;189:475-86.

193. X Wei, Xu H, Kufe D. *MUC1 oncoprotein stabilizes and activates estrogen receptor alpha*. Molecular cell 2006;21:295-305.

194. CM Klinge, Radde BN, Imbert-Fernandez Y, et al. *Targeting the intracellular MUC1 C-terminal domain inhibits proliferation and estrogen receptor transcriptional activity in lung adenocarcinoma cells*. Molecular cancer therapeutics 2011;10:2062-71.

195. EM Jung, An BS, Yang H, Choi KC, Jeung EB. *Biomarker genes for detecting estrogenic activity of endocrine disruptors via estrogen receptors*. International journal of environmental research and public health 2012;9:698-711.

196. J Lundy, Thor A, Maenza R, et al. *Monoclonal antibody DF3 correlates with tumor differentiation and hormone receptor status in breast cancer patients*. Breast cancer research and treatment 1985;5:269-76.

197. XJ Ma, Wang Z, Ryan PD, et al. *A two-gene expression ratio predicts clinical outcome in breast cancer patients treated with tamoxifen*. Cancer cell 2004;5:607-16.

198. RJ Critchley-Thorne, Simons DL, Yan N, et al. *Impaired interferon signaling is a common immune defect in human cancer*. Proceedings of the National Academy of Sciences of the United States of America 2009;106:9010-5.

199. EF Need, Atashgaran V, Ingman WV, Dasari P. *Hormonal regulation of the immune microenvironment in the mammary gland*. Journal of mammary gland biology and neoplasia 2014;19:229-39.

200. AK Dunbier, Ghazoui Z, Anderson H, et al. *Molecular profiling of aromatase inhibitor-treated postmenopausal breast tumors identifies immune-related correlates of resistance*. Clinical cancer research : an official journal of the American Association for Cancer Research 2013;19:2775-86.

201. KE de Visser, Eichten A, Coussens LM. *Paradoxical roles of the immune system during cancer development*. Nature reviews Cancer 2006;6:24-37.

202. P Dasari, Sharkey DJ, Noordin E, et al. *Hormonal regulation of the cytokine microenvironment in the mammary gland*. Journal of reproductive immunology 2014.

203. M Tavallai, Booth L, Roberts JL, Poklepovic A, Dent P. *Rationally Repurposing Ruxolitinib (Jakafi ((R))) as a Solid Tumor Therapeutic*. Frontiers in oncology 2016;6:142.

204. CR Hagan, Regan TM, Dressing GE, Lange CA. *ck2-dependent phosphorylation of progesterone receptors (PR) on Ser81 regulates PR-B isoform-specific target gene expression in breast cancer cells*. Molecular and cellular biology 2011;31:2439-52.

205. CM Perou, Jeffrey SS, van de Rijn M, et al. *Distinctive gene expression patterns in human mammary epithelial cells and breast cancers*. Proceedings of the National Academy of Sciences of the United States of America 1999;96:9212-7.

206. TC Wagner, Velichko S, Vogel D, et al. *Interferon signaling is dependent on specific tyrosines located within the intracellular domain of IFNAR2c. Expression of IFNAR2c tyrosine mutants in U5A cells*. The Journal of biological chemistry 2002;277:1493-9.

207. A Yoshimura, Naka T, Kubo M. *SOCS proteins, cytokine signalling and immune regulation*. Nat Rev Immunol 2007;7:454-65.

208. DJ Zhou, Pompon D, Chen SA. *Stable expression of human aromatase complementary DNA in mammalian cells: a useful system for aromatase inhibitor screening*. Cancer research 1990;50:6949-54.

APPENDIX A: MANUSCRIPT-EVEROLIMUS DOWNREGULATES ESTROGEN RECEPTOR AND INDUCES AUTOPHAGY IN AROMATASE INHIBITOR-RESISTANT BREAST CANCER CELLS

The PI3K/Akt/ mTOR pathway is one system that is thought to promote AI-resistance in breast cancer. As such, several inhibitors of this pathway are being investigated in clinical trials in various combinations with endocrine therapy with the goal of preventing or reversing resistance. In this study, we investigated the therapeutic benefits of the newest mTOR inhibitor to be approved by the FDA, everolimus/RAD001, in our models of AI-resistant breast cancer.

Lui A, New J, Ogony J, Thomas S and Lewis-Wambi, J. *Everolimus downregulates estrogen receptor and induces autophagy in aromatase inhibitor-resistant breast cancer cells.* BMC Cancer. 2016 Jul 16;16:487. PMCID:4947349.

ABSTRACT

Background: mTOR inhibition of aromatase inhibitor (AI)-resistant breast cancer is currently under evaluation in the clinic. Everolimus/RAD001 (Afinitor®) has had limited efficacy as a solo agent but is projected to become part of combination therapy for AI-resistant breast cancer. This study was conducted to investigate the anti-proliferative and resistance mechanisms of everolimus in AI-resistant breast cancer cells.

Methods: In this study we utilized two AI-resistant breast cancer cell lines, MCF-7:5C and MCF-7:2A, which were clonally derived from estrogen receptor positive (ER+) MCF-7 breast cancer cells following long-term estrogen deprivation. Cell viability assay, colony formation assay, cell cycle analysis and soft agar anchorage-independent growth assay were used to determine the efficacy of everolimus in inhibiting the proliferation and tumor forming potential of MCF-7, MCF-7:5C, MCF-7:2A and MCF10A cells. Confocal microscopy and transmission electron microscopy were used to evaluate LC3-II production and autophagosome formation,_while ERE-luciferase reporter, Western blot, and RT-PCR analyses were used to assess ER expression and transcriptional activity.

Results: Everolimus inhibited the proliferation of MCF-7:5C and MCF-7:2A cells with relatively equal efficiency to parental MCF-7 breast cancer cells. The inhibitory effect of everolimus was due to G1 arrest as a result of downregulation of cyclin D1 and p21. Everolimus also dramatically reduced estrogen receptor (ER) expression (mRNA and protein) and transcriptional activity in addition to the ER chaperone, heat shock protein 90 protein (HSP90). Everolimus restored 4-hydroxy-tamoxifen (4OHT) sensitivity in MCF-7:5C cells and enhanced 4OHT sensitivity in MCF-7 and MCF-7:2A cells. Notably,

we found that autophagy is one method of everolimus insensitivity in MCF-7 breast cancer cell lines.

Conclusion: This study provides additional insight into the mechanism(s) of action of everolimus that can be used to enhance the utility of mTOR inhibitors as part of combination therapy for AI-resistant breast cancer.

KEYWORDS

Breast Cancer, Aromatase Inhibitor, RAD001, Everolimus, PI3K/Akt/mTOR, Estrogen Receptor, Autophagy

BACKGROUND

Estrogen deprivation using aromatase inhibitors (AIs) is currently the standard of care for patients with estrogen receptor-positive (ER+) breast cancer. Unfortunately, ~30% of breast cancer patients develop resistance to AIs following long-term treatment [209]. The mechanism by which AI resistance develops is still not completely understood, however, several contributing factors have been identified including; alterations in ER signaling, enhanced growth factor signaling, and imbalance in the phosphoinositide 3-kinase/protein kinase B/mammalian target of rapamycin (PI3K/Akt/mTOR) pathway [29,30]. The activation of the PI3K/Akt/mTOR pathway is considered clinically relevant for tumor escape from hormone dependence in breast cancer, promoting the survival of breast cancer cells in estrogen-deprived conditions.[210] Additionally, upregulation of the PI3K/Akt/mTOR pathway is associated with poor outcome for breast cancer patients and has been observed in AI-resistant breast cancer models.[155,211] As a result, a variety of PI3K/Akt/mTOR pathway inhibitors have been under study, including everolimus/RAD001 (Afinitor®).

Everolimus is a rapamycin analog that is currently approved for treatment of metastatic breast cancer. It inhibits the PI3K/Akt/mTOR signaling pathway by preventing the phosphorylation of mTORC1, which interrupts the signaling cascade and results in inhibition of cell proliferation and growth.[212] Everolimus treatment has shown promising anti-cancer effects in preclinical studies; however, when used as a single agent, it does not significantly decrease tumor size.[213] As a result, recent clinical trials have focused instead on simultaneous targeting of the PI3K/AKT/mTOR and ER pathways in ER+ breast cancer.[214-216] The results from these trials have been very encouraging due to

significant improvements in response rate and progression free survival for both AI-sensitive and AI-resistant patients.[217-219] Subsequent laboratory studies have focused on comparison of everolimus in combination with endocrine therapies [154,220] as well as other PI3K/Akt/mTOR inhibitors in a variety of breast cancer cell lines [153,221] and these studies have reported synergy between tamoxifen or AI therapy and everolimus. However, these studies have not investigated the anti-cancer mechanisms of everolimus alone in AI-resistant breast cancer cells.

Everolimus and other PI3K/Akt/mTOR inhibitors are known to induce autophagy in both solid and blood tumors [222,223]; however, to our knowledge, the phenomenon has not been reported in breast cancer. Autophagy allows cells to degrade dysfunctional organelles and proteins, and recycle their components. Autophagy can support tumor survival during treatment, making it a possible mechanism for AI-resistance.[224,225] This process is dependent upon the cleavage of microtubule associated light chain 3 (LC3) to LC3-I and subsequent lipidation to LC3-II which allows for final formation of the autophagosome membrane.[226] A group of small proteins, called heat shock proteins (HSPs), promote cell survival during stress reactions by promoting the refolding of denatured proteins and directly regulating autophagy. Specifically, HSP70 is thought to be required for the induction of autophagy [227,228] in response to inhibition of the PI3K/Akt/mTOR pathway by either starvation or rapamycin treatment [229,230]. Another heat shock protein, HSP27, allows cells to survive a variety of cytotoxic stimuli [231,232] and is thought to be degraded during starvation and rapamycin-induced autophagy.[233] Due to the link between drug resistance and autophagy, we hypothesized

that the induction of autophagy may contribute to everolimus insensitivity in MCF-7 breast cancer cell lines.

In this study, we investigated the effects of everolimus, as a single agent, or in combination with 4-hydroxy tamoxifen (4-OHT) or chloroquine on cell proliferation, anchorage-independent growth, PI3K/Akt/mTOR signaling, ER expression and transcriptional activity, LC3 turnover, and autophagosome induction in AI-sensitive MCF-7 and AI-resistant MCF-7:5C and MCF-7:2A breast cancer cells. We report that everolimus exerts similar anti-proliferative effects in both the AI-sensitive and AI-resistant breast cancer cell lines and that its inhibitory activity is associated with G1 arrest and down regulation of ERα expression. Everolimus also reverses and enhances 4OHT sensitivity during long-term co-treatment of the AI-resistant cell lines. Lastly, we report that autophagy is a mechanism of everolimus insensitivity in MCF-7, MCF-7:5C and MCF-7:2A cells, possibly explaining the equal response of these cell lines to treatment. The information from this study may enhance future selection of everolimus containing combination therapies for AI-resistant breast cancer.

MATERIALS AND METHODS

Cell lines and culture conditions

The MCF-7 cell line [42,132] was obtained from Dr. V. Craig Jordan (University of Texas MD Anderson Cancer Center, Houston) and maintained in RPMI-1640 medium supplemented with 10% fetal bovine serum, 2 mM glutamine, Antibiotic/Antimitotic mix, MEM Non-Essential Amino Acids (Invitrogen, Waltham, MA), and bovine insulin at 6 ng/mL (Sigma Aldrich, St. Louis, MO). The long-term estrogen deprived human breast cancer cell lines; MCF-7:5C [42,48] and MCF-7:2A [122,132] were cloned from parental MCF-7 cells following long term (> 12 months) culture in estrogen-free medium composed of phenol red-free RPMI-1640, 10% fetal bovine serum treated three times with dextran-coated charcoal (SFS), 2 mM glutamine, bovine insulin at 6 ng/mL, Antibiotic/Antimitotic mix, and MEM Non-Essential Amino Acids (Invitrogen). The MCF10A cell line was purchased from the American Type Tissue Culture Collection. They are maintained in Dulbecco's Modified Eagle Medium: Nutrient Mixture F-12 (DMEM/F12) in a 1:1 mixture and supplemented with 5% horse serum, Antibiotic/Antimitotic mix (100 IU/mL penicillin, 100 µg/mL streptomycin, 25 µg/mL of Fungizone® from Invitrogen, Grand Island, NY), 20ng/ml EGF (Millipore), 0.5mg/ml hydrocortisone, 100ng/ml cholera toxin (Sigma Aldrich). All cell lines were cultured at 37°C under 5% CO_2. After overnight acclimatization period, cells were cultured with 20 nM everolimus alone or in combination with 1 µM 4-hydroxytamoxifen (Sigma Aldrich) or 50 µM Chloroquine (InvivoGen, San Diego, CA), in their normal culture medium.

Cell Viability

Cells were assayed for viability in 24-well plates using the Cell-Titer Blue Assay Kit (Promega, Madison, WI) per the manufacturer's instructions. Assay plates were kept at 37˚C in 5% CO_2 for 3 hours and read at 560-590 nM on a BioTek Synergy 4 microplate reader using the Gen 5 data analysis software (BioTek Instruments, Winooski, VT).

Western blotting

Cells were seeded in 6-well plates, collected using a cell scraper and suspended in RIPA buffer (Thermo Scientific, Pittsburgh, PA) supplemented with protease inhibitor cocktail and phosphatase inhibitor (Sigma Aldrich). Cells were homogenized over ice by sonication. After purification of the sample by centrifugation, protein concentration was determined by protein assay (Bio-Rad, Hercules, CA). The proteins were separated by 4-12% SDS–polyacrylamide gel electrophoresis (SDS–PAGE) and electrically transferred to a polyvinylidene difluoride membrane (Santa Cruz Biotechnology). After blocking the membrane using 5% non-fat milk, target proteins were detected using either Anti-mTOR, anti-phospho-mTOR, anti- LC3A/B (Cell Signaling, Beverly, MA), anti-p70S6K, anti-phospho-p70S6K, anti-AKT, anti-phospho-AKT (S473) or anti-ERα (Santa Cruz Biotechnology) antibodies. Membranes were stripped and re-probed for β-actin (Cell Signaling) or β-tubulin (Sigma Aldrich). The appropriate horseradish peroxidase (HRP)-conjugated secondary antibody was applied and the positive bands were detected using Amersham ECL Plus Western blotting detection reagents (GE Health care, Piscataway, NJ). In the case of LC3 analysis, cells were treated with 50 µM chloroquine (CQ) for 24 or 48 hours to allow for LC3-II accumulation. Immunoreactivity was detected using anti-mouse or anti-rabbit IgG conjugated to Dylight 680 or 800

fluorochromes (Thermo Scientific, Waltham, MA), respectively. Blots were visualized on Odyssey imager (LiCor, Lincoln, NE). Quantitation of immunoreactive signals was done by densitometry using ImageJ 1.46r software (NIH, Bethesda, MA). The ratio of protein expression to β-tubulin in each lane was calculated and presented relative to the respective controls within each experiment.

Cell Cycle Analysis

Cells were incubated in the appropriate cell culture media with and without drug treatment. Cells were harvested at the indicated time points by trypsinization. They were washed once with cold PBS and stained with 50 µg/mL Propidium Iodide and 100 µg/mL RNase A in PBS (Invitrogen). Samples were analyzed using a BD FACSAria™ II Flow Cytometer (BD, Franklin Lakes, NJ) and the data were analyzed with FlowJo software (Ashland, OR).

Clonogenic Proliferation Assay

Cells were seeded at 1,000 cells per well in 6-well plate in singe cell suspension. After 24 hour acclimatization, they were treated every three days and allowed to proliferate and establish colonies for 9 days. Cells were stained with 0.5% crystal violet in 1:7 acetic acid: methanol and imaged at 1X in a Bio-Rad ChemiDoc™ XRS+ System with Image Lab™ Software (Bio-Rad Laboratories Inc., Hercules, CA). Colonies were counted and measured using Image J software (The National Institute of Health, Bethesda, MD).

Soft Agar Anchorage-independent Growth Assay

6-well plates were coated with 1 mL of 0.8% agarose in the appropriate culture media. Cells were then suspended in 0.48% agarose and immediately overlaid on the pre-

coated plates. Once the agarose was solid, 1mL of culture medium with or without 20 nM everolimus was added and replaced every 4 days for 15 days. Cultures were then stained with 0.005% crystal violet in PBS, washed with PBS until the background was clear and imaged microscopically at 10X for measurement of colony diameter. Plates were also imaged at 1X in a Bio-Rad ChemiDoc™ XRS+ System with Image Lab™ Software (Bio-Rad). Colonies were counted and measured using Image J software (NIH).

Real Time PCR

Cells were seeded in 6-well plates and allowed to acclimatize overnight. Following 72 hour treatment with 20 nM everolimus, cells were harvested by cell scraping in RLT lysis buffer and total RNA was isolated using the Qiagen RNeasy kit (Venlo, Limburg). First strand cDNA synthesis was performed from 3 µg total RNA using MulV Reverse Transcriptase (Applied Biosystems, Carlsbad, CA) on a Bio Rad MyCycler™. RT-PCR was conducted using the ViiA™ 7 Real-Time PCR system (Applied Biosystems) and SYBR Green Reagent (Life Technologies, Carlsbad, CA) with primers specific for ERα and the housekeeping gene PUM1. Primers for ERα: Forward 5'–AAGAGGGTGCCAGGCTTTGT–3', Reverse 5'–CAGGATCTCTAG CCAGGCACAT –3'. Primers for PUM1: Forward-TCACCGAGGCCCCTCTGAACCCTA Reverse-GGCAGTAATCTCCTTCTGCATCCT (Integrated DNA Technologies, Coralville, Iowa). Relative ERα mRNA expression level was determined as the ratio of the signal intensity to that of PUM1 using the formula: $2^{-\Delta CT}$. When treated with everolimus, fold change in ERα expression was normalized to PUM1 and then compared to the untreated value for that cell line using the formula: $2^{-\Delta\Delta CT}$.

Luciferase Reporter Assay

Cells were seeded in 12-well tissue culture plates overnight for attachment before transfection. The cells were transfected using Lipofectamine 2000™ Transfection Reagent (Invitrogen, San Diego) according to the manufacturer's recommendations. Briefly, 4μL of Lipofectamine 2000, 0.8 μg of ERE Luciferase plasmid DNA and 0.01 μg of the pRL CMV Renilla (Promega) were diluted individually in 250-μl aliquots of OptiMEM Reduced-Serum Medium (Invitrogen). Cells were incubated for 24 h after transfection, and then treated with 20 nM EVE or vehicle in complete media for 24 hours. The Luciferase and Renilla activities were measured using the dual luciferase assay kit (Promega) according to the manufacturer's instructions. To confirm the specificity of the ERE Luciferase construct, EVE treated cells were also compared to those treated with 1nM 17β-estradiol and 1nM Fulvestrant, a pure anti-estrogen (Sigma). Relative Fluorescence Units (RFUs) were calculated as a ratio of Luciferase to Renilla signal intensity. The ERE Luciferase reporter construct was a kind gift from Dr. Clodia Osipo (Loyola University, Chicago, IL).

Immunofluorescence microscopy

Cells grown on glass coverslips were washed in PBS and fixed with 100% ice cold methanol for 10 minutes. After permeabilization by 0.1% Triton X-100 in PBS for 10 min, cells were incubated with 5% normal horse serum/PBS for 30 min, followed by incubation with ERα or LC3B antibody, 2 μg/mL in 0.01% Triton X-100 /PBS overnight (Santa Cruz Biotechnology). Cells were stained with fluorescein isothiocyanate (FITC)-conjugated labeled goat anti-rabbit IgG (Cell Signaling), 4 μg/mL in PBS for 1 h, followed by coverslip mounting with the ProLong® Gold anti-fade reagent with DAPI

(Life Technologies). Samples were imaged on a Leica TCS SPE confocal microscope in the Confocal Imaging Core at The University of Kansas Medical Center. Images were collected and analyzed using the Leica LAS AF Lite software (Leica Biosystems, Nussloch, Germany). For quantification, mean fluorescent intensity was determined using Image J software on green (FITC) channel images.

Electron Microscopy

1 x10^6 cells were seeded in 6-well plates and treated after an overnight acclimatization. After 72 hours of treatment cells were harvested by scraping and fixed for 24 hours at 4^0C in 0.1 M cacodylate buffer supplemented with 2% glutaraldehyde. Samples were then processed in The Electron Microscopy Research Laboratory at KU Medical Center as follows. Briefly, cell pellets were washed in 0.1M cacodylate buffer for 10 min, and resuspended. Cell pellets were post fixed in 1% osmium tetroxide buffered in 0.1M cacodylate, rinsed in distilled water 3X's and then dehydrated in a graded series of ethanol as follows: 50%,70%,80%,95%,100%,100% 10 min each step. Cells were placed into propylene oxide for 20 min, then into a 50:50 mixture of propylene oxide and Embed 812 resin medium overnight at room temperature. Samples were cured overnight in beem capsules at 60 degrees and then sectioned with a diamond knife on a Leica UC-7. Sections were cut at 80nm and contrasted with uranyl acetate and lead citrate and imaged on a JEOL 100CX II Transmission Electron Microscope (Tokyo, Japan).

Statistical analysis

At least three separate experiments were performed for each measurement unless otherwise indicated. All quantitative data were expressed as means with error bars

representing 1 standard deviation (mean ± 1SD). Comparisons between two treatments were analyzed using a two-way student t-test with P-value of < 0.05 considered to be statistically significant. $*p < 0.05$, $**p<0.01$, $***p < 0.001$ unless otherwise indicated.

RESULTS

Everolimus inhibits proliferation through induction of G1 arrest

We tested the anti-proliferative effect of everolimus in two AI-resistant breast cancer cell lines, MCF-7:5C and MCF-7:2A and their parental AI-sensitive cell line, MCF-7. We found that everolimus inhibited the proliferation of MCF-7:5C and MCF-7:2A cells with relatively equal efficiency compared to MCF-7 breast cancer cells (Fig. 1a, upper panel). The IC_{50} values for MCF-7, MCF-7:5C and MCF-7:2A cells were 25 nM, 38 nM and 20 nM, respectively, indicating only minor differences in sensitivity to everolimus between these cell lines (Fig. 1a, lower panel). Treatment with 20 nM everolimus achieved maximal inhibition of all three cell lines (Fig. 1a) as early as 24 hours post-treatment (Fig. 1b). Additionally, the everolimus mediated inhibition of proliferation could be maintained with treatment every three days under clonogenic assay conditions (Fig. 1c). In contrast, everolimus had no effect on the proliferation of the immortalized normal breast epithelium cell line, MCF10A (Additional File 1: Figure S1a and b).

Cell cycle analysis of MCF-7, MCF-7:5C, and MCF-7:2A cells treated with everolimus indicated that the anti-proliferative effect of the drug was due to G1 arrest. The percentage of cells in G1 phase increased by at least 20% in all three cells lines as early as 24 hours after treatment (Fig. 2a) and this persisted through 72 hours (Fig. 2b). Everolimus had no effect on the cycling of the normal breast epithelial cell line MCF10A (Additional File 1: Figure S1c). Additionally, we found that the expression of cyclin D1 and p21 were significantly reduced in MCF-7, MCF-7:5C and MCF-7:2A cells 48 and 72

hours after treatment (Fig. 2c). This data indicates that everolimus is effective at inhibiting the proliferation of breast cancer cells due to marked induction of G1 arrest.

Everolimus reduces the anchorage-independent growth

The ability of cancer cells to grow in an anchorage-independent manner is a critical marker of tumor forming and metastatic potential. We compared the abilities of MCF-7, MCF-7:5C and MCF-7:2A cells to grow in an anchorage-independent manner using the soft-agar 3D colony formation assay. We found that MCF-7:5C cells produced three times more 3D colonies than the MCF-7 and MCF-7:2A cells. Additionally, 20 nM everolimus significantly reduced the number of 3D colonies in all three cell lines (Fig. 3a). The 3D colonies formed by the MCF-7:5C cells averaged 18 μM^2, while those formed by the MCF-7 and MCF-7:2A cells averages 40 and 35 μM^2 respectively. Upon microscopic inspection, we found that 20 nM everolimus dramatically reduced the size of 3D colonies in all three cell lines, with the most pronounced effect being on the MCF-7:5C cells (Fig. 3b). These data indicate that everolimus inhibits not just the proliferation of breast cancer cells, but also their tumor forming and metastatic potential

Effects of everolimus on the PI3K/Akt/mTOR pathway

We also examined the effect of everolimus treatment on the activation of the PI3K/Akt/mTOR pathway. We found that everolimus significantly inhibited mTOR phosphorylation as early as 30 minutes post treatment but not Akt, p70S6K and 4EBP1 (Fig. 4, upper panels). Everolimus inhibited the phosphorylation of downstream members of the PI3K/Akt/mTOR pathway at 12 hours. This was most prominent at 24 hours in MCF-7, MCF-7:5C and MCF-7:2A cells (Fig. 4, bottom panels). 25 nM everolimus was sufficient to inhibit PI3K/mTOR/Akt signaling at 12 and 24 hours but

higher doses were more effective at blocking phosphorylation. Notably, inhibition of p70S6K phosphorylation was observed by 60 minutes in the AI-sensitive MCF-7 cell line, especially with higher doses, but not in the AI-resistant MCF-7:5C and MCF-7:2A cells until 12 hours post-treatment (Fig. 4). Reduction of phospho- mTOR, p70S6K and Akt were maintained by 20 nM everolimus through 48 and 72 hours (Additional File 2: Figure S2). Everolimus successfully targets the Akt/mTOR pathway in AI-sensitive and AI-resistant breast cancer cells.

Everolimus reduces estrogen receptor (ER) expression and transcriptional activity

The activity of ERα can be regulated by the PI3K/Akt/mTOR pathway and is critical to the survival and proliferation of AI-sensitive MCF-7 cells, as well as the AI-resistant MCF-7:5C and MCF-7:2A cell lines. The ligand-independent activity of ER maintains the growth and survival of AI-resistant breast cancer cells.[22,234] We found that treatment with everolimus significantly reduced ER transcriptional activity and protein expression (Fig. 5a and b). This was compared to the action of the pure anti-estrogen fulvestrant (Fig. 5a and b). Everolimus also dramatically reduced ERα mRNA expression (Fig. 5c) in addition to protein expression of the ER chaperone, HSP90 (Fig. 5d). Downregulation of ER expression was confirmed by immunofluorescent confocal microscopy (Fig. 5e). Notably, there was higher ER transcriptional activity in AI-resistant MCF-7:5C and MCF-7:2A cells compared to parental MCF-7 cells, confirming estrogen-independent ER action in the resistant cells (Fig. 5a). Taken together, these data indicate that everolimus, and therefore PI3K/Akt/mTOR signaling, is capable of

regulating ER expression and transcriptional activity in both wild-type MCF-7 cells and AI-resistant MCF-7:5C and MCF-7:2A cells.

Everolimus reverses 4-OH tamoxifen resistance

Due to earlier studies that have found synergy between tamoxifen and everolimus in endocrine-sensitive breast cancer cell models and patients, we investigated the efficacy of this combination in our MCF-7, MCF-7:5C and MCF-7:2A cells. We have previously shown that the AI-resistant MCF-7:5C cells are not responsive to 4OHT, whereas MCF-7:2A are partially sensitive to 4OHT.[234] In this study, 1μM 4OHT significantly inhibited the proliferation of MCF-7 and MCF-7:2A cells, reducing the number of 2D colonies by 20% and 10% respectively, but had no effect on MCF-7:5C cells (Fig. 6a). Treatment with 20 nM everolimus for 9 days significantly reduced the proliferation of all three cell lines, reducing colony numbers by ~ 60% (Fig. 6a). Co-treatment of MCF-7, MCF-7:5C and MCF-7:2A cells with 1μM 4OHT and 20 nM everolimus reduced colony formation in MCF-7 and MCF-7:2A cells by ~ 95% and also had added benefit in the 4OHT-resistant MCF-7:5C cells, bringing the anti-proliferative effect from 60% to 76%. Synergy between 4OHT and everolimus treatment was present despite reductions in ERα expression in all three cell lines (Fig. 6b). This data supports clinical observations that the combination of tamoxifen with everolimus has therapeutic benefit in patients with ER+ breast cancer and can re-sensitize AI-resistant breast cancer to endocrine therapy.

Everolimus induces autophagy in breast cancer cells, which mediates insensitivity

We investigated whether everolimus treatment induced autophagy in MCF-7, MCF-7:5C and MCF-7:2A cells. We found that everolimus reduced the levels of HSP70 and HSP27 in all three cell lines (Fig. 7a). Interestingly, everolimus also induced PARP cleavage (Fig. 7a); however, this was not associated with apoptosis by annexin v/PI staining (data not shown). Chloroquine was used as an autophagic flux inhibitor, and basal autophagy was assessed with and without everolimus treatment. Both immunofluorescent microscopy and western blot (Fig. 7b and 7c), indicate that everolimus markedly enhanced LC3-II above basal level, respectively. A lysosomal protease inhibitor cocktail (100 μM leupeptin, 10μg/mL pepstatin A and 10μg/mL e-64d for 24 hours) was also used to inhibit autophagic flux but results were not as robust as with 50 μM chloroquine (data not shown). As further indication of everolimus' ability to induce autophagy, the number of autophagosomes identified by electron microscopy in all three cell lines was also increased (Fig. 8a and 8b). Combined inhibition of autophagy with 50 μM CQ significantly improved the efficacy of everolimus treatment on cell proliferation, indicating that autophagy is a method of everolimus insensitivity in MCF-7 cell lines (Fig. 8c). Under normal conditions, the MCF-7:5C cell line displayed dilated endoplasmic reticulum, and both AI-resistant cell lines had pleomorphic mitochondria, indicating that aberrant metabolism is likely part of the phenotype of these AI-resistant breast cancer models (Fig. 8a). These data suggest that MCF-7, MCF-7:5C and MCF-7:2A cells use autophagy as a method of everolimus resistance and that this response may be inhibited to improve the efficacy of everolimus treatment in breast cancer.

FIGURES

Figure 1

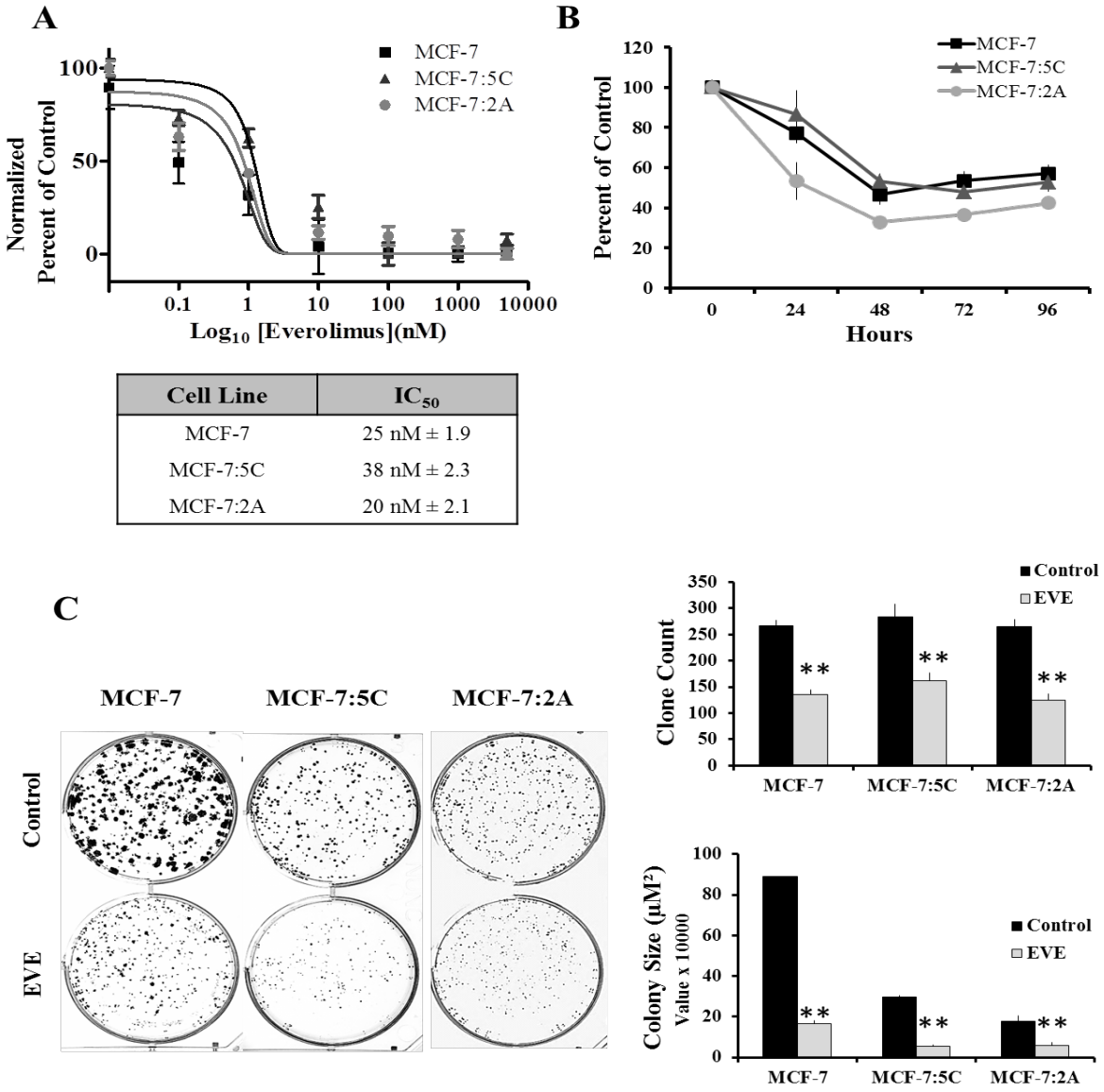

Cell Line	IC_{50}
MCF-7	25 nM ± 1.9
MCF-7:5C	38 nM ± 2.3
MCF-7:2A	20 nM ± 2.1

Fig. 1 Everolimus inhibits the proliferation of AI-sensitive and AI-resistant breast cancer cells. **(a)** MCF-7, MCF-7:5C and MCF-7:2A cells were treated with 20 nM everolimus or vehicle (control) for 72 hours. The percent of viable cells after everolimus treatment was determined by cell viability assay and compared to control. IC_{50} values for each of the cell lines were determined by nonlinear regression on normalized values. Values represent means of three experiments conducted in quadruplet. **(b)** MCF-7, MCF-7:5C and MCF-7:2A cells were seeded in 24-well plates and treated with 20 nM everolimus or vehicle after overnight acclimatization (Day 0). The percentage of viable cells was determined at 24, 48, 72 and 96 hours post treatment by comparison to vehicle treated cells. **(c)** Cells were seeded in single cell suspension and allowed to proliferate for 9 days in the presence of 20nM everolimus or vehicle (control). The plates were photographed at 1X magnification (left panel) and the number of colonies and colony size were quantified using Image J (right panel). Bar graphs represent the data from three independent experiments in triplicate and values are mean ± SD. ** p< 0.01

Figure 2

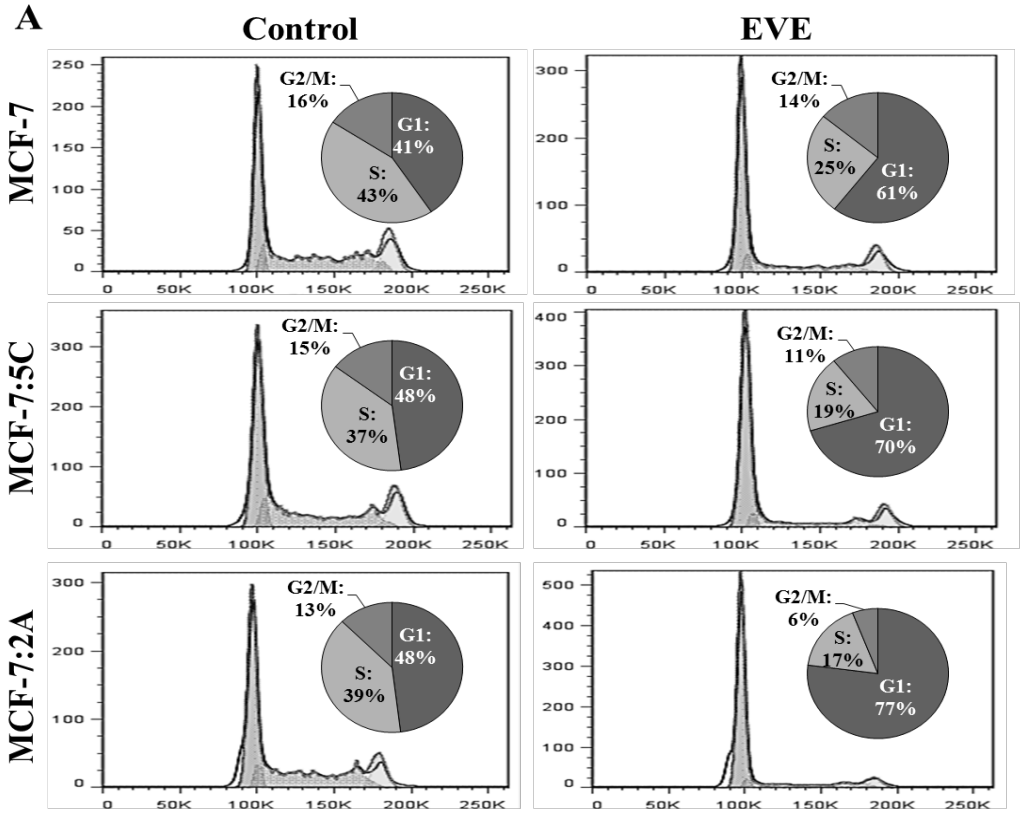

B

Cell Line	24 Hours		48 Hours		72 Hours	
	Control	EVE**	Control	EVE**	Control	EVE**
MCF-7	42.5 ± 4	60.7 ± 9	50.2 ± 5	62.2 ± 1	58.9 ± 1	66.1 ± 2
MCF-7:5C	48.1 ± 5	73.1 ± 6	56.5 ± 2	69.9 ± 4	57.8 ± 2	69.1 ± 4
MCF-7:2A	55.2 ± 7	74.4 ± 2	51.1 ± 2	70.3 ± 9	55.9 ± 4	68.8 ± 8

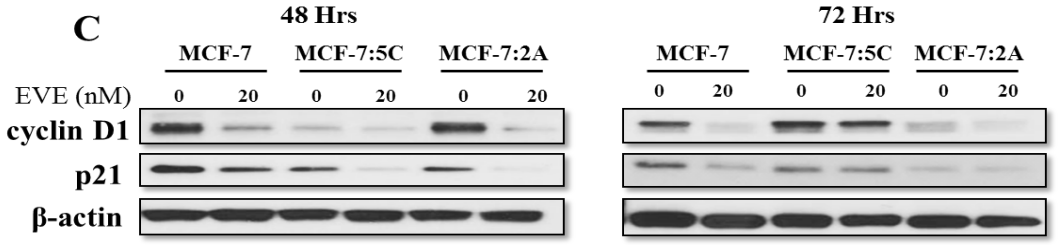

Fig. 2 Everolimus induces G1 arrest. (a) MCF-7, MCF-7:5C and MCF-7:2A cells were treated for 24 hours with 20 nM everolimus or vehicle and then harvested by trypsinization. Samples were fixed with methanol, stained with propidium iodide and analyzed by flow cytometry. The percent of cells in each phase of the cell cycle from a representative experiment are indicated in pie charts. (b) Samples from cells treated for 24, 48 and 72 hours are summarized in the table. Values are means from three independent experiments analyzed in duplicate and are displayed as mean ± SD. ** $p < 0.01$. (c) Cyclin D1 and p21 expression in MCF-7, MCF-7:5C and MCF-7:2A cells following treatment with everolimus (20 nM) for 48 and 72 hours.

Figure 3

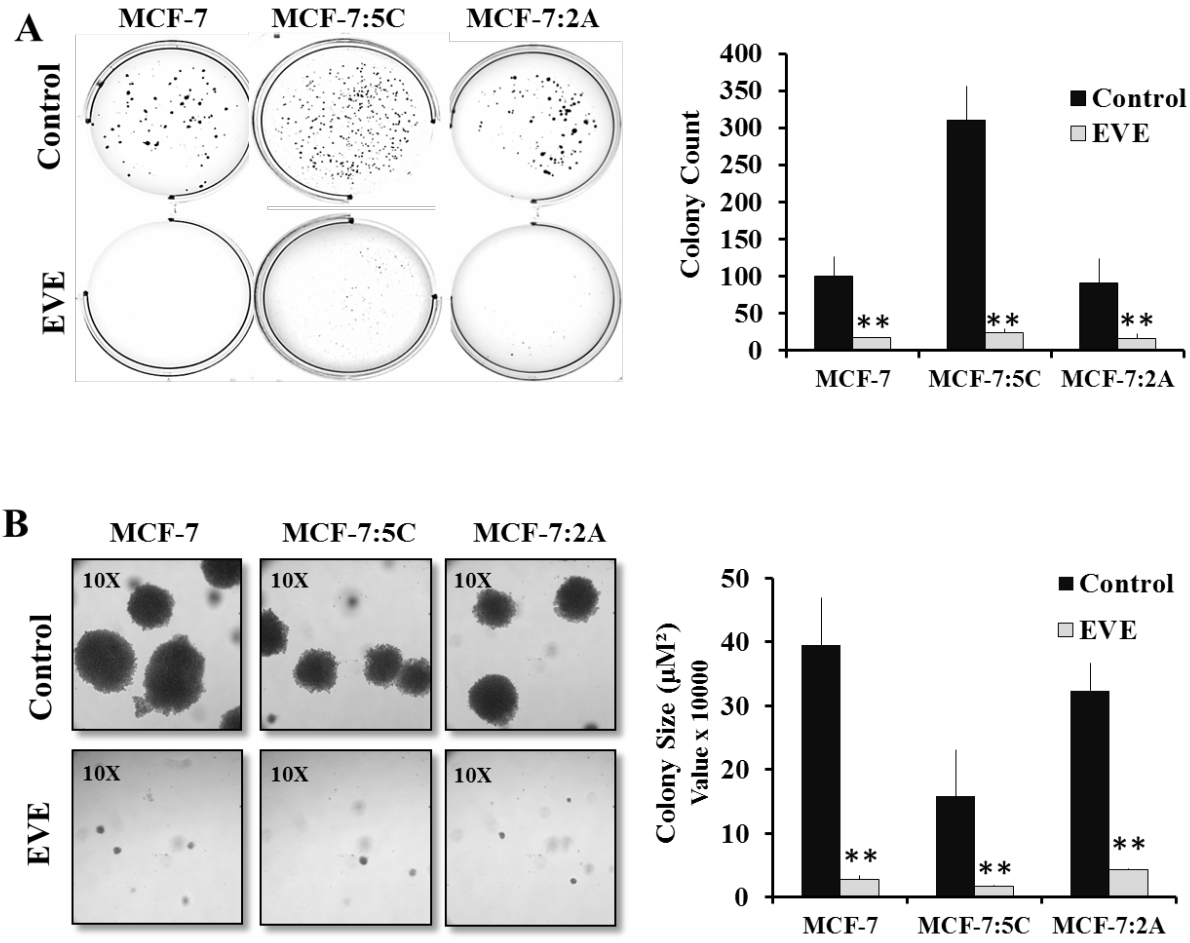

Fig. 3 Everolimus reduces anchorage-independent growth. (a) MCF-7, MCF-7:5C and MCF-7:2A cells were seeded in single cell suspension within a layer of 0.5% agarose gel. Cells were treated with 20 nM everolimus or vehicle every 48 hours for 17 days. Images were taken at 1X magnification and the number of colonies quantified using Image J. **(b)** Images of the same wells were taken at 10X magnification and colony diameter in μm^2 is shown. Bar graphs represent the data from three independent experiments in duplicate. The displayed values are mean ± SD. ** $p < 0.01$.

Figure 4

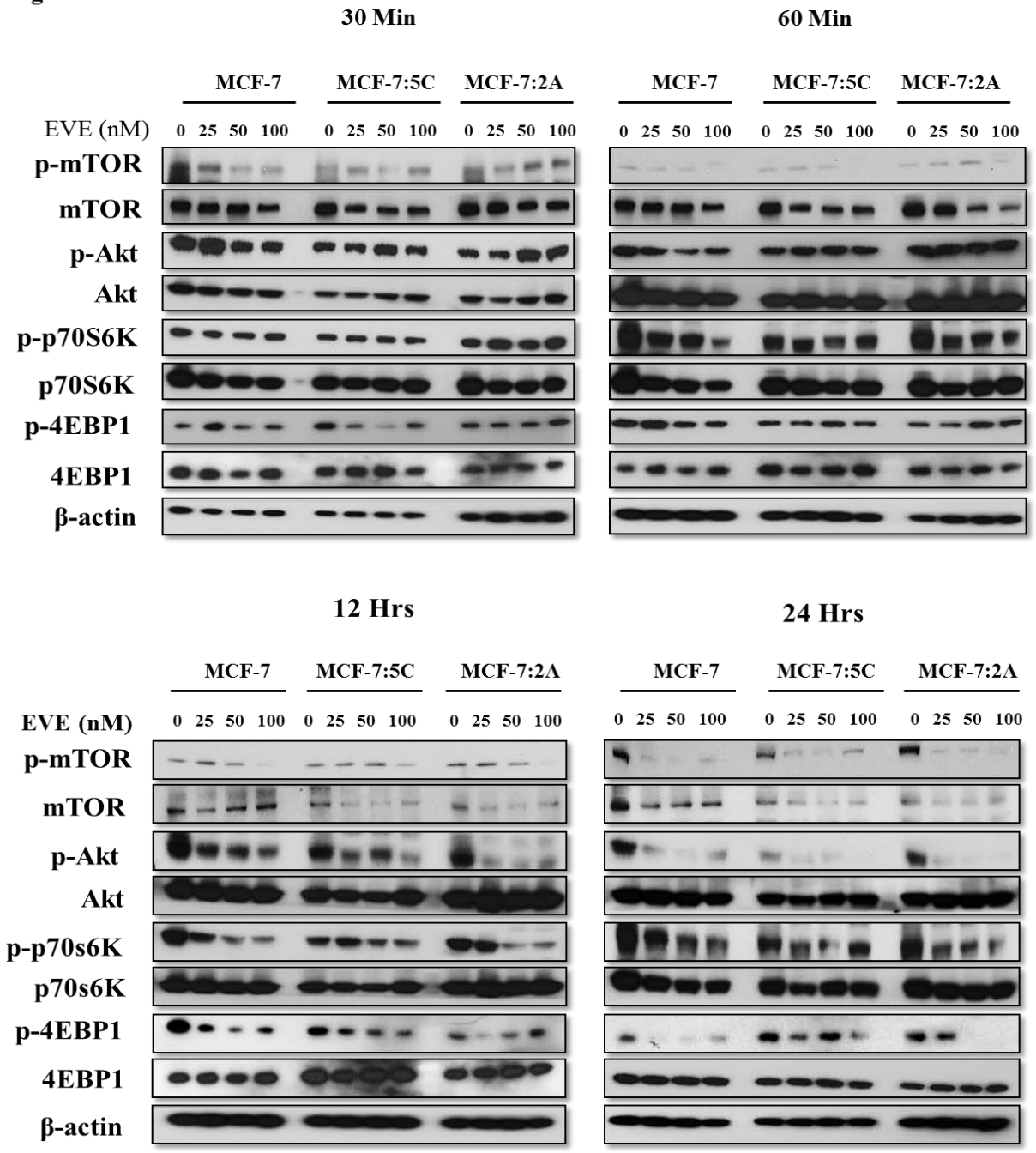

Fig. 4 Everolimus targets the mTOR/Akt pathway. AI-sensitive MCF-7 and AI-resistant MCF-7:5C and MCF-7:2A cells were treated with 25, 50 and 100nM everolimus. Phosphorylation of mTOR, AKT, p70s6K, 4EBP1 and total protein levels are shown at 30mins, 60mins, 12 and 24 hours. Images are representative of three independent experiments.

Figure 5

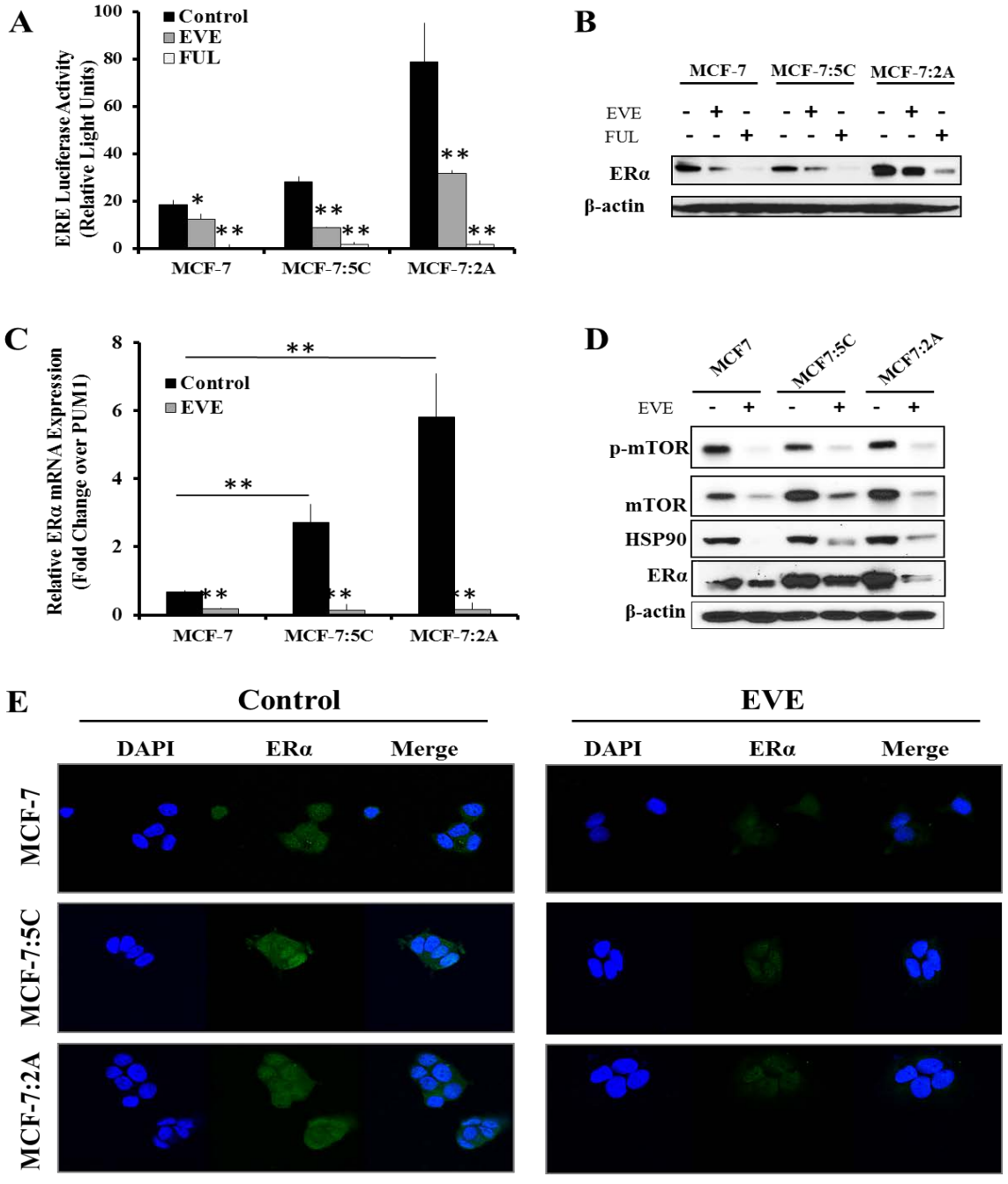

Fig. 5 Everolimus treatment inhibits estrogen receptor α expression and activity. (a) ER transcriptional activity after 24 hour treatment of MCF-7, MCF-7:5C and MCF-7:2A cells with 20 nM everolimus (EVE) and 1μM fulvestrant (FUL) is demonstrated using an ERE luciferase reporter. **(b)** Corresponding expression of estrogen receptor α (ERα) after 48 hours of treatment is shown by western blot. **(c)** RT-PCR demonstrates the impact of 20 nM everolimus on ERα mRNA production in all three cell lines after 24 hours. **(d)** The effect of everolimus treatment on mTOR phosphorylation as well as HSP90 and ERα expression is shown. **(e)** Immunofluorescent confocal microscopy illustrates the impact of 20 nM everolimus on ERα expression and localization (green). Cell nuclei are stained with DAPI (blue). Bar graphs represent means from two independent experiments analyzed in quadruplet and are displayed as mean ± SD. ** $p < 0.01$.

Figure 6

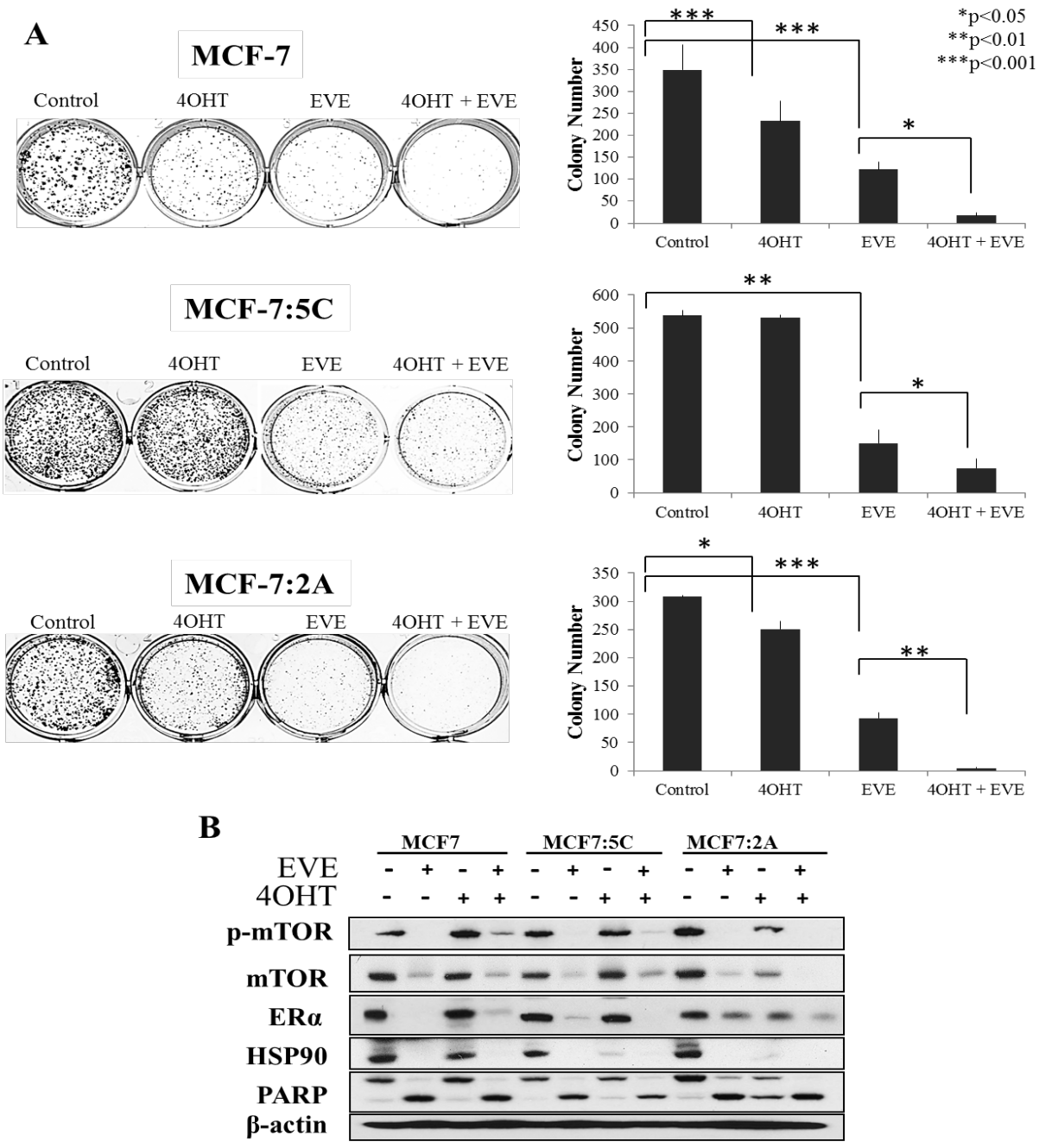

Fig. 6 Everolimus enhances tamoxifen sensitivity. (a) MCF-7, MCF-7:5C and MCF-7:2A cells were seeded in single cell suspension and allowed to proliferate for 9 days in the presence of 20 nM everolimus, 1μM 4-hydroxy tamoxifen (4OHT) or vehicle for 48 hours. The plates were photographed and the number of colonies was quantified using Image J. Bar graphs represent the data from three independent experiments in triplicate and values are mean ± SD. *p<0.05, **p<0.01. *** p< 0.001. **(b)** Western blot indicates the effect of each treatment on mTOR phosphorylation and ERα, HSP90 expression and cleaved PARP.

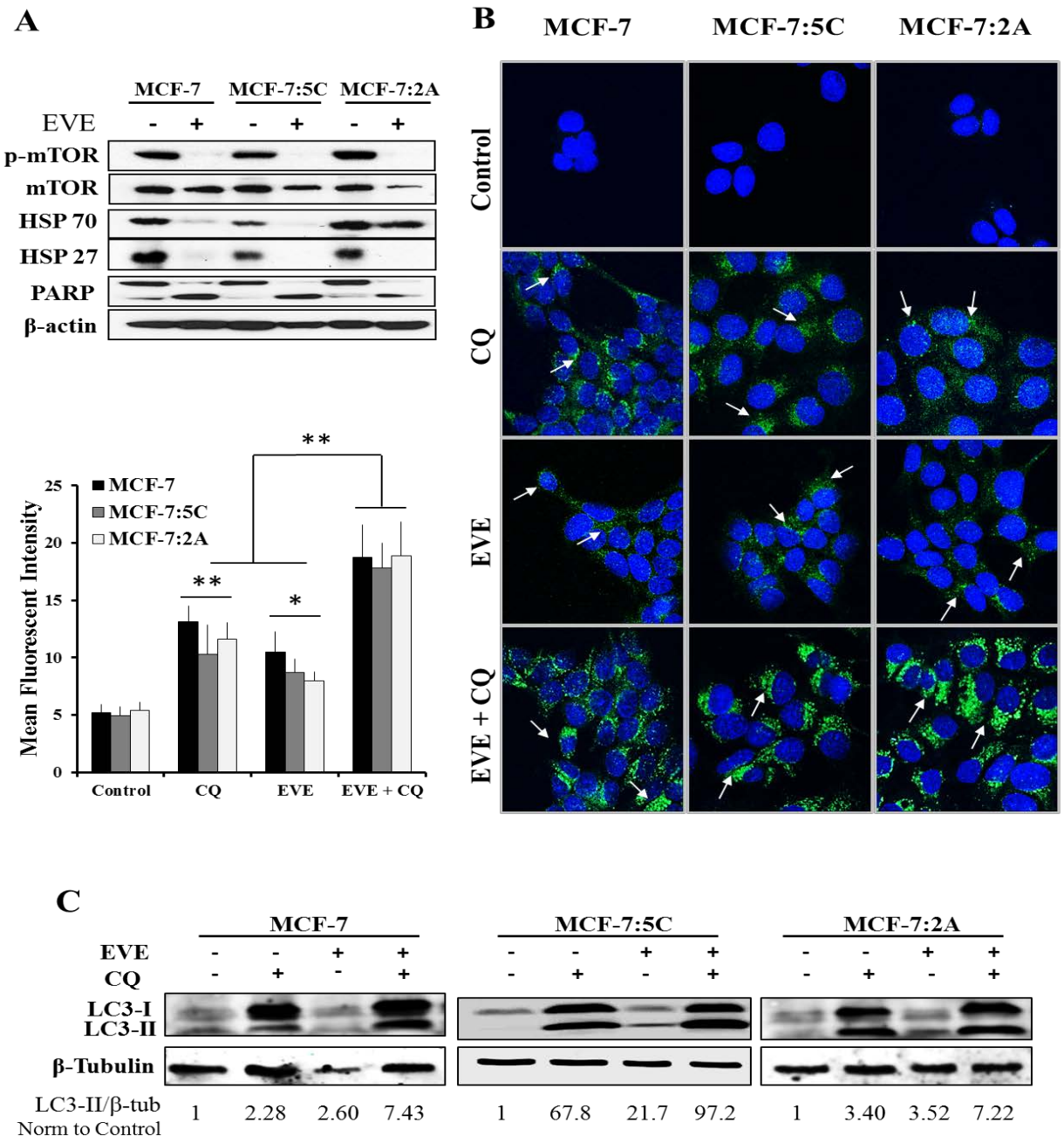

Fig. 7 Everolimus modifies autophagic cell markers. (a) Inhibition of mTOR phosphorylation, downregulation of HSP70 and HSP27 as well as induction of PARP cleavage by 20 nM everolimus are shown by western blot. **(b)** MCF-7, MCF-7:5C and MCF-7:2A cells were treated with vehicle, 20 nM everolimus, 50μM chloroquine (CQ) or both for 24 hours. LC3B is shown by immunofluorescent confocal microscopy. Punctate LC3B granules (green) are indicated with white arrows. Cell nuclei are stained with DAPI (blue). Mean fluorescent intensity was determined using Image J. **(c)** Cells were treated with vehicle, 20 nM everolimus, 50μM chloroquine (CQ) or both for 48 hours and LC3-I and -II assessed by western blot. The ratio of LC3-II/β-Tubulin normalized to control was determined by densitometry with Image J and is shown below the blots.

Figure 8

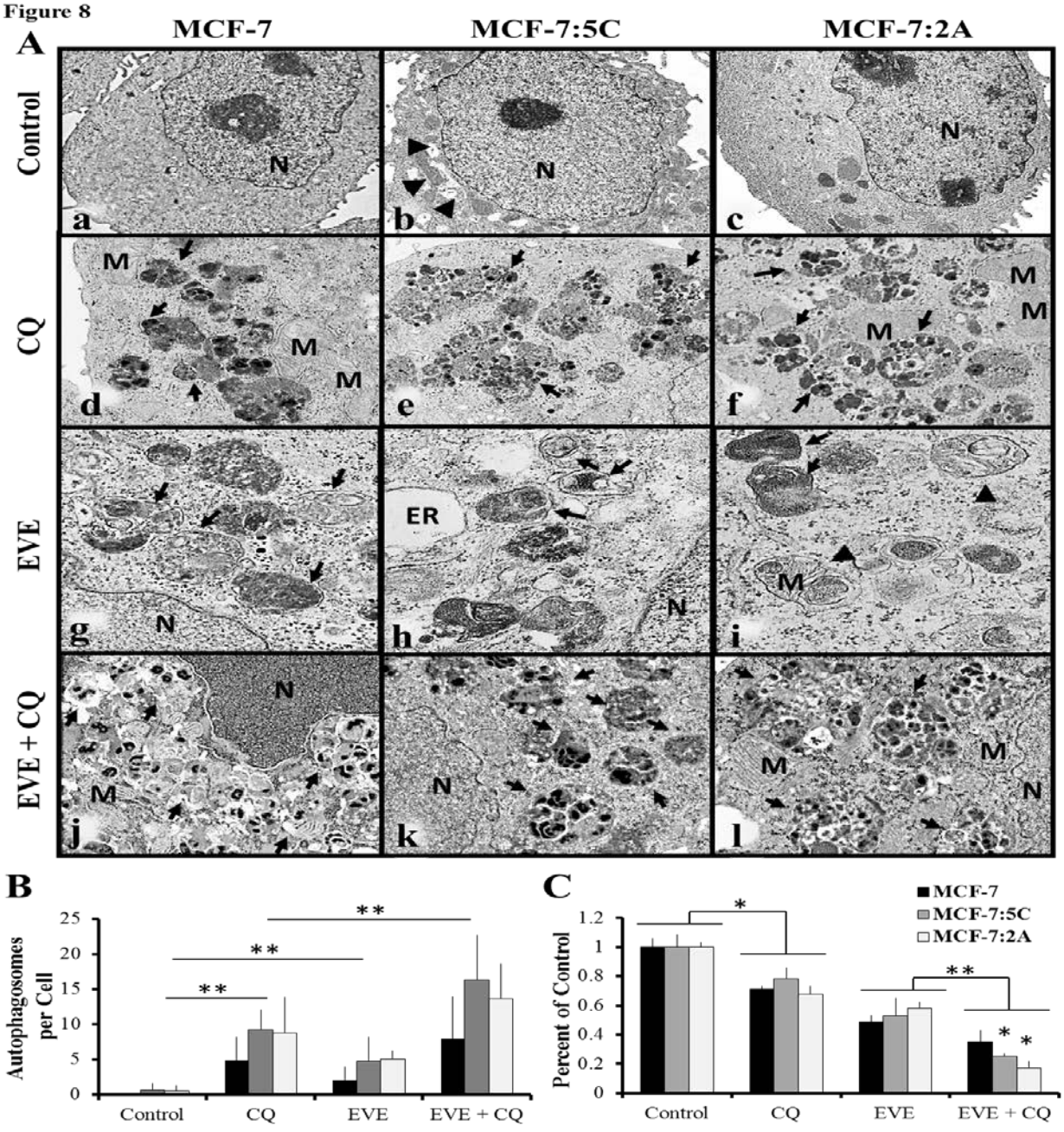

Fig. 8 Everolimus treatment induces autophagy, which mediates insensitivity. (a) MCF-7, MCF-7:5C and MCF-7:2A cells were treated with vehicle (a-c), 50μM chloroquine (CQ) (d-f), 20 nM everolimus (EVE) (g-i) or both EVE and CQ (j-l) for 48 hours and imaged using electron microscopy. Arrows indicate double membrane bound autophagosomes and arrow heads indicate pleomorphic mitochondria and dilated endoplasmic reticulum, which could also be seen in untreated MCF-7:5C cells. Images a-c are shown at 2000 X magnification while d-f**,** g-i and j-l are shown at 5000X, 8000X and 6000X respectively. M, mitochondria; N, nucleus; ER, endoplasmic reticulum. **(b)** Autophagosomes in a minimum of 10 random cells were recorded using de-identified samples. Values are average autophagosomes per cell and represent three trials from two separate experiments. **(c)** Cells were seeded in 24-well plates and treated with vehicle, 20 nM everolimus (EVE), 50μM chloroquine or both for 7 days. The percentage of viable cells is shown as compared to vehicle treated cells. Bar graphs represent the data from three independent experiments in duplicate and values are mean ± SD. * p< 0.05, ** p< 0.01

Supplemental Figure 1

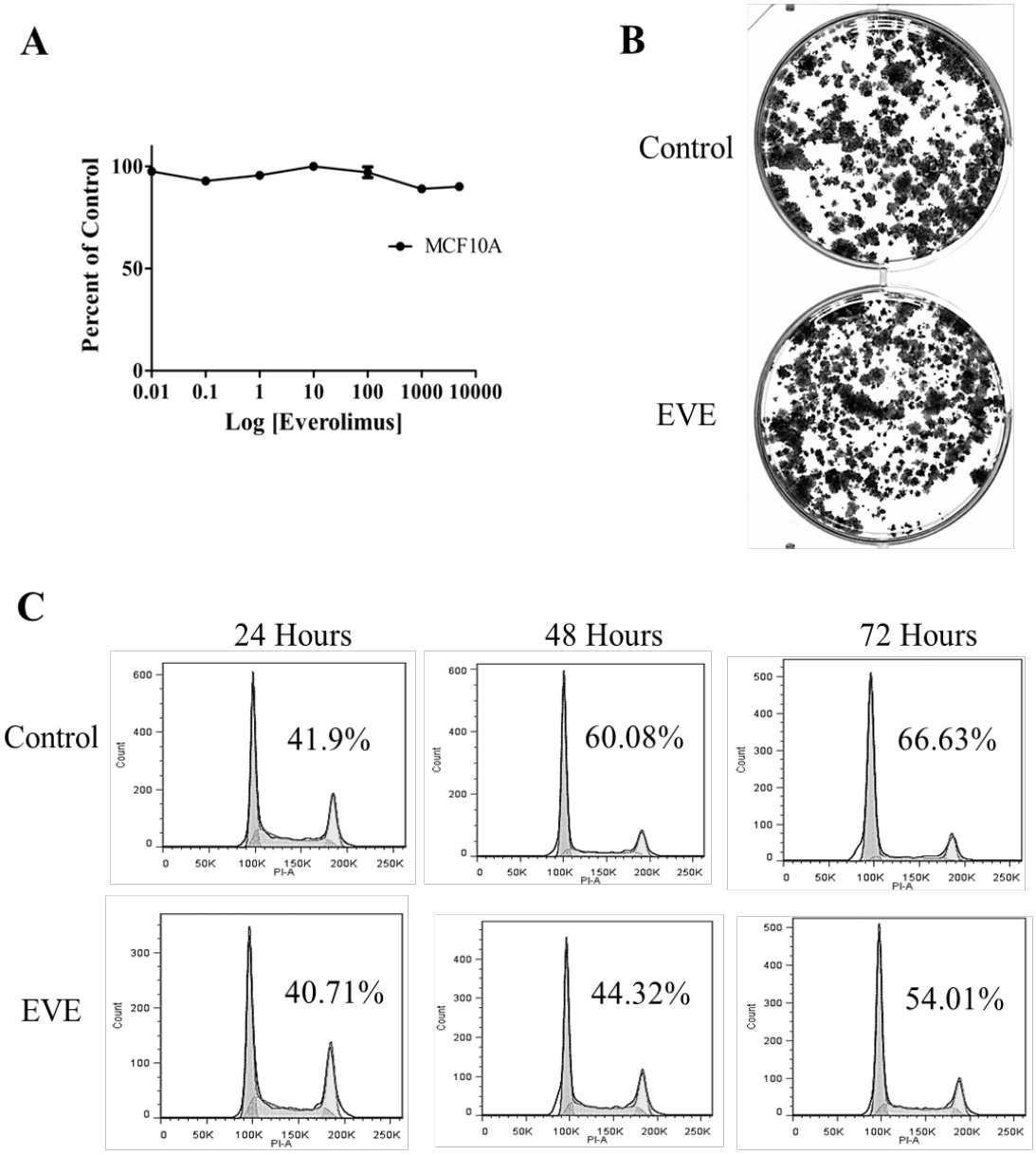

Supplemental Fig. 1 Everolimus does not impact the proliferation or cycling of normal breast cells
a MCF10A cells were seeded in 24-well plates and treated with a range of everolimus doses. The percentage of viable cells was determined after 72 hours of everolimus treatment. **b** MCF10A cells were seeded in 6-well plates in single cell suspension and treated with 20 nM everolimus for 9 days. The number and size of clones was quantified and represents means from two independent experiments conducted in triplicate. **c** After 24, 48 and 72 hours of 20 nM everolimus treatment in 6-well plates, MCF10A cells were subjected to cell cycle analysis. The percent of cells in G1 phase is highlighted.

Supplemental Figure 2

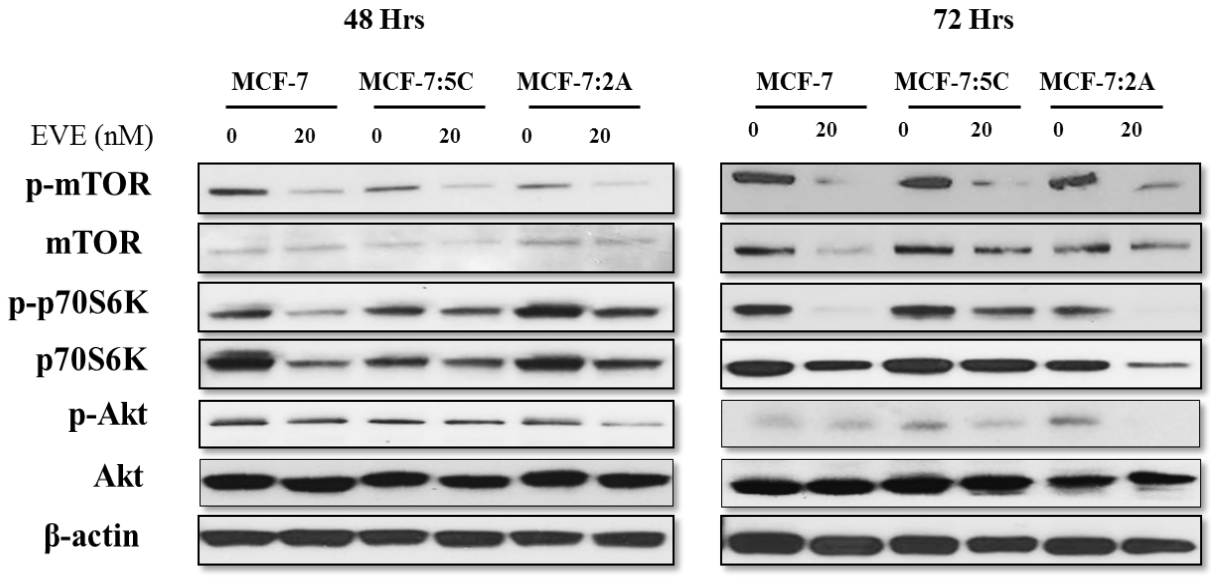

Supplemental Fig. 2 Everolimus targets the phosphorylation of the PI3K/mTOR/Akt pathway at 48 and 72 hours MCF-7, MCF-7:5C and MCF-7:2A cells were seeded in 6-well plates and treated with 25, 50 or 100 nM everolimus or vehicle. Cells were harvested at 48 and 72 hours and protein expression analyzed by western blot.

DISCUSSION

This study was conducted to provide mechanistic insights into the anti-proliferative effects of everolimus in AI-resistant MCF-7:5C and MCF-7:2A breast cancer cells, and AI-sensitive MCF-7 cells. We found that everolimus was equally effective against all three breast cancer cell lines. The anti-proliferative mechanisms included downregulation of ER expression and transcriptional activity, possibly through the suppression of HSP90. We also demonstrated that everolimus enhanced 4OHT sensitivity in all three cell lines. Everolimus treatment significantly induced autophagy, which was associated with downregulation of HSP70 and HSP27 expression. Additionally, we confirmed that everolimus inhibits the activation of the PI3K/Akt/mTOR pathway, resulting in the downregulation of cyclin D1 and p21 expression, which induced G1 arrest.

MCF-7 cells and their derivatives are more resistant to everolimus as compared to other luminal A breast cancer cell lines.[235,236] Our study is consistent with this observation, as total inhibition of the MCF-7, MCF-7:5C and MCF-7:2A cells did not exceed 60%, making them suitable to model a patient population that is not highly sensitive to everolimus. Additionally, our IC_{50} values were consistent with the frequent use of 20 nM everolimus when studying MCF-7 cell lines.[153,237,238] The enhanced insensitivity of the MCF-7:5C cells may be due to increased expression of c-myc, which is thought to confer some resistance in ER+ breast cancer. [108,239] The slightly enhanced sensitivity of the MCF-7:2A cells to everolimus may be related to comparatively lower levels of PTEN.[108] It should be noted that the MCF-7 and MCF-7:2A cells are progesterone receptor-positive (PR+), while the MCF-7:5C cells are PR-negative (PR-)

and they overexpresses interferon stimulated genes [59]. These differences do not seem to mediate any variances in everolimus sensitivity, suggesting that the MCF-7 background of these cell lines is the most prominent determinant of response.

Elevated ER expression and signaling has been observed in both endocrine resistance cells and endocrine resistant tumors.[29,30,240,241] The ability of everolimus to reduce ER transcriptional activity and phospho-ER (p-ER) expression in MCF-7/LTED cells has been previously reported but was not assessed in wild type MCF-7 cells.[220] In our study, we found that the inhibition of ER transcriptional activity was due to profound downregulation of total ER expression in all cell models. MCF-7:5C and MCF-7:2A cells are selected clones maintained in estrogen-free media that have retained ER transcriptional activity by upregulation of ER expression and ligand-independent ER signaling. In contrast, the MCF-7/LTED cells are a mixed population of cells that have developed hypersensitivity to estrogen.[242] Additionally, the studies by Martin and colleagues were conducted after acute insulin deprivation, which probably contributed to the enhanced sensitivity to everolimus and to the impact on both p-ER and p-Akt expression in their study. The clinical efficacy of everolimus as a solo agent was thought to be limited by a compensatory increase in Akt phosphorylation through mTORC2.[153] We did not observe this reflexive increase in Akt phosphorylation in our cells lines. Our results suggest that everolimus as a single agent has the ability to function in a manner similar to combination therapy by inhibiting both growth factor and ER signaling simultaneously in some systems. Downregulation of total ER expression by everolimus has not, to our knowledge, been previously reported.

The downregulation of ER expression was likely due to reduced expression of HSP90, a well-known ER chaperone. HSP expression in general is controlled by the PI3K/Akt/mTOR pathway through phosphorylation of the transcription factor HSF1 and is consistent with the loss of HSP90, HSP27 and HSP70 expression observed in this study. [243] Everolimus induced loss of HSP90 mRNA expression has been observed in other cancers [222] and a loss of HSP90 expression has been linked to autophagic cell death.[244] Two HSP90 inhibitors, NVP-AUY922 and STA-9090, are currently in clinical trials for the treatment of breast cancer. [245,246] HSP90 inhibitor therapy has been limited by reflexive increase in HSP signaling, especially enhanced HSP27 expression.[247,248] Here, we report that everolimus inhibits HSP27 in our cell lines, and so may potentiate HSP90 inhibitor treatment. These results suggest that everolimus may be combined with HSP90 inhibitors or drugs that target HSP90 clients for the treatment of AI-resistant breast cancer.

AI-resistant tumors are known to retain dependence on ER signaling for growth and survival. Given that everolimus reduces ER expression, our observation that it also enhances 4OHT sensitivity during long-term co-treatment is very interesting and warrants further investigation. It should be noted, however, that everolimus has previously been shown to inhibit ER phosphorylation on serine 167 despite documented synergy between everolimus and tamoxifen in AI-resistant models and patients. [153,215,220] It is likely that these two drugs exhibit synergy by targeting ER signaling through separate but complementary mechanisms. Our results indicate that everolimus reduces ER expression through inhibition of ER mRNA transcription, while tamoxifen targets the ER protein. Combining everolimus and tamoxifen ensures that ER signaling

is inhibited continuously over time in all cells within a heterogeneous breast tumor. The improved efficacy of everolimus in combination with 4OHT in our study is consistent with results from the TAMRAD clinical trial.[215] The data from our study suggest that everolimus could benefit AI-resistant patients with ligand-independent ER activity by targeting ER expression and signaling.

We have demonstrated that everolimus dramatically induces autophagy, and is associated with significant downregulation of HSP90, HSP70 and HSP27. Loss of HSP70 and HSP27 is associated with starvation-induced autophagy and rapamycin treatment, both of which target the PI3K/Akt/mTOR pathway.[229,233] Autophagy is a mechanism of drug insensitivity in cancer because it allows tumors to recycle cellular components and survive treatment. [224,225] Inhibition of autophagy significantly improved the anti-proliferative effects of everolimus in MCF-7, MCF-7:5C and MCF-7:2A cells. This is consistent with a previous study reporting enhanced inhibition of MCF-7 cell proliferation when combining chloroquine and everolimus.[249] Everolimus and other PI3K/Akt/mTOR inhibitors are known to induce autophagy in both solid and blood tumors [222,223]; however, to our knowledge, this phenomenon has not been reported in breast cancer cells. We conclude that the induction of autophagy is likely a mechanism of everolimus insensitivity in MCF-7 [235,236], MCF-7:5C and MCF-7:2A cells.

Although everolimus treatment induced PARP cleavage in all three cell lines, we did not observe apoptotic cell death normally associated with PARP cleavage. PARP cleavage is thought to mediate autophagy rather than apoptosis in response to certain stimuli.[250] Since HSP70 is known to stabilize PARP [251], loss of HSP70-mediated stability offers an explanation for the everolimus induced PARP cleavage seen in this study.

While there have been reports of autophagic and apoptotic cell death in leukemia [222] and nasopharyngeal carcinoma cells [252], everolimus is not known to induce cell death in breast cancer cells on its own. [222,252] To our knowledge, everolimus induced cell death in breast cancer has only been observed in aromatase expressing MCF-7/Aro cells when combined with letrozole. [212] We have shown that induction of autophagy limits the anti-proliferative response of everolimus treatment, hence a combination of everolimus with the autophagy inhibitors chloroquine or hydroxychloroquine, which are currently in clinical trials as part of combination therapy [253], may be beneficial in the treatment of AI-resistant breast cancer.

CONCLUSION

Overall, this study demonstrated that everolimus inhibits the proliferation of AI-resistant breast cancer cells through down regulation of ER expression and also that induction of autophagy is a method of everolimus insensitivity. We found that everolimus had similar effect on the proliferation of both our AI-sensitive (MCF-7) and AI-resistant (MCF-7:5C and MCF-7:2A) models, suggesting that the MCF-7 background of these cell lines overrides any other differences that might impact everolimus sensitivity. The inhibition of proliferation was seen regardless of PR status, PTEN expression, type 1interferon signaling, and 4OHT sensitivity, supporting a conclusion that everolimus holds promise as part of combination therapy for a wide variety of AI-resistant patients, for whom AI treatment is not an option.

Abbreviations

AI	Aromatase inhibitor
CQ	Chloroquine
EGF	Epidermal growth factor
ER	Estrogen receptor
EVE	Everolimus;
FUL	Fulvestrant
HER2	human epidermal growth factor receptor 2
HIF-1 α	hypoxia inducible factor 1 alpha subunit
HSP27	Heat shock protein 27
HSP70	Heat shock protein 70
HSP90	Heat shock protein 90
IC_{50}	Drug concentration that provides 50% maximal growth inhibition
LC3B	Microtubule associated light chain 3
mTOR	Mammalian target of rapamycin
PARP	Poly ADP ribose polymerase
PI3K	Phosphoinositide 3-kinase
PR	Progesterone receptor
PTEN	Phosphatase and tensin homolog
P21	Cyclin dependent kinas inhibitor 1
p70S6K	p70 S6 ribosomal protein kinase
TSC	Tuberous sclerosis complex
4OHT	4- hydroxytamoxifen
4EBP1	Eukaryotic translation initiation factor 4E-bidning protein

Ethics Approval and Consent to Participate

Not Applicable

Consent for Publication

Not Applicable

Availability of Data and Materials

All data supporting the findings in this study are included within the manuscript and the two supplementary figures.

Competing Interests

The authors declare that they have no competing interests to report.

Funding

This study was supported, in part, by grants from the Department of Defense (W81XWH-12-1-0139 to JLW), the National Cancer Institute (K01CA120051 to JLW), start-up funds from the University of Kansas Medical Center (to JLW), the KUMC Biomedical Research Training Program (BRTP to AL), the National Cancer Institute (1F30CA203160-01 to AL), and the University of Kansas Cancer Center (CCSG grants P30 CA168524-0 to ST and JLW).

Authors Contributions

AL designed and executed this study and wrote the manuscript. JN assisted with the experiments concerning analysis of autophagy and contributed to the manuscript. JO edited the manuscript and contributed intellectually to the study. ST oversaw the autophagy analysis and edited the manuscript. JLW, conceived of the study and edited the manuscript. All authors have read and approved the final manuscript.

Acknowledgements

We would like to thank the Flow Cytometry Core Laboratory at the University of Kansas Medical Center, which is sponsored, in part, by the NIH/NIGMS COBRE grant P30 GM103326. We also wish to acknowledge the University of Kansas Medical Center Electron Microscopy Research Lab (EMRL) facility for assistance with

the electron microscopy. The EMRL is supported in part, by NIH COBRE grant 9P20GM104936. The JEOL JEM-1400 TEM used in the study was purchased with funds from NIH grant S10RR027564.

REFERENCES

22. JS Lewis, Jordan VC. *Selective estrogen receptor modulators (SERMs): mechanisms of anticarcinogenesis and drug resistance*. Mutation research 2005;591:247-63.

29. R Clarke, Liu MC, Bouker KB, et al. *Antiestrogen resistance in breast cancer and the role of estrogen receptor signaling*. Oncogene 2003;22:7316-39.

30. S Ali, Coombes RC. *Endocrine-responsive breast cancer and strategies for combating resistance*. Nature reviews Cancer 2002;2:101-12.

42. SY Jiang, Wolf DM, Yingling JM, Chang C, Jordan VC. *An estrogen receptor positive MCF-7 clone that is resistant to antiestrogens and estradiol*. Molecular and cellular endocrinology 1992;90:77-86.

48. JS Lewis, Meeke K, Osipo C, et al. *Intrinsic mechanism of estradiol-induced apoptosis in breast cancer cells resistant to estrogen deprivation*. Journal of the National Cancer Institute 2005;97:1746-59.

59. HJ Choi, Lui A, Ogony J, Jan R, Sims PJ, Lewis-Wambi J. *Targeting interferon response genes sensitizes aromatase inhibitor resistant breast cancer cells to estrogen-induced cell death*. Breast cancer research : BCR 2015;17:6.

108. JS Lewis-Wambi, Cunliffe HE, Kim HR, Willis AL, Jordan VC. *Overexpression of CEACAM6 promotes migration and invasion of oestrogen-deprived breast cancer cells*. European journal of cancer (Oxford, England : 1990) 2008;44:1770-9.

122. JS Lewis-Wambi, Kim HR, Wambi C, et al. *Buthionine sulfoximine sensitizes antihormone-resistant human breast cancer cells to estrogen-induced apoptosis*. Breast cancer research : BCR 2008;10:R104.

132. JJ Pink, Jiang SY, Fritsch M, Jordan VC. *An estrogen-independent MCF-7 breast cancer cell line which contains a novel 80-kilodalton estrogen receptor-related protein*. Cancer research 1995;55:2583-90.

153. X Chen, Zhao M, Hao M, et al. *Dual Inhibition of PI3K and mTOR Mitigates Compensatory AKT Activation and Improves Tamoxifen Response in Breast Cancer*. Molecular cancer research : MCR 2013;11:1269-78.

154. Y Liu, Zhang X, Liu J, Hou G, Zhang S, Zhang J. *Everolimus in combination with letrozole inhibit human breast cancer MCF-7/Aro stem cells via PI3K/mTOR pathway: an experimental study*. Tumour biology : the journal of the International Society for Oncodevelopmental Biology and Medicine 2014;35:1275-86.

155. I Barone, Cui Y, Herynk MH, et al. *Expression of the K303R estrogen receptor-alpha breast cancer mutation induces resistance to an aromatase inhibitor via addiction to the PI3K/Akt kinase pathway*. Cancer research 2009;69:4724-32.

209. J Cuzick, Sestak I, Baum M, et al. *Effect of anastrozole and tamoxifen as adjuvant treatment for early-stage breast cancer: 10-year analysis of the ATAC trial*. The Lancet Oncology 2010;11:1135-41.

210. LA deGraffenried, Friedrichs WE, Russell DH, et al. *Inhibition of mTOR activity restores tamoxifen response in breast cancer cells with aberrant Akt Activity*. Clinical cancer research : an official journal of the American Association for Cancer Research 2004;10:8059-67.

211. H Kurokawa, Arteaga CL. *ErbB (HER) receptors can abrogate antiestrogen action in human breast cancer by multiple signaling mechanisms*. Clinical cancer research : an official journal of the American Association for Cancer Research 2003;9:511s-5s.

212. A Boulay, Rudloff J, Ye J, et al. *Dual inhibition of mTOR and estrogen receptor signaling in vitro induces cell death in models of breast cancer*. Clinical cancer research : an official journal of the American Association for Cancer Research 2005;11:5319-28.

213. SL Ellard, Clemons M, Gelmon KA, et al. *Randomized phase II study comparing two schedules of everolimus in patients with recurrent/metastatic breast cancer: NCIC*

Clinical Trials Group IND.163. Journal of clinical oncology : official journal of the American Society of Clinical Oncology 2009;27:4536-41.

214. J Baselga, Semiglazov V, van Dam P, et al. *Phase II randomized study of neoadjuvant everolimus plus letrozole compared with placebo plus letrozole in patients with estrogen receptor-positive breast cancer*. Journal of clinical oncology : official journal of the American Society of Clinical Oncology 2009;27:2630-7.

215. T Bachelot, Bourgier C, Cropet C, et al. *Randomized phase II trial of everolimus in combination with tamoxifen in patients with hormone receptor-positive, human epidermal growth factor receptor 2-negative metastatic breast cancer with prior exposure to aromatase inhibitors: a GINECO study*. Journal of clinical oncology : official journal of the American Society of Clinical Oncology 2012;30:2718-24.

216. JA Beaver, Park BH. *The BOLERO-2 trial: the addition of everolimus to exemestane in the treatment of postmenopausal hormone receptor-positive advanced breast cancer*. Future oncology (London, England) 2012;8:651-7.

217. JT Beck, Hortobagyi GN, Campone M, et al. *Everolimus plus exemestane as first-line therapy in HR(+), HER2(-) advanced breast cancer in BOLERO-2*. Breast cancer research and treatment 2014;143:459-67.

218. S Noguchi, Masuda N, Iwata H, et al. *Efficacy of everolimus with exemestane versus exemestane alone in Asian patients with HER2-negative, hormone-receptor-positive breast cancer in BOLERO-2*. Breast cancer (Tokyo, Japan) 2014;21:703-14.

219. DA Yardley, Noguchi S, Pritchard KI, et al. *Everolimus plus exemestane in postmenopausal patients with HR(+) breast cancer: BOLERO-2 final progression-free survival analysis*. Advances in therapy 2013;30:870-84.

220. LA Martin, Pancholi S, Farmer I, et al. *Effectiveness and molecular interactions of the clinically active mTORC1 inhibitor everolimus in combination with tamoxifen or letrozole in vitro and in vivo*. Breast cancer research : BCR 2012;14:R132.

221. NJ Jordan, Dutkowski CM, Mottram HJ, et al. *Impact of dual mTORC1/2 mTOR kinase inhibitor AZD8055 on acquired endocrine resistance in breast cancer in vitro*. Breast cancer research : BCR 2014;16:R12.

222. R Baraz, Cisterne A, Saunders PO, et al. *mTOR inhibition by everolimus in childhood acute lymphoblastic leukemia induces caspase-independent cell death*. PloS one 2014;9:e102494.

223. M Santoni, Pantano F, Amantini C, et al. *Emerging strategies to overcome the resistance to current mTOR inhibitors in renal cell carcinoma*. Biochimica et biophysica acta 2014;1845:221-31.

224. R Clarke, Shajahan AN, Riggins RB, et al. *Gene network signaling in hormone responsiveness modifies apoptosis and autophagy in breast cancer cells*. The Journal of steroid biochemistry and molecular biology 2009;114:8-20.

225. AC Crawford, Riggins RB, Shajahan AN, Zwart A, Clarke R. *Co-inhibition of BCL-W and BCL2 restores antiestrogen sensitivity through BECN1 and promotes an autophagy-associated necrosis*. PloS one 2010;5:e8604.

226. H Weidberg, Shvets E, Shpilka T, Shimron F, Shinder V, Elazar Z. *LC3 and GATE-16/GABARAP subfamilies are both essential yet act differently in autophagosome biogenesis*. The EMBO journal 2010;29:1792-802.

227. HL Chiang, Terlecky SR, Plant CP, Dice JF. *A role for a 70-kilodalton heat shock protein in lysosomal degradation of intracellular proteins*. Science (New York, NY) 1989;246:382-5.

228. FA Agarraberes, Terlecky SR, Dice JF. *An intralysosomal hsp70 is required for a selective pathway of lysosomal protein degradation*. The Journal of cell biology 1997;137:825-34.

229. K Dokladny, Zuhl MN, Mandell M, et al. *Regulatory coordination between two major intracellular homeostatic systems: heat shock response and autophagy*. The Journal of biological chemistry 2013;288:14959-72.

230. MA Park, Yacoub A, Rahmani M, et al. *OSU-03012 stimulates PKR-like endoplasmic reticulum-dependent increases in 70-kDa heat shock protein expression, attenuating its lethal actions in transformed cells*. Molecular pharmacology 2008;73:1168-84.

231. C Garrido, Bruey JM, Fromentin A, Hammann A, Arrigo AP, Solary E. *HSP27 inhibits cytochrome c-dependent activation of procaspase-9*. FASEB journal : official publication of the Federation of American Societies for Experimental Biology 1999;13:2061-70.

232. AP Arrigo, Firdaus WJ, Mellier G, et al. *Cytotoxic effects induced by oxidative stress in cultured mammalian cells and protection provided by Hsp27 expression*. Methods (San Diego, Calif) 2005;35:126-38.

233. CY Chen, Chen HF, Gi SJ, et al. *Decreased heat shock protein 27 expression and altered autophagy in human cells harboring A8344G mitochondrial DNA mutation*. Mitochondrion 2011;11:739-49.

234. JS Lewis-Wambi, Kim H, Curpan R, Grigg R, Sarker MA, Jordan VC. *The selective estrogen receptor modulator bazedoxifene inhibits hormone-independent breast cancer cell growth and down-regulates estrogen receptor alpha and cyclin D1*. Molecular pharmacology 2011;80:610-20.

235. S Hurvitz, Kalous O, Conklin D, et al. *In vitro activity of the mTOR inhibitor everolimus, in a large panel of breast cancer cell lines and analysis for predictors of response*. Breast cancer research and treatment 2015;149:669-80.

236. EY Leung, Askarian-Amiri M, Finlay GJ, Rewcastle GW, Baguley BC. *Potentiation of Growth Inhibitory Responses of the mTOR Inhibitor Everolimus by Dual mTORC1/2 Inhibitors in Cultured Breast Cancer Cell Lines*. PloS one 2015;10:e0131400.

237. EC Martin, Rhodes LV, Elliott S, et al. *microRNA regulation of mammalian target of rapamycin expression and activity controls estrogen receptor function and RAD001 sensitivity*. Molecular cancer 2014;13:229.

238. H Liu, Zang C, Schefe JH, et al. *The mTOR inhibitor RAD001 sensitizes tumor cells to the cytotoxic effect of carboplatin in breast cancer in vitro*. Anticancer research 2011;31:2713-22.

239. T Bihani, Ezell SA, Ladd B, et al. *Resistance to everolimus driven by epigenetic regulation of MYC in ER+ breast cancers*. Oncotarget 2015;6:2407-20.

240. CM Staka, Nicholson RI, Gee JM. *Acquired resistance to oestrogen deprivation: role for growth factor signalling kinases/oestrogen receptor cross-talk revealed in new MCF-7X model*. Endocrine-related cancer 2005;12 Suppl 1:S85-97.

241. KL Henriksen, Rasmussen BB, Lykkesfeldt AE, Moller S, Ejlertsen B, Mouridsen HT. *An ER activity profile including ER, PR, Bcl-2 and IGF-IR may have potential as selection criterion for letrozole or tamoxifen treatment of patients with advanced breast cancer*. Acta oncologica (Stockholm, Sweden) 2009;48:522-31.

242. WS Shim, Conaway M, Masamura S, et al. *Estradiol hypersensitivity and mitogen-activated protein kinase expression in long-term estrogen deprived human breast cancer cells in vivo*. Endocrinology 2000;141:396-405.

243. SD Chou, Prince T, Gong J, Calderwood SK. *mTOR is essential for the proteotoxic stress response, HSF1 activation and heat shock protein synthesis*. PloS one 2012;7:e39679.

244. W-B Wang, Feng L-X, Yue Q-X, et al. *Paraptosis accompanied by autophagy and apoptosis was induced by celastrol, a natural compound with influence on proteasome, ER stress and Hsp90*. Journal of Cellular Physiology 2012;227:2196-206.

245. K Jhaveri, Ochiana SO, Dunphy MPS, et al. *Heat shock protein 90 inhibitors in the treatment of cancer: current status and future directions*. Expert opinion on investigational drugs 2014;23:611-28.

246. R Schulz, Marchenko ND, Holembowski L, et al. *Inhibiting the HSP90 chaperone destabilizes macrophage migration inhibitory factor and thereby inhibits breast tumor progression*. The Journal of Experimental Medicine 2012;209:275-89.

247. L Whitesell, Lindquist S. *Inhibiting the transcription factor HSF1 as an anticancer strategy*. Expert opinion on therapeutic targets 2009;13:469-78.

248. K Sidera, Patsavoudi E. *HSP90 inhibitors: current development and potential in cancer therapy*. Recent patents on anti-cancer drug discovery 2014;9:1-20.

249. CR Loehberg, Strissel PL, Dittrich R, et al. *Akt and p53 are potential mediators of reduced mammary tumor growth by cloroquine and the mTOR inhibitor RAD001*. Biochemical pharmacology 2012;83:480-8.

250. JA Munoz-Gamez, Rodriguez-Vargas JM, Quiles-Perez R, et al. *PARP-1 is involved in autophagy induced by DNA damage*. Autophagy 2009;5:61-74.

251. P Kotoglou, Kalaitzakis A, Vezyraki P, et al. *Hsp70 translocates to the nuclei and nucleoli, binds to XRCC1 and PARP-1, and protects HeLa cells from single-strand DNA breaks*. Cell stress & chaperones 2009;14:391-406.

252. Y Cai, Xia Q, Su Q, et al. *mTOR inhibitor RAD001 (everolimus) induces apoptotic, not autophagic cell death, in human nasopharyngeal carcinoma cells*. International journal of molecular medicine 2013;31:904-12.

253. R Rangwala, Chang YC, Hu J, et al. *Combined MTOR and autophagy inhibition: phase I trial of hydroxychloroquine and temsirolimus in patients with advanced solid tumors and melanoma*. Autophagy 2014;10:1391-402.